

CHEMISTRY, A SUSTAINABLE BRIDGE FROM WASTE TO MATERIALS FOR ENERGY AND ENVIRONMENT

EDITED BY: Francesca Deganello, Enrico Traversa and Ana C. Tavares
PUBLISHED IN: *Frontiers in Chemistry*





frontiers

Frontiers eBook Copyright Statement

The copyright in the text of individual articles in this eBook is the property of their respective authors or their respective institutions or funders. The copyright in graphics and images within each article may be subject to copyright of other parties. In both cases this is subject to a license granted to Frontiers.

The compilation of articles constituting this eBook is the property of Frontiers.

Each article within this eBook, and the eBook itself, are published under the most recent version of the Creative Commons CC-BY licence.

The version current at the date of publication of this eBook is CC-BY 4.0. If the CC-BY licence is updated, the licence granted by Frontiers is automatically updated to the new version.

When exercising any right under the CC-BY licence, Frontiers must be attributed as the original publisher of the article or eBook, as applicable.

Authors have the responsibility of ensuring that any graphics or other materials which are the property of others may be included in the CC-BY licence, but this should be checked before relying on the CC-BY licence to reproduce those materials. Any copyright notices relating to those materials must be complied with.

Copyright and source acknowledgement notices may not be removed and must be displayed in any copy, derivative work or partial copy which includes the elements in question.

All copyright, and all rights therein, are protected by national and international copyright laws. The above represents a summary only. For further information please read Frontiers' Conditions for Website Use and Copyright Statement, and the applicable CC-BY licence.

ISSN 1664-8714

ISBN 978-2-88966-571-6

DOI 10.3389/978-2-88966-571-6

About Frontiers

Frontiers is more than just an open-access publisher of scholarly articles: it is a pioneering approach to the world of academia, radically improving the way scholarly research is managed. The grand vision of Frontiers is a world where all people have an equal opportunity to seek, share and generate knowledge. Frontiers provides immediate and permanent online open access to all its publications, but this alone is not enough to realize our grand goals.

Frontiers Journal Series

The Frontiers Journal Series is a multi-tier and interdisciplinary set of open-access, online journals, promising a paradigm shift from the current review, selection and dissemination processes in academic publishing. All Frontiers journals are driven by researchers for researchers; therefore, they constitute a service to the scholarly community. At the same time, the Frontiers Journal Series operates on a revolutionary invention, the tiered publishing system, initially addressing specific communities of scholars, and gradually climbing up to broader public understanding, thus serving the interests of the lay society, too.

Dedication to Quality

Each Frontiers article is a landmark of the highest quality, thanks to genuinely collaborative interactions between authors and review editors, who include some of the world's best academicians. Research must be certified by peers before entering a stream of knowledge that may eventually reach the public - and shape society; therefore, Frontiers only applies the most rigorous and unbiased reviews.

Frontiers revolutionizes research publishing by freely delivering the most outstanding research, evaluated with no bias from both the academic and social point of view. By applying the most advanced information technologies, Frontiers is catapulting scholarly publishing into a new generation.

What are Frontiers Research Topics?

Frontiers Research Topics are very popular trademarks of the Frontiers Journals Series: they are collections of at least ten articles, all centered on a particular subject. With their unique mix of varied contributions from Original Research to Review Articles, Frontiers Research Topics unify the most influential researchers, the latest key findings and historical advances in a hot research area! Find out more on how to host your own Frontiers Research Topic or contribute to one as an author by contacting the Frontiers Editorial Office: frontiersin.org/about/contact

CHEMISTRY, A SUSTAINABLE BRIDGE FROM WASTE TO MATERIALS FOR ENERGY AND ENVIRONMENT

Topic Editors:

Francesca Deganello, Consiglio Nazionale delle Ricerche Italiano (CNR), Italy
Enrico Traversa, University of Electronic Science and Technology of China, China
Ana C. Tavares, Research Centre for Energy Materials Telecommunications (INRS), Canada

Citation: Deganello, F., Traversa, E., Tavares, A. C., eds. (2021). Chemistry, a Sustainable Bridge from Waste to Materials for Energy and Environment. Lausanne: Frontiers Media SA. doi: 10.3389/978-2-88966-571-6

Table of Contents

- 04 Editorial: Chemistry, a Sustainable Bridge From Waste to Materials for Energy and Environment**
Francesca Deganello, Ana C. Tavares and Enrico Traversa
- 06 Influence of Dimethylsulfoxide and Dioxygen in the Fructose Conversion to 5-Hydroxymethylfurfural Mediated by Glycerol's Acidic Carbon**
Tatiane C. Tudino, Renan S. Nunes, Dalmo Mandelli and Wagner A. Carvalho
- 17 Synthesis of Porous Biochar Containing Graphitic Carbon Derived From Lignin Content of Forestry Biomass and Its Application for the Removal of Diclofenac Sodium From Aqueous Solution**
Nguyen Thi Minh Tam, Yun-guo Liu, Hassan Bashir, Peng Zhang, Shao-bo Liu, Xiaofei Tan, Ming-yang Dai and Mei-fang Li
- 34 Bio-based Substances From Compost as Reactant and Active Phase for Selective Capture of Cationic Pollutants From Waste Water**
Giuliana Magnacca, Flavio Neves Dos Santos and Razieh Sadraei
- 45 Activated Carbons From Winemaking Biowastes for Electrochemical Double-Layer Capacitors**
Lorena Alcaraz, Alberto Adán-Más, Pablo Arévalo-Cid, Maria de Fatima Montemor and Félix A. López
- 55 Advancements and Complexities in the Conversion of Lignocellulose Into Chemicals and Materials**
Giulia Fiorani, Claudia Crestini, Maurizio Selva and Alvis Perosa
- 61 A Way to Close the Loop: Physicochemical and Adsorbing Properties of Soybean Hulls Recovered After Soybean Peroxidase Extraction**
Maria Laura Tummino, Valentina Tolardo, Mery Malandrino, Razieh Sadraei, Giuliana Magnacca and Enzo Laurenti
- 73 Waste-Derived Nanoparticles: Synthesis Approaches, Environmental Applications, and Sustainability Considerations**
Sabah M. Abdelbasir, Kelli M. McCourt, Cindy M. Lee and Diana C. Vanegas
- 91 Adsorption of Orange II Onto Zn₂Al-Layered Double Hydroxide Prepared From Zinc Ash**
Andra Tămaș, Ioana Cozma, Laura Coheci, Lavinia Lupa and Gerlinde Rusu



Editorial: Chemistry, a Sustainable Bridge From Waste to Materials for Energy and Environment

Francesca Deganello^{1*}, Ana C. Tavares² and Enrico Traversa³

¹Istituto per lo Studio dei Materiali Nanostrutturati, Consiglio Nazionale delle Ricerche Italiano (CNR), Rome, Italy, ²Centre Énergie Matériaux Télécommunications, Institut National de la Recherche Scientifique, Varennes, QC, Canada, ³School of Materials and Energy, University of Electronic Science and Technology of China, Chengdu, China

Keywords: waste—a misplaced resource, materials from waste, environment and energy application, chemistry, sustainable synthesis

Editorial on the Research Topic

Chemistry, a Sustainable Bridge From Waste to Materials for Energy and Environment

The recent acceleration of climate changes and associated catastrophic phenomena worldwide is calling for unprecedented efforts for protecting our environment. The United Nations Sustainable Development Goals (SDGs) are now playing a major role in the policies of many governments. One of the main tools for reaching sustainability is adopting the concept of circular economy. We cannot afford anymore the unlimited growth of waste as in the linear economy model, but we should go toward reusing and recycling of commodities at their end of life cycle. In this framework, the transition to sustainability needs new sustainable approaches in chemical synthesis, since chemistry has a predominant role in the production of new materials.

The present research topic focuses on the possibility to use waste-derived precursors for preparing new materials (**Figure 1**) for environmental remediation or for sustainable energy applications. The general idea is based on the sustainability concepts, which consider both the limitation of a damage and the creation of a benefit. Thus, the use of waste, which needs to be eliminated, often at some cost, could be seen as a damage limitation. The production of materials from waste-precursors is considered benefic for the society and economy. If the material is used for environmental and energy applications, benefit is further increased, and damage is further limited.

The majority of the research work in this field still concerns organic waste, which can be transformed into carbon-based materials to be used in the formulation of heterogeneous catalysts and electrochemical double-layer capacitors or as pollutant absorbents. For example, the lignin fraction of the pitch pine sawdust was extracted and transformed into a porous biochar containing graphitic carbon through a two-step activation process. The waste derived carbon was used as adsorbent for the removal of wastewater pharmaceutical pollutants, through an absorption mechanism that changes with pH (Tam et al.). Bagasse and cluster stalks from winemaking waste were transformed into microporous-mesoporous carbon structures through a hydrothermal process followed by alkaline activation. These materials display high electrochemical double-layer capacitance and stability and can be considered for application as negative electrodes in electrochemical energy storage devices (Alcaraz et al.). A detailed knowledge on the physical-chemical and catalytic properties of activated carbons derived from commercial glycerol and of their interaction with reaction reagents and solvents gives an important contribute to the use of biomass derived carbons to produce platform molecules (Tudino et al.).

New materials can be obtained from specific waste-derived precursors, taking advantage of the specific waste features, usually related to the chemical composition of the waste precursor or to its microstructure/morphology. For example, Magnacca et al. evidenced some peculiar properties of

OPEN ACCESS

Edited and reviewed by:

Valeria Conte,
University of Rome Tor Vergata, Italy

*Correspondence:

Francesca Deganello
francesca.deganello@cnr.it

Specialty section:

This article was submitted to
Green and Sustainable Chemistry,
a section of the journal
Frontiers in Chemistry

Received: 13 December 2020

Accepted: 23 December 2020

Published: 27 January 2021

Citation:

Deganello F, Tavares AC and
Traversa E (2021) Editorial: Chemistry,
a Sustainable Bridge From Waste to
Materials for Energy and Environment.
Front. Chem. 8:641129.
doi: 10.3389/fchem.2020.641129

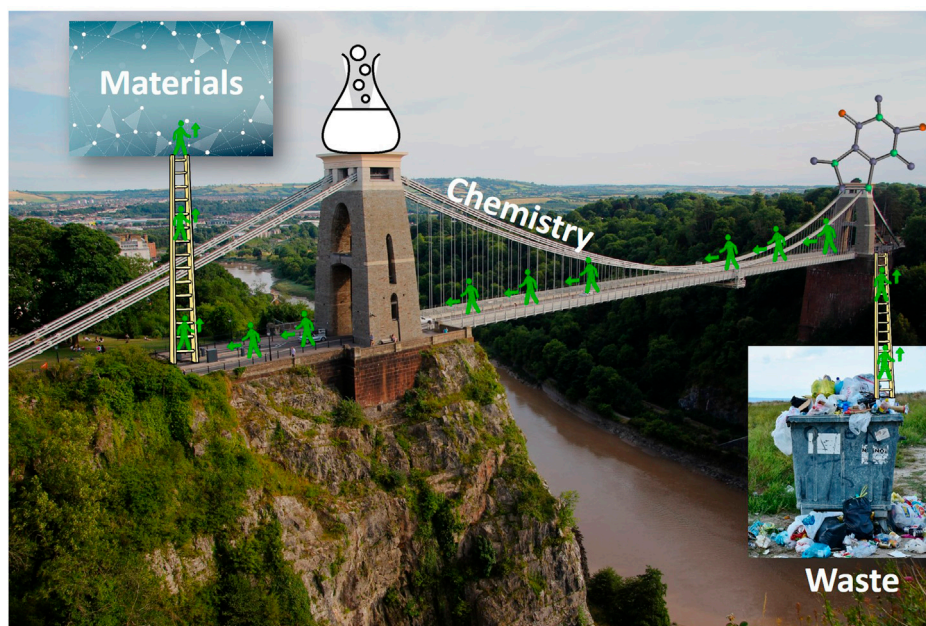


FIGURE 1 | In this Research Topic, Chemistry is presented as a bridge connecting waste to materials, that can be further used for a greener and sustainable world.

porous alumina membranes prepared from bio-based substances from compost, resulting in a selective adsorption of cationic species. In their perspective article, Fiorani et al. describe the chemical complexity of plant-based biomasses, pointing out to the urgency of reliable and convergent chemical strategies for their transformation into platform molecules. As reported by Tummino et al., soybean hulls from agro-industrial scraps can be still used after peroxidase extraction as adsorbents for inorganic and organic pollutants present in wastewater. The authors also evidenced that the adsorption efficiency is strongly dependent on the extraction conditions.

There are plenty opportunities for research work on the chemical synthesis of materials derived from inorganic waste. Therefore, we encourage the scientific community to intensify the research in this specific field, being convinced that any advancement of knowledge in this direction may also have a considerable impact on society. It is enough to consider for example the electric/electronic waste, the waste tires, wastewater, sludges and other types of inorganic industrial waste that are at the moment seldom recycled. Abdelbasir et al. report here a strategy to transform inorganic waste into inorganic nanoparticles for use in environmental applications. However, toxicological and life-cycle aspects should be taken into consideration for upscaling the synthesis process (Abdelbasir et al.). Another strategy is the extraction of metal cations from industrial inorganic waste and their use as inorganic precursors for the synthesis of materials, as described by Tamas et al. for Zn ash used as a Zn precursor. A further step will be to use the inorganic waste directly in the synthesis without any acid/base extraction.

Finally, we would like to thank all authors and reviewers who contributed to this Research Topic. The papers collection under this Research Topic gave a substantial contribution to the knowledge on the use of waste-derived precursors in the synthesis of materials for energy and environmental applications. In the next future, new synthesis procedures need to be explored and greater flexibility will be required to maximize the economic and technological advantages of waste-derived materials production. In this sense, the role of Chemistry as “a sustainable bridge from waste to materials for energy and environment” needs to be further consolidated, in order to facilitate the transition from ideas to real industrial-social opportunities.

AUTHOR CONTRIBUTIONS

FD wrote the first draft, ET and AT corrected and integrated it.

Conflict of Interest: The authors declare that the research was conducted in the absence of any commercial or financial relationships that could be construed as a potential conflict of interest.

Copyright © 2021 Deganello, Tavares and Traversa. This is an open-access article distributed under the terms of the Creative Commons Attribution License (CC BY). The use, distribution or reproduction in other forums is permitted, provided the original author(s) and the copyright owner(s) are credited and that the original publication in this journal is cited, in accordance with accepted academic practice. No use, distribution or reproduction is permitted which does not comply with these terms.



Influence of Dimethylsulfoxide and Dioxygen in the Fructose Conversion to 5-Hydroxymethylfurfural Mediated by Glycerol's Acidic Carbon

Tatiane C. Tudino, Renan S. Nunes, Dalmo Mandelli and Wagner A. Carvalho*

Center for Natural Sciences and Humanities, Federal University of ABC (UFABC), Santo André, Brazil

OPEN ACCESS

Edited by:

Francesca Deganello,
Italian National Research Council, Italy

Reviewed by:

Maria Luisa Testa,
Italian National Research Council, Italy
Miguel Angel Centeno,
Instituto de Ciencia de Materiales de
Sevilla (ICMS), Spain

*Correspondence:

Wagner A. Carvalho
wagner.carvalho@ufabc.edu.br

Specialty section:

This article was submitted to
Green and Sustainable Chemistry,
a section of the journal
Frontiers in Chemistry

Received: 27 January 2020

Accepted: 18 March 2020

Published: 08 April 2020

Citation:

Tudino TC, Nunes RS, Mandelli D and
Carvalho WA (2020) Influence of
Dimethylsulfoxide and Dioxygen in the
Fructose Conversion to
5-Hydroxymethylfurfural Mediated by
Glycerol's Acidic Carbon.
Front. Chem. 8:263.
doi: 10.3389/fchem.2020.00263

Both the catalytic production of 5-hydroxymethylfurfural (5-HMF) from carbohydrates and the use of a catalyst obtained from residues stand out for adding value to by-products and wastes. These processes contribute to the circular economy. In this work it was evaluated optimized conditions for 5-HMF production from fructose with high yield and selectivity. The reaction was catalyzed by an acidic carbon obtained from glycerol, a byproduct of the biodiesel industry. Special attention has been given to the use of dimethyl sulfoxide (DMSO) as a solvent and its influence on system activity, both in the presence and absence of O₂. Glycerol's carbon with acidic properties can be effectively used as catalyst in fructose dehydration, allowed achieving conversions close to 100% with 5-HMF selectivities higher than 90%. The catalyst can be reused in consecutive batch runs. The influence of DMSO in the presence of O₂ should be considered in the catalytic activity, as the stabilization of a reaction intermediate by the [O₂:DMSO] complex is favored and, both fructose conversion and 5-HMF yield increase.

Keywords: acid-assisted hydrothermal carbonization, sulfonated carbons, glycerol, fructose dehydration, DMSO, 5-HMF

INTRODUCTION

5-Hydroxymethylfurfural (5-HMF) is considered as a platform molecule composed by a furan ring and aldehyde and alcohol functional groups. This structure favors its conversion into several chemical compounds with wide industrial applicability, from fine chemistry to biofuels (Putten et al., 2013). It can be obtained by dehydration of all types of C6 carbohydrates (**Figure 1**), including monomers and polymeric carbohydrates such as fructose, glucose, sucrose, starch, inulin and cellulose, as well as other biomass raw materials (Teong et al., 2014; Nunes et al., 2020). The use of glucose-based polysaccharides or glucose monomers as starting materials in the reaction is economically preferred if we consider that these substrates are more abundant than fructose. However, converting these types of substrates generally requires severe reaction conditions and consequently less selectivity for 5-HMF due to the decomposition and polymerization reactions of this product (Fang et al., 2014; Yi et al., 2015; Shahangi et al., 2017).

The use of heterogeneous catalysts has been studied for the production of 5-HMF due to several advantages compared to typically used homogeneous catalysts, such as the reduced reactor corrosion and reduced residue formation (Yi et al., 2015). However, solids commonly used as support for the reaction-active acidic functional groups [silicas (Wang et al., 2019), aluminas

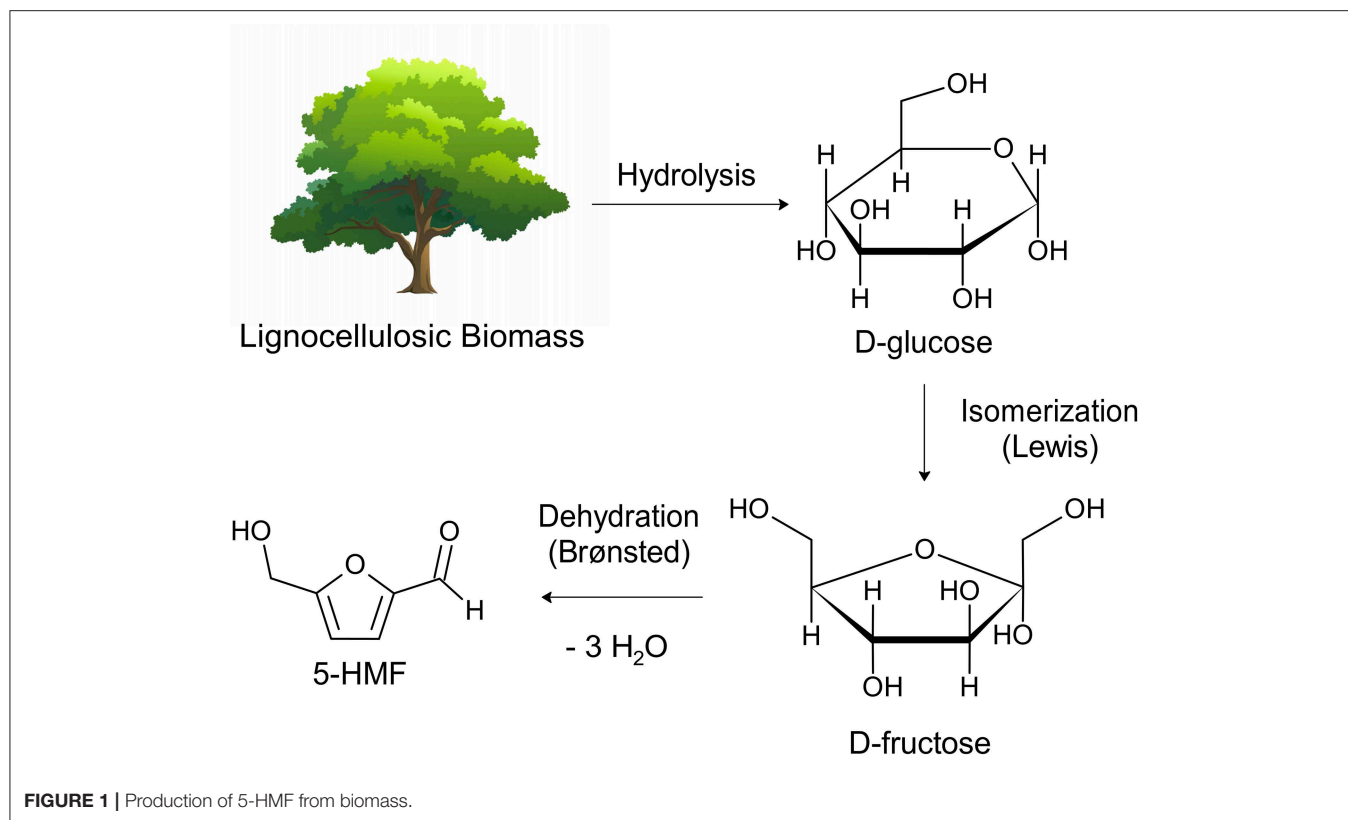


FIGURE 1 | Production of 5-HMF from biomass.

(Tong et al., 2010; Solis Maldonado et al., 2017), zeolites (Wang et al., 2018), zirconias (Ni et al., 2019), etc] typically require extensive synthesis processes. Generally acidic groups are inserted by post-synthesis processes by adding numerous preparation steps. In addition, in many cases high concentrations of functionalizing agents, such as organic and mineral acids, or high temperatures are used (Fang et al., 2014). Among the types of heterogeneous catalysts most used in carbohydrate dehydration are carbons, which can be produced from carbon-based agro-industrial residues. These processes have been highlighted by adding value to waste, contributing to the Circular Economy in the industry (Adib et al., 2015). A wide variety of wastes, including coffee grounds (Gonçalves et al., 2016b), rice husks (Boonpoke et al., 2013), palm tree (Adinata et al., 2007), coconut (Daud and Ali, 2004), almond (González et al., 2009), glycerin and glycerol (Monteiro et al., 2018), has already been used for this process and the carbons obtained have a wide applicability, being used as catalysts in many hydrogenation reactions (Madduluri et al., 2020), environmental catalysis (Restivo et al., 2017), and photocatalysis (Velasco et al., 2013). The high temperatures used in the carbonization of these residues result in catalysts with poorly developed porosity and surface area, and some carbons undergo a later stage of chemical activation to increase both their porosity and surface area (Lin et al., 2019). Although several reaction types show a significant improvement in results, it is experimentally observed in carbohydrate dehydration that a higher selectivity to 5-HMF is not dependent on a higher surface area, but rather on a

higher concentration of total acidic sites on the carbons surface (Wang et al., 2018). High selectivity to 5-HMF was obtained in a previous study using glycerin and glycerol-based catalysts with a low surface area. The catalysts were obtained after only 15 min of carbonization and *in situ* functionalization (Mantovani et al., 2018). A high density of total acidic groups of 4.1 mmol/g was obtained in the catalyst. Sulfonated and oxygenated groups, such as carboxylic acids and lactones, were found on their surface (Mantovani et al., 2018). Their presence has been shown to be crucial for dehydration of fructose. Zhao et al. (2016) produced glycerol carbons with only oxygenated groups on their surface and by testing their catalytic activity in fructose dehydration, a 64.3% conversion of fructose was obtained with a 5-HMF selectivity of 57%. The introduction of sulfonic groups led to fructose conversion reaching 97% and 5-HMF selectivity of 77%. However, a loss in 5-HMF selectivity was also observed when using carbon with high number of sulfonic groups.

Although the interaction between fructose and sulfonic groups is predominant, higher densities of total acid groups have shown a greater influence on 5-HMF yield and selectivity compared to higher densities of strong acidic groups. The synergistic action of sulfonic and oxygenated groups allows a better catalytic performance for the production of 5-HMF (Thapa et al., 2017). Recently, Yu et al. (2020) also demonstrated that Brønsted acid sites with adjacent carboxyl present higher catalytic ability than isolated ones.

The search for green solvents has been carried out by several researchers, but without success so far. Ideally, water

should be used as a solvent. However, in the presence of acidic species 5-HMF tends to easily decompose upon rehydration, forming levulinic and formic acids as byproducts (Wang et al., 2019). Therefore the production of 5-HMF in aqueous systems occurs parallel to a high yield of levulinic and formic acids (Yi et al., 2015).

The yields obtained in aqueous media are much lower, essentially when compared to those obtained using DMSO, a solvent widely used in the production of 5-HMF (Wang et al., 2011, 2019). DMSO-based solvent systems are one of the most attractive due to DMSO abundance, low cost, manufacturing by an environmentally friendly process, low toxicity, and the outstanding properties when compared to competing solvents and potential applications. Currently some studies have been performed in order to analyze the influence of DMSO on 5-HMF production and an apparent catalytic activity has been proposed by decomposition in H_2SO_4 (Tong and Li, 2010; Zhang et al., 2016), or by solvation (Kimura et al., 2013; Whitaker et al., 2019). Amarasekara et al. (2008) found a change in the anomeric composition of D-fructose in DMSO when the solution is heated to 150°C, with subsequent formation of 5-HMF after 15 min reaction time. Some examples of DMSO activity in fructose dehydration are found in the literature (Musau and Munavu, 1987; Amarasekara et al., 2008; Shimizu et al., 2009; Binder et al., 2010; Liu et al., 2014; Hu et al., 2015). In these works, 5-HMF yields range from 1.8 to 72% at temperatures in the range of 100° to 160°C. Typically, the highest yields were obtained at higher temperatures and in the presence of O_2 . However, there is no assessment of the influence of O_2 on reaction systems. Thus, the objective of this work is to evaluate the best conditions to obtain higher selectivities to 5-HMF using carbon as a catalyst as well as to analyze the influence of DMSO as solvent in this process.

MATERIALS AND METHODS

Chemicals

Carbon was produced utilizing glycerol 99% from Vetec (São Paulo, São Paulo), sulfuric acid >98% from LabSynth (Diadema, São Paulo) and acetone from Cosmoquímica Indústria e Comércio (Barueri, São Paulo). Characterization techniques used KBr 99.5% from Sigma-Aldrich (São Paulo, São Paulo), NaOH 99% from Vetec (São Paulo, São Paulo), NaHCO_3 99.5% from Sigma-Aldrich (São Paulo, São Paulo), HCl 36.5–38.0% from Vetec (São Paulo, São Paulo). Catalytic tests were performed with D(-)-fructose >99.9% from Sigma Aldrich (São Paulo, São Paulo) and Dimethylsulfoxide >99.9% from Synth (Diadema, São Paulo). All chemicals were used as received and without any treatment.

Catalyst Preparation

Carbon was prepared as reported in a previous study (Mantovani et al., 2018). In a typical process, glycerol (10 g) was mixed with concentrated sulfuric acid (30 g) in a Teflon-coated stainless-steel autoclave reactor. Then the system was heated to 180°C in an oven and kept to that temperature for 15 min. At the end of the process the solid obtained was washed repeatedly with distilled water until a pH value above 4 and then with acetone to remove

non-carbonized organic matter. Precipitation tests with BaCl_2 were also performed to confirm the absence of sulfate ions in the washing solution. The obtained materials were oven dried at 60°C for 6 h. The washing process was repeated twice under the same conditions.

Catalyst Characterization

Surface functional groups were analyzed by Fourier Transform Infrared spectroscopy (FTIR) analysis using a Varian-Agilent 640-IR FT-IR Spectrometer. The analyses were performed mixing dried carbons with KBr in a 3:100 weight ratio and ground into fine powder. These mixtures were dried at 60°C for 12 h and thin pellets were made in a manual press. The spectra were acquired by accumulating 32 scans at 4 cm^{-1} resolution in the 4,000–400 cm^{-1} range.

X-ray photoelectron spectroscopy (XPS) data were obtained on a K-alpha + ThermoFisher Scientific or a VG-Microtech Multilab 3000 spectrometer, equipped with a hemispherical electron analyzer with X-ray source Mg $K\alpha$ ($h = 1253.6 \text{ eV}$) 300 W X-ray source.

Boehm's method (Boehm, 1994) was used to estimate the acid-base properties of samples. For the test, 300 mg of the carbon was added in 25 mL of NaOH 0.1 mol/L to quantify all Brønsted acids groups in the carbon surface or NaHCO_3 0.1 mol/L to quantify sulfonic and carboxylic acid groups. A blank was prepared for each experimental condition. The suspensions were degassed with N_2 , and the bottles were closed and shaken for 24 h at room temperature. Aliquots of filtered solutions were titrated with HCl 0.1 mol/L in an automatic titrator Metrohm 905 Titrand.

Carbon, oxygen, and sulfur content were obtained in an elemental analyzer (EA1112 Thermo Scientific FLASH) using 3 mg of samples previously dried at 60°C for 12 h.

Catalytic Tests

Reactions were performed in a Teflon-lined stainless-steel reactor (Parr 4848). In a typical run, a 2.5 or 5 wt.% fructose solution in DMSO was added in the reactor with 2.5–10 wt.% of catalyst and kept under mechanical stirring for 2 h under synthetic air or N_2 . The temperature was kept at the desired value, ranging from 80 to 130°C. Blank reactions (in absence of catalyst) were also performed.

The reaction products were analyzed by high performance liquid chromatography (HPLC Agilent 1200 series, equipped with a refractive index detector and ROA Organic Acid column, 300 × 7.8 mm). The mobile phase used was a 4 mmol/L aqueous solution of H_2SO_4 previously filtered through 0.45 μm membrane and degassed by ultrasound. The column was maintained at 60°C with 0.6 mL/min mobile phase (isocratic) flow. Reaction products were identified and quantified by pure standards and previously constructed analytical curves of fructose, 5-HMF, levulinic acid and formic acid. Fructose was detected by Refractive Index Detector (RID) at 40°C while 5-HMF, formic acid and levulinic acid were detected by Diode Array Detector (DAD) at 254, 210, and 210 nm, respectively.

The stability of the prepared materials was evaluated by performing consecutive batch runs under the same reaction conditions, in order to investigate the reusability of the catalyst.

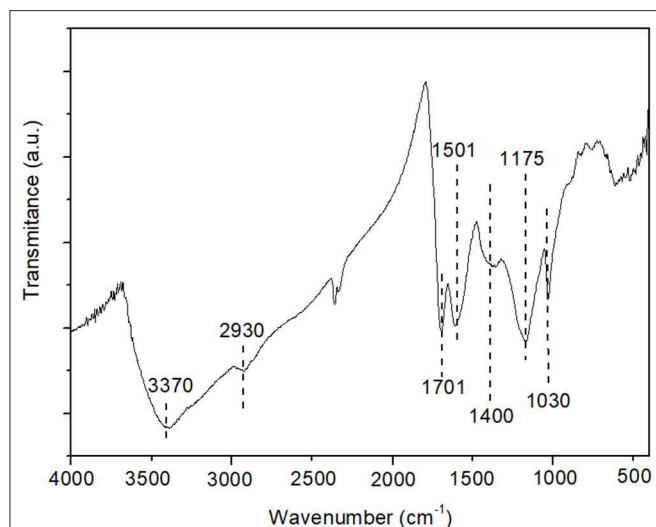


FIGURE 2 | FTIR spectrum for the prepared carbon.

After each reaction run, the solid was removed from the reaction solution, washed with acetone to remove the reactants adsorbed on the surface and dried at 333 K for 12 h and then used for the next run without any reactivation or purification.

Fructose conversion into products and yield and selectivity for the identified products (5-HMF, levulinic acid and formic acid) were calculated as follows.

$$\text{Conversion (\%)} = \left(\frac{\text{moles of fructose reacted}}{\text{initial moles of fructose}} \right) \times 100 \quad (1)$$

$$\text{Yield}_{\text{prod}} (\%) = \left(\frac{\text{moles of product}}{\text{initial moles of fructose}} \right) \times 100 \quad (2)$$

$$\text{Selectivity}_{\text{prod}} (\%) = \frac{\text{Yield}_{\text{prod}}}{\text{Conversion}} \quad (3)$$

RESULTS AND DISCUSSION

Catalyst Characterization

The methodology used in this work allowed the formation of sulfonic and carboxylic acidic groups in the carbon as can be seen by FTIR analysis (Figure 2). The presence of sulfonic acidic groups is confirmed by characteristic bands observed in the spectrum at 1,030 and 1,175 cm^{-1} . These bands correspond to the asymmetric and symmetrical vibrational stretching of SO_2 , respectively (Zhao et al., 2016; Mantovani et al., 2018). The 3,370 cm^{-1} centered broadband is attributed to O-H stretching of -COOH groups while the band around 1,590 cm^{-1} can be attributed to the C=C double bond stretch characteristic of carbons (Thapa et al., 2017; Yu et al., 2020). One band at 1,701 cm^{-1} is characteristic of carbonyls from -COOH group and another at 2,930 cm^{-1} is attributed to the elongation vibrations of methylene groups (Zhao et al., 2017).

A high density of total acidic groups was obtained by Boehm Titration. The amount of total acidic groups was 4.2 mmol/g, of which 1.7 mmol/g correspond to carboxylic and sulfonic

acid groups. In addition to the strong acid groups, groups with weak, and moderate acidity are also produced, including lactones, phenols and carbonyls, as previously reported (Gonçalves et al., 2016a). As expected, the non-activation of carbon and the *in situ* functionalization method used resulted in a high concentration of total acidic groups even with the use of a lower precursor: acid ratio (Table 1).

Unlike what was done in this work, the methodology of preparation of non-activated carbons developed by Gonçalves et al. (2016a) and by Wataniyakul et al. (2018) considered the sulfuric acid functionalization step after hydrothermal carbonization. Although these authors used a longer functionalization time, a higher temperature and a higher precursor: acid mass ratio, a lower density of total acidic groups was obtained compared to the results obtained in this work. *In situ* sulfonation favors the formation of a greater number of functional groups throughout the carbonaceous structure that is being produced. As the structure is less organized, it is easier to insert acidic groups. Thus, keeping the functionalizing agent present while the precursor is carbonized, it is possible to increase the amount of functional groups formed throughout the structure, whether on the surface or not. Thus, the *in situ* functionalization method allowed reaching a higher density of acidic groups on the carbon surface.

The pyrolysis carbonization method is another factor that hinders the functionalization process of the carbons. Mo et al. (2008) promoted pyrolysis of D-glucose under N_2 for 15 h at 400°C. Then, the carbon obtained was sulfonated using precursor: acid mass ratio of 1:36.8 at 160°C for 13 h. A lower density of total acidic groups was obtained compared to the values obtained in this work. It has been suggested that carbon produced from pyrolysis processes has a higher degree of crosslinking as treatment is done at higher temperatures (Xiong et al., 2018). This is the reason why activated carbons cannot be easily functionalized (the more graphitized the structure, the more difficult it is to functionalize). The increase in temperature associated or not with a longer carbonization time, increases the fixed carbon content, while the ratios of O/C and H/C decreased. The number of acidic functional groups also decreased as a function of pyrolysis temperature, especially carboxylic groups (Marsh and Rodríguez-Reinoso, 2006; Saleh, 2011). Thus, the carbon structure becomes more hydrophobic and less flexible, making it difficult to insert acidic groups in a later stage of functionalization (Zhong and Sels, 2018). In this case, it is common to use high concentrations of acids at elevated temperatures for more efficient functionalization (Ormsby et al., 2012; Villanueva and Marzioletti, 2018; Lin et al., 2019). On the other hand, the presence of carboxyl and hydroxyl groups in sulfonated carbon can make the surface more polar for substrate adsorption such as fructose and lead to hydrogen bond formation (Dong et al., 2015). Sulfonated carbons are promising materials and can be used as acidic catalysts due to its high density of surface acidic groups, especially carboxylic and sulfonic, acting as Brønsted acid sites. However, other functional groups with acidic characteristics present on the surface (such as phenolic and lactonic) influence the catalytic activity. Xiong et al. (2018) proposed that these groups can act by establishing hydrogen

TABLE 1 | Values of total acid groups in non-activated and activated carbons.

Reference	Carbon	Precursor:acid mass ratio	Functionalization	Total acidic groups (mmol/g)
This work	Non-activated	Glycerol: sulfuric acid (1:3)	15 min at 180°C	4.20
Gonçalves et al. (2016b)	Non-activated	Coffee grounds: sulfuric acid (5:92)	2 h at 180°C	3.00
Gonçalves et al. (2016b)	Non-activated	Coffee grounds: sulfuric acid (5:92)	5 h at 180°C	3.40
Wataniyakul et al. (2018)	Non-activated	Glycerol: sulfuric acid (5:92)	15 h at 150°C under N ₂	1.08
Mo et al. (2008)	Non-activated	D-glucose: sulfuric acid (1:36,8)	13 h at 160°C	0.60
Maneechakr and Karnjanakom (2017)	Non-activated	β -cyclodextrin: hydroxyethyl sulfonic acid (1:4)	4 h at 180°C	1.82
Lin et al. (2019)	Activated	Furfural residue: sulfuric acid (1:36,8)	5 h at 150°C	2.72
Ormsby et al. (2012)	Activated	Biochar: sulfuric acid (12,5:36,8)	12–18 h at 100°C	2.59
Villanueva and Marzalletti (2018)	Activated	Activated carbon: sulfuric acid (5:184)	16 h at 150°C	5.30

bonds with the carbohydrates tested as substrate and increasing the polarity of the carbon surface, improving its contact with the sulfonic and carboxylic groups. Recently, Yu et al. (2020) showed that adjacent acid sites on carbon surface cooperatively catalyze the fructose dehydration. The adjacent Brønsted sites lead to co-interaction with the fructose, then accelerating the dehydration. The co-interaction also results in more stable dehydration intermediates, enhancing the selectivity.

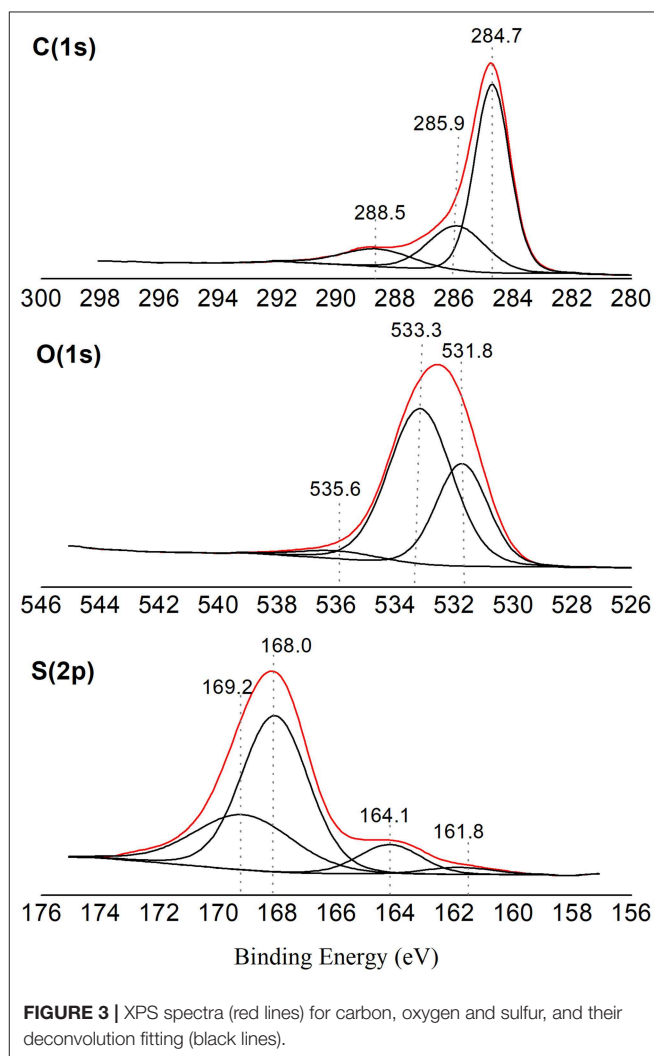
From the elemental analysis of the carbon the composition 65.9% C, 3.8% H, 3.4% S, and 26.9% O was obtained. Considering the glycerol mass composition (39.1% carbon, 8.8% hydrogen, and 52.1% oxygen) there is, as expected, an increase in the carbon content and a decrease in the amount of oxygen and hydrogen due to the carbonization process. X-ray photoelectron spectroscopic analysis indicated the composition 78.2% C, 19.5% O, and 2.3% S. When comparing these values with those obtained by elemental analysis, it is noted that the O and S contents are lower than those previously obtained. This is because the XPS analysis considers only the elements present on the carbon surface and therefore available to act as active sites.

From the XPS analysis, it was also possible to identify the oxidation state of each element on the carbon surface, as can be observed in the spectra shown in **Figure 3**. The carbon spectrum (C1s) shows the presence of C–C bonds with centralized bonding energy at 284.7 eV. The presence of oxygen groups has also been confirmed by the peaks at 285.9 and 288.5 eV, which are attributed to C–C and COOH carbon bond belonging to carboxylic groups, respectively (Shimizu et al., 2009; Binder et al., 2010). In addition, peaks at 531.8 and 533.3 eV in the oxygen spectrum can also be attributed to the C–OH and C=O bonds, respectively, confirming the presence of these groups.

The sulfur spectrum (S2p) peaked at 168.0 eV is assigned to a higher oxidation state of sulfur, –SO₃H (Aldana-Pérez et al., 2012). Peaks at 161.8 and 164.1 eV observed in the S2p spectrum belong to photoelectrons of groups with reduced sulfur forms (Fraga et al., 2016).

Catalytic Tests

Preliminary tests allowed to evaluate the behavior of the catalytic system in relation to the temperature and the carbon: substrate mass ratio. The results showed that the increase in temperature favorably influenced the process, leading to an



increase in both fructose conversion and 5-HMF yield, without losses in its selectivity. By increasing the temperature from 80 to 130°C, the yield of 5-HMF increased from 12.6 to 55.6% (**Figure 4**).

In the literature this behavior was also observed by Zhao et al. (2016), who obtained a conversion of 12.8% and a selectivity of

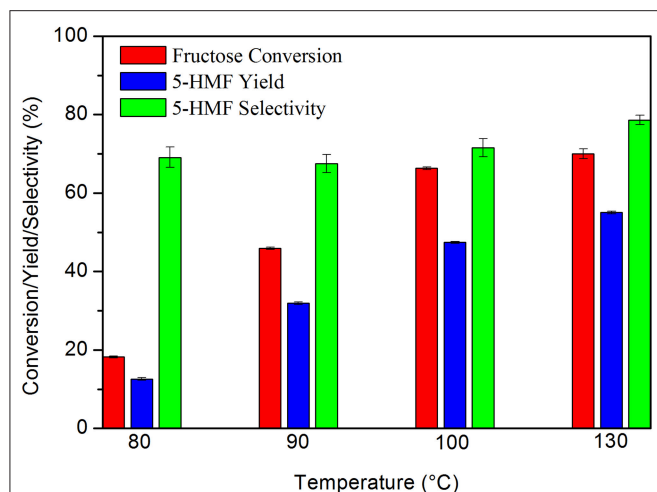


FIGURE 4 | Fructose dehydration reaction at different temperatures.

Conditions: 5% fructose in DMSO, 5 wt.% catalyst, 2 h reaction time under synthetic air.

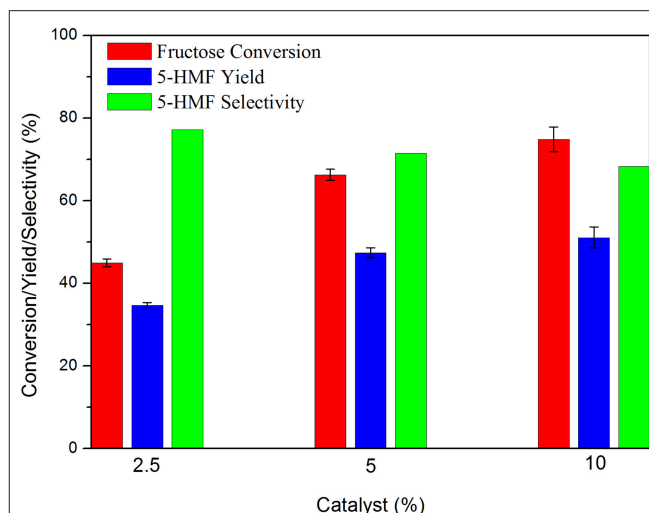


FIGURE 5 | Fructose dehydration reaction in the presence of different catalyst:substrate mass ratios.

Conditions: 5% fructose in DMSO, 100°C, 2 h reaction time under synthetic air.

40.5% at 100°C. By increasing the temperature to 160°C these values increased to 100 and 76.3%, respectively. Wang et al. (2011) also obtained an increase in 5-HMF yield by increasing the temperature from 70 to 130°C, reaching a yield of 91.2% at 130°C. However, these authors used catalyst: substrate mass ratios as high as 0.8:1 and 5-HMF selectivity decreased quickly at temperatures above or below 130°C. The authors justified this behavior due to the existence of partial dehydrated intermediates and the formation of humins, respectively.

Often, the literature brings results promoted by the use of high amounts of catalyst. In this work the best amount of carbon for the reactions was 5 wt.% relative to the substrate, which resulted in the highest yield and selectivity values for 5-HMF. The use of 10 wt.% increased fructose conversion but decreased 5-HMF selectivity resulting in minimal difference in yield (Figure 5).

The decrease in 5-HMF selectivity can be attributed to the increased number of available acidic sites due to the increased amount of carbon used. This condition favored rehydration and polymerization reactions of 5-HMF, as previously discussed. Zhao et al. (2016) were able to increase 5-HMF yield from 60.7 to 75.4% by increasing the catalyst: substrate mass ratio from 5 to 20%. However, by increasing the mass ratio to 40% 5-HMF yield decreased to 70.8%.

Thus, different catalytic tests were performed with solutions containing 5% fructose and 5 wt.% catalyst, varying the temperature (100 or 130°C), the reaction atmosphere (synthetic air or N₂) and the reaction time. Catalytic tests were also performed in the absence of catalyst, whose fructose conversion values can be seen in Figure 6. Fructose conversion and 5-HMF selectivity values obtained in the carbon catalyzed reactions are shown in Figure 7.

In blank reactions, it is evident that the solvent is catalytically active for fructose dehydration in the presence of O₂. Even under inert atmosphere, a reduced activity was observed. In all cases fructose conversion started only after 30 min of reaction.

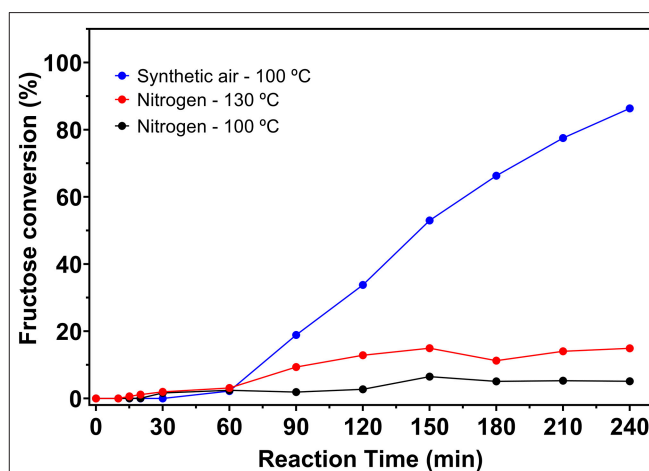


FIGURE 6 | Fructose conversion values for blank reactions under nitrogen at 100 and 130°C and under synthetic air at 100°C, from 5% fructose solutions in DMSO.

Zhang et al. (2016) demonstrated that, under inert atmosphere, DMSO stabilizes the intermediate carbocation resulting from the removal of the first water molecule from fructose, with the formation of a [carbocation-DMSO] complex. This complex is immediately converted to other intermediates as the second and third water molecules are removed from fructose, when 5-HMF is then produced. Therefore, it can be considered that the induction period observed in blank reaction is related to the time required to remove the first water molecule from fructose.

In the presence of O₂, the system is much more active. Some authors have proposed that the catalytic activity of DMSO is attributed to its decomposition into H₂SO₄, which in turn is catalytically active in the reaction (Tong and Li, 2010; Zhang et al., 2016). However, recently a detailed study by Whitaker

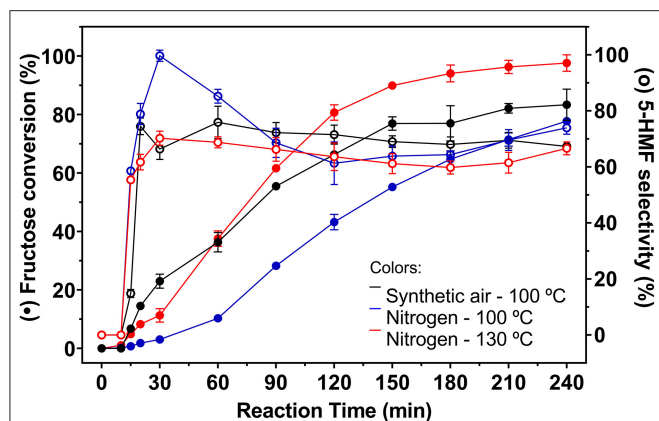


FIGURE 7 | Fructose conversion and 5-HMF selectivity values (full and empty symbols, respectively) for carbon catalyzed reactions under inert atmosphere at 100 and 130°C and under synthetic air at 100°C. Conditions: 5% fructose in DMSO, 5 wt.% catalyst.

et al. (2019) concluded that DMSO does not decompose at temperatures below 190°C and the catalytic activity of the solvent would be attributed to “solvation effects.” Ren et al. (2017) when performing theoretical studies concluded that the homogeneous species $[\text{DMSOH}^+]$, catalytically active, can be formed during the reaction when acidic Brønsted species are present. In the absence of acidic species, DMSO stabilizes an intermediate of fructose dehydration, similar to that proposed by Zhang et al. (2016). This ability of the solvent to stabilize the reaction intermediate is responsible by the conversion, even limited, of fructose and 5-HMF production under inert atmosphere. In addition to this ability, the results of this work combined with literature data indicated the positive effect of the presence of O_2 on both fructose conversion and 5-HMF production. Lindberg et al. (2018) used density functional theory (DFT) calculations to predict the interaction energy between O_2 and different electrolytes, among them DMSO. The geometry of the most stable complex for the $[\text{O}_2:\text{DMSO}]$ combination corresponds to the interaction of oxygen atoms of O_2 with hydrogen atoms of methyl groups in DMSO. Belletti et al. (2019) demonstrated by DFT calculations that nine DMSO molecules are surrounding the O_2 molecule in the first coordination sphere. Thus, it can be assumed that in the presence of O_2 there is the formation of a $[\text{O}_2:\text{DMSO}]$ complex where solvent molecules stabilize a positive charge (from a fructose dehydration intermediate) more easily, favoring the mechanism of 5-HMF production. According to Kimura et al. (2013), this non-catalytic fructose conversion in DMSO allowed the production of 5-HMF after about 45 min of reaction at 90°C. Prior to this, fructose is converted into a primary precursor, which will undergo subsequent dehydration give 5-HMF.

With longer reaction times, similar fructose conversion values were obtained in the presence of O_2 , in the blank reaction and in the carbon catalyzed reaction (Figures 6, 7). However, reactions in the absence of heterogeneous catalyst showed lower selectivity to 5-HMF compared to values obtained in the carbon catalyzed reactions.

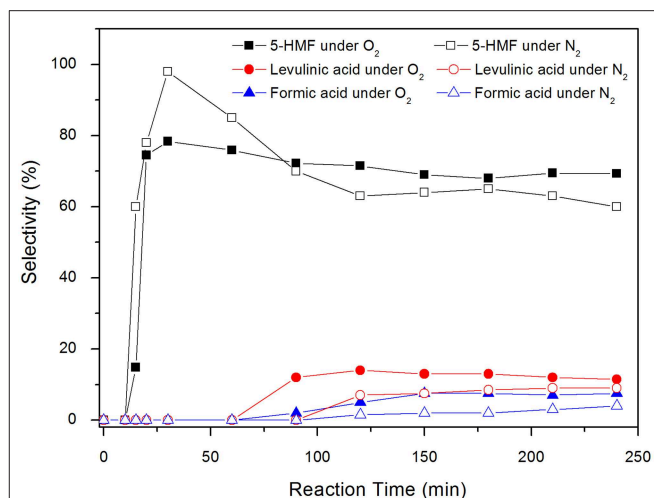


FIGURE 8 | Selectivities toward 5-HMF, formic acid and levulinic acid for carbon catalyzed reactions under inert atmosphere and under synthetic air at 100°C. Conditions: 5% fructose in DMSO, 5 wt.% catalyst.

At the same temperature, the catalyzed reactions under synthetic air allowed a higher conversion of fructose. After 1 h of reaction under N_2 the maximum conversion was 10.3% while in the presence of O_2 fructose conversion reached 36.3%. The system under N_2 remains less active at longer reaction times, but a smaller difference was observed. After 4 h reaction time a maximum fructose conversion of 77.8% was obtained under N_2 , while under synthetic air this value reached 83.3%. In contrast, the values obtained for the 5-HMF selectivity in reactions under N_2 was higher than those obtained under synthetic air until 1 h reaction time, reaching a selectivity of 99.7% after 0.5 h at 100°C. After the first hour of reaction, the drop in 5-HMF selectivity is more pronounced under N_2 , but no significant increase in levulinic and formic acids production was observed.

The selectivities toward 5-HMF, levulinic acid, and formic acid in the carbon catalyzed reactions are presented in Figure 8.

Levulinic acid is only observed after 90 min of reaction. It is worth noting that, in the presence of carbon, 5-HMF is produced from the beginning of the reaction (Figure 8), reaches a maximum after 30 min and then slightly decreases throughout the reaction. In the absence of carbon, the system takes about 30 min to produce 5-HMF and after 90 min of reaction the production of levulinic acid begins. Up to 30 min reaction time, the selectivity values of 5-HMF are increasing, reaching a maximum of 98%. In this initial stage of the reaction, part of the fructose must be in the form of intermediates that correspond to the dehydration steps necessary for the formation of 5-HMF. Although they were not quantified by HPLC, these intermediaries were already identified by different techniques (Zhang et al., 2016), where the authors found behavior similar to that shown in the Figure 7.

The selectivity values for the by-products levulinic and formic acids were higher in the blank reactions. 5-HMF was only identified after 1 h reaction time under N_2 , with a selectivity of 58%. This value remained practically unchanged throughout the

reaction, reaching 56.5% after 4 h. Levulinic acid was observed only after 90 min, reaching a maximum selectivity of 23% after 2 h reaction time. After that, selectivity suffered a continuous reduction of up to 12% in 4 h. The behavior of formic acid was similar, with a maximum selectivity of 15% in 2 h and 10% after 4 h.

The yield of levulinic acid in the reaction carried out under synthetic air reached 9.1%, while in the reaction under inert atmosphere, this value was 7.0%. Similarly, formic acid yield reached 6.2% under synthetic air and 3.1% under N₂. This result corroborates the assumption made by Whitaker et al. (2019), who suggested that the production of organic acids is enhanced in the presence of oxygen. The production of humins increases during the reaction, reaching a yield of 10.1% in the presence of O₂ and 21.0% under inert atmosphere. Over time, a strong brown color, indicative of a higher concentration of humins, was observed in reactions under N₂ in both temperatures, 130° and 100°C. The color intensity was higher than that observed in reactions made under synthetic air. The favoring of humins formation at higher temperatures is reported in the literature by Shahangi et al. (2017) who observed that as reactions were promoted at higher temperatures, there was a loss in selectivity of 5-HMF and the formation of an increasingly intense brown color, indicating the presence of humins.

Comparing the reactions under synthetic air or N₂ at the same temperature, the higher formation of humins in inert atmosphere is related to the high amount of 5-HMF present in the former reaction period. Yalpani (1985) and Petronijevic et al. (2013) demonstrated several reactions in which DMSO shows crosslinking agent behavior with polysaccharides, when in the presence of aldehydes and organic acids. The presence of high concentrations of 5-HMF and fructose in the reaction medium must have enhanced the ability of DMSO to promote crosslinking, favoring fructose polymerization and humin formation. It is noteworthy that Tsilomelekis et al. (2016) demonstrated that levulinic acid is not significantly incorporated into humins, but aldolic condensation between 5-HMF and the ketone group must occur. Therefore, inhibition of DMSO catalytic activity under inert atmosphere reduced the formation of levulinic and formic acids, but there is still the formation of humins as a byproduct.

Since fructose and 5-HMF can polymerize, the fructose concentration in the system may be an important factor to consider in order to avoid the formation of humins. The influence of fructose concentration and catalyst amount is reported by Thapa et al. (2017). When the authors trying to produce levulinic acid from fructose, they noticed that the use of a higher fructose concentration and a lower catalyst amount caused a lower selectivity to levulinic acid and the consequent accumulation of fructose and 5-HMF led to a higher concentration of humins. Thus, solutions containing 2.5% fructose in DMSO were used to evaluate reaction behavior in the presence of lower fructose concentration. Fructose conversion and 5-HMF selectivity data are presented in Figure 9.

Fructose conversion reached similar values in both reactions, meaning that less fructose remained in solution when the reaction was conducted from a solution containing 2.5% fructose

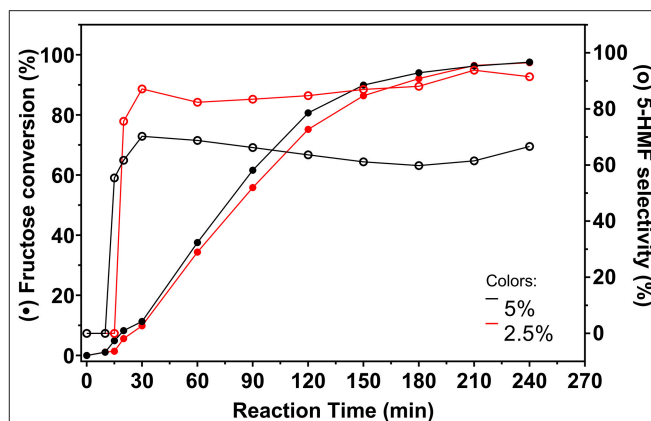


FIGURE 9 | Fructose conversion and 5-HMF selectivity values (full and empty symbols, respectively) for carbon catalyzed reactions promoted from 2.5 and 5% fructose solutions in DMSO. Conditions: 130°C, inert atmosphere, 5 wt.% catalyst.

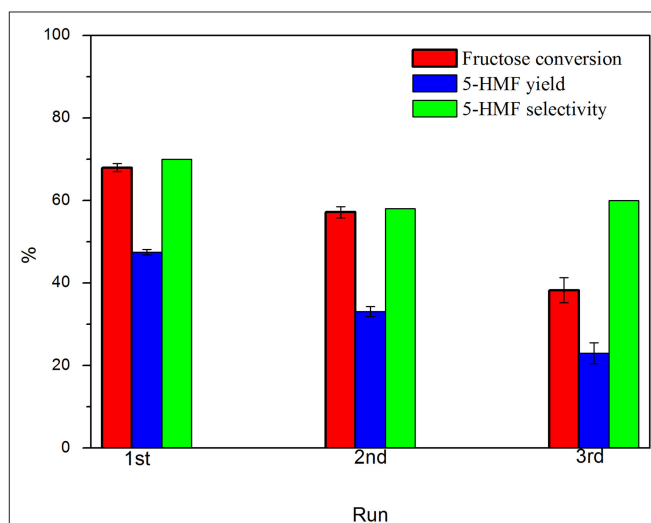


FIGURE 10 | Catalyst reusability in fructose dehydration in DMSO. Conditions: 100°C, 5% fructose in DMSO, 5 wt.% catalyst, 2 h under synthetic air.

in DMSO. Selectivity to 5-HMF increased considerably with decreasing fructose concentration. This behavior is related to the minimization of polymerization reactions, since less fructose is available in the reaction medium. Much less intense staining was observed in reactions with 2.5% fructose, indicating that polymerization was better controlled.

In order to investigate the reusability of the catalyst, consecutive batch runs were performed under the same reaction conditions. Results are presented in Figure 10.

It was observed a gradual lost in the catalyst performance after each run. From 1st to 2nd run, it was observed that the fructose conversion reduced from 68.5 to 57.2%, with a decrease of 12.5 percentual points in the 5-HMF selectivity. From 2nd to 3rd run, conversion reduced from 57.2 to 38.3%, while the 5-HMF selectivity has stabilized. This behavior is similar to that

previously observed (Nunes et al., 2020) and also reported in other works (Portillo Perez et al., 2019; Rusanen et al., 2019). The main reasons found in the literature are (I) loss of -COOH/-SO₃H groups and (II) deactivation of the acid sites by deposition/anchoring of humins on carbon surface. Some groups from the solid surface can leach to the reaction medium under the reaction conditions, thus leading to homogeneous catalysis. In order to investigate the surface groups leaching, a reaction was performed, wherein the catalyst was removed from the reaction medium after 30 min of reaction, keeping the system temperature at 100°C, as proposed by Sheldon et al. (Sheldon et al., 1998). Fructose conversion value observed after 30 min remained for 3 h after catalyst removal. This means that the homogenous contribution, arising from the leached soluble groups, can be considered negligible. On the other hand, several authors have observed that a minimal amount of humins can block the acidic sites of the catalyst, leading to its gradually deactivation (Portillo Perez et al., 2019; Nunes et al., 2020). A XPS analysis on the spent catalyst provided the composition 78.8% C, 20.2% O, and 1.0% S. When comparing the result with the values obtained previously, it is noted that a slight increase in the oxygen content, while the amount of sulfur on the surface has been drastically reduced. The results corroborate the hypothesis of the humins deposit on the catalyst surface, blocking the original acid groups. In some cases, a washing process with acetone was able to remove the humins and recover the activity of the catalyst. In conditions similar to this work, it was observed that the removal of humins by a solvent washing is not efficient enough for the reactivation of the catalyst and, in this case, a recarbonization process allows the maintenance of the catalyst activity, suggesting that humins on the spent catalyst were carbonized and incorporated on carbon surface, creating a new layer of acidic sites.

CONCLUSIONS

The catalyst based on *in situ* carbonization and sulfonation allowed to achieve fructose conversions close to 100% with 5-HMF selectivities higher than 90%. This catalyst can be used in consecutive batch runs, but it was observed a gradual lost in the catalyst performance after each run due to deposition of humins on the carbon surface. Maintaining the activity requires recarbonization of the solid.

Proper control of DMSO catalytic activity can be achieved in an inert atmosphere. The presence of oxygen in the reaction medium accelerates the occurrence of fructose dehydration reaction, which may provide a higher production of 5-HMF, but also favors the decomposition of this product, with higher formation of levulinic and formic acids. In reactions under inert

atmosphere the occurrence of rehydration reactions can be better controlled. Therefore, DMSO activity, in the presence of oxygen and at high temperatures, was considered as the major influence for the occurrence of rehydration and polymerization reactions parallel to the formation of 5-HMF.

Decreasing the initial concentration of fructose and the catalyst content in the reaction medium minimized polymerization reactions, enabling higher selectivity to 5-HMF even under high temperature conditions where polymerization is favored.

Despite the catalytic capacity of DMSO in the presence of O₂, the use of a glycerol carbon as catalyst favored fructose conversion and 5-HMF production. It is noteworthy that several studies in the literature do not consider the blank reaction and, consequently, the contribution of DMSO to the conversion of fructose, especially at temperatures above 80°C and in the presence of oxygen, mistakenly attributing all activity to the heterogeneous catalyst.

The results indicated the appropriate conditions for using DMSO, contributing to the search for green solvents, since there is a compromise between effectiveness of the DMSO application as a solvent and its relative abundance, low cost and reduced toxicity when compared to competing solvents.

DATA AVAILABILITY STATEMENT

All datasets generated for this study are included in the article/Supplementary-Material.

AUTHOR CONTRIBUTIONS

WC and DM contributed conception and design of the study, TT performed the synthesis and analysis, TT and RN wrote the first draft of the manuscript, WC wrote the final version of the manuscript. All authors contributed to manuscript revision, read, and approved the submitted version.

FUNDING

This research was supported by the FAPESP (Project Nr. 2017/24931-4 and 2016/05006-5), CAPES (Finance Code 001) and CNPq (Project Nr. 404843/2018-2).

ACKNOWLEDGMENTS

The authors also acknowledge the Multi-User Central Facilities (CEM/UFABC) for the experimental support.

REFERENCES

- Adib, M., Al-qodah, Z., and Ngah, C. W. Z. (2015). Agricultural bio-waste materials as potential sustainable precursors used for activated carbon production : a review. *Renew. Sustain. Energy Rev.* 46, 218–235. doi: 10.1016/j.rser.2015.02.051
- Adinata, D., Wan Daud, W. M. A., and Aroua, M. K. (2007). Preparation and characterization of activated carbon from palm shell by chemical activation with K₂CO₃. *Bioresour. Technol.* 98, 145–149. doi: 10.1016/j.biortech.2005.11.006
- Aldana-Pérez, A., Lartundo-Rojas, L., Gómez, R., and Niño-Gómez, M. E. (2012). Sulfonic groups anchored on mesoporous carbon Starbons-300 and its use for the esterification of oleic acid. *Fuel* 100, 128–138. doi: 10.1016/j.fuel.2012.02.025
- Amarasekara, A. S., Williams, L. T. D., and Ebade, C. C. (2008). Mechanism of the dehydration of d-fructose to 5-hydroxymethylfurfural in dimethyl

- sulfoxide at 150°C: an NMR study. *Carbohydr. Res.* 343, 3021–3024. doi: 10.1016/j.carres.2008.09.008
- Belletti, G. D., Schulte, E., Colombo, E., Schmickler, W., and Quaino, P. (2019). Development of force fields for binary systems: Application to a dimethylsulfoxide (DMSO) – Oxygen mixture. *Chem. Phys. Lett.* 735:136778. doi: 10.1016/j.cplett.2019.136778
- Binder, J. B., Cefali, A. V., Blank, J. J., and Raines, R. T. (2010). Mechanistic insights on the conversion of sugars into 5-hydroxymethylfurfural. *Energy Environ. Sci.* 3, 765–771. doi: 10.1039/b923961h
- Boehm, H. P. (1994). Some aspects of the surface chemistry of carbon blacks and other carbons. *Carbon N. Y.* 32, 759–769. doi: 10.1016/0008-6223(94)90031-0
- Boonpoke, A., Chiarakorn, S., Laosiripojana, N., Towprayoon, S., and Chidthaisong, A. (2013). Synthesis of activated carbon and MCM-41 from bagasse and rice husk and their carbon dioxide adsorption capacity. *J. Sustain. Environ.* 2, 77–81. Available online at: <http://www.jseejournal.com/searchresult.php?search=Boonpoke>
- Daud, W. M. A. W., and Ali, W. S. W. (2004). Comparison on pore development of activated carbon produced from palm shell and coconut shell. *Bioresour. Technol.* 93, 63–69. doi: 10.1016/j.biortech.2003.09.015
- Dong, T., Gao, D., Miao, C., Yu, X., Degan, C., and Garcia-Pérez, M. (2015). Two-step microalgal biodiesel production using acidic catalyst generated from pyrolysis-derived bio-char. *Energy Convers. Manag.* 105, 1389–1396. doi: 10.1016/j.enconman.2015.06.072
- Fang, Z., Liu, B., Luo, J., Ren, Y., and Zhang, Z. (2014). Efficient conversion of carbohydrates into 5-hydroxymethylfurfural catalyzed by the chromium-exchanged montmorillonite K-10 clay. *Biomass Bioenergy* 60, 171–177. doi: 10.1016/j.biombioe.2013.12.002
- Fraga, A., Do, C., Quitete, C. P. B., Ximenes, V. L., Sousa-Aguiar, E. F., Fonseca, I. M., et al. (2016). Biomass derived solid acids as effective hydrolysis catalysts. *J. Mol. Catal. A Chem.* 422, 248–257. doi: 10.1016/j.molcata.2015.12.005
- Gonçalves, M., Rodrigues, R., Galhardo, T. S., and Carvalho, W. A. (2016a). Highly selective acetalization of glycerol with acetone to solketal over acidic carbon-based catalysts from biodiesel waste. *Fuel* 181, 46–54. doi: 10.1016/j.fuel.2016.04.083
- Gonçalves, M., Soler, F. C., Isoda, N., Carvalho, W. A., Mandelli, D., and Sepúlveda, J. (2016b). Glycerol conversion into value-added products in presence of a green recyclable catalyst: acid black carbon obtained from coffee ground wastes. *J. Taiwan Inst. Chem. Eng.* 60, 294–301. doi: 10.1016/j.jtice.2015.10.016
- González, J. F., Román, S., Encinar, J. M., and Martínez, G. (2009). Pyrolysis of various biomass residues and char utilization for the production of activated carbons. *J. Anal. Appl. Pyrolysis* 85, 134–141. doi: 10.1016/j.jaap.2008.11.035
- Hu, L., Tang, X., Wu, Z., Lin, L., Xu, J., and Xu, N. (2015). Magnetic lignin-derived carbonaceous catalyst for the dehydration of fructose into 5-hydroxymethylfurfural in dimethylsulfoxide. *Chem. Eng. J.* 263, 299–308. doi: 10.1016/j.cej.2014.11.044
- Kimura, H., Nakahara, M., and Matubayasi, N. (2013). Solvent effect on pathways and mechanisms for d-fructose conversion to 5-hydroxymethyl-2-furaldehyde: *in situ* 13C NMR study. *J. Phys. Chem. A* 117, 2102–2113. doi: 10.1021/jp312002h
- Lin, Q. X., Zhang, C. H., Wang, X. H., Cheng, B. G., Mai, N., and Ren, J. L. (2019). Impact of activation on properties of carbon-based solid acid catalysts for the hydrothermal conversion of xylose and hemicelluloses. *Catal. Today* 319, 31–40. doi: 10.1016/j.cattod.2018.03.070
- Lindberg, J., Endrödi, B., Åvall, G., Johansson, P., Cornell, A., and Lindbergh, G. (2018). Li salt anion effect on O₂ solubility in a Li–O₂ battery. *J. Phys. Chem.* 122, 1913–1920. doi: 10.1021/acs.jpcc.7b09218
- Liu, Y., Zhu, L., Tang, J., Liu, M., Cheng, R., and Hu, C. (2014). One-pot, one-step synthesis of 2,5-diformylfuran from carbohydrates over Mo-containing keggins heteropolyacids. *ChemSusChem* 7, 3541–3547. doi: 10.1002/cssc.2014.02468
- Madduluri, V. R., Mandari, K. K., Velpula, V., Varkolu, M., Kamaraju, S. R. R., and Kang, M. (2020). Rice husk-derived carbon-silica supported Ni catalysts for selective hydrogenation of biomass-derived furfural and levulinic acid. *Fuel* 261:116339. doi: 10.1016/j.fuel.2019.116339
- Maneechakr, P., and Karnjanakom, S. (2017). Catalytic transformation of furfural into bio-based succinic acid via ultrasonic oxidation using β -cyclodextrin-SO₃H carbon catalyst: a liquid biofuel candidate. *Energy Convers. Manag.* 154, 299–310. doi: 10.1016/j.enconman.2017.10.069
- Mantovani, M., Mandelli, D., Gonçalves, M., and Carvalho, W. A. (2018). Fructose dehydration promoted by acidic catalysts obtained from biodiesel waste. *Chem. Eng. J.* 348, 860–869. doi: 10.1016/j.cej.2018.05.059
- Marsh, H., and Rodríguez-Reinoso, F. (2006). *Activated Carbon*. Amsterdam: Elsevier.
- Mo, X., Lopez, D., Suwannakarn, K., Liu, Y., Lotero, E., Goodwin, J. G., Jr., et al. (2008). Activation and deactivation characteristics of sulfonated carbon catalysts. *J. Catal.* 254, 332–338. doi: 10.1016/j.jcat.2008.01.011
- Monteiro, M. R., Kugelmeier, C. L., Pinheiro, R. S., Batalha, M. O., and da Silva César, A. (2018). Glycerol from biodiesel production: technological paths for sustainability. *Renew. Sustain. Energy Rev.* 88, 109–122. doi: 10.1016/j.rser.2018.02.019
- Musau, R. M., and Munavu, R. M. (1987). The preparation of 5-hydroxymethyl-2-furaldehyde (HMF) from d-fructose in the presence of DMSO. *Biomass* 13, 67–74. doi: 10.1016/0144-4565(87)90072-2
- Ni, W., Li, D., Zhao, X., Ma, W., Kong, K., and Gu, Q. (2019). Catalytic dehydration of sorbitol and fructose by acid-modified zirconium phosphate. *Catal. Today* 319, 66–75. doi: 10.1016/j.cattod.2018.03.034
- Nunes, R., Tudino, T., Vieira, L., Mandelli, D., and Carvalho, W. (2020). Rational production of highly acidic sulfonated carbons from kraft lignins employing a fractionation process combined with acid-assisted hydrothermal carbonization. *Bioresour. Technol.* 303:122823. doi: 10.1016/j.biortech.2020.122822
- Ormsby, R., Kastner, J. R., and Miller, J. (2012). Hemicellulose hydrolysis using solid acid catalysts generated from biochar. *Catal. Today* 190, 89–97. doi: 10.1016/j.cattod.2012.02.050
- Petronijevic, Z., Maluckov, B., and Smelcerovic, A. (2013). Crosslinking of polysaccharides with activated dimethylsulfoxide. *Tetrahedron Lett.* 54, 3210–3214. doi: 10.1016/j.tetlet.2013.04.050
- Portillo Perez, G., Mukherjee, A., and Dumont, M. J. (2019). Insights into HMF catalysis. *J. Ind. Eng. Chem.* 70, 1–34. doi: 10.1016/j.jiec.2018.10.002
- Putten, R., Waal, J., Jong, E., Rasrendra, C. B., Heeres, H. J., and Vries, J. (2013). Hydroxymethylfurfural, a versatile platform chemical made from renewable resources. *Chem. Rev.* 113, 1499–1597. doi: 10.1021/cr300182k
- Ren, L. K., Zhu, L. F., Qi, T., Tang, J. Q., Yang, H. Q., and Hu, C. W. (2017). Performance of dimethyl sulfoxide and brønsted acid catalysts in fructose conversion to 5-Hydroxymethylfurfural. *ACS Catal.* 7, 2199–2212. doi: 10.1021/acscatal.6b01802
- Restivo, J., Soares, O. S. G. P., Órfão, J. J. M., and Pereira, M. F. R. (2017). Catalytic reduction of bromate over monometallic catalysts on different powder and structured supports. *Chem. Eng. J.* 309, 197–205. doi: 10.1016/j.cej.2016.10.025
- Rusanen, A., Lahti, R., Lappalainen, K., Kärkkäinen, J., Hu, T., Romar, H., et al. (2019). Catalytic conversion of glucose to 5-hydroxymethylfurfural over biomass-based activated carbon catalyst. *Catal. Today*. doi: 10.1016/j.cattod.2019.02.040. [Epub ahead of print].
- Saleh, T. A. (2011). The influence of treatment temperature on the acidity of MWCNT oxidized by HNO₃ or a mixture of HNO₃/H₂SO₄. *Appl. Surf. Sci.* 257, 7746–7751. doi: 10.1016/j.apsusc.2011.04.020
- Shahangi, F., Najafi Chermahini, A., and Saraji, M. (2017). Dehydration of fructose and glucose to 5-hydroxymethylfurfural over Al-KCC-1 silica. *J. Energy Chem.* 27, 769–780. doi: 10.1016/j.jechem.2017.06.004
- Sheldon, R. A., Wallau, M., Arends, I. W. C. E., and Schuchardt, U. (1998). Heterogeneous catalysts for liquid-phase oxidations: philosophers' stones or trojan horses? *Acc. Chem. Res.* 31, 485–493. doi: 10.1021/ar9700163
- Shimizu, K.-I., Uozumi, R., and Satsuma, A. (2009). Enhanced production of hydroxymethylfurfural from fructose with solid acid catalysts by simple water removal methods. *Catal. Commun.* 10, 1849–1853. doi: 10.1016/j.catcom.2009.06.012
- Solis Maldonado, C., De la Rosa, J. R., Lucio-Ortiz, C. J., Valente, J. S., and Castaldi, M. J. (2017). Synthesis and characterization of functionalized alumina catalysts with thiol and sulfonic groups and their performance in producing 5-hydroxymethylfurfural from fructose. *Fuel* 198, 134–144. doi: 10.1016/j.fuel.2016.10.004
- Teong, S. P., Yi, G., and Zhang, Y. (2014). Hydroxymethylfurfural production from bioresources: past, present and future. *Green Chem.* 16, 2015–2026. doi: 10.1039/c3gc42018c
- Thapa, I., Mullen, B., Saleem, A., Leibig, C., Baker, R. T., and Giorgi, J. B. (2017). Efficient green catalysis for the conversion of fructose to levulinic acid. *Appl. Catal. A Gen.* 539, 70–79. doi: 10.1016/j.apcata.2017.03.016

- Tong, X., and Li, Y. (2010). Efficient and selective dehydration of fructose to 5-hydroxymethylfurfural catalyzed by brønsted-acidic ionic liquids. *ChemSusChem* 3, 350–355. doi: 10.1002/cssc.200900224
- Tong, X., Ma, Y., and Li, Y. (2010). Biomass into chemicals: conversion of sugars to furan derivatives by catalytic processes. *Appl. Catal. A Gen.* 385, 1–13. doi: 10.1016/j.apcata.2010.06.049
- Tsilomelekis, G., Orella, M. J., Lin, Z., Cheng, Z., Zheng, W., Nikolakis, V., et al. (2016). Molecular structure, morphology and growth mechanisms and rates of 5-hydroxymethyl furfural (HMF) derived humins. *Green Chem.* 18, 1983–1993. doi: 10.1039/C5GC01938A
- Velasco, L. F., Maurino, V., Laurenti, E., Fonseca, I. M., Lima, J. C., and Ania, C. O. (2013). Photoinduced reactions occurring on activated carbons. A combined photooxidation and ESR study. *Appl. Catal. A Gen.* 452, 1–8. doi: 10.1016/j.apcata.2012.11.033
- Villanueva, N. I., and Marzalletti, T. G. (2018). Mechanism and kinetic parameters of glucose and fructose dehydration to 5-hydroxymethylfurfural over solid phosphate catalysts in water. *Catal. Today* 302, 100–107. doi: 10.1016/j.cattod.2017.04.049
- Wang, J., Xu, W., Ren, J., Liu, X., Lu, G., and Wang, Y. (2011). Efficient catalytic conversion of fructose into hydroxymethylfurfural by a novel carbon-based solid acid. *Green Chem.* 13, 2678–2681. doi: 10.1039/c1gc15306d
- Wang, L., Guo, H., Xie, Q., Wang, J., Hou, B., Jia, L., et al. (2018). Conversion of fructose to furfural or 5-hydroxymethylfurfural over HY zeolites selectively in γ -butyrolactone. *Appl. Catal. A Gen.* 572, 51–60. doi: 10.1016/j.apcata.2018.12.023
- Wang, L., Zhang, L., Li, H., Ma, Y., and Zhang, R. (2019). High selective production of 5-hydroxymethylfurfural from fructose by sulfonic acid functionalized SBA-15 catalyst. *Compos. Part B Eng.* 156, 88–94. doi: 10.1016/j.compositesb.2018.08.044
- Wataniyakul, P., Boonnoun, P., Quitain, A. T., Kida, T., Laosiripojana, N., and Shotipruk, A. (2018). Preparation of hydrothermal carbon acid catalyst from defatted rice bran. *Ind. Crops Prod.* 117, 286–294. doi: 10.1016/j.indcrop.2018.03.002
- Whitaker, M. R., Parulkar, A., Ranadive, P., Joshi, R., and Brunelli, N. A. (2019). Examining acid formation during the selective dehydration of fructose to 5-hydroxymethylfurfural in dimethyl sulfoxide and water. *ChemSusChem* 12, 2211–2219. doi: 10.1002/cssc.201803013
- Xiong, X., Yu, I. K. M., Chen, S. S., Tsang, D. C. W., Cao, L., and Song, H. (2018). Sulfonated biochar as acid catalyst for sugar hydrolysis and dehydration. *Catal. Today* 314, 52–61. doi: 10.1016/j.cattod.2018.02.034
- Yalpani, M. (1985). A survey of recent advances in selective chemical and enzymic polysaccharide modifications. *Tetrahedron* 41, 2957–3020. doi: 10.1016/S0040-4020(01)96652-9
- Yi, X., Delidovich, I., Sun, Z., Wang, S., Wang, X., and Palkovits, R. (2015). A heteropoly acid ionic crystal containing Cr as an active catalyst for dehydration of monosaccharides to produce 5-HMF in water. *Catal. Sci. Technol.* 5, 1–5. doi: 10.1039/C4CY01555J
- Yu, X., Chu, Y., Zhang, L., Shi, H., Xie, M., Peng, L., et al. (2020). Adjacent acid sites cooperatively catalyze fructose to 5-hydroxymethylfurfural in a new, facile pathway. *J. Energy Chem.* 47, 112–117. doi: 10.1016/j.jechem.2019.11.020
- Zhang, J., Das, A., Assary, R. S., Curtiss, L. A., and Weitz, E. (2016). A combined experimental and computational study of the mechanism of fructose dehydration to 5-hydroxymethylfurfural in dimethylsulfoxide using amberlyst 70, PO_4^{3-} /niobic acid, or sulfuric acid catalysts. *Appl. Catal. B Environ.* 181, 874–887. doi: 10.1016/j.apcatb.2014.10.056
- Zhao, J., Zhou, C., He, C., Dai, Y., Jia, X., and Yang, Y. (2016). Efficient dehydration of fructose to 5-hydroxymethylfurfural over sulfonated carbon sphere solid acid catalysts. *Catal. Today* 264, 123–130. doi: 10.1016/j.cattod.2015.07.005
- Zhao, K., Liu, S., Li, K., Hu, Z., Yuan, Y., Yan, L., et al. (2017). Fabrication of $-\text{SO}_3\text{H}$ functionalized aromatic carbon microspheres directly from waste camellia oleifera shells and their application on heterogeneous acid catalysis. *Mol. Catal.* 433, 193–201. doi: 10.1016/j.mcat.2017.02.032
- Zhong, R., and Sels, B. F. (2018). Sulfonated mesoporous carbon and silica-carbon nanocomposites for biomass conversion. *Appl. Catal. B Environ.* 236, 518–545. doi: 10.1016/j.apcatb.2018.05.012

Conflict of Interest: The authors declare that the research was conducted in the absence of any personal, professional or financial relationships that could potentially be construed as a conflict of interest.

Copyright © 2020 Tudino, Nunes, Mandelli and Carvalho. This is an open-access article distributed under the terms of the Creative Commons Attribution License (CC BY). The use, distribution or reproduction in other forums is permitted, provided the original author(s) and the copyright owner(s) are credited and that the original publication in this journal is cited, in accordance with accepted academic practice. No use, distribution or reproduction is permitted which does not comply with these terms.



Synthesis of Porous Biochar Containing Graphitic Carbon Derived From Lignin Content of Forestry Biomass and Its Application for the Removal of Diclofenac Sodium From Aqueous Solution

Nguyen Thi Minh Tam^{1,2*}, Yun-guo Liu^{1,2*}, Hassan Bashir¹, Peng Zhang^{1,2}, Shao-bo Liu^{3,4}, Xiaofei Tan^{1,2}, Ming-yang Dai^{1,2} and Mei-fang Li^{1,2}

¹ College of Environmental Science and Engineering, Hunan University, Changsha, China, ² Key Laboratory of Environmental Biology and Pollution Control, Ministry of Education, Changsha, China, ³ School of Metallurgy and Environment, Central South University, Changsha, China, ⁴ School of Architecture and Art, Central South University, Changsha, China

OPEN ACCESS

Edited by:

Francesca Deganello,
Italian National Research Council, Italy

Reviewed by:

Elisa I. Garcia-Lopez,
University of Palermo, Italy
Xuefeng Zhang,
Mississippi State University,
United States

*Correspondence:

Nguyen Thi Minh Tam
tamnm@hnu.edu.cn
Yun-guo Liu
hnuliyunguo@gmail.com;
liuyunguo_hnu@163.com

Specialty section:

This article was submitted to
Green and Sustainable Chemistry,
a section of the journal
Frontiers in Chemistry

Received: 27 December 2019

Accepted: 20 March 2020

Published: 23 April 2020

Citation:

Tam NTM, Liu Y, Bashir H, Zhang P,
Liu S, Tan X, Dai M and Li M (2020)
Synthesis of Porous Biochar
Containing Graphitic Carbon Derived
From Lignin Content of Forestry
Biomass and Its Application for the
Removal of Diclofenac Sodium From
Aqueous Solution.
Front. Chem. 8:274.
doi: 10.3389/fchem.2020.00274

Porous biochar containing graphitic carbon materials have received great attention from various disciplines, especially for environmental pollutant treatment, due to their cost-effective and specific textural properties. This study exhibited a two-step strategy to compose lignin-porous biochar containing graphitic carbon (LPGC) from pitch pine sawdust and investigated its adsorptive removal for diclofenac sodium (DCF) from an aqueous solution. Sulfuric acid (H_2SO_4) was utilized to obtain lignin content from biomass and potassium ferrate (K_2FeO_4) and was adopted to fulfill the synchronous carbonization and graphitization of LPGC. Through slow pyrolysis in atmospheric N_2 ($900^\circ\text{C} - 2\text{ h}$), the structure of the as-prepared sample was successfully modified. Using SEM images, a stripped layer structure was observed on the H_2SO_4 -treated sample for both one-step and two-step activated samples, indicating the pronounced effect of H_2SO_4 in the layering of materials. K_2FeO_4 acted as an activator and catalyst to convert biomass into the porous graphitic structure. The BET surface area, XRD and Raman spectra analyses demonstrated that LPGC possessed a micro/mesoporous structure with a relatively large surface area ($457.4\text{ m}^2\text{ g}^{-1}$) as well as the presence of a graphitic structure. Further adsorption experiments revealed that LPGC exhibited a high DCF adsorption capacity ($q_{\text{max}} = 159.7\text{ mg g}^{-1}$ at 298 K , $\text{pH} = 6.5$). The effects of ambient conditions such as contact time, solution pH, temperature, ionic strength, electrolyte background on the uptake of DCF were investigated by a batch adsorption experiment. Results indicated that the experimental data were best fitted with the pseudo second-order model and Langmuir isotherm model. Furthermore, the adsorption of DCF onto the LPGC process was spontaneous and endothermic. Electrostatic interaction, H-bonding interaction, and $\pi-\pi$ interaction are the possible adsorption mechanisms. The porous biochar containing graphitic carbon obtained from the lignin content of pitch pine sawdust may be a potential material for eliminating organic pollutants from water bodies.

Keywords: graphitic carbon, porous biochar, diclofenac sodium, potassium ferrate, lignin content, adsorption

INTRODUCTION

Over the past few decades, along with the development of medicine, the human healthcare products manufacturing industry has also grown to serve the demand of more than 7 billion people worldwide. Among the products, pharmaceuticals are widely used for preventing and treating diseases in humans and animals. It was estimated that the worldwide average per capita consumption of pharmaceuticals is around 15 g per year (Alder et al., 2006; Zhang et al., 2008). Environmentalists consider pharmaceuticals as emerging contaminants (ECs), which include various groups such as: analgesics, antibiotics, anti-inflammatories, regulatory blood lipid, and natural and synthetic hormones (Ahmed and Hameed, 2018). Because the conventional wastewater treatment plants are not specifically designed to remove pharmaceuticals and residues, they are almost unobstructed, flowing into water bodies and causing damage to animals and human beings (Alidina et al., 2014). It is especially dangerous for the environment and can even cause damage in marine life such as hormonal disorders and sex reversal in fish and amphibians. Many studies about the effect of ECs on the environment and human health have been conducted (Letzel et al., 2009; Michael et al., 2013; Alves et al., 2017; Batt et al., 2017; Benson et al., 2017). Among the pharmaceutical products, diclofenac (DCF) is known as the “world’s most popular pain killer” and is listed as an environmental threat by the European Union (EU) and the US Environmental Protection Agency (USEPA) (Framework, 2013; Lonappan et al., 2016). DCF has been detected in water all over the world both in a low concentration ($0.08 \mu\text{g L}^{-1}$) and a significant concentration ($2.51 \mu\text{g L}^{-1}$) (Heberer, 2002) in wastewater effluents. It was reported that currently 0.1–8.3% of the total length of Europe’s rivers could exceed the suggested EU Environmental Quality Standards for diclofenac (100 ng L^{-1}) (Johnson et al., 2013). It is estimated that the world consumes about $1,443 \pm 58$ tons of DCF annually (Acuña et al., 2015), and hundreds of tons of it has been discharged into the environment. The contaminant is partly absorbed by the natural ecosystem and the rest blends into the marine environment. It was reported that even at very low concentrations, DCF can cause cytological alterations in rainbow trout ($1 \mu\text{g L}^{-1}$), or tissue damage in several mussel species ($250 \mu\text{g L}^{-1}$) (Ericson et al., 2010). Thus, DCF should be removed from wastewater by proper physicochemical treatment methods before disposal into the natural environment.

Various technologies such as adsorption, degradation, coagulation, oxidation degradation and so on have been applied in polluted water treatment. Among these methods, adsorption has the advantage of being easy to operate, is low cost, is highly efficient, has strong reproducibility, and is available as different adsorbents (Liu et al., 2019). Thus, it has been proven to be an effective and economically viable method of removing organic contaminants. One of the important materials used in adsorption techniques is biochar. Biochar is known as a type of solid carbonaceous material with profound properties (the presence of surface functional groups, moderate surface area, and porosity) which can effectively adsorb organic pollutants from the water environment. Many studies have been conducted

to derive biochar from different types of biomass, such as shells, flowers, rice residues, bamboo, tobacco, sawdust, and sewage sludge, etc. Among the feedstocks, biochar derived from herbaceous plant materials is more favorable than others, due to its beneficial characteristics (e.g., abundant feedstock, easy to harvest, high potential to produce sustainable adsorbents and green supercapacitors; Tan et al., 2015). However, the raw biochar has limited ability to adsorb contaminants from aqueous solutions, especially for wastewater that contain high concentrations of pollution (Yao et al., 2013; Tan et al., 2016). Furthermore, biochar is an amorphous powder and is not easy to separate from the aqueous solution due to its small particle size (Tan et al., 2016). Thus, it is essential to enhance the biochar structure to improve its adsorption performance. For this reason, porous graphitic carbon materials (PGCs) have been developed and has increasingly attracted attention from various disciplines, especially in the field of environmental micro-pollutant treatment (Edathil et al., 2017; Siyasukh et al., 2018; Gupta et al., 2019; Shittu et al., 2019) and advanced materials for storing energy (Jiang et al., 2019; Kim et al., 2019; Xi et al., 2019; Xing et al., 2019). To obtain PGCs, researchers developed several methods such as catalytic activation of biomass (Sevilla and Fuertes, 2010; Wang et al., 2013; Navarro-Suárez et al., 2014) or sacrificial template methods using silica or surfactants (Gibot et al., 2016; Nita et al., 2016; Yan et al., 2017). The advantage of graphitic carbon over amorphous carbon materials is that the honeycomb structure facilitates the absorption of aromatic compounds including aromatic pharmaceuticals through π - π stacking. Nevertheless, the further development of PGCs fabrication process is limited by the consumption of expensive precursors and multiple time-consuming steps. It is therefore sensible to develop a low-cost, environmentally friendly, and effective approach to synthesize porous graphitic carbon.

The herbaceous plant biomass contains about 85–90% of cellulose, hemicellulose, and lignin, while organic extractives and inorganic minerals constitute the rest (Pasangulapati et al., 2012). Lignin, because of its aromatic molecule structure with a high degree of cross linking between the phenylpropane and β -O-4, presents an incentive feedstock for graphite production (Chatterjee et al., 2014a,b). This connection makes lignin more thermally stable than hemicellulose (Ramiah, 1970). In this study, we propose an approach for deriving a porous biochar containing graphitic carbon material from pitch pine sawdust. A graphitic structure was obtained through the structural separation of biomass components. Sulfuric acid (H_2SO_4) was employed to eliminate the cellulose/hemicellulose components in sawdust. Potassium ferrate (K_2FeO_4) is known as a strong oxidant reagent that can be directly applied in wastewater treatment without producing any polluting byproducts (Jiang et al., 2006; He et al., 2018). In addition, potassium ferrate was also utilized as an activated agent to modify the biochar structure (Wu J. et al., 2019). Zhang et al. (2019) used Fe—a transition metal—as a catalyst agent to form a graphitic structure of biochar while Demir et al. (2015) proposed graphitic biocarbon from the metal-catalyzed hydrothermal carbonization of lignin. To the best of our knowledge, the study on applications of potassium ferrate to convert lignin content of plant biomass is limited. In this study,

K_2FeO_4 was utilized to simultaneously convert the lignin content of pitch pine biomass into a porous and graphitic structure. The nano composite was labeled as lignin-porous biochar containing graphitic carbon (LPGC). DCF was employed as a representative organic contaminant and its removal process from aqueous solution using LPGC was investigated.

Taking into account the advantageous characteristics of biochar and the necessity of removing DCF from the natural environment, the aims of our study were to: (1) prepare and characterize the LPGC; (2) explore the adsorption capacity of LPGC for DCF through studies of kinetics and isotherms; (3) investigate the impact of the DCF concentration, reaction temperature, solution pH, ionic strengths, and background electrolytes on the adsorption capacity of LPGC toward DCF; and to (4) examine the possible adsorption mechanism between adsorbent LPGC and adsorbate DCF.

MATERIALS AND METHODS

Chemical Reagents

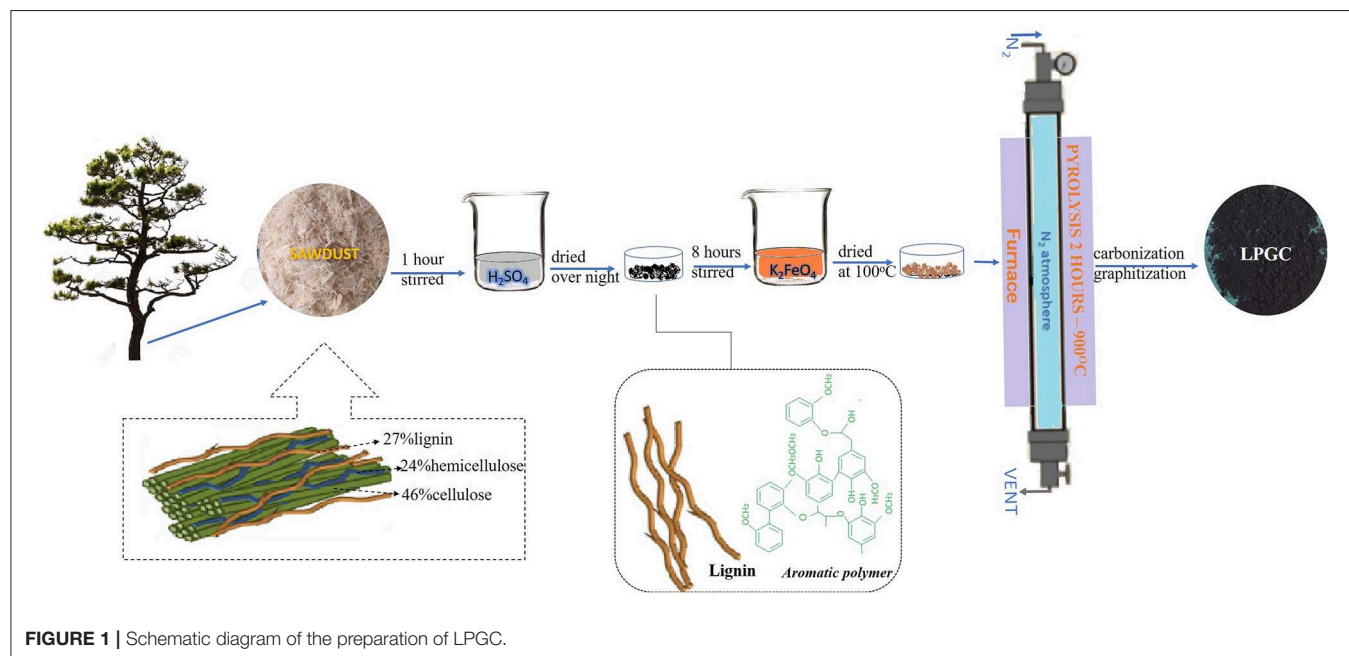
The pitch pine (*Pinus rigida*) sawdust, a byproduct of the wood manufacturing industry was utilized in this study. The chemical compositions of cellulose, hemicellulose, and lignin in pitch pine wood are 46, 24, and 27%, respectively (Rangabhashiyam and Balasubramanian, 2019). The biomass used was obtained from a furniture factory located in Changsha (Hunan, China). Diclofenac sodium salt (purity 99%) was purchased from Shanghai Yien Chemical Technique Co., Ltd. The chemical structure and physicochemical properties of DCF are described in the **Table S1**. The other chemical reagents used were supplied by Shanghai Macklin Biochemical Co., Ltd. The water used in all experiments was prepared in Milli-Q water (18.25 M Ω .cm at 25°C) obtained from a Millipore water purification system. All chemicals used in this study were of analytical grade.

To prepare DCF stock solution (5 g L⁻¹), 0.5 g DCF solid (99% purity) was dissolved in 10 ml pure methanol before continuously being mixed into deionized water (90 ml). The solution was then stored in an amber colored bottle at 4 ± 1°C for later use. For each experiment, different working solutions were derived by diluting the as-prepared solution with deionized water.

Synthesis of Lignin Biochar Containing Graphitic Carbon and Other Compared Materials

First, pitch pine sawdust was mixed in H_2SO_4 (72%) solution at a ratio of 10% w/v to obtain the lignin component of the biomass. The mixed solution was stirred magnetically at room temperature for 1 h to eliminate cellulose and hemicellulose components. The solution concentration was then adjusted to 4% by deionized water and kept at 120°C for 1 h. After that, 0.45 μ m filter paper was used to refine the slurry. The sample was washed several times to remove the excess chemicals and dried overnight at 60°C. After evaporating, we obtained a solid sample. The solid sample was then crushed into powder and dispersed in 0.1 M K_2FeO_4 solution (100 ml) and continuously stirred in 8 h and dried overnight at 100°C to obtain a solid mixture. The mixture was then transferred into a tube furnace and heated at 900°C for 2 h with a heating rate of 5°C min⁻¹ in atmospheric N_2 . Ultimately, the sample was collected and washed with deionized water, followed by drying at 80°C. The resultant sample was denoted as LPGC. The preparation process is schematically illustrated in **Figure 1**.

For comparison, three different samples were prepared. A H_2SO_4 -treated sample was made by mixing sawdust with an H_2SO_4 (72%) solution at a ratio of 10% of w/v and stirred continuously for 1 h. The concentration of H_2SO_4 was adjusted to 4% by adding deionized water. The sample was incubated at



120°C for 1 h then filtered by 0.45 µm filter paper and dried overnight at 60°C to obtain a solid mixture. At the same time, a K₂FeO₄-treated sample was prepared by adding 3.0 g of sawdust to the K₂FeO₄ solution (100 ml, 0.1 M) and continuously stirred for 8 h, then dried overnight at 100°C. Subsequently, a similar pyrolysis process as described above was carried out with the H₂SO₄-treated sample, K₂FeO₄-treated sample, and no-treated sample. All the samples were transferred into a tube furnace and heated at 900°C for 2 h with a heating rate of 5°C min⁻¹ in atmospheric N₂. The resultant H₂SO₄-treated, K₂FeO₄-treated, and no-treated samples were collected and labeled as lignin biochar (LBC), cellulose/lignin biochar (C/LBC), and pristine biochar (BC), respectively.

Characterizations

The morphological studies of the samples were carried out by scanning electron microscopy (SEM) (S4800, Hitachi, Japan) and transmission electron microscopy (TEM) (Tecnai G2 20, FEI, USA). The elemental composition of samples was observed with energy-dispersive X ray spectroscopy (EDS) (Genesis, Edax, USA). To obtain a X-ray diffraction (XRD) pattern of the samples, a Bruker AXS D8 Advance diffractometer was used with Cu Kα radiation (acceleration voltage of 40 kV, 2 theta interval 0.02°, scan speed 0.1 sec/step, λ = 0.15418 nm). The Raman spectra was obtained from a LabRAM HR UV Raman spectrometer at the laser excitation wavelength of 532 nm and power 10 mV. The spectrum was measured at room temperature in the spectral range of 4,000–400 cm⁻¹. The BET surface areas and pore structure of the samples were investigated by Nitrogen adsorption-desorption method temperature of liquid nitrogen (Quantachrome Instruments Quadrasorb EVO, USA). The surface chemistry and chemical state of elements were analyzed by X-ray photoelectron spectroscopy (XPS) (ESCALAB 250Xi, Thermo Fisher, USA) under Al- Kα (hν = 1486.6 eV), power 150 W, 500 µm beam spot. FT-IR studies were performed by a spectrophotometer (IR Tracer-100, Shimadzu, Japan) in the wavenumber range of 400–4,000 cm⁻¹. For zeta potential analysis, 25 mg of adsorbents was added to 25 ml Milli-Q water and the pH was adjusted in the range of 2.0–10.0 with 0.1 M NaOH or HCl. Zeta potential meter (Zetasizer Nano-ZS90, Malvern Instruments, Malvern, UK) was used to perform the results.

Adsorption Experiments

For adsorption experiments, DCF solution with a concentration of 20 mg L⁻¹ was chosen and derived by diluting stock solution into deionized water. NaOH and HCl with negligible volumes were used to adjust the pH to desired values. In all batch sorption experiments, 0.005 g of adsorbents was added in conical flasks (volume 100 ml) with 50 ml DCF solution (20 mg L⁻¹). The conical flasks were put in a rotary thermostatic oscillator and shaken at a constant speed (160 rpm) at a temperature of 25°C for 24 h and then the supernatants were collected by filtration with 0.45 µm membrane filters.

The concentration of DCF in both the initial and adsorbent solutions were examined by an UV-VIS spectrophotometer (UV-2550, Shimadzu, Japan) at the wavelength of the highest

absorbance 276 nm (Bhadra et al., 2016). A linear coefficient was obtained from the calibration curve of DCF and used to convert the absorbance to the concentration through Equation 1 (Rosset et al., 2019).

$$S = \frac{A}{a} \quad (1)$$

Where: S is the solution concentration (mg L⁻¹); A is the absorbance at wavelength 276 nm; a is the linear coefficient of the calibration curve.

The adsorbed DCF amount was calculated by the difference between the sorption solution concentrations at initial time and equilibrium time. The adsorption capacities were obtained by the following equation:

$$q_e = \frac{(C_o - C_e)V}{m} \quad (2)$$

where C_o is the initial and C_e is the equilibrium concentration of DCF (mg L⁻¹), V and m are the volume of the solution (L), and adsorbents doses (g), respectively.

DCF adsorption kinetic experiments were carried out to determine the minimum time required to reach adsorption equilibrium state. Fifty microgram of adsorbents was added to 50 ml of DCF 20 mg L⁻¹ solution at pH ≈ 6.5 and 298 K. All samples were then shaken for different time intervals (ranging from 0.17 to 24 h). Two models, Pseudo first-order and Pseudo second-order were used to evaluate the adsorption process. The equations of each model are given as Equation (1s) and (2s) in the **Supplementary Materials**.

To obtain information about the maximum adsorption capacities, DCF adsorption isotherm experiments were conducted at pH ≈ 6.5 under three different temperatures (298, 308, and 318 K). The initial concentration of the DCF solution ranged from 5 to 25 mg L⁻¹. Two isotherm models, namely Langmuir isotherm and Freundlich isotherm, were used to simulate the adsorption process. The isotherm model equations are given as Equation (3s) and (4s) in the **Supplementary Materials**.

A thermodynamics study can reveal information on the inherent energy change of adsorbent and the adsorption mechanism between adsorbent and adsorbate (Sun et al., 2014; Jiang et al., 2015). The effects of temperature on adsorption were explored through some thermodynamic parameters, such as Gibbs free energy of adsorption (ΔG°), heat of the adsorption (ΔH°) and standard entropy changes (ΔS°) (Suriyanon et al., 2013). Here, the thermodynamics adsorption of DCF on LPGC was carried out at various temperatures (298, 308, and 318 K), 50 mg LPGC was added into the 20 mg L⁻¹ DCF solution (50 ml) at pH ≈ 6.5, contact time 24 h. Thermodynamic parameters calculation equations are given as Equation (5s) and (6s) in the **Supplementary Materials**.

To investigate the influence of pH onto the adsorption process, batch experiments with the same conditions of kinetic experiments (excluded pH value) were conducted. The range of initial pH was from 2.0 to 10.0, and 0.1 M NaOH or 0.1 M HCl with negligible volumes were used to adjust the pH of the solution.

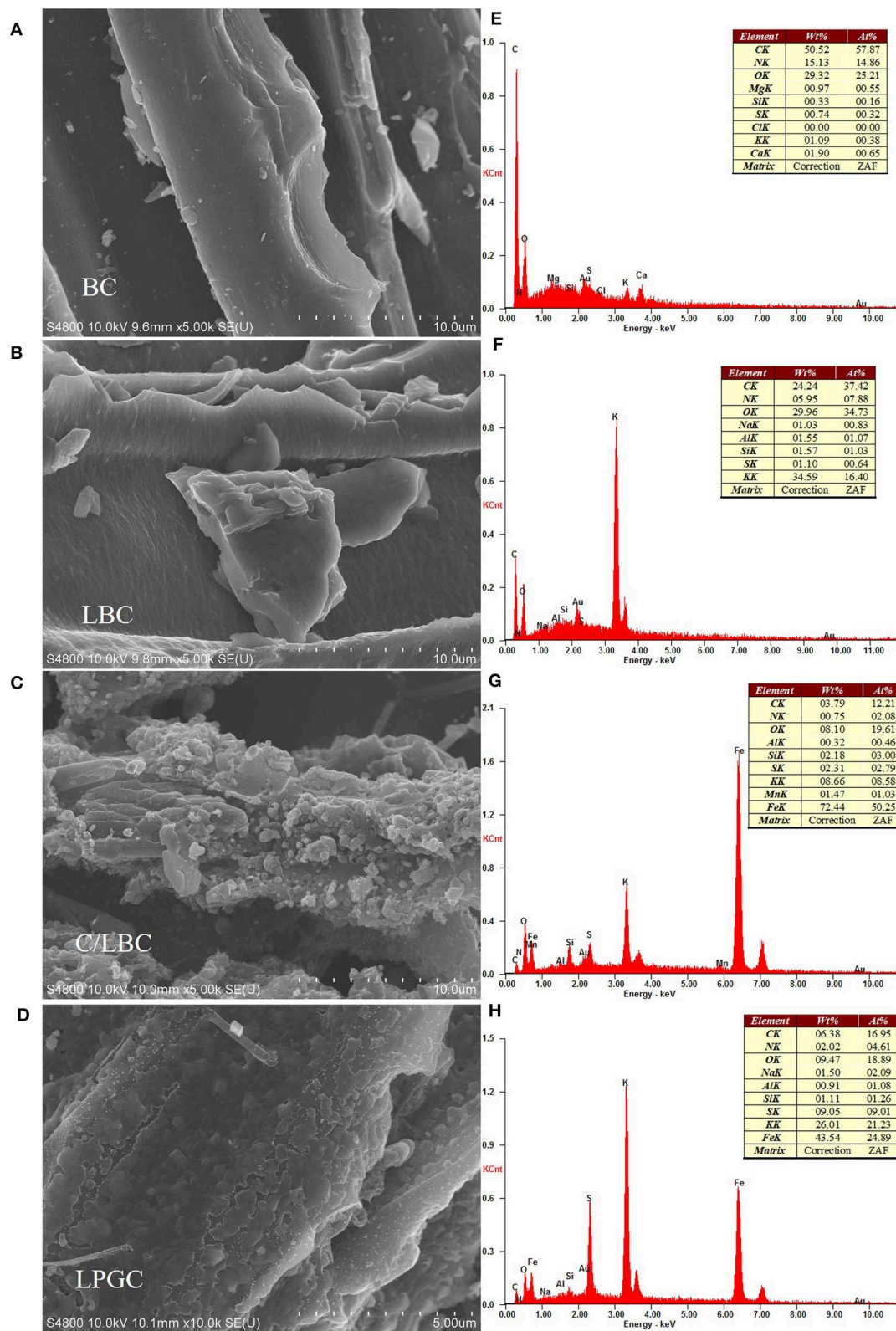


FIGURE 2 | Scanning electron microscopy (SEM) images of **(A)** BC, **(B)** LBC, **(C)** C/LBC, and **(D)** LPGC, and the corresponding EDS image of **(E)** BC, **(F)** LBC, **(G)** C/LBC, and **(H)** LPGC.

NaCl with different concentrations varying from 0.001 to 0.1 M were used to explore the effect of ionic strength on the removal of DCF from the aqueous solution by as-prepared materials. The experiment conditions were the same as the kinetic experiment conditions.

Along with other ambient factors, background electrolyte ions also have an impact on the adsorption process. To examine the effect of this factor onto DCF adsorption by LPGC, several background electrolyte ions such as Na^+ , K^+ , Mg^{2+} , Ca^{2+} , NO_3^- , SO_4^{2-} , and PO_4^{3-} were used. The electrolyte ions with three different concentrations (0.001, 0.01, and 0.1 M) were added into 50 mL DCF solution (20 mg L^{-1}) containing 50 mg LPGC at 298 K and $\text{pH} \approx 6.5$, respectively.

RESULTS AND DISCUSSION

Characterization of Adsorbents Surface Morphology Analysis

The combination of the scanning electron microscope (SEM) and energy-dispersive X-ray spectroscopy (EDS) provides a powerful tool for exploring the morphological, topographical information of the biochar, while transmission electron microscopy (TEM) can reveal the structural quality and the layer state of material. The SEM images of BC, LBC, C/LBC, and LPGC are shown in **Figures 2A–D**. The EDS images of as-prepared samples are displayed in **Figures 2E,F**. The TEM image of LPGC is presented in **Figure 3E**. As can be observed, there are many nanoparticles on the surface of LPGC and C/LBC compared with BC. The original surface of BC possessed a relatively smooth surface with a plate-like morphology (**Figure 2A**). After one step modification, the H_2SO_4 -treated sample (LBC) obtained a stripped layer structure with small and even ripples (**Figure 2B**). Meanwhile the morphology was totally changed for the K_2FeO_4 -treated sample (C/LBC). Its surface became rough and uneven with various lumps of different diameters (**Figure 2C**). **Figure 2D** displays the outer shape of LPGC—the two-step modification sample. Compared with the previous samples, LGBC exhibited a different surface structure with very high roughness and many parallel stripped scratches. In addition, it is easy to recognize that many solid particles appeared on the surface of C/LBC and LPGC, which confirmed the loading of iron particles. Moreover, the EDS results (**Figures 2G,H**) show that 72.44 and 43.45 wt% of Fe were found in C/LBC and LPGC, respectively. It could be concluded that Fe molecules successfully attached on to the samples treated with K_2FeO_4 . Furthermore, the TEM image of LPGC (**Figure 3E**) indicated the presence of graphitic carbon.

XRD and Raman Analysis

The composition and crystalline phase of the as-prepared samples were investigated by XRD and Raman spectra. The XRD patterns of samples are shown in **Figure 3A**. There was a broad peak in BC and some characteristic peaks at θ values of 24.2° , 30.1° , and 31.3° in LBC, which could be ascribed to amorphous carbon (Tseng et al., 2011; Jiang et al., 2018), while in the LPGC and C/LBC these peaks are weaker, indicating the significant changes of their carbon characteristic. Furthermore, it can be observed that two diffraction peaks at θ values of 26.6° and 44.7° in C/LBC were obviously higher in LPGC, which can be

indexed to typical (002) and (001) reflection of graphitic carbon (JCPDS No. 41-1487) (Gong et al., 2017). New diffraction peaks at 65.0° and 82.3° can also be seen in both C/LBC and LPGC, indicating the presence of Fe (JCPDS No. 06-0696) (Jiang et al., 2018). Furthermore, some peaks at θ value between 40° and 50° that corresponded to cementite (Fe_3C) were observed in the XRD pattern of C/LBC and LPGC (Yan et al., 2018). It again confirmed that Fe nanoparticles were successfully loaded on the surface of two K_2FeO_4 -treated materials (C/LBC and LPGC) during the synthesis process. Additionally, the peaks between 30° and 35° in LPGC could be attributed to iron oxide bands (JCPDS No. 19-0629) (Macías-Martínez et al., 2016; Atul et al., 2019). The presence of all the peaks in the LPGC XRD pattern showed the formation of the desired porous graphitic carbon. In addition, the graphitic structure was also demonstrated by Raman spectroscopy. As can be seen in **Figure 3B**, two peaks were present which belong to the D-band and G-band in the Raman spectra of all samples. Basically, the D-band (near $1,350 \text{ cm}^{-1}$) exhibits additional first-order bands, corresponding to defect sites or disordered sp^2 -hybridized carbon atoms of graphite and the G-band (near $1,580 \text{ cm}^{-1}$) associated with the zone-center phonon of sp^2 -bonded carbon atoms (Gong et al., 2017; Li et al., 2018). In LPGC Raman spectra, the intensity of the D-band was lower than other samples, it may be attributable to the fact that the amorphous structure in LPGC was reduced, and instead there was the formation of another structure. In addition, in comparison with other samples, it was notable that Raman spectra of LPGC showed a peak at the wavenumber of $2,685 \text{ cm}^{-1}$, which corresponds to the 2D-band—a signature of the graphitic carbon (Li et al., 2018). This indicated that the Raman spectrum of LPGC is referring to its graphitic portion. Generally, the intensity ratio of the D-band to G-band (I_D/I_G) was used as an useful parameter to determine the degree of order or disorder in crystalline structures of carbonaceous materials (Sadezky et al., 2005). The I_D/I_G values of LPGC were relatively low (0.48) compared with that of C/LBC (1.07) and BC (1.22). In short, the XRD and Raman spectra analysis confirmed that after two-step modification, the LPGC was successfully converted into porous biochar containing graphitic carbon.

N_2 Adsorption-Desorption Isotherms

N_2 adsorption-desorption isotherms and the porosity distribution of LPGC are shown in **Figure 3C**. Based on the International Union of Pure and Applied Chemistry (IUPAC) classification, the adsorption/desorption isotherm of LPGC belongs to Type-IV isotherm. It can be seen that the isotherm curve showed a hysteresis loop in the relative vapor pressure range of 0.4–1.0 bar, which demonstrated the presence of a hierarchical micro/mesoporous system on the surface of LPGC (Abo El Naga et al., 2019). This was further confirmed by the Barrett-Joyner-Halenda (BJH) pore-size distribution result. As can be observed in **Figure 3D**, the pore sizes of LPGC were allocated in a range of 1–133 nm, focused between 1.6 and 18.7 nm. The N_2 adsorption with the pore diameter distribution curves of C/LBC and BC are shown in **Figure S1**. The corresponding porosity data of LPGC and comparison samples are listed in **Table 1**. After a process of pyrolysis at 900°C , the BET surface area of LPGC was 457.4

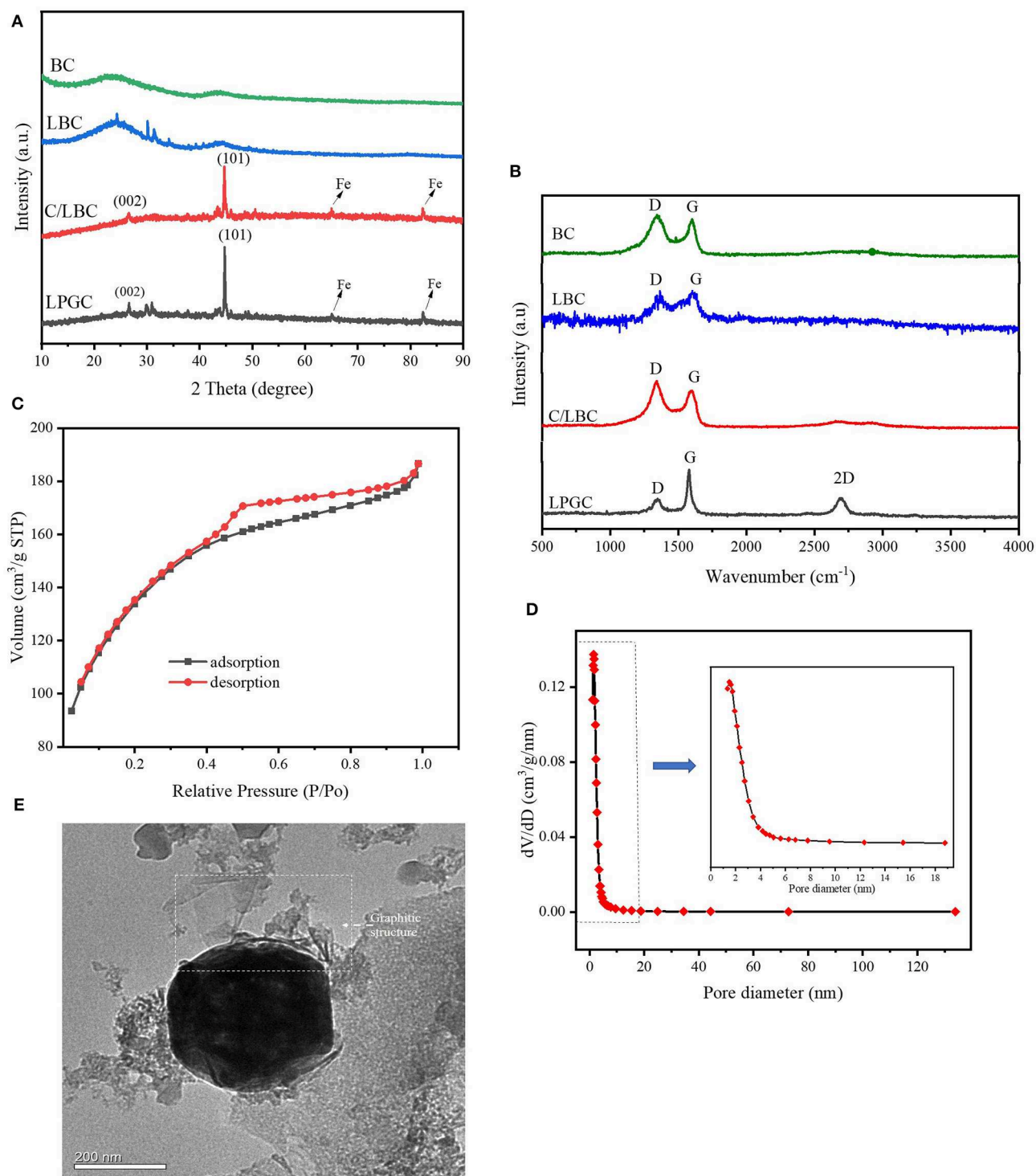


FIGURE 3 | (A) XRD patterns and **(B)** Raman spectra of LPGC and other samples; **(C)** N₂ adsorption-desorption isotherm, **(D)** pore size distribution, and **(E)** transmission electron microscopy (TEM) image of LPGC sample.

$\text{m}^2 \text{g}^{-1}$, while those of C/LBC and BC were 175.8 and 426.7 $\text{m}^2 \text{g}^{-1}$, respectively. Kim et al. (2012) carried out research on the influence of pyrolysis temperature on physicochemical

properties of biochar obtained from the pyrolysis of pitch pine (*Pinus rigida*). The study reported that at different pyrolysis temperatures, the *Pinus rigida* sawdust derived biochar possessed

TABLE 1 | Parameters describe the surface area and pore structure of LPGC and comparison samples.

Samples	Isotherms type	BET surface area (m ² g ⁻¹)	Total pore volume (cm ³ g ⁻¹)	Micropore volume (cm ³ g ⁻¹)	Mesopore volume (cm ³ g ⁻¹)	Ratio of mesopore on total pore volume (%)	Average pore diameter (nm)
LPGC	IV	457.4	0.288	0.143	0.145	50.3	2.524
C/LBC	IV	175.8	0.141	0.049	0.092	65.2	3.214
BC	I	426.7	0.265	0.154	0.111	41.8	2.449

different BET surface areas with an increasing trend (2.9, 4.8, and 175 m² g⁻¹, corresponding with the pyrolysis temperature at 300, 400, and 500°C, respectively). Tan et al. (2015) also confirmed that pyrolytic temperature plays a significant role in changing biochar characteristics. In this study, the BC sample without chemical activation obtained a relatively high BET surface area (426.7 m² g⁻¹), which might be due to the influence of a high pyrolysis temperature. Furthermore, it can be seen from the SEM images (**Figures 2C,D**), that plenty of nano particles appeared on the LPGC and C/LBC surface, which might block the small pores on their surfaces. In addition, in **Figure 3C** there is the appearance of an “ink bottle” between the isotherm adsorption—desorption curves of LPGC. It can be hypothesized that there were micropores inside of mesopores resulting in the process of N₂ desorption, thus, after N₂ liquid in the mesopores desorbed, the N₂ gas bound in the micropore would suddenly escape. By analyzing the BET results, the surface area of the C/LBC (one-step activated) was significantly decreased while the surface area of LPGC (two-step activated) insignificantly increased, compared with the BET surface of no-treated biochar (BC).

XPS Analysis

To explore the surface chemical compositions of the as-prepared samples, X-ray photoelectron spectroscopy (XPS) was applied. **Figure 4A** shows the survey spectra of LPGC, C/LBC, LBC, and BC samples. It can be observed that C, O, N, K, and Fe in the XPS spectrum of LBC and C/LBC were present, which is consistent with the EDS characterization results. **Figures 4B–E** shows the high-resolution (H-R) C 1s and O 1s XPS spectra of as-prepared samples. The H-R XPS spectrum of Fe 2p for LPGC and C/LBC are presented in **Figure 4F**.

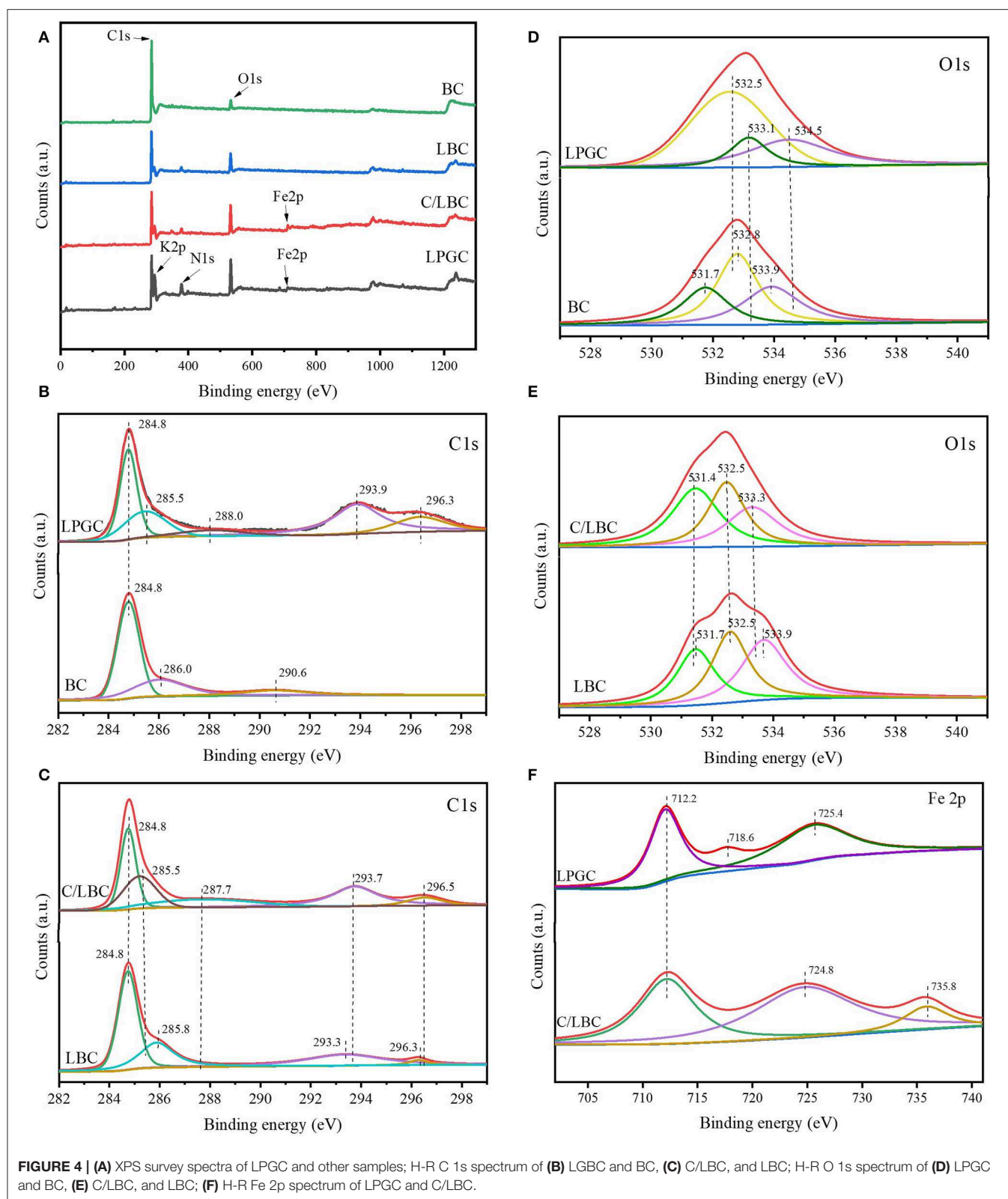
Regarding the C 1s, as can be seen in **Figures 4B,C**, the peak located at 284.8 eV corresponded to the C-C bonds with a sp² hybridization zone and appeared in all samples. The peak at 285.5 eV was associated with the contribution of both C-O and C-OH functional groups (Rojas et al., 2016) and can only be observed at LPGC and C/LBC. There were other peaks at 287.7, 293.7, and 296.5 eV in the C/LBC H-R C 1s XPS spectrum which can be ascribed to C-O, C=C, O=C-O, and π-π* “shake-up” satellites characteristic of graphite-like carbon (Chang et al., 2019). Those peaks then slightly shifted to higher binding energy in the C 1s spectrum of LPGC (288.0, 293.9, and 296.5 eV). This finding suggested that the changes in electron cloud density in the carbon atoms, were likely due to the more graphitic structure of LPGC compared with C/LBC. For the O 1s, XPS spectra for all samples are shown in **Figures 4D,E**. There was a peak at 531.7 eV in BC and LBC, which represented surface OH groups (Lu et al., 2018), but it did not present in C/LBC and LPGC,

instead, there was the presence of a peak at 532.5 eV (in both LPGC and C/LBC). This peak can be attributed to the signal of C-O/C=O bonds with a larger contribution from C-O bonds than from C=O bonds. The next peaks at 533.1 eV in LPGC and 533.3 eV in C/LBC corresponded to C-OH bonds, while the peak at 534.5 eV, only seen in LPGC-, was associated with oxygen in water molecules (Rojas et al., 2016). Additionally, the H-R XPS spectrum for Fe 2p of LPGC (**Figure 4F**) shows two peaks around the binding energy of 712.2 and 725.4 eV, which were ascribed to Fe 2p_{3/2} and Fe 2p_{1/2}, respectively (Gao et al., 2017), and the peak at 718.6 eV was attributed to the satellite peak of Fe (Li et al., 2019). For C/LBC, the peak at 712.2 eV was also observed on the Fe 2p spectrum, while the peaks at 724.8 eV could be assigned to Fe 2p_{1/2} (Li et al., 2019) and the peak at 735.8 eV presented a contribution of Fe³⁺ (Peña et al., 2019). The XPS results indicated that the surface of LPGC was significantly changed by using a two-step modification process. The XPS of BC and LBC only showed the existence of the sp² hybridization zone, while multiple polar functional groups could be observed on the C/LBC and LPGC surface which might contribute to the formation of a porous graphitic structure of these samples.

DCF Adsorption Kinetics

Adsorption kinetics display a strong relationship with the physical and/or chemical characteristics of the biochar (Tan et al., 2015). The adsorption kinetics of DCF onto LPGC, C/LBC, LBC, and BC are displayed in **Figure 5A**. The uptake of DCF onto LPGC and C/LBC increased rapidly in the first 4 h, then gradually increased from 4 to 12 h, while the adsorption capacity of LBC and BC were insignificant. The maximum adsorption capacity was reached at about 24 and 20 h for LPGC and C/LBC, respectively; and 8 h for LBC and BC. Twenty-four hours was therefore chosen as the reaction time, while LPGC and BC were chosen as adsorbents in further adsorption experiments.

To further understand the mechanism of adsorption, two conventional kinetic models (Pseudo first-order and Pseudo second-order) were used to analyze and simulate the experiment results of DCF adsorption. The model descriptions are given in the **Supplementary Materials**. The kinetic parameters and correlation coefficients (*R*²) of two kinetic models are listed in **Table 2**. As can be seen, the determined coefficients of the Pseudo second-order model were higher than those of the Pseudo first-order model for all samples. In addition, the simulated adsorption capacity results, which were provided by the Pseudo second-order model, were very close to the experimental data. It further confirmed the feasibility of the



Pseudo second-order model to fit the kinetic DCF adsorption results. The trend indicated that the chemisorption might be the primary mechanism for the uptake of DCF onto LGBC and other

samples. It is worth noting that the DCF adsorption capacity of K_2FeO_4 -treated samples (112.1 and 91.3 $mg\ g^{-1}$ corresponding to LPGC and C/LBC) are much higher than those of non-

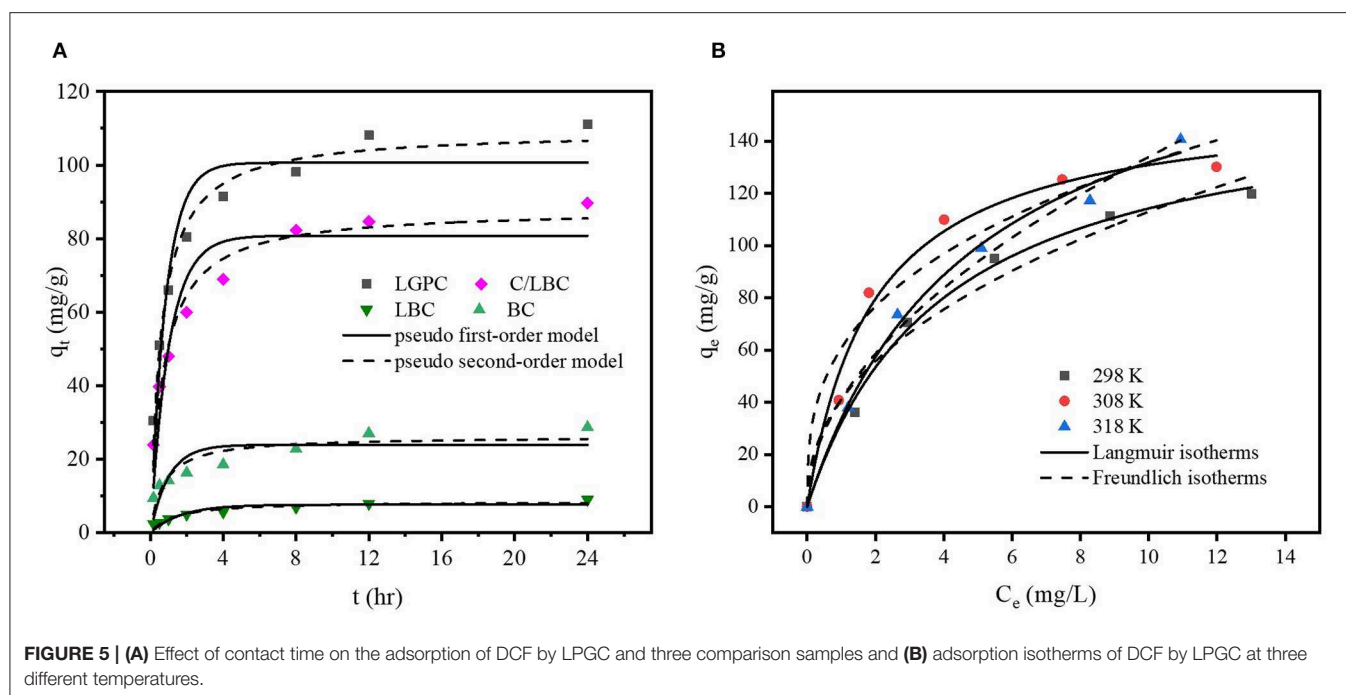


TABLE 2 | Kinetic parameters adsorption of DCF on LPGC and comparison samples.

Absorbents	$q_{e,exp}$ ($mg\ g^{-1}$)	Pseudo-first-order model			Pseudo-second-order model		
		$q_{e,1}$ ($mg\ g^{-1}$)	k_1 ($t\ h^{-1}$)	R^2	$q_{e,2}$ ($mg\ g^{-1}$)	k_2 ($g\ mg^{-1}\ h^{-1}$)	R^2
LPGC	111.09	105.4	1.17	0.90	112.1	0.015	0.98
C/LBC	89.66	85.3	0.97	0.87	91.3	0.015	0.96
LBC	9.00	8.3	0.59	0.80	9.2	0.091	0.90
BC	28.75	26.2	1.00	0.63	28.3	0.053	0.80

Experimental conditions: $m/V = 0.1\ mg/mL$, $C_0 = 20\ mg\ L^{-1}$, $T = 298\ K$, $pH = 6.5$.

TABLE 3 | Isotherm model parameters of DCF adsorption by LPGC and BC at three temperatures.

Adsorbents	Temperature (K)	Langmuir			Freundlich		
		q_{max} (mg/g)	K_L (L/mg)	R^2	K_F [(mg/g)/ (mg/L) $^{1/n}$]	n	R^2
LPGC	298	159.7	0.25	0.98	41.11	0.44	0.91
	308	165.9	0.52	0.96	60.72	0.33	0.83
	318	195.1	0.21	0.98	41.08	0.51	0.97
BC	298	35.2	0.36	0.93	14.32	0.26	0.96
	308	37.4	0.33	0.96	14.55	0.28	0.98
	318	46.3	0.30	0.98	16.84	0.29	0.99

Experimental conditions: $m/V = 0.1\ mg/mL$, C_0 ranged $5\text{--}25\ mg\ L^{-1}$, $T = 298, 308, 318\ K$, $pH = 6.5$, $t = 24\ h$.

K_2FeO_4 -treated samples (9.2 and $28.3\ mg\ g^{-1}$ corresponding to LBC and BC). Furthermore, the results of the characterization of adsorbents confirmed the presence of Fe iron particles on the LPGC and C/LBC surface. Thus, Fe plays an important role in the removal efficiency of LPGC and C/LBC toward DCF, and the effect of Fe-based technologies for pharmaceutical removal from water is further discussed in a study by Liu et al. (2016).

DCF Adsorption Isotherm

To explore the adsorption phenomena in the liquid phase at equilibrium, adsorption isotherm experiments were conducted. **Figure 5B** shows the uptake of DCF by LPGC at three different temperatures and **Figure S2** illustrates the DCF adsorption by BC at three temperatures (298, 308, and 318 K, respectively). As can be seen, the uptake of DCF onto LPGC significantly increased with low initial DCF concentration. It might be the result of numerous active sites located on the surface of the adsorbent, which was easy to access. However, when the concentration of the

DCF solution increased, the adsorption capacity of LPGC tended to decrease. This revealed that the active sites became fewer when the reaction state was near the equilibrium point. Two adsorption isotherm models, namely Langmuir and Freundlich, were used to investigate the mechanism of the adsorption equilibrium. Theoretical aspects regarding adsorption isotherm models are given in the **Supplementary Materials**. The relevant results simulated from those equations are listed in **Table 3**. The Langmuir parameter q_{max} corresponds to the monolayer's maximum adsorption capacity, while the Freundlich constant K_F roughly reflects the adsorption capacity for comparing multiple adsorbent-adsorbate systems (Tong et al., 2019). Results in **Table 3** indicate that the Langmuir model exhibited a higher correlation coefficient value than the Freundlich model and it could be assumed that the DCF adsorption by LPGC was a monolayer reaction, which may occur on homogeneous

adsorption sites. Furthermore, the adsorption isotherm results of BC were fitted to both models with an insignificant difference between the R^2 values of the Langmuir and Freundlich models. It was also reported that q_{\max} tended to be related with the reaction temperature; the higher the q_{\max} value, the higher the heat of sorption. This could be the base for the formation of stronger bonds (Ofomaja et al., 2010). In this study, the simulated maximum adsorption capacity (q_{\max}) of the Langmuir model increased when experimental temperature increased (from 298 to 318 K), which indicated that a higher temperature could be more favorable for the uptake of DCF onto LPGC.

DCF Adsorption Thermodynamic

The thermodynamic parameters were calculated from the data in Figure 5B by Equation (5s) and (6s) (Supplementary Materials). The results are shown in Table 4. The values of ΔG° were found to be negative at all temperatures, which revealed that the whole process was spontaneous. The positive value of ΔH° implied that the adsorption reaction was an endothermic process, which was suggested by the experimental results that the adsorption capacity of DCF increased when the temperature was raised. Furthermore, the positive value of ΔS° suggested that the randomness of the adsorbate-adsorbent interface could be increased during the reaction process.

TABLE 4 | Thermodynamic parameters of DCF adsorption on LPGC.

T (K)	$\ln K^0$	ΔG° (kJ mol ⁻¹)	ΔS° (J K ⁻¹ mol ⁻¹)	ΔH° (kJ mol ⁻¹)
298	1.22	-3.02	0.015	1.562
308	1.36	-3.50		
318	1.26	-3.34		

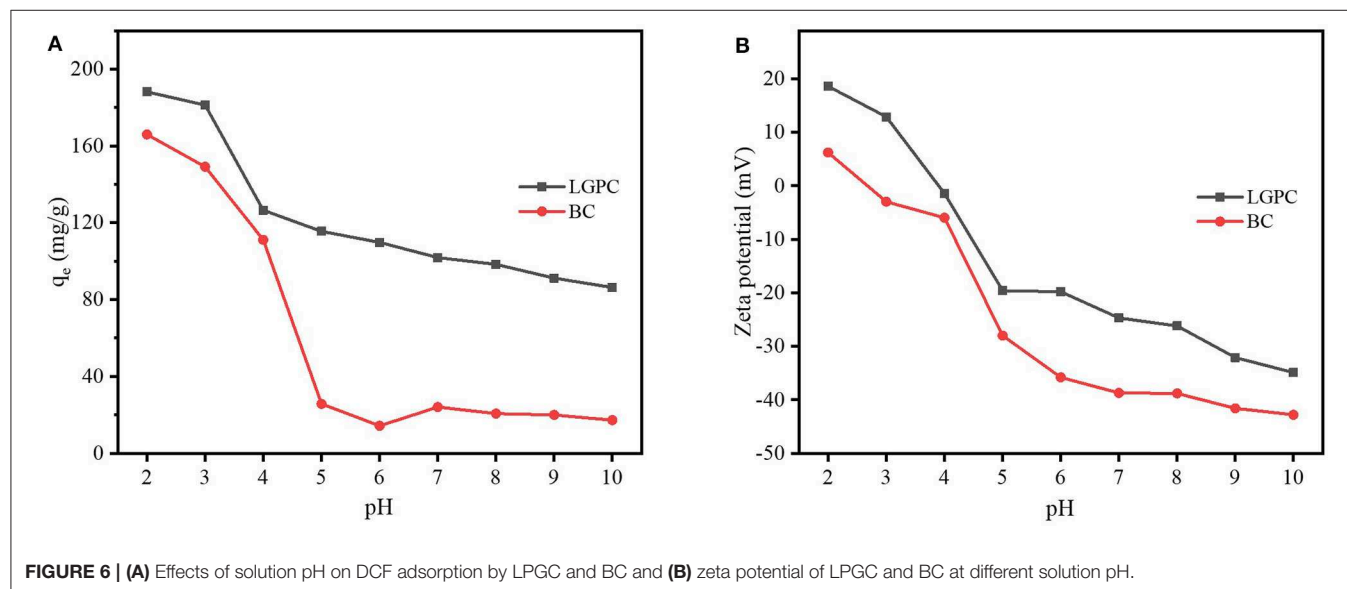
Experimental conditions: $m/V = 0.1$ mg/mL, $C_0 = 20$ mg L⁻¹, $T = 298, 308, 318$ K, $pH = 6.5$, $t = 24$ h.

Impact of Solution pH

The value of solution pH is an important parameter for investigating the adsorption mechanism, since adsorption is a surface-controlled process and the variation of the pH value can change the surface charge of the adsorbent or the allocation of adsorbate in solution as well. Figure 6A shows the impact of initial pH solutions on DCF adsorption by LPGC and BC with a pH value ranging from 2.0 to 10.0. The results showed that the adsorption capacity was relatively high when the pH value was 2 and 3. It was then dramatically decreased at pH = 4.0 with LPGC and pH = 5.0 with BC. This phenomenon was consistent with the results of zeta potential (Figure 6B). The zeta potential value of LPGC and BC changed from positive to negative when the pH value increased. It demonstrated a negative charge on the LPGC surface over a wide range of pH values, and this surface charged value decreased with the increase of pH values. The zero point of charge (pH_{zpc}) was found to be equal to 4.0, and at this point the LPGC surface became negatively charged. The DCF molecules could then be isolated to the anionic form, creating an electrostatic repulsive interaction between the negative charge of DCF anions and LGBC, which may result in a lower adsorption capacity of DCF onto adsorbents (Figure 6A). In addition, it was reported that the solubility of DCF was low (<2.37 mg/L) at pH values lower than its pK_a (4.15), indicating a presence of DCF in its neutral form (Bhadra et al., 2016; Larous and Meniai, 2016). It might explain the decreasing trend in adsorption capacity when the pH value increased above 4.2 ($pH > pK_a$), since the solubility of DCF became higher.

Impact of Ionic Strength

It was reported that wastewater contains not only organic contaminants but also various salts with ionic strengths, which may influence the elimination of contaminants (Xu et al., 2012). NaCl was chosen to explore the impact of ionic strength on the removal of DCF by LPGC due to its widespread presence in wastewater as well as other water sources. A series of experiments



were conducted by adding different concentrations of NaCl into DCF compiled adsorbents (LPGC and BC), the results of which are shown in **Figure 7**. As can be seen, DCF adsorption capacity was improved in the presence of NaCl, and it was more obvious with adsorbent LPGC (q_e increased 8.83% when added NaCl 0.1 M into the solution). The enhanced coefficient activity of hydrophobic organic compounds that resulted in their solubility reduction, might be due to the increase in ionic strength, which was beneficial for the adsorption process (Zhang et al., 2010). In addition, Wu L. et al. (2019) used NaCl 10 mM as the background ionic strength during their experiment to enhance adsorption capacity of adsorbents, confirming its favorable role for DCF adsorption.

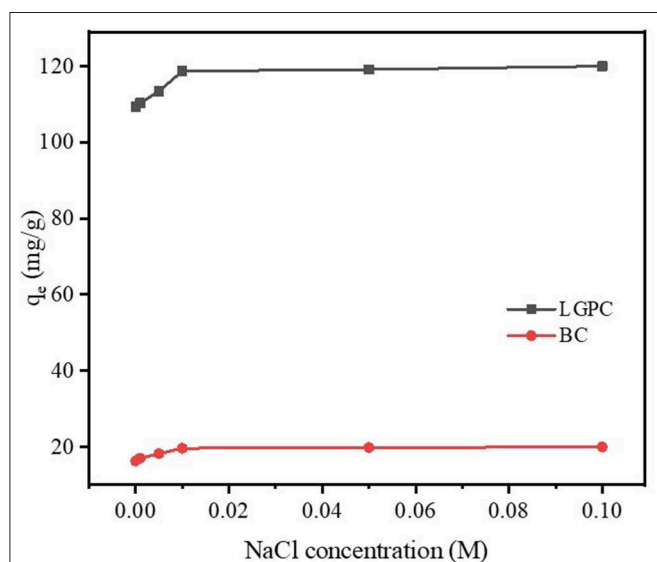


FIGURE 7 | Effect of the ionic strength on DCF adsorption by LPGC and BC.

Impact of Background Electrolyte

Several types of background electrolyte ions such as Na^+ , K^+ , Mg^{2+} , Ca^{2+} , Cl^- , NO_3^- , SO_4^{2-} , and PO_4^{3-} were simultaneously presented with contaminants in wastewater, which may influence the removal efficiency of contaminants from wastewater effluents. Thus, the impact of those background electrolytes on DCF adsorption was studied in the presence of cations (Na^+ , K^+ , Mg^{2+} , and Ca^{2+}) and anions (Cl^- , NO_3^- , SO_4^{2-} , and PO_4^{3-}) at three different concentrations (0.001, 0.01, and 0.1 M) for each type of ion; the results are shown in **Figure 8**. As can be seen in **Figure 8A**, the cations supported the adsorption process and the adsorption capacity increased with higher concentrations of cations. It may be due to the fact that the surface charge of DCF molecules at the studied pH (≈ 6.5) was negative, which led to an electrostatic interaction between the cations and the negatively charged DCF. On the contrary, the anions might hinder the adsorption of DCF onto LPGC (**Figure 8B**). Obviously, the adsorption capacity significantly declined in the presence of anions NO_3^- and PO_4^{3-} . The phenomena might be mainly attributed to the occupation of NO_3^- and PO_4^{3-} for limited adsorption sites on the LPGC surface, which resulted in a decrease in its adsorption capacity.

Comparisons Between Studied Materials and Different Biomass-Derived Adsorbents

Table 5 provides an overview of different biomass-derived adsorbents used for DCF adsorption in terms of adsorption capacity. A straightforward comparison may not be objective since the experimental condition and the synthesized methodologies were different. Though, from the perspective of the efficiency of adsorbents, the comparison may provide a perception of the performance of a porous biochar containing graphitic carbon, obtained from the lignin content of pitch pine biomass (LPGC). From **Table 5**, it can be shown that the LPGC presents a significant adsorption capacity for DCF compared

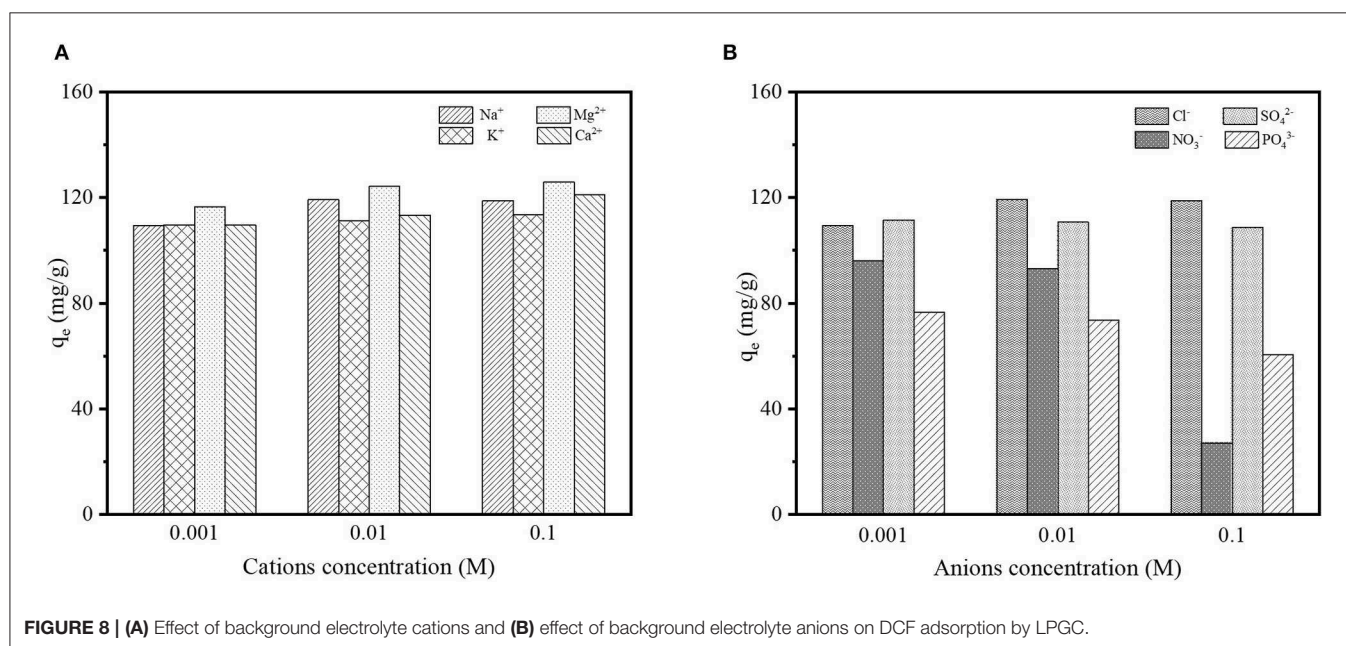
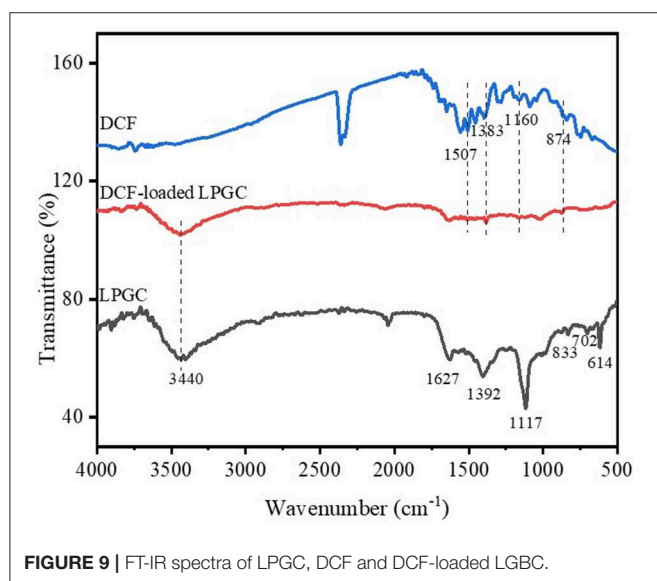


FIGURE 8 | (A) Effect of background electrolyte cations and **(B)** effect of background electrolyte anions on DCF adsorption by LPGC.

TABLE 5 | Comparison of DCF adsorption capacity with other biochar derived adsorbents.

Material	BET surface area (m ² /g)	Adsorption ambient conditions				Maximum adsorption capacity (mg g ⁻¹)	References
		pH	Temperature (K)	Adsorbent dose (g)	Initial concentration of DCF solution (mg L ⁻¹)		
Rice straw	287.8	7	293	0.3	15.9	277.8	Xia et al., 2019
Pinewood	13.3	6.5	298	2	0.5	1.1	Lonappan et al., 2019
Pig manure	43.5	6.5	298	2	0.5	4.1	Lonappan et al., 2019
Sugarcane	1145.0	2	298	0.4	50.0	315.0	Abo El Naga et al., 2019
Isabel grape	2.0	5	295	0.0005	10.0	11.1	Antunes et al., 2012
Potato peel	866	5	–	10	50.0	68.5	Bernardo et al., 2016
Cocoa shell	619	7	298	2.5	100.0	63.5	Saucier et al., 2015
Tea waste	865.4	6.47	–	0.3	30.0	62.5	Malhotra et al., 2018
LPGC	457.4	6.5	298	0.05	20.0	159.7	This study
C/LBC	175.8	6.5	298	0.05	20.0	91.3	This study
BC	426.7	6.5	298	0.05	20.0	35.2	This study

**FIGURE 9** | FT-IR spectra of LPGC, DCF and DCF-loaded LGBC.

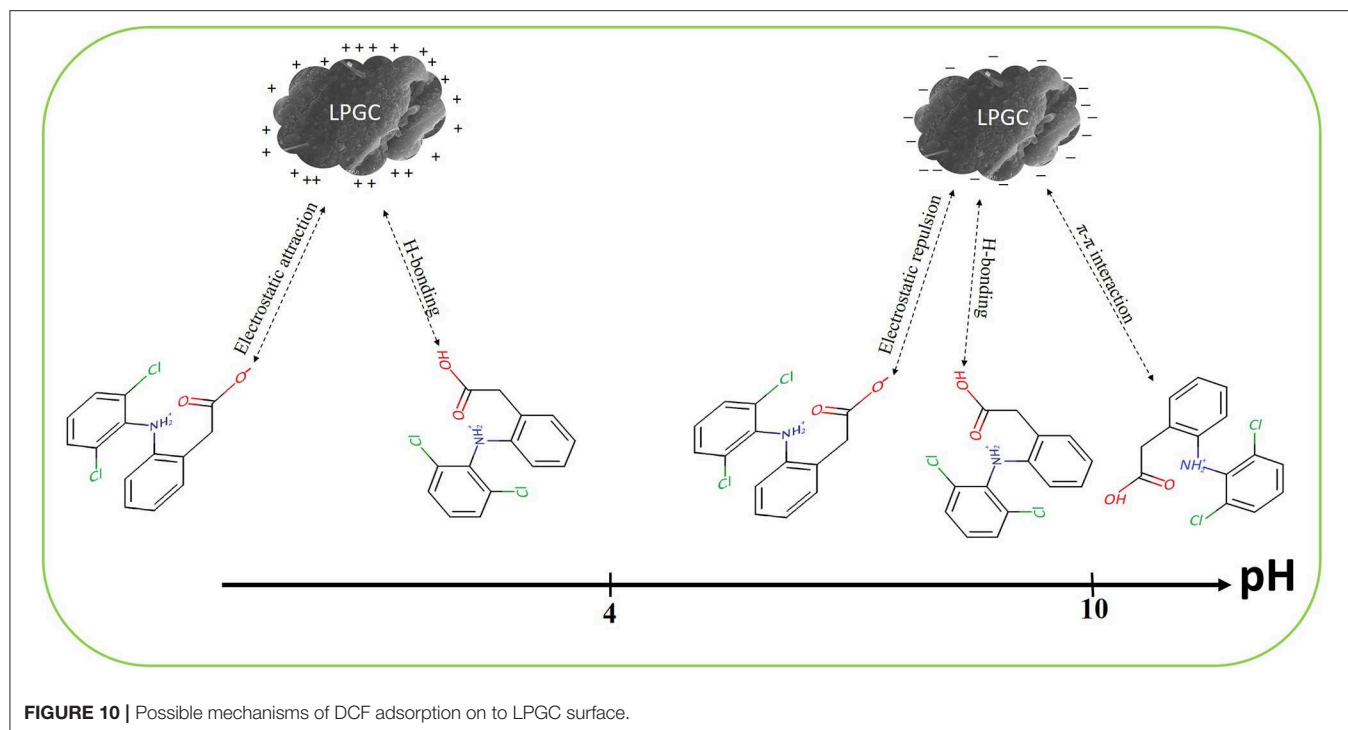
to the other biomass derived adsorbents such as pine wood, pig manure, Isabel grape bagasse, potato peel, cocoa shell, and tea waste, etc. However, the performance of LPGC on DCF adsorption was weaker than some other adsorbents such as rice straw (277.78 mg g⁻¹) or sugarcane bagasse (315.0 mg g⁻¹). Nevertheless, the dosage of LPGC used in adsorption experiments was small compared with rice straw and sugarcane bagasse. Therefore, LPGC can still be evaluated as a potential adsorbent for the efficient removal of DCF from wastewater.

Possible Mechanisms

DCF is known as a hydrophobic compound with a weak acidity (pK_a is around 4.15). As can be seen in section Impact of Solution pH, the higher adsorption capacity of LPGC was observed at an acidic pH due to the interaction between adsorbent microparticles and ionizable micropollutants through electrostatic attraction or repulsion. The adsorption capacity increased with the decrease of solution pH and this phenomenon

can be explained by the repulsive electrostatic interactions between the negative surface charge of LPGC and the negatively charged anionic form of DCF (-COO⁻) (Liang et al., 2019).

To investigate the possible adsorption mechanisms of the removal of DCF by LPGC, the FT-IR spectra of LPGC before and after DCF adsorption are shown in **Figure 9** (scanning ranged from 500 to 4,000 cm⁻¹). As can be seen from the FT-IR spectra, the left half region above 2,000 cm⁻¹ usually presents few common bands for all materials, while the right half region shows a greater number of bands as well as their intensity variability. Among them, the broad peak at 3,440 cm⁻¹ of original LPGC represented for the stretching vibration of O-H groups (dos Santos et al., 2019); and the peak located at 1,632 and 1,392 cm⁻¹, were due to the skeletal vibration of aromatic C=C bonds (Jiang et al., 2015; Zhang et al., 2019). It can be seen that quite a few new peaks appeared at 1,507, 1,383, 1,160, and 874 cm⁻¹, confirming the successful adsorbed DCF molecules on the surface of LPGC. Moreover, after DCF adsorption, the peak at 1,627 cm⁻¹ shifted to 1,632 cm⁻¹ and these peaks corresponded to the skeletal vibration of C=C bonds. This revealed the presence of a π - π interaction between aromatic rings of DCF and LPGC in the adsorption process (Wang et al., 2014). Moreover, Abo El Naga et al. (2019) reported that in relatively high pH conditions (pH \geq 10), the adsorbent still had a considerable adsorption capacity, which might be attributed by the π - π electron donor acceptor interaction. Compared with the DCF adsorption capacity of LPGC at pH = 10, q_e reached a value of 86.3 mg g⁻¹, which confirmed that the π - π interaction might be the mechanism for DCF removal by LPGC. It can be seen that the wavenumber peak at 1,117 cm⁻¹ was prominent on LPGC, which attributed to C-O stretches (Guerrero et al., 2010), but it was no longer seen on DCF-loaded LPGC. It might shift to a small peak at 1,022 cm⁻¹. A similar phenomenon appeared at the 614 cm⁻¹ peaks and could be assigned for COO⁻ stretching (Arivuselvi and Kumar, 2015). The intelligible changes indicated that the interaction between DCF microparticles and oxygen-containing functional groups of LPGC occurred. These functional groups might be H-bonding between the DCF and LPGC. Thus, it could be hypothesized that H-bonding interaction, along with



electrostatic interaction and π - π interaction were the possible mechanisms of DCF adsorption by LPGC and the adsorption mechanism can be illustrated in **Figure 10**.

CONCLUSION

In the present work, a porous biochar containing graphitic carbon (LPGC) was successfully synthesized from structurally separated pitch pine sawdust biomass using a two-step activation process. The H_2SO_4 treatment separated the biomass into a lignin component whereas K_2FeO_4 was adopted as an activated agent and catalyst for carbonization and graphitization processes, respectively. The one-step H_2SO_4 -treated sample, K_2FeO_4 -treated sample, and non-treated sample were used to investigate the advanced characteristics of as-proposed material. The obtained LPGC has a micro-mesoporous structure with a relatively high surface area ($457.4 \text{ m}^2 \text{ g}^{-1}$), as well as the presence of a graphitic structure. Through these characteristics, LPGC showed an excellent adsorption capacity for DCF adsorption from an aqueous solution. Result from the Langmuir isotherm model indicated that the maximum adsorption capacity of LPGC for DCF was 159.7 mg g^{-1} at experimental conditions of temperature 298 K, contact time 24 h, and pH 6.5 and this is a considerable DCF adsorption capacity compared with other biomass-derived adsorbents. The kinetic and isotherm parameters were highly fitted with the Pseudo second-order kinetic model and Langmuir isotherms, respectively. The results of the thermodynamic study demonstrated that the DCF adsorption by LPGC process was spontaneous and endothermic. The adsorption capacity was significantly influenced by the pH solution, followed by an increasing trend with the decrease of pH value and obtained maximum adsorption capacity at the value

of pH = 2.0. The adsorption process by LPGC was enhanced with the presence of NaCl in the DCF solution. In addition, the study about the effect of background electrolytes indicated that the adsorption capacity was positively affected by the presence of cations (Na^+ , K^+ , Ca^{2+} , and Mg^{2+}) but was negatively affected by the presence of anions (Cl^- , NO_3^- , SO_4^{2-} , and PO_4^{3-}). The possible adsorption mechanism that was expected, is that the H-bonding interaction, electrostatic interaction, and π - π interaction took part in the process of DCF removal from the solution by LPGC. Finally, from a sustainability perspective, the synthesis process of LPGC can be assessed as an advantageous method due to its ability to provide a cost-effective and efficient adsorbent for the removal of DCF from aqueous solutions.

DATA AVAILABILITY STATEMENT

The raw data supporting the conclusions of this article will be made available by the authors, without undue reservations, to any qualified researcher.

AUTHOR CONTRIBUTIONS

NT conducted the experimental work, wrote the first draft, and corrected the final manuscript. YL and SL supervised the work. HB, PZ, and MD further analyzed the data and worked on the subsequent version of the manuscript. XT and ML contributed to thorough discussions of the work.

FUNDING

This work was financially supported by the NSFC of China (51521006, 51609268, 51809019, and 51809089) and the Natural

Science Foundation of Hunan Province, China (2018JJ3096 and 2018JJ3040).

ACKNOWLEDGMENTS

The authors thank the Key Laboratory of Environmental Biology and Pollution Control, College of Environment Science and

Engineering—Hunan University for their support during the experiment process.

SUPPLEMENTARY MATERIAL

The Supplementary Material for this article can be found online at: <https://www.frontiersin.org/articles/10.3389/fchem.2020.00274/full#supplementary-material>

REFERENCES

- Abo El Naga, A. O., El Saied, M., Shaban, S. A., and El Kady, F. Y. (2019). Fast removal of diclofenac sodium from aqueous solution using sugar cane bagasse-derived activated carbon. *J. Mol. Liquids* 285, 9–19. doi: 10.1016/j.molliq.2019.04.062
- Acuña, V., Ginebreda, A., Mor, J. R., Petrovic, M., Sabater, S., Sumpter, J., et al. (2015). Balancing the health benefits and environmental risks of pharmaceuticals: diclofenac as an example. *Environ. Int.* 85, 327–333. doi: 10.1016/j.envint.2015.09.023
- Ahmed, M. J., and Hameed, B. H. (2018). Removal of emerging pharmaceutical contaminants by adsorption in a fixed-bed column: a review. *Ecotoxicol. Environ. Safe.* 149, 257–266. doi: 10.1016/j.ecoenv.2017.12.012
- Alder, A. C., Bruchet, A., Carballa, M., Clara, M., Joss, A., Löffler, D., et al. (2006). “Consumption and occurrence,” in *Human Pharmaceuticals, Hormones and Fragrances. The Challenge of Micropollutants in Urban Water Management*, eds T. A. Ternes and A. Joss (London: IWA Publishing), 15–54.
- Alidina, M., Li, D., Ouf, M., and Drewes, J. E. (2014). Role of primary substrate composition and concentration on attenuation of trace organic chemicals in managed aquifer recharge systems. *J. Environ. Manag.* 144, 58–66. doi: 10.1016/j.jenvman.2014.04.032
- Alves, R. N., Maulvault, A. L., Barbosa, V. L., Cunha, S., Kwadijk, C. J. A. F., Álvarez-Muñoz, D., et al. (2017). Preliminary assessment on the bioaccessibility of contaminants of emerging concern in raw and cooked seafood. *Food Chem. Toxicol.* 104, 69–78. doi: 10.1016/j.fct.2017.01.029
- Antunes, M., Esteves, V. I., Guégan, R., Crespo, J. S., Fernandes, A. N., and Giovanela, M. (2012). Removal of diclofenac sodium from aqueous solution by Isabel grape bagasse. *Chem. Eng. J.* 192, 114–121. doi: 10.1016/j.cej.2012.03.062
- Arivuselvi, R., and Kumar, A. R. (2015). Growth of non linear optical zinc thiosemicarbazide sulfate single crystal and its studies on FT-Raman, XRD, mechanical and dielectric studies. *Int. J. ChemTech Res.* 8, 1304–1309. Available online at: [http://sphinxσαι.com/2015/ch_vol8_no3/6/\(1304-1309\)V8N3.pdf](http://sphinxσαι.com/2015/ch_vol8_no3/6/(1304-1309)V8N3.pdf)
- Atul, K. M., Sharma, A., Maurya, I. K., Thakur, A., and Kumar, S. (2019). Synthesis of ultra small iron oxide and doped iron oxide nanostructures and their antimicrobial activities. *J. Taibah Univ. Sci.* 13, 280–285. doi: 10.1080/16583655.2019.1565437
- Batt, A. L., Furlong, E. T., Mash, H. E., Glassmeyer, S. T., and Kolpin, D. W. (2017). The importance of quality control in validating concentrations of contaminants of emerging concern in source and treated drinking water samples. *Sci. Total Environ.* 579, 1618–1628. doi: 10.1016/j.scitotenv.2016.02.127
- Benson, R., Conerly, O. D., Sander, W., Batt, A. L., Boone, J. S., Furlong, E. T., et al. (2017). Human health screening and public health significance of contaminants of emerging concern detected in public water supplies. *Sci. Total Environ.* 579, 1643–1648. doi: 10.1016/j.scitotenv.2016.03.146
- Bernardo, M., Rodrigues, S., Lapa, N., Matos, I., Lemos, F., Batista, M. K. S., et al. (2016). High efficacy on diclofenac removal by activated carbon produced from potato peel waste. *Int. J. Environ. Sci. Technol.* 13, 1989–2000. doi: 10.1007/s13762-016-1030-3
- Bhadra, B. N., Seo, P. W., and Nhung, S. H. (2016). Adsorption of diclofenac sodium from water using oxidized activated carbon. *Chem. Eng. J.* 301, 27–34. doi: 10.1016/j.cej.2016.04.143
- Chang, R., Sohi, S. P., Jing, F., Liu, Y., and Chen, J. (2019). A comparative study on biochar properties and Cd adsorption behavior under effects of ageing processes of leaching, acidification and oxidation. *Environ. Pollut.* 254:113123. doi: 10.1016/j.envpol.2019.113123
- Chatterjee, S., Clingenpeel, A., McKenna, A., Rios, O., and Johs, A. (2014a). Synthesis and characterization of lignin-based carbon materials with tunable microstructure. *RSC Adv.* 4, 4743–4753. doi: 10.1039/C3RA46928J
- Chatterjee, S., Jones, E. B., Clingenpeel, A. C., McKenna, A. M., Rios, O., McNutt, N. W., et al. (2014b). Conversion of lignin precursors to carbon fibers with nanoscale graphitic domains. *ACS Sustain. Chem. Eng.* 2, 2002–2010. doi: 10.1021/sc500189p
- Demir, M., Kahveci, Z., Aksoy, B., Palapati, N. K. R., Subramanian, A., Cullinan, H. T., et al. (2015). Graphitic biocarbon from metal-catalyzed hydrothermal carbonization of lignin. *Ind. Eng. Chem. Res.* 54, 10731–10739. doi: 10.1021/acs.iecr.5b02614
- dos Santos, J. M. N., Pereira, C. R., Foletto, E. L., and Dotto, G. L. (2019). Alternative synthesis for ZnFe₂O₄/chitosan magnetic particles to remove diclofenac from water by adsorption. *Int. J. Biol. Macromol.* 131, 301–308. doi: 10.1016/j.ijbiomac.2019.03.079
- Edathil, A. A., Pal, P., and Banat, F. (2017). Alginate derived porous graphitic carbon for highly efficient remediation of sulfide from wastewater. *J. Environ. Chem. Eng.* 5, 1998–2009. doi: 10.1016/j.jece.2017.04.009
- Ericson, H., Thorsén, G., and Kumblad, L. (2010). Physiological effects of diclofenac, ibuprofen and propranolol on Baltic Sea blue mussels. *Aquat. Toxicol.* 99, 223–231. doi: 10.1016/j.aquatox.2010.04.017
- Framework, E. W. (2013). *Directive 2013/39/EU of the European Parliament and of the Council of 12 August 2013 Amending Directives 2000/60/EC and 2008/105/EC as Regards Priority Substances in the Field of Water Policy Text with EEA Relevance*, Brussels.
- Gao, Y., Li, S., Li, Y., Yao, L., and Zhang, H. (2017). Accelerated photocatalytic degradation of organic pollutant over metal-organic framework MIL-53(Fe) under visible LED light mediated by persulfate. *Appl. Catal. B Environ.* 202, 165–174. doi: 10.1016/j.apcatb.2016.09.005
- Gibot, P., Schnell, F., and Spitzer, D. (2016). Enhancement of the graphitic carbon nitride surface properties from calcium salts as templates. *Microporous Mesoporous Mater.* 219, 42–47. doi: 10.1016/j.micromeso.2015.07.026
- Gong, Y., Li, D., Luo, C., Fu, Q., and Pan, C. (2017). Highly porous graphitic biomass carbon as advanced electrode materials for supercapacitors. *Green Chem.* 19, 4132–4140. doi: 10.1039/C7GC01681F
- Guerrero, P., Retegi, A., Gabilondo, N., and De la Caba, K. (2010). Mechanical and thermal properties of soy protein films processed by casting and compression. *J. Food Eng.* 100, 145–151. doi: 10.1016/j.jfoodeng.2010.03.039
- Gupta, K., Gupta, D., and Khatri, O. P. (2019). Graphene-like porous carbon nanostructure from Bengal gram bean husk and its application for fast and efficient adsorption of organic dyes. *Appl. Surf. Sci.* 476, 647–657. doi: 10.1016/j.apsusc.2019.01.138
- He, Z.-W., Liu, W.-Z., Gao, Q., Tang, C.-C., Wang, L., Guo, Z.-C., et al. (2018). Potassium ferrate addition as an alternative pre-treatment to enhance short-chain fatty acids production from waste activated sludge. *Bioresour. Technol.* 247, 174–181. doi: 10.1016/j.biortech.2017.09.073
- Heberer, T. (2002). Tracking persistent pharmaceutical residues from municipal sewage to drinking water. *J. Hydrol.* 266, 175–189. doi: 10.1016/S0022-1694(02)00165-8
- Jiang, J.-Q., Panagouloupoulos, A., Bauer, M., and Pearce, P. (2006). The application of potassium ferrate for sewage treatment. *J. Environ. Manag.* 79, 215–220. doi: 10.1016/j.jenvman.2005.06.009
- Jiang, L.-H., Liu, Y.-G., Zeng, G.-M., Xiao, F.-Y., Hu, X., Hu, X., et al. (2015). Removal of 17 β -estradiol by few-layered graphene oxide nanosheets from

- aqueous solutions: external influence and adsorption mechanism. *Chem. Eng. J.* 284, 93–103. doi: 10.1016/j.cej.2015.08.139
- Jiang, P., Deng, W., Zhou, X., Feng, J., and Liu, Z. (2019). Vapor-assisted synthesis of hierarchical porous graphitic carbon materials towards energy storage devices. *J. Power Sour.* 425, 10–16. doi: 10.1016/j.jpowsour.2019.03.117
- Jiang, X., Guo, Y., Zhang, L., Jiang, W., and Xie, R. (2018). Catalytic degradation of tetracycline hydrochloride by persulfate activated with nano FeO immobilized mesoporous carbon. *Chem. Eng. J.* 341, 392–401. doi: 10.1016/j.cej.2018.02.034
- Johnson, A. C., Dumont, E., Williams, R. J., Oldenkamp, R., Cisowska, I., and Sumpter, J. P. (2013). Do concentrations of ethinylestradiol, estradiol, and diclofenac in European rivers exceed proposed EU environmental quality standards? *Environ. Sci. Technol.* 47, 12297–12304. doi: 10.1021/es4030035
- Kim, K. H., Kim, J.-Y., Cho, T.-S., and Choi, J. W. (2012). Influence of pyrolysis temperature on physicochemical properties of biochar obtained from the fast pyrolysis of pitch pine (*Pinus rigida*). *Bioresour. Technol.* 118, 158–162. doi: 10.1016/j.biortech.2012.04.094
- Kim, M.-H., Tang, J., Jang, S.-J., Pol, V. G., and Roh, K. C. (2019). Porous graphitic activated carbon sheets upcycled from starch-based packing peanuts for applications in ultracapacitors. *J. Alloys Compd.* 805, 1282–1287. doi: 10.1016/j.jallcom.2019.05.359
- Larous, S., and Meniai, A.-H. (2016). Adsorption of diclofenac from aqueous solution using activated carbon prepared from olive stones. *Int. J. Hydrogen Energ.* 41, 10380–10390. doi: 10.1016/j.ijhydene.2016.01.096
- Letzel, M., Metzner, G., and Letzel, T. (2009). Exposure assessment of the pharmaceutical diclofenac based on long-term measurements of the aquatic input. *Environ. Int.* 35, 363–368. doi: 10.1016/j.envint.2008.09.002
- Li, L., Ma, P., Hussain, S., Jia, L., Lin, D., Yin, X., et al. (2019). FeS₂/carbon hybrids on carbon cloth: a highly efficient and stable counter electrode for dye-sensitized solar cell. *Sustain. Energy Fuels* 3, 1749–1756. doi: 10.1039/C9SE00240E
- Li, X., Liu, Y., Zeng, Z., Wang, P., Fang, Y., and Zhang, L. (2018). Investigation on tip enhanced Raman spectra of graphene. *Spectrochim. Acta A Mol. Biomol. Spectroscopy* 190, 378–382. doi: 10.1016/j.saa.2017.07.069
- Liang, X. X., Omer, A. M., Hu, Z.-H., Wang, Y. G., Yu, D., Ouyang, X.-H., et al. (2019). Efficient adsorption of diclofenac sodium from aqueous solutions using magnetic amine-functionalized chitosan. *Chemosphere* 217, 270–278. doi: 10.1016/j.chemosphere.2018.11.023
- Liu, S.-J., Liu, Y.-G., Tan, X.-F., Liu, S.-B., Li, M.-F., Liu, N., et al. (2019). Facile synthesis of MnOx-loaded biochar for the removal of doxycycline hydrochloride: effects of ambient conditions and co-existing heavy metals. *J. Chem. Technol. Biotechnol.* 94, 2187–2197. doi: 10.1002/jctb.6000
- Liu, W., Sutton, N. B., Rijnaarts, H. H. M., and Langenhoff, A. A. M. (2016). Pharmaceutical removal from water with iron- or manganese-based technologies: a review. *Crit. Rev. Environ. Sci. Technol.* 46, 1584–1621. doi: 10.1080/10643389.2016.1251236
- Lonappan, L., Brar, S. K., Das, R. K., Verma, M., and Surampalli, R. Y. (2016). Diclofenac and its transformation products: environmental occurrence and toxicity - a review. *Environ. Int.* 96, 127–138. doi: 10.1016/j.envint.2016.09.014
- Lonappan, L., Rouissi, T., Liu, Y., Brar, S. K., and Surampalli, R. Y. (2019). Removal of diclofenac using microbiochar fixed-bed column bioreactor. *J. Environ. Chem. Eng.* 7:102894. doi: 10.1016/j.jece.2019.102894
- Lu, L., Wang, G., Zou, M., Wang, J., and Li, J. (2018). Effects of calcining temperature on formation of hierarchical TiO₂/g-C₃N₄ hybrids as an effective Z-scheme heterojunction photocatalyst. *Appl. Surf. Sci.* 441, 1012–1023. doi: 10.1016/j.apsusc.2018.02.080
- Macías-Martínez, B. I., Cortés-Hernández, D. A., Zugasti-Cruz, A., Cruz-Ortiz, B. R., and Múzquiz-Ramos, E. M. (2016). Heating ability and hemolysis test of magnetite nanoparticles obtained by a simple co-precipitation method. *J. Appl. Res. Technol.* 14, 239–244. doi: 10.1016/j.jart.2016.05.007
- Malhotra, M., Suresh, S., Garg, A. J. E. S., and Research, P. (2018). Tea waste derived activated carbon for the adsorption of sodium diclofenac from wastewater: adsorbent characteristics, adsorption isotherms, kinetics, and thermodynamics. *Environ. Sci. Pollut. Res. Int.* 25, 32210–32220. doi: 10.1007/s11356-018-3148-y
- Michael, I., Rizzo, L., McArdell, C. S., Manaia, C. M., Merlin, C., Schwartz, T., et al. (2013). Urban wastewater treatment plants as hotspots for the release of antibiotics in the environment: a review. *Water Res.* 47, 957–995. doi: 10.1016/j.watres.2012.11.027
- Navarro-Suárez, A. M., Carretero-González, J., Roddatis, V., Goikolea, E., Ségolini, J., Redondo, E., et al. (2014). Nanoporous carbons from natural lignin: study of structural-textural properties and application to organic-based supercapacitors. *RSC Adv.* 4, 48336–48343. doi: 10.1039/C4RA08218D
- Nita, C., Bensafia, M., Vaulot, C., Delmotte, L., and Matei Ghimbeu, C. (2016). Insights on the synthesis mechanism of green phenolic resin derived porous carbons via a salt-soft templating approach. *Carbon* 109, 227–238. doi: 10.1016/j.carbon.2016.08.011
- Ofomaja, A. E., Unuabonah, E. I., and Oladoja, N. A. (2010). Competitive modeling for the biosorptive removal of copper and lead ions from aqueous solution by *Mansonia* wood sawdust. *Bioresour. Technol.* 101, 3844–3852. doi: 10.1016/j.biortech.2009.10.064
- Pasangulapati, V., Ramachandriya, K. D., Kumar, A., Wilkins, M. R., Jones, C. L., and Huhnke, R. L. (2012). Effects of cellulose, hemicellulose and lignin on thermochemical conversion characteristics of the selected biomass. *Bioresour. Technol.* 114, 663–669. doi: 10.1016/j.biortech.2012.03.036
- Peña, S. S., Cruz-Pacheco, A., Garzón-Fontecha, A., Vargas, C. P., and De la Cruz, W. (2019). "Structural, morphological and surface properties of the samarium modified BiFeO₃ perovskite," in *Journal of Physics: Conference Series*, Vol. 12043 (Bucaramanga: IOP Publishing). doi: 10.1088/1742-6596/1247/1/012043
- Ramiah, M. V. (1970). Thermogravimetric and differential thermal analysis of cellulose, hemicellulose, and lignin. *J. Therm. Anal. Calorim.* 14, 1323–1337. doi: 10.1002/app.1970.070140518
- Rangabhashiyam, S., and Balasubramanian, P. (2019). The potential of lignocellulosic biomass precursors for biochar production: performance, mechanism and wastewater application—a review. *Ind. Crops Prod.* 128, 405–423. doi: 10.1016/j.indcrop.2018.11.041
- Rojas, J. V., Toro-Gonzalez, M., Molina-Higgins, M. C., and Castano, C. E. (2016). Facile radiolytic synthesis of ruthenium nanoparticles on graphene oxide and carbon nanotubes. *Mater. Sci. Eng. B* 205, 28–35. doi: 10.1016/j.mseb.2015.12.005
- Rosset, M., Sfreddo, L. W., Hidalgo, G. E. N., Perez-Lopez, O. W., and Férís, L. A. (2019). Adsorbents derived from hydrotalcites for the removal of diclofenac in wastewater. *Appl. Clay Sci.* 175, 150–158. doi: 10.1016/j.clay.2019.04.014
- Sadezky, A., Muckenhuber, H., Grothe, H., Niessner, R., and Pöschl, U. (2005). Raman microspectroscopy of soot and related carbonaceous materials: spectral analysis and structural information. *Carbon* 43, 1731–1742. doi: 10.1016/j.carbon.2005.02.018
- Saucier, C., Adebayo, M. A., Lima, E. C., Cataluña, R., Thue, P. S., Prola, L. D. T., et al. (2015). Microwave-assisted activated carbon from cocoa shell as adsorbent for removal of sodium diclofenac and nimesulide from aqueous effluents. *J. Hazard. Mater.* 289, 18–27. doi: 10.1016/j.jhazmat.2015.02.026
- Sevilla, M., and Fuertes, A. B. (2010). Graphitic carbon nanostructures from cellulose. *Chem. Phys. Lett.* 490, 63–68. doi: 10.1016/j.cplett.2010.03.011
- Shittu, I., Achazhiyath Edathil, A., Alsaedi, A., Al-Asheh, S., Polychronopoulou, K., and Banat, F. (2019). Development of novel surfactant functionalized porous graphitic carbon as an efficient adsorbent for the removal of methylene blue dye from aqueous solutions. *J. Water Process Eng.* 28, 69–81. doi: 10.1016/j.jwpe.2019.01.001
- Siyasukh, A., Chimupala, Y., and Tonaon, N. (2018). Preparation of magnetic hierarchical porous carbon spheres with graphitic features for high methyl orange adsorption capacity. *Carbon* 134, 207–221. doi: 10.1016/j.carbon.2018.03.093
- Sun, J., Liao, Z.-H., Si, R.-W., Kingori, G., Chang, F.-X., Gao, L., et al. (2014). Adsorption and removal of triphenylmethane dyes from water by magnetic reduced graphene oxide. *Water Sci. Technol.* 70, 1663–1669. doi: 10.2166/wst.2014.427
- Suriyanon, N., Punyapalakul, P., and Ngamcharussrivichai, C. (2013). Mechanistic study of diclofenac and carbamazepine adsorption on functionalized silica-based porous materials. *Chem. Eng. J.* 214, 208–218. doi: 10.1016/j.cej.2012.10.052
- Tan, X., Liu, Y., Zeng, G., Wang, X., Hu, X., Gu, Y., et al. (2015). Application of biochar for the removal of pollutants from aqueous solutions. *Chemosphere* 125, 70–85. doi: 10.1016/j.chemosphere.2014.12.058
- Tan, X.-F., Liu, Y.-G., Gu, Y.-L., Xu, Y., Zeng, G.-, Hu, X.-J., et al. (2016). Biochar-based nano-composites for the decontamination of wastewater: a review. *Bioresour. Technol.* 212, 318–333. doi: 10.1016/j.biortech.2016.04.093

- Tong, Y., McNamara, P., and Mayer, B. (2019). Adsorption of organic micropollutants onto biochar: a review of relevant kinetics, mechanisms and equilibrium. *Environ. Sci. Water Res. Technol.* 5, 821–838. doi: 10.1039/C8EW00938D
- Tseng, H.-H., Su, J.-G., and Liang, C. (2011). Synthesis of granular activated carbon/zero valent iron composites for simultaneous adsorption/dechlorination of trichloroethylene. *J. Hazard. Mater.* 192, 500–506. doi: 10.1016/j.jhazmat.2011.05.047
- Wang, J., Chen, Z., and Chen, B. (2014). Adsorption of polycyclic aromatic hydrocarbons by graphene and graphene oxide nanosheets. *Environ. Sci. Technol.* 48, 4817–4825. doi: 10.1021/es405227u
- Wang, L., Mu, G., Tian, C., Sun, L., Zhou, W., Yu, P., et al. (2013). Porous graphitic carbon nanosheets derived from cornstarch biomass for advanced supercapacitors. 6, 880–889. doi: 10.1002/cssc.201200990
- Wu, J., Lu, T., Bi, J., Yuan, H., and Chen, Y. (2019). A novel sewage sludge biochar and ferrate synergetic conditioning for enhancing sludge dewaterability. *Chemosphere* 237:124339. doi: 10.1016/j.chemosphere.2019.07.070
- Wu, L., Du, C., He, J., Yang, Z., and Li, H. (2019). Effective adsorption of diclofenac sodium from neutral aqueous solution by low-cost lignite activated cokes. *J. Hazard. Mater.* 384:121284. doi: 10.1016/j.jhazmat.2019.121284
- Xi, Y., Wang, Y., Yang, D., Zhang, Z., Liu, W., Li, Q., et al. (2019). K₂CO₃ activation enhancing the graphitization of porous lignin carbon derived from enzymatic hydrolysis lignin for high performance lithium-ion storage. *J. Alloys Compd.* 785, 706–714. doi: 10.1016/j.jallcom.2019.01.039
- Xia, W. J., Xu, J., Liu, F., Huang, T. Y., Wang, Z. M., and Chen, J. B. (2019). Adsorption of diclofenac on straw-biochar. *Zhongguo Huanjing Kexue/China Environ. Sci.* 39, 1054–1060. Available online at: <https://www.scopus.com/inward/record.uri?eid=2-s2.0-85069687789&partnerID=40&md5=ca5168a1392379ffa5d869bd60ea6457>
- Xing, B., Zhang, C., Liu, Q., Zhang, C., Huang, G., Guo, H., et al. (2019). Green synthesis of porous graphitic carbons from coal tar pitch templated by nano-CaCO₃ for high-performance lithium-ion batteries. *J. Alloys Compd.* 795, 91–102. doi: 10.1016/j.jallcom.2019.04.300
- Xu, J., Wang, L., and Zhu, Y. (2012). Decontamination of bisphenol A from aqueous solution by graphene adsorption. *Langmuir* 28, 8418–8425. doi: 10.1021/la301476p
- Yan, Q., Li, J., Zhang, X., Hassan, E. B., Wang, C., Zhang, J., et al. (2018). Catalytic graphitization of kraft lignin to graphene-based structures with four different transitional metals. *J. Nanopart. Res.* 20:223. doi: 10.1007/s11051-018-4317-0
- Yan, X., Sahimi, M., and Tsotsis, T. T. (2017). Fabrication of high-surface area nanoporous SiOC ceramics using pre-ceramic polymer precursors and a sacrificial template: precursor effects. *Microporous Mesoporous Mater.* 241, 338–345. doi: 10.1016/j.micromeso.2016.12.027
- Yao, Y., Gao, B., Chen, J., and Yang, L. (2013). Engineered biochar reclaiming phosphate from aqueous solutions: mechanisms and potential application as a slow-release fertilizer. *Environ. Sci. Technol.* 47, 8700–8708. doi: 10.1021/es4012977
- Zhang, P., Tan, X., Liu, S., Liu, Y., Zeng, G., Ye, S., et al. (2019). Catalytic degradation of estrogen by persulfate activated with iron-doped graphitic biochar: process variables effects and matrix effects. *Chem. Eng. J.* 378:122141. doi: 10.1016/j.cej.2019.122141
- Zhang, S., Shao, T., Bekaroglu, S. S. K., and Karanfil, T. (2010). Adsorption of synthetic organic chemicals by carbon nanotubes: effects of background solution chemistry. *Water Res.* 44, 2067–2074. doi: 10.1016/j.watres.2009.12.017
- Zhang, Y., Geißen, S.-U., and Gal, C. (2008). Carbamazepine and diclofenac: removal in wastewater treatment plants and occurrence in water bodies. *Chemosphere* 73, 1151–1161. doi: 10.1016/j.chemosphere.2008.07.086

Conflict of Interest: The authors declare that the research was conducted in the absence of any commercial or financial relationships that could be construed as a potential conflict of interest.

Copyright © 2020 Tam, Liu, Bashir, Zhang, Liu, Tan, Dai and Li. This is an open-access article distributed under the terms of the Creative Commons Attribution License (CC BY). The use, distribution or reproduction in other forums is permitted, provided the original author(s) and the copyright owner(s) are credited and that the original publication in this journal is cited, in accordance with accepted academic practice. No use, distribution or reproduction is permitted which does not comply with these terms.



Bio-based Substances From Compost as Reactant and Active Phase for Selective Capture of Cationic Pollutants From Waste Water

Giuliana Magnacca^{1,2*}, Flavio Neves Dos Santos¹ and Razieh Sadraei³

¹ Dipartimento di Chimica, Università di Torino, Turin, Italy, ² Centre for Nanostructured Interfaces and Surfaces (NIS) Interdepartmental Centre, Università di Torino, Turin, Italy, ³ Faculty of Science and Engineering, University of Wolverhampton, Wolverhampton, United Kingdom

OPEN ACCESS

Edited by:

Ana C. Tavares,
Research Centre for Energy Materials
Telecommunications (INRS), Canada

Reviewed by:

Hassan Ait Ahsaine,
University Mohamed VI
Polytechnics, Morocco
Wenbo Wang,
Lanzhou Institute of Chemical Physics
(CAS), China

*Correspondence:

Giuliana Magnacca
giuliana.magnacca@unito.it

Specialty section:

This article was submitted to
Green and Sustainable Chemistry,
a section of the journal
Frontiers in Chemistry

Received: 03 March 2020

Accepted: 28 May 2020

Published: 21 July 2020

Citation:

Magnacca G, Neves Dos Santos F
and Sadraei R (2020) Bio-based
Substances From Compost as
Reactant and Active Phase for
Selective Capture of Cationic
Pollutants From Waste Water.
Front. Chem. 8:550.
doi: 10.3389/fchem.2020.00550

Alumina porous monoliths were successfully fabricated using a simple and reproducible synthesis dispersing gamma alumina phase from commercial boehmite (GAB) in water containing water-soluble bio-based substances (BBSs) obtained from composted biowaste. The wet mixture obtained was shaped in form of small spheres and then dried and calcined at 500°C in order to burn the organic matter and obtain mesoporous monoliths. They were successively functionalized with BBSs in order to introduce BBS functional groups and obtain an efficient adsorbing system. Therefore, in this work, BBSs acted as template/binder for the production of monoliths and as functionalizing agent of the produced monoliths. The reference powders, deeply studied in a published article (Sadraei et al., 2019b), and the monoliths of GAB before and after functionalization were characterized by means of x-ray diffraction to evidence their crystal structure, Fourier transform infrared spectroscopy for evaluating the presence of BBSs on the supports, thermogravimetric analysis to measure the thermal stability of the materials and quantify the functionalizing BBS amount immobilized on the supports, nitrogen adsorption at 77 K for the investigation of the surface area and porosity of the systems, and zeta potential measurements to analyze the effect of BBS immobilization on the surface charge of the supports and to predict the type of interaction, which can be established with substrates. Finally, the systems were applied in removal of pollutants with different charge, polarity, and molecular structure, such as dyes (crystal violet and acid orange 7) and contaminants of emerging concern (carbamazepine and atenolol). Only the cationic dye CV is captured by the adsorbing material, and this allows envisaging a possible use of the functionalized monoliths for selective adsorption of cationic substrates.

Keywords: bio-based substances, alumina, porous monolith, organic/inorganic hybrid, removal of pollutant, cationic molecules

INTRODUCTION

Refuse accumulation is a heavy burden for our society, as the normal human activities imply an increasing production of wastes accumulating in dedicated places organized by the municipalities or often abandoned in non-regulated areas. Wastes are generated by domestic, industrial, agricultural, commercial, municipal, and sanitary processes. They can contaminate air, water, and land affecting in turn the health of the biosphere. Part of the problem is faced by a process called waste management, taking into account the management of the already existing refuses, but another complementary approach to reduce the impact of refuses, and the consequent earth pollution, is the Zero Waste Philosophy (<https://www.epa.gov/transforming-waste-tool/how-communities-have-defined-zero-waste>). It considers that a sustainable life passes through the reduction of wastes and their transformation into raw materials; therefore, it promotes the ideas of recycling and upcycling the waste we produce and increasing the sustainability of the production processes of objects that will be transformed into refuses at the end of their life.

In this perspective, compost is a renewable source of carbonaceous compounds, alternative to the less sustainable petroleum, and bio-based substances (BBSs), isolated from composted urban refuses, are interesting amphiphilic reactants (Montoneri et al., 2008, 2009, 2011). Bio-based substances have been used as binder/templating agents to produce siliceous mesoporous monoliths useful as support for a variety of applications. In 2012, they were employed to support an enzyme in order to obtain a heterogeneous biocatalysts for hydrogen peroxide activation (Magnacca et al., 2012), in this article, the same procedure has been applied to produce alumina-based mesoporous monoliths. In this case, the application of the material was chosen in the field of wastewater remediation, as water contamination, similarly to refuse accumulation, has become a serious worldwide concern that can cause many health problems, particularly in industrial countries. Scientists are facing the issue developing simple, fast, and environmentally friendly methods for decomposition or removal, in general, of pollutants, in particular of organic ones (de Paul Obade and Moore, 2018; Jaramillo and O'Shea, 2018; Vega et al., 2018; Ren et al., 2019).

Among the possible techniques for wastewater treatment, the adsorption process by solid adsorbents demonstrates a high potential as one of the most efficient methods for capturing organic contaminants from wastewaters avoiding the risk of secondary pollution brought by decomposition methods. Several adsorbents, such as activated carbon (Jalcour-Lebigue et al., 2012), silica gel (Fan et al., 2012), organic clay (Unuabonah et al., 2013), alumina (Serbezov et al., 2011; Tang et al., 2018; Sadraei, 2019), iron powders (Yu et al., 2013; Zeng et al., 2018), and mesoporous silica (Ko et al., 2014; Ye et al., 2017), have been successfully applied for the removal of dyes from water, but the development of handleable materials that can operate much more easily, in particular in terms of recovery and reusability, is necessary. As the open-framework nature and large pore size (2–50 nm) are the key factors for a good diffusion of the

molecules inside the adsorbing materials and a consequent fast adsorption process (Alauzun et al., 2011; Masika and Mokaya, 2011), the production of massive materials possessing these features is pursued, and alumina-based monoliths perfectly fit the requirements.

In addition to this aspect, the adsorption capacity of materials can be enhanced introducing functional groups with high affinity for different substrates by means of functionalization processes. The choice of functional groups allows defining a specific activity of the adsorbing material toward a specific substrate. Oxides carrying OH groups at the surface are very good candidates for being surface-modified, as they can be easily functionalized exploiting several strategies reported in the literature, some of them basing on physical methods, whereas others basing on chemical ones (Nayak et al., 2019; Sadraei et al., 2019a,b; Shanaghi et al., 2019). As in a previous article, we reported the performances of BBS-functionalized alumina powders (Sadraei et al., 2019b). In this work, we are considering the upscaling of the previous study producing mesoporous gamma alumina-based monoliths (GAB-M) functionalized with BBSs (GAB-M-BBSs).

Summarizing, the current research comprehends the following points: (1) the fabrication of new alumina monoliths using BBSs as binder/templating agents, (2) the simple monolith functionalization with BBSs acting as active phase to enhance the adsorption properties, (3) the physicochemical characterization of the produced materials compared with the parent alumina powder, and (4) the adsorption study.

MATERIALS AND METHODS

Materials for Synthesis

Commercial boehmite was kindly supplied by Centro Ricerche FIAT and used to prepare gamma-Al₂O₃ (GAB) after calcination in a furnace at 500°C for 3 h, as reported in the literature (Sadraei et al., 2019b).

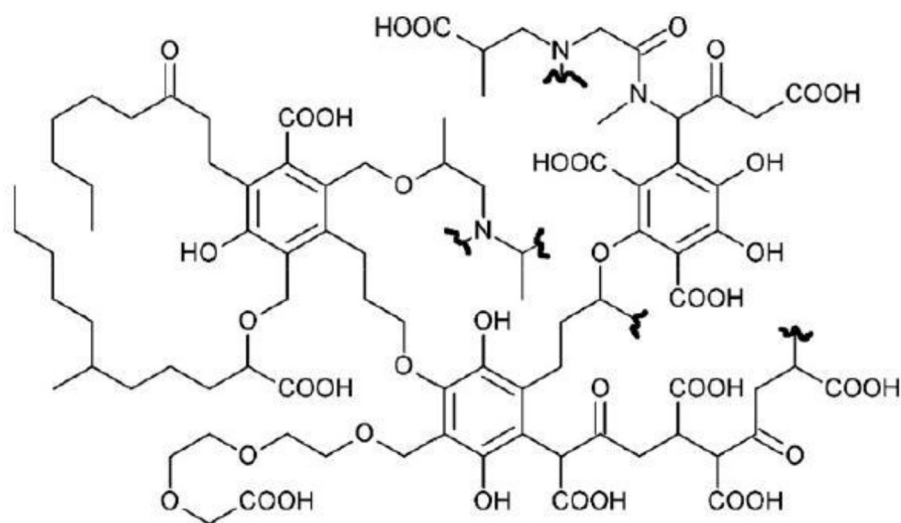
Bio-based substances were extracted from composted organic refuses aged for more than 180 days supplied by ACEA Pinerolese Industriale. The extraction procedure was described by Montoneri et al. (2008, 2009, 2011). A hypothetical structure of BBS is reported in **Scheme 1**.

Materials and Methods for Characterization Study

Scanning electron microscope (SEM) image of the monolith surface was obtained by means of a scanning microscope ZEISS EVO50 XVP equipped with LaB₆ source and a secondary electron detector. The samples prior to the SEM investigation were sputtered with ~20 nm of a gold layer in order to avoid charging effects using a Bal-tec SCD050 sputter coater.

X-ray diffraction (XRD) analysis was used to investigate the morphology and crystal structure of powders and monoliths. The measurements were performed by using a X'Pert PRO MPD diffractometer from PANalytical, equipped with Cu anode worked at 45 kV and 40 mA in a Bragg–Brentano geometry. In this work, the flat sample-holder configuration was employed.

Fourier transform infrared (FTIR) spectroscopy was applied in a transmission mode by using Bruker Vector 22



SCHEME 1 | Virtual molecular fragments of BBS.

spectrophotometer equipped with Globar source and DTGS detector, and working in the transmission mode in the range of $4000\text{--}400\text{ cm}^{-1}$ at 4 cm^{-1} resolution. Before investigation all the samples were mixed with KBr powder (1:20 ratio) and pressed to form pellets.

Nitrogen adsorption–desorption measurements at 77 K were carried out by means of ASAP 2020 Micromeritics gas-volumetric apparatus. Prior to the experiments, the samples before and after functionalization were activated at 300 and 40°C , respectively, for 24 h. Specific surface areas were calculated by applying the Brunauer–Emmett–Teller (BET) method (Thommes et al., 2015). Pore volumes and pore size distribution were determined by using the Barrett–Joyner–Halenda method (Thommes et al., 2015) applied to the isotherm adsorption branch.

Thermogravimetric analysis (TGA) was performed by means of TA Q600 (TA Instruments). Materials before and after functionalization were heated at a rate of $10^\circ\text{C}/\text{min}$ from 40 to 650°C under air.

Zeta potential (ZP) measurements have been used in order to determine the surface charge of the particles in water at different pH and the point of zero charge of the dispersions (Sadraei et al., 2019b). They were performed using the instrument Zetasizer by Malvern (model ZS90). The suspensions were prepared by mixing 10 mg of sample (after finely crushing in an agate mortar in the case of monoliths) in 20 mL of deionized water under constant stirring (400 rpm) for 15 min. The pH of the suspensions was adjusted in different pH in the range of 3 to 11 by addition of 0.1 M HCl and 0.1 M NaOH solutions. The suspensions were shaken at 25°C temperature for 15 min until the pH had stabilized. A digital pH meter (Metrohm, model 827 pH lab, Swiss mode) was used to measure the pH. In all batch experiments, the refractive index value of alumina was selected.

Materials and Methods for Adsorption Study

UV-Vis spectrophotometer (Varian Cary 300 Scans) was applied to study the adsorption of the dyes crystal violet (CV, positively charged, maximum absorbance at 584 nm) and acid orange 7 (AO, negatively charged, maximum absorbance at 480 nm) and of the contaminants atenolol (polar, maximum absorbance at 224 nm) and carbamazepine (apolar, maximum absorbance at 284 nm).

The kinetics of the adsorption was carried out contacting 20 mg of adsorbents materials with 10 ppm of contaminant solutions in the total volume of 10 mL at pH 6.5 and keeping under shaking at the temperature of $22 \pm 2^\circ\text{C}$. The removal was evaluated considering the residual contaminant concentrations after separation of the supernatant and measurement of contaminant absorption using a calibration curve.

RESULTS AND DISCUSSION

Preparation of Materials

Preparation of Monoliths as Support

Following the procedure previously applied for preparation of silica monolith (Magnacca et al., 2012), 0.5 g of BBSs was stored under stirring in 7.5 mL water at room temperature (RT) for 2 h. GAB (2 g) was added to the BBS solution. Five milliliters of water was then added, and the mixture was stirred for 2 h. The mixture was left at ambient condition for relaxing and dried at ambient temperature for the time needed to obtain a mud in order to model small spheres of $\sim 0.5\text{ cm}$ of diameter. These spheres were dried overnight at RT and then calcined in furnace at 500°C for 4 h in order to remove all organics and yield a mechanically stable, porous monolith named GAB-M. The image of the spheres after calcination is presented in the inset of **Figure 1** together with the SEM image of the monolith surface.

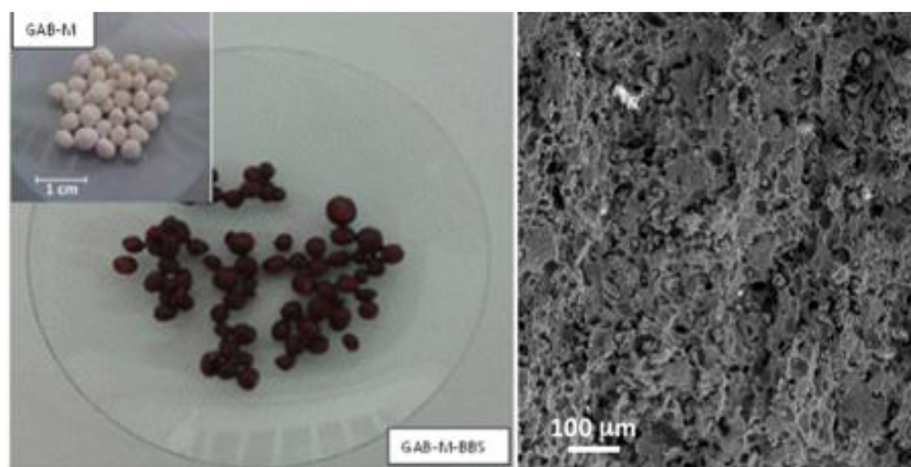


FIGURE 1 | GAB-M before (in the inset) and after functionalization with BBSs (left section) and an SEM image of the monolith surface (right section).

BBS Functionalization of Monoliths

As alumina powders were successfully BBS-functionalized, thanks to a simple electrostatic interaction occurring in water at circumneutral pH (Sadraei et al., 2019b), we tried the same procedure to functionalize the surface of GAB-M. The functionalized monoliths were prepared using 1 g of GAB-M dispersed in water at natural pH (~ 6.5) containing 20 g/L of water-soluble BBSs and two different procedures:

The mixture container was sealed and gently shaken (in order to avoid the monolith breakage) using an orbital mixing plate with rotation at 1000 rpm for 24 h at $25 \pm 2^\circ\text{C}$.

The mixture contained was sealed and, after shaking at RT, was placed in an oven at 60°C overnight and then cooled down and again placed in an oven at 80°C overnight.

At the end of both procedures, the samples were washed with 10 mL of water several times until no signal of leached BBS molecules from GAB-M-BBS samples were evidenced in the UV-Vis spectra of the washing medium. The following drying process was carried out in the oven at 40°C for 24 h.

The first procedure did not allow a complete functionalization of the monolith as the BBS brown color was present only in the outermost layer of the spheres, whereas the second treatment allowed a complete functionalization. The image of the functionalized porous monoliths, named GAB-M-BBSs, is reported in **Figure 1**. These samples were used for the subsequent characterization, and the powders obtained in the previous work (Sadraei et al., 2019b), GAB and GAB-BBSs, were used as reference materials for comparison.

The preparation route of the non-functionalized monoliths and the following functionalization methods were carried out several times in order to define the reproducibility of the procedures. In all the attempts, the samples presented very similar behaviors, as witnessed by FTIR spectra, XRD, TGA, and N_2 adsorption/desorption analyses.

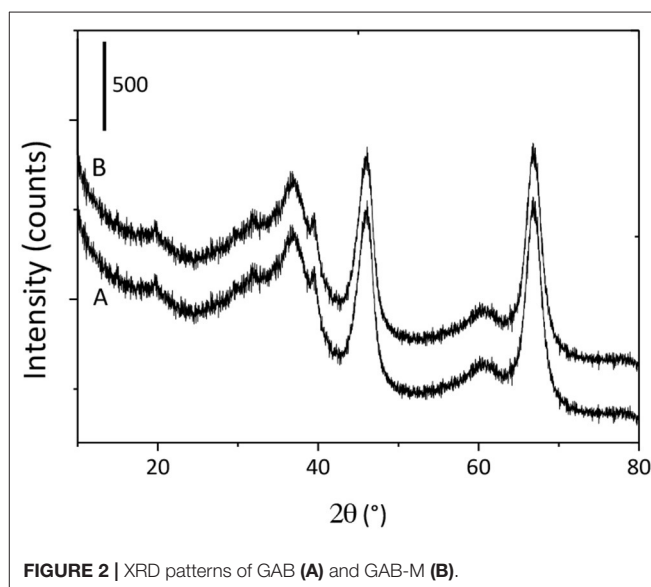
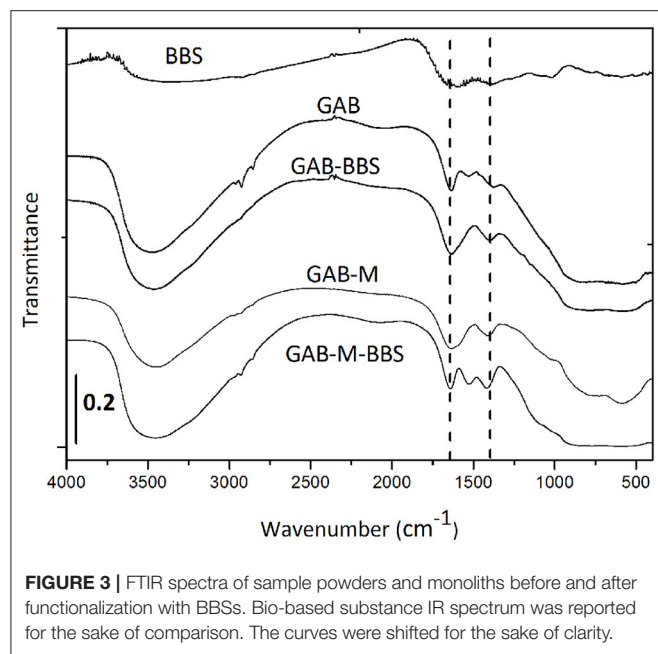


FIGURE 2 | XRD patterns of GAB (A) and GAB-M (B).

Material Characterization

XRD Measurements

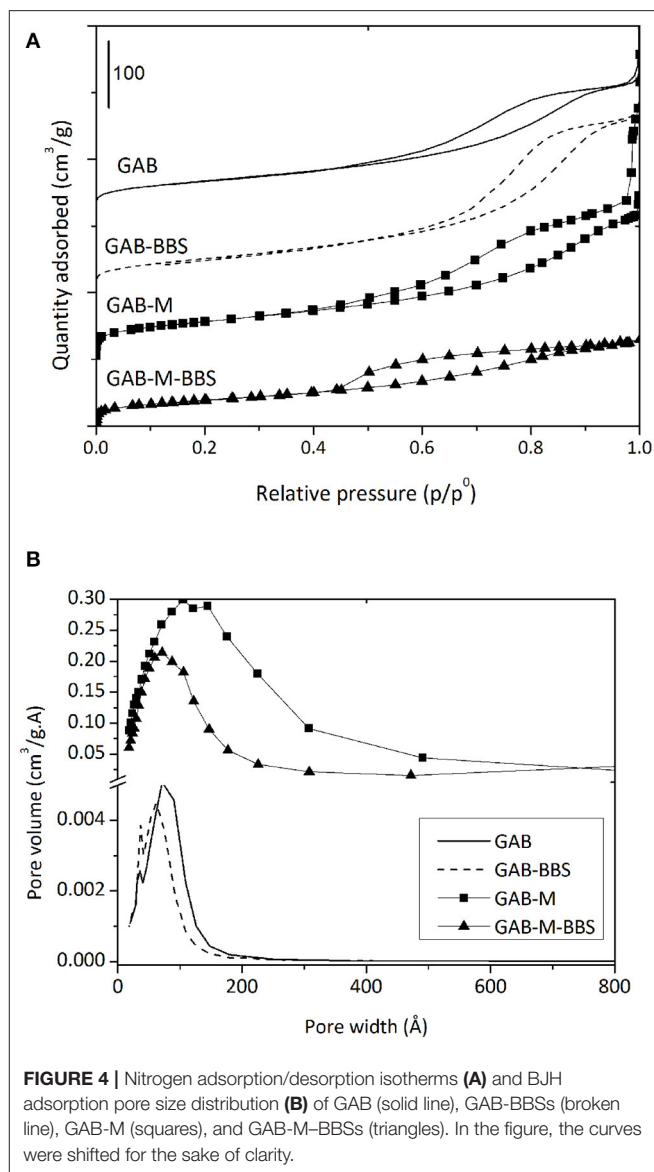
X-ray diffraction analysis was performed to investigate the effect of monolith fabrication process on the crystal structure of GAB powder. **Figure 2** shows the diffraction patterns for both GAB and GAB-M samples. As it can be seen, the crystallographic patterns of the monoliths GAB-M are not different from GAB one. The typical reflections of cubic $\gamma\text{-Al}_2\text{O}_3$ [reference pattern 01-075-0921 and (Sifontes et al., 2014)] can be evidenced in both diffractograms; in detail: the signals at $2\theta = 39, 46$, and 67° corresponding to the reflection of the planes (311), (400), and (440). An analogous curve, not reported for the sake of brevity, can be observed for monoliths after BBS functionalization.



FTIR Spectroscopy

The IR spectra of GAB powder before and after functionalization are reported in **Figure 3**. The presence of BBSs is clearly visible in the GAB-BBS spectrum. In fact, as for pure BBS sample, it shows the presence of OH groups and atmospheric moisture interacting with the surface and producing a signal at $\sim 3500\text{ cm}^{-1}$ (ν_{OH} vibrations), a large signal at 1600 cm^{-1} due to both carbonylic stretching ($\nu_{\text{C=O}}$) and vibration of water molecules adsorbed at the surface (δ_{HOH} signal), and other two signals at 1400 and 1000 cm^{-1} due to carboxylic acid/C-H bending and OCO vibrations, respectively. Other weak signals due to ν_{CH} stretching vibrations are visible at around 3000 cm^{-1} (Nisticò et al., 2015; Bianco Prevot et al., 2019; Sadraei et al., 2019b). In addition to these bands, the alumina samples are characterized by a very intense absorption $>1000\text{ cm}^{-1}$ due to the bulk vibrations of the solid framework.

The infrared spectra of GAB-M before and after functionalization were collected in the same figure. The spectrum of GAB-M before functionalization is dominated by a very large signal at $\sim 3400\text{ cm}^{-1}$ and by a couple of bands at ~ 1650 and 1300 cm^{-1} . All of them derive from the interaction of the solid samples with the molecules present in the atmosphere, H_2O and CO_2 . In fact, the burning off of BBSs, in the process of monolith formation, leaves in the material some inorganic residues naturally present in the BBSs (namely, cationic and anionic species such as Mg^{2+} , K^+ , Ca^{2+} , NO_3^- , Cl^-), and these species interact very easily with moisture and CO_2 leading to the formation of intense ν_{OH} signals at high frequency and to the formation of symmetric and antisymmetric vibrations of surface carbonate-like groups at low frequency, respectively. In addition to these absorptions, the BBS functionalization causes the formation of BBS typical bands, as mentioned for GAB-BBS sample.



Gas-Volumetric N_2 Adsorption at 77 K

Gas-volumetric analysis of N_2 adsorbed at 77 K was carried out for all samples including reference powders. According to the International Union of Pure and Applied Chemistry classification, the adsorption/desorption isotherms of all samples, reported in **Figure 4A**, are of the IV type, with hysteresis loops at relative pressures higher than 0.4, confirming that all materials are mesoporous or even macroporous. The formation of monolith from alumina powder does not affect significantly the specific surface area (198 vs. $186\text{ m}^2/\text{g}$), but changes significantly the porosity, which appears higher and made up of larger mesopores and macropores of width up to 600 Å with respect to the pure powder (**Table 1** and **Figure 4B**). This effect was already evidenced in the previous work dealing with silica monolith formation from powder (Magnacca et al., 2012), and it

TABLE 1 | Textural features of the samples.

Materials	BET-specific surface area (m ² /g)	BJH pore volume (cm ³ /g)
GAB	186	0.42
GAB-BBSs	165	0.29
GAB-M	198	0.32
GAB-M-BBSs	141	0.19

is due to the templating effect brought by BBS molecules during alumina particle aggregation.

In the case of monolith and reference powder, the functionalization process affects the specific surface area and the mesoporosity of all systems, as BBSs occupy part of the pores (the largest ones) leading to a decrease of the total mesoporosity and consequently to the material surface area. This result confirms the BBS functionalization reaches also the core of the monolith pores, as also suggested by the visual examination of the internal part of the monoliths after functionalization.

Thermogravimetric Analysis

The results of TGA analysis on GAB and GAB-M before and after immobilization of BBSs are shown in **Figure 5A**. **Figure 5B** shows the curve due to BBS weight loss measured in the same conditions and reports two main regions of weight loss for pure BBS materials, the first one in the range of 40–200°C due to water molecules elimination, and the second one is in the range of 200–650°C due to the oxidation of BBSs. In order to interpret the TGA curve of GAB-BBSs and GAB-M-BBSs, we do need the BBSs, GAB, and GAB-M curves as references. As it can be seen in **Figure 5A**, all the curves report the two important weight losses described in the case of BBS sample, but while the foster occurs in the range of 40–200°C and is related to the removal of physisorbed and chemisorbed water molecules, the latter one, falling in the range of 200–650°C, is due to a couple of contributions, namely, (i) loss of water obtained from OH groups condensation and (ii) loss of organic matter by oxidation with formation of CO₂ and H₂O (Sadraei et al., 2019b). To calculate the amount of organic matter present in the functionalized samples, it is needed to eliminate the contribution due to the condensation of OH groups. The results of this comparison are reported in **Table 2**. The amount of BBSs loaded onto GAB-BBSs is higher than that observed in the case of GAB-M-BBSs, indicating that a small amount of BBS molecules can be hosted in the mesoporous structure of the monoliths with respect to the parent powder.

The amount of water physisorbed and chemisorbed present on the samples and determined by the weight loss in the range 40–200°C confirms that the presence of inorganic residues present on the plain monoliths GAB-M and the additional presence of BBSs present in the functionalized monolith GAB-M-BBSs make the materials much more hydrophilic than the relative powdery ones.

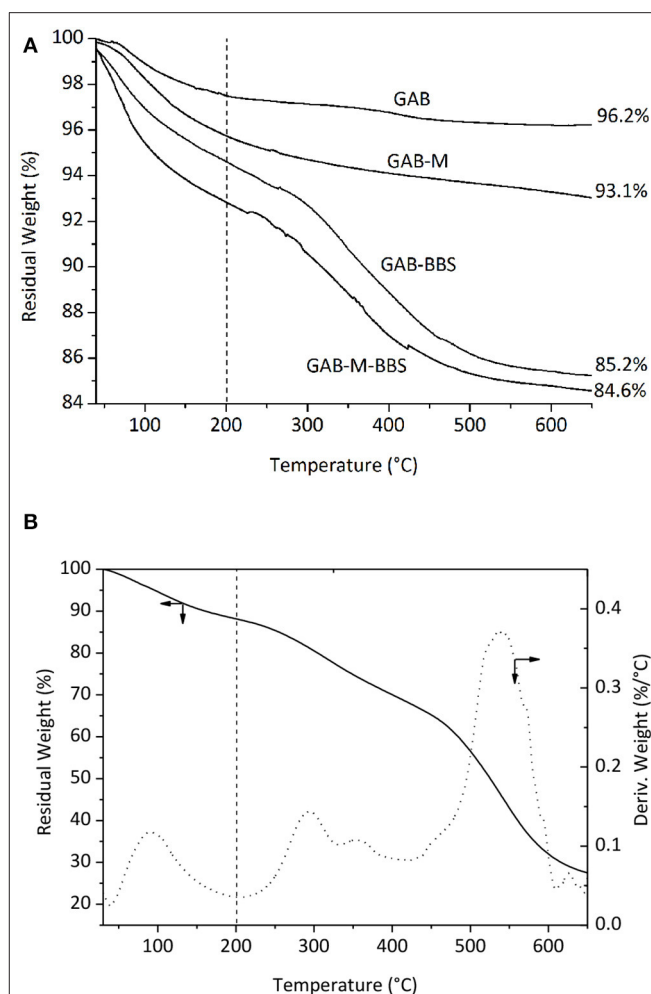


FIGURE 5 | Thermogravimetric analysis curves obtained in air for GAB, GAB-BBSs, GAB-M, and GAB-M-BBSs in (A); weight (solid line) and derivate weight (dotted line) curves of BBSs in (B). The values indicated in the figure represent the residual weight measured for the materials at 650°C; the vertical broken lines indicate the temperature of 200°C used for the quantification of water and organics loss.

TABLE 2 | Weight losses observed for references and hybrid materials.

Materials	40–200°C adsorbed water %	200–650°C organic content and OH groups %	OH groups %	Measured organic content % ± 0.1
GAB	2.5	1.3	1.3	–
GAB-BBSs	5.4	9.4	1.3	8.1
GAB-M	4.3	2.6	2.6	–
GAB-M-BBSs	7.2	8.2	2.6	5.6

Zeta Potential

Zeta potential (ZP) measurements were obtained in order to evaluate the surface charge of the materials before and after

immobilization of BBSs, as this is a very useful indication dealing with adsorption process in order to predict the type of substrate suitable for an efficient interaction with the adsorbent. The variations of the ZP values of the samples in the range of pH 3.0–11.0 are reported in **Figure 6**. GAB possesses a positive surface charge in the range of pH 4–7.9, and then it becomes negative. Water-soluble BBS molecules bring a negative charge at circumneutral pH caused by the presence of dissociated COOH and OH groups (Montoneri et al., 2009); therefore, they can interact quite easily with GAB support. After functionalization, the point of zero charge of GAB-BBS shifts from 7.9 to 5.2, leading to a hybrid material with negatively charged surface at circumneutral pH, prone to the interaction with positive or even partially positive (i.e., polar) substrates (Sadraei et al., 2019b). On the contrary, GAB-M and GAB-M-BBSs show a negative charge in the entire pH range examined, with no substantial modifications brought by BBS functionalization. This feature suggests that only positively charged substrates should interact with these materials.

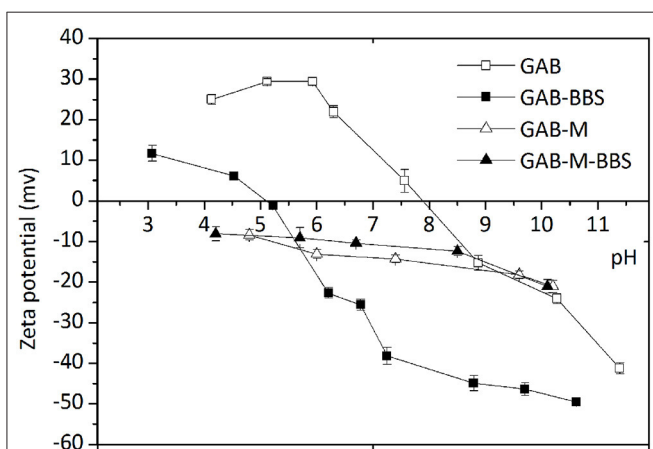


FIGURE 6 | Zeta potential values of GAB, GAB-BBSs, GAB-M, and GAB-M-BBSs as a function of pH. The measurements were carried out on 10 mg of crushed sample dispersed in 20 mL of deionized water. pH was adjusted by addition of HCl or NaOH 0.1 M and stabilized for 15 min.

Application of Materials in Contaminant Removal

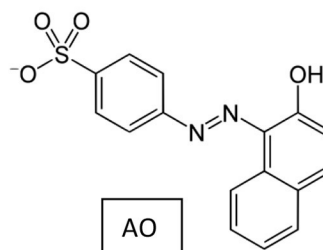
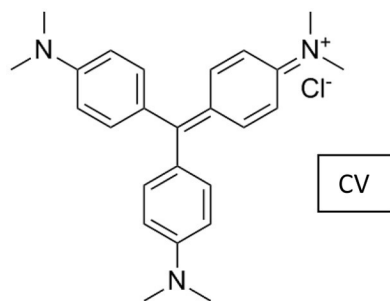
Removal of Dyes

Positively charged CV and negatively charged AO (whose molecular structures are shown in **Scheme 2**) were selected as model adsorptives to evaluate the mechanism at the base of the interaction substrate monoliths. For the sake of comparison, CV adsorption on the reference powdery materials GAB and GAB-BBSs was taken into consideration.

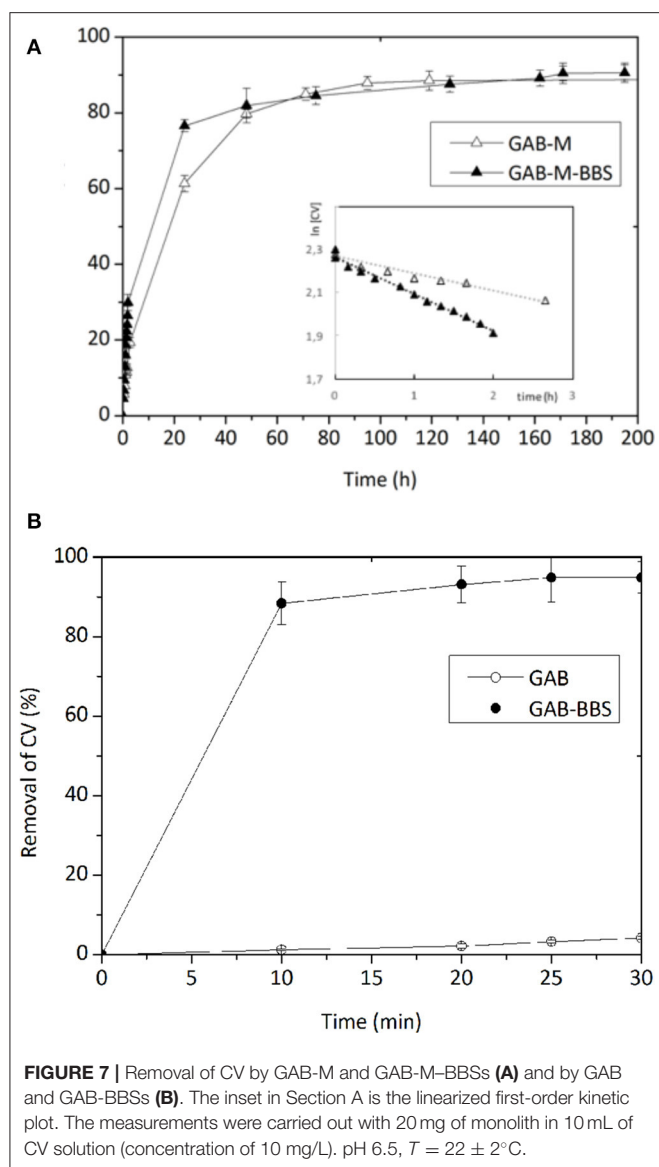
Figure 7 shows the adsorption kinetics of CV on the monoliths GAB-M and GAB-M-BBSs (Section A) and on the reference powdery GAB and GAB-BBSs (Section B). No adsorption was evidenced contacting the negatively charged AO with the monolith systems.

As reported in Sadraei et al. (2019b), the adsorption of CV on the powdery GAB-BBSs occurs very quickly and to a large extent, favored by the opposite charges carried by material and substrate. As already evidenced in Sadraei et al. (2019b) and as expected considering the positive charge carried by both material and substrate, the plain GAB powder does not give a good interaction.

The adsorption kinetic curves of CV on GAB-M and GAB-M-BBSs are reported in **Figure 7B**. In these cases, the interaction occurs in longer time (the experiments took up to 8 days), as the large but flexible CV molecules need to diffuse into the mesopores of monoliths to be adsorbed. Indeed, no significant differences are evidenced for the plain and the functionalized systems in terms of maximum removal, as expected considering the ZP curves and BET measurements discussed in the previous paragraph: both systems are slightly negative and possess similar surface areas; therefore, they can interact almost the same way with the positive substrate. The only change observable is related to the adsorption rate, higher in the case of GAB-M-BBS system, although smaller pores are present in this material with respect to the non-functionalized one. This means that diffusion of dye molecules into the porous adsorbing material is not a steady step for the adsorption process; therefore, we have to consider the high chemical affinity between the negatively charged support and the positively charged CV molecules. In the case of BBSs containing monoliths, the negative charge can be identified with carboxylate groups brought by BBSs, whereas for plain monoliths, a dispersed charge, not localized in one



SCHEME 2 | Molecular structure of crystal violet (CV) and acid orange 7 (AO).



specific site, should be taken into account. In an adsorption process of this kind, a second-order kinetic law is expected, as two species should be responsible of the process, namely, the negative adsorbing surface and the positive dye molecules. In the case of GAB-M-BBS material, it is also possible to try evaluating the relative amounts of adsorbing sites and adsorbed molecules considering the number of carboxylate groups, the number of CV adsorbed molecules, and a stoichiometry of the interaction 1:1. The amount of BBS immobilized on monolith support is 5.6% in weight (as measured by TGA), the corresponding amount of carboxylate groups is 1.40 mmol COOH/g BBSs (Magnacca et al., 2014), and the amount of CV immobilized within 3 h is ~ 3 ppm, corresponding to $\sim 7 \cdot 10^{-8}$ mol. We can see that the amount of carboxylic groups available for adsorption is in large excess with respect to the amount of adsorbed dye molecules, so the kinetic law should depend only

from CV concentration. In this situation, a kinetic constant of the pseudo-first order could be determined from the kinetic trend. For GAB-M-BBSs, the pseudo $k = 0.172 \text{ h}^{-1}$, whereas for GAB-M, k , calculated with analogous procedure, corresponds to 0.080 h^{-1} , one-half of the GAB-M-BBS ones. In conclusion, the thermodynamic of the adsorption does not change with or without BBSs, but the BBS presence slightly influences the kinetic of the process.

No AO adsorption was revealed by GAB-M and GAB-M-BBSs, neither for prolonged time of contact, as expected given the negative charge of the dye.

For a comparison with literature data, the CV adsorption capacity of the monoliths was calculated (Liu et al., 2015):

$$q_t = \frac{(C_0 - C_t) V}{W}$$

In the Equation, C_0 and C_t (mg/L) are the concentration of CV in solution before and after adsorption, respectively, V (L) is the volume of the solution, and W (g) is the mass of adsorbents.

As reported in **Table 3**, the efficiency toward CV adsorption of monoliths studied in this article is similar to or higher than that of other literature adsorbing systems. In principle, therefore, both plain and BBS-functionalized monoliths could be applied to the removal of cationic contaminants. The BBS functionalization, therefore, seems not be functional to the adsorption application. Indeed, this system shows a further advantage with respect to other materials. In fact, it is known that BBSs possess photosensitizing properties (Bianco Prevot et al., 2019), being able of producing Reactive oxygen species (ROS) when irradiated with visible light. The produced ROS (typically the highly reactive OH radicals) can attack and degrade organic molecules until mineralization (complete abatement with formation of CO_2 and H_2O), with consequent increase of the applicative interest of this material. The challenge, so far, is the possibility of irradiating all the BBS molecules present in the material, including the molecules immobilized inside the porosities of the monolith, in order to achieve a high abatement efficiency. Thus, once a suitable shape of the support is elaborated, development of the material in photocatalytic applications could be pursued.

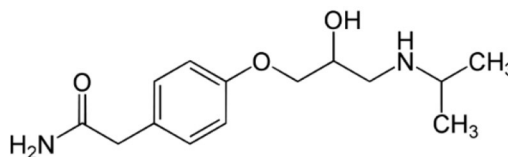
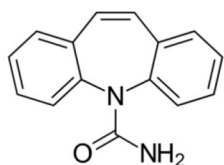
Removal of Contaminants of Emerging Concern

The molecular structure of the contaminants analyzed is reported in **Scheme 3**.

Contrary to what happened with reference powders and reported in Sadraei et al. (2019b), atenolol (polar non-charged substrate) and carbamazepine (essentially apolar substrate) did not give valuable adsorption on monoliths, even if the large pores of these systems should favor the diffusion and consequent adsorption of the substrates. Probably the simple van der Waals forces that could establish between the poorly charged monoliths and the non-charged substrates are not enough to produce a stable interaction.

TABLE 3 | Efficiency of various adsorbents toward CV removal from aqueous solutions.

Adsorbent	Amount adsorbed (mg/g)	References	Experimental condition (pH, initial concentration, temperature)
Multiwalled carbon nanotubes	4.48	Gabal et al., 2014	pH 8 Concentration: 5 mg/L Temperature: 25–50°C
<i>Calotropis procera</i> leaf	4.14	Ali and Shah, 2008	pH 5 Concentration: 25 mg/L Temperature: 20°C
CaCO ₃ bare	3.35	Liu et al., 2015	pH 6 Concentration: 40 mg/L Temperature: 25°C
Unexpanded perlite	3.30	Dogan and Alkan, 2003	pH 11 Concentration: 122 mg/L Temperature: 30 ± 1°C
Coir pith	2.56	Namasivayam et al., 2001	pH 6.5 Concentration: 40 mg/L Temperature: 30 ± 2°C
Expanded perlite	1.14	Dogan and Alkan, 2003	pH 11 Concentration: 122 mg/L Temperature: 30 ± 1°C
GAB-M/GAB-M-BBSs	4.48	This work	pH 6.5 Concentration: 10 mg/L Temperature: 22 ± 2°C

**SCHEME 3** | Molecular structure of carbamazepine (left side) and atenolol (right side).

CONCLUSIONS

γ -Alumina-based monoliths were prepared following a previously developed procedure (Magnacca et al., 2012). The results showed that they can be prepared in a reproducible way, with good mechanical property, large mesoporosity/macroporosity, and a surface area similar to the parent powdery system. With respect to the pure powder, the monoliths contain some inorganic residues deriving from the BBSs used as template/binder that remain in the alumina framework after the calcination was performed to remove the organic matter and obtain the monoliths. The inorganic residues are responsible of the interaction with atmospheric moisture and CO₂, the last forming carbonate-like species on the monolith surface, and of the slightly negative surface charge of the material.

Bio-based substance molecules were also used to functionalize the alumina monolith in order to reproduce the results obtained with parent alumina powder and obtain a good adsorbent for polar pollutants, handleable, and therefore useful for upscaling the material to real application. The interaction of the functionalized monoliths with positive, negative, polar non-charged, and apolar molecules (chosen in the family

of dyes and contaminants of emerging concern) evidenced a good interaction with positively charged species, opening the way to the use of the BBS-containing monoliths for the selective capture of pollutants based on their charge.

DATA AVAILABILITY STATEMENT

All datasets generated for this study are included in the article/supplementary material.

AUTHOR CONTRIBUTIONS

GM followed the experiments and revised the manuscript. FN carried out the experiments and most part of the data elaboration. RS helped in carrying out the experiments and wrote the manuscript. All authors contributed to the article and approved the submitted version.

FUNDING

This project has received funding from the European Union's Horizon 2020 research and innovative programme under

the Marie Skłodowska-Curie grant agreement no. 645551. The authors thank the contribution of Compagnia di San Paolo supplied under the pluriannual Convention (2016–2018) between the University of Turin and Compagnia di

San Paolo (Ex-post projects). The Department of Chemistry of University of Turin will fund the publication expenses. I also received a 45% waiver for publication from Frontiers (January 2020).

REFERENCES

- Alaun, J. G., Ungureanu, S., Brun, N., Bernard, S., Miele, P., Backov, R., et al. (2011). Novel monolith-type boron nitride hierarchical foams obtained through integrative chemistry. *J. Mater. Chem.* 21, 14025–14030. doi: 10.1039/c1jm12751a
- Ali, H., and Shah, K. M. (2008). Biosorption of crystal violet from water on leaf biomass of *Calotropis procera*. *J. Environ. Sci. Technol.* 3, 143–150. doi: 10.3923/jest.2008.143.150
- Bianco Prevot, A., Arques, A., Carlos, L., Laurenti, E., Magnacca, G., and Nisticò, R. (2019). “Innovative sustainable materials for the photoinduced remediation of polluted waters,” in *Sustainable Water and Wastewater Processing*, eds C. M. Galanakis and E. Agrafioti (Amsterdam: Elsevier), 203–238.
- de Paul Obade, V., and Moore, R. (2018). Synthesizing water quality indicators from standardized geospatial information to remedy water security challenges: a review. *Environ. Int.* 119, 220–231. doi: 10.1016/j.envint.2018.06.026
- Dogan, M., and Alkan, M. (2003). Removal of methyl violet from aqueous solution by perlite. *J. Colloid Interface Sci.* 267, 32–41. doi: 10.1016/S0021-9797(03)00579-4
- Fan, H. T., Fan, X., Li, J., Guo, M., Zhang, D., Yan, F., et al. (2012). Selective removal of arsenic(V) from aqueous solution using a surface-ion-imprinted amine-functionalized silica gel sorbent. *Ind. Eng. Chem. Res.* 51, 5216–5223. doi: 10.1021/ie202655x
- Gabal, M. A., Al-Harthy, E. A., Al Angari, Y. M., and Abdel Salam, M. (2014). MWCNTs decorated with $Mn_{0.8}Zn_{0.2}Fe_2O_4$ nanoparticles for removal of crystal-violet dye from aqueous solutions. *Chem. Eng. J.* 255, 156–164. doi: 10.1016/j.cej.2014.06.019
- Jaramillo, M., and O'Shea, K. E. (2018). Analytical methods for assessment of cyanotoxin contamination in drinking water sources. *Curr. Opin. Environ. Sci. Health* 7, 45–51. doi: 10.1016/j.coesh.2018.10.003
- Julcour-Lebigue, C., Krou, N. J., Andriantsiferana, C., Wilhelm, A. M., and Delmas, H. (2012). Assessment and modeling of a sequential process for water treatment-adsorption and batch CWAO regeneration of activated carbon. *Ind. Eng. Chem. Res.* 51, 8867–8874. doi: 10.1021/ie2020312
- Ko, Y. G., Lee, H. J., Kim, J. Y., and Choi, U. S. (2014). Hierarchically porous aminosilica monolith as a CO_2 adsorbent. *ACS Appl. Mater. Interf.* 6, 12988–12996. doi: 10.1021/am5029022
- Liu, Y., Jiang, Y., Hu, M., Li, S., and Zhai, Q. (2015). Removal of triphenylmethane dyes by calcium carbonate-lentinan hierarchical mesoporous hybrid materials. *Chem. Eng. J.* 273, 371–380. doi: 10.1016/j.cej.2015.03.109
- Magnacca, G., Allera, A., Montoneri, E., Celi, L., Benito, D. E., Gagliardi, L. G., et al. (2014). Novel magnetite nanoparticles coated with waste-sourced biobased substances as sustainable and renewable adsorbing materials. *ACS Sustain. Chem. Eng.* 2, 1518–1524. doi: 10.1021/sc500213j
- Magnacca, G., Laurenti, E., Vigna, E., Franzoso, F., Tomasso, L., Montoneri, E., et al. (2012). Refuse derived bio-organics and immobilized soybean peroxidase for green chemical technology. *Process Biochem.* 47, 2025–2031. doi: 10.1016/j.procbio.2012.07.021
- Masika, E., and Mokaya, R. (2011). Mesoporous aluminosilicates from a zeolite BEA recipe. *Chem. Mater.* 23, 2491–2498. doi: 10.1021/cm200706n
- Montoneri, E., Boffa, V., Savarino, P., Perrone, D., Ghezzi, M., Montoneri, C., et al. (2011). Acid soluble bio-organic substances isolated from urban bio-waste. Chemical composition and properties of products. *Waste Manage.* 31, 10–17. doi: 10.1016/j.wasman.2010.08.029
- Montoneri, E., Boffa, V., Savarino, P., Perrone, D. G., Musso, G., Mendichi, R., et al. (2009). Biosurfactants from urban green waste. *ChemSusChem* 2, 239–247. doi: 10.1002/cssc.200800199
- Montoneri, E., Boffa, V., Quagliotto, P. L., Mendichi, R., Chierotti, M. R., Gobetto, R., et al. (2008). Humic acid-like matter isolated from green urban wastes. Part I: structure and surfactant properties. *Bioresources* 3, 123–141.
- Namasivayam, C., Kumar, M. D., Selvi, K., Begum, R. A., Vanathi, T., and Yamuna, R. T. (2001). ‘Waste’ coir pith — a potential biomass for the treatment of dyeing wastewaters. *Biomass Bioenergy* 21, 477–483. doi: 10.1016/S0961-9534(01)00052-6
- Nayak, N., Huertas, R., Crespo, J. G., and Portugal, C. A. M. (2019). Surface modification of alumina monolithic columns with 3-aminopropyltriethoxysilane (APTES) for protein attachment. *Separat. Purif. Technol.* 2019:115674. doi: 10.1016/j.seppur.2019.115674
- Nisticò, R., Barrasso, M., Carrillo Le Roux, G. A., Seckler, M. M., Sousa, W., Malandrino, M., et al. (2015). Biopolymers from composted biowaste as stabilizers for the synthesis of spherical and homogeneously sized silver nanoparticles for textile applications on natural fibers. *ChemPhysChem* 7, 3902–3909. doi: 10.1002/cphc.201500721
- Ren, A., Zahid, A., Fan, D., Yang, X., Imran, M. A., Alomainy, A., et al. (2019). State-of-the-art in terahertz sensing for food and water security – a comprehensive review. *Trends Food Sci. Technol.* 85, 241–251. doi: 10.1016/j.tifs.2019.01.019
- Sadraei, R. (2019). Fast, green and easy adsorption of dye and emerging contaminants by functionalized γ -AACH. *J. Environ. Chem. Eng.* 8:100632. doi: 10.1016/j.jece.2019.103616
- Sadraei, R., Murphy, R. S., Laurenti, E., and Magnacca, G. (2019a). Characterization methodology to evaluate the activity of supported soybean peroxidase. *Ind. Eng. Chem. Res.* 58, 19082–19089. doi: 10.1021/acs.iecr.9b03495
- Sadraei, R., Paganini, M. C., Calza, P., and Magnacca, G. (2019b). An easy synthesis for preparing bio-based hybrid adsorbent useful for fast adsorption of polar pollutants. *Nanomaterials* 9:731. doi: 10.3390/nano9050731
- Serbezov, A., Moore, J. D., and Wu, Y. (2011). Adsorption equilibrium of water vapor on selexsorb-CDX commercial activated alumina adsorbent. *J. Chem. Eng. Data* 56, 1762–1769. doi: 10.1021/je100473f
- Shanaghi, A., Soury, A. R., Rafie, M., and Chu, P. K. (2019). Nano-mechanical properties of zirconia-alumina-benzotriazole nano-composite coating deposited on Al2024 by the sol-gel method. *Thin Solid Films* 689:137417. doi: 10.1016/j.tsf.2019.137417
- Sifontes, Á. B., Gutierrez, B., Mónaco, A., Yanez, A., Díaz, Y., Méndez, F. J., Llovera, L., Cañizales, E., and Brito, J. L. (2014). Preparation of functionalized porous nano- γ - Al_2O_3 powders employing colophony extract. *Biotechnol. Rep.* 4, 21–29. doi: 10.1016/j.btre.2014.07.001
- Tang, H., Hao, L., Chen, J., Wang, F., Zhang, H., and Guo, Y. (2018). Surface modification to fabricate superhydrophobic and superoleophilic alumina membranes for oil/water separation. *Energy Fuels* 32, 3627–3636. doi: 10.1021/acs.energyfuels.7b03344
- Thommes, M., Kaneko, K., Neimark, A. V., Olivier, J. P., Rodriguez-Reinos, F., Rouquerol, J., et al. (2015). Physisorption of gases, with special reference to the evaluation of surface area and pore size distribution (IUPAC Technical Report). *Pure Appl. Chem.* 87, 1051–1069. doi: 10.1515/pac-2014-1117
- Unuabonah, E. I., Günter, C., Weber, J., Lubahn, S., and Taubert, A. (2013). Hybrid clay: a new highly efficient adsorbent for water treatment. *ACS Sustain. Chem. Eng.* 1, 966–973. doi: 10.1021/sc400051y
- Vega, M., Nerenberg, R., and Vargas, I. T. (2018). Perchlorate contamination in Chile: legacy, challenges, and potential solutions. *Environ. Res.* 164, 316–326. doi: 10.1016/j.envres.2018.02.034

- Ye, S., Liu, Y., and Feng, J. (2017). Low-density, mechanical compressible, water-induced self-recoverable graphene aerogels for water treatment. *ACS Appl. Mater. Interfaces* 9, 22456–22464. doi: 10.1021/acsami.7b04536
- Yu, Z., Zhang, X., and Huang, Y. (2013). Magnetic chitosan-iron(III) hydrogel as a fast and reusable adsorbent for chromium(VI) removal. *Ind. Eng. Chem. Res.* 52, 11956–11966. doi: 10.1021/ie400781n
- Zeng, H., Yin, C., Qiao, T., Yu, Y., Zhang, J., and Li, D. (2018). As(V) removal from water using a novel magnetic particle adsorbent prepared with iron-containing water treatment residuals. *ACS Sustain. Chem. Eng.* 6, 14734–14742. doi: 10.1021/acssuschemeng.8b03270

Conflict of Interest: The authors declare that the research was conducted in the absence of any commercial or financial relationships that could be construed as a potential conflict of interest.

Copyright © 2020 Magnacca, Neves Dos Santos and Sadraei. This is an open-access article distributed under the terms of the Creative Commons Attribution License (CC BY). The use, distribution or reproduction in other forums is permitted, provided the original author(s) and the copyright owner(s) are credited and that the original publication in this journal is cited, in accordance with accepted academic practice. No use, distribution or reproduction is permitted which does not comply with these terms.



Activated Carbons From Winemaking Biowastes for Electrochemical Double-Layer Capacitors

Lorena Alcaraz^{1*}, Alberto Adán-Más², Pablo Arévalo-Cid², Maria de Fatima Montemor² and Félix A. López¹

¹ Centro Nacional de Investigaciones Metalúrgicas (CENIM), Consejo Superior de Investigaciones Científicas (CSIC), Madrid, Spain, ² Departamento Engenharia Química, Centro de Química Estrutural-CQE, Instituto Superior Técnico, Universidade de Lisboa, Lisbon, Portugal

OPEN ACCESS

Edited by:

Enrico Traversa,
University of Electronic Science and
Technology of China, China

Reviewed by:

Mohammad Boshir Ahmed,
Gwangju Institute of Science and
Technology, South Korea
Raffaele Cucciniello,
University of Salerno, Italy

*Correspondence:

Lorena Alcaraz
alcaraz@cenim.csic.es

Specialty section:

This article was submitted to
Green and Sustainable Chemistry,
a section of the journal
Frontiers in Chemistry

Received: 14 May 2020

Accepted: 01 July 2020

Published: 14 August 2020

Citation:

Alcaraz L, Adán-Más A, Arévalo-Cid P,
Montemor MdF and López FA (2020)
Activated Carbons From Winemaking
Biowastes for Electrochemical
Double-Layer Capacitors.
Front. Chem. 8:686.
doi: 10.3389/fchem.2020.00686

Revalorizing organic biowaste is critical to achieve a full circular economy, where waste is transformed into resources. One of the main strategies is to produce activated carbons and use them as functional materials for electrochemical energy storage. In this study, winemaking wastes, bagasse (BAG), and cluster stalks (CS) were recovered and used in the preparation of activated carbons by a hydrothermal process. Then, they were chemically activated using KOH and investigated for electrochemical capacitor applications. The activation treatment resulted in microporous structures, characterized by a type I isotherm for low partial pressures (P/P_0), and a type IV for higher pressures, as observed by Brunauer–Emmett–Teller surface analysis, with specific surfaces of 1,861 and 2,662 $\text{m}^2\cdot\text{g}^{-1}$ for BAG and CS, respectively. These microporous structures were also investigated by means of scanning electron microscopy, revealing a high porous degree. Micro-Raman spectroscopy and X-ray photoelectron spectroscopy measurements displayed bands associated to disorder of the structure of the carbonaceous material. The electrochemical performance of the resulting materials was investigated for electrochemical energy storage applications, as supercapacitor electrode, in 1 M KOH aqueous electrolyte. These biowaste-derived materials displayed electrochemical double-layer capacitance, with 129 $\text{F}\cdot\text{g}^{-1}$ at 10 $\text{A}\cdot\text{g}^{-1}$ in the 0.1 to -1.0 V vs. saturated calomel electrode. For that reason, they are pin-pointed as potential negative electrodes for electrochemical double-layer supercapacitors and hybrid or asymmetric supercapacitors.

Keywords: wine biowastes, biomass reuse, activated carbon, electrochemical double-layer capacitor, supercapacitors

INTRODUCTION

The increasing demographic evolution over the last century alongside the industrial development of highly populated countries, such as India or China, has led to an increased demand for raw materials. This need entails a great environmental risk associated with the overexploitation of natural resources and the release of industrial waste. Nowadays, new habits to minimize the environmental impact have emerged, including a growing interest on the use of natural and bio-based products (Sardella et al., 2015). In addition, different valorization processes of waste are being considered as a mean to generate more efficient and tailored materials.

In this sense, obtaining activated carbons from waste is, currently, one important goal. Practically any raw materials with high carbon content, including several wastes, may yield interesting and useful materials (Deiana et al., 2009). Various waste sources have been proposed for the preparation of activated carbon, from biodiesel (Gonçalves et al., 2019) to food processing waste (Ramón-Gonçalves et al., 2019; Senophiyah-Mary et al., 2019; Yaglikci et al., 2020) or agriculture industry residues (Ukanwa et al., 2019), all of them with great attractiveness owing to their large-scale production and low price. Winemaking-derived waste is a major issue in the wine industry, being Spain, the origin of the precursor wine used in this work, the third world producer of wine (Maicas and Mateo, 2020). Among others, a great amount of skins, seeds, and stems left are generated in the process (Mingo et al., 2016). In this sense, bagasse is the residual material obtained after the pressing of grapes to extract the must, and contains grape skin, pulp, and seeds. Cluster stalks are waste generated after the grapes are removed from their woody support.

Different methods have been used to obtain activated carbons such as carbonization/leaching (Deiana et al., 2009), pyrolysis (Rajamani et al., 2018), impregnation with several activation agents (Chen et al., 2017), demineralization (Chan et al., 2011), or extraction with organic solvent (Jiménez-Cordero et al., 2014), among others. However, these processes need high-temperature treatments, increasing the total cost of the process, and usually yield materials with low specific surface areas with limited use. To increase cost-effectiveness while improving the final properties of the resulting material, hydrothermal pre-carbonization is gaining attention for the preparation of carbon-based materials from several biowastes (Jain et al., 2016). The benefits of this process as pre-treatment of precursor biowaste are two-fold. On the one hand, it reduces the total cost of the production because hydrothermal carbonization followed by chemical activation leads to increased efficiency of the subsequent activation process. On the other hand, the two-step process improves the microstructural features of the final material and, as a result, the properties of the activated carbon can be tailored to the application.

Among all the potential uses of activated carbons, such as catalyst or catalyst support [Sadashiv Bhubanale and Shivashankar, 2017], pollutant adsorption (Alguacil et al., 2018; Alcaraz et al., 2019, 2020), or hydrogen production (Tsytarski et al., 2015; Prabu et al., 2019), their application in energy storage as electrodes for electrochemical double-layer capacitors (EDLCs) (Chang and Zainal, 2019) has attracted an immense interest from the scientific community.

EDLCs store energy in the form of electrostatic charge at the electrode–electrolyte interface. Large active surface area materials are required to attain large capacitance values, and, for that reason, active carbons are generally used. In contrast to classical batteries, there is no Faradaic reaction involved, which would imply diffusion-controlled chemical reactions in the material that imply slower response. Therefore, EDLCs exhibit better power capabilities (Lei et al., 2013) and the absence of chemical reactions allows to extend their useful lifetime to over 100,000 charge–discharge cycles.

Although previous studies have reported the use of activated carbons from winemaking waste for energy storage applications (Jiménez-Cordero et al., 2014; Guardia et al., 2018, 2019), most literature focuses on their performance in two-electrode systems. Studying their performance in three-electrode systems is key to understanding their applicability in asymmetric and hybrid devices. Moreover, to the best of our knowledge, the study of electrochemical properties for this type of materials has been scarcely investigated in certain cases, without an in-depth investigation on their cycling stability or their performance at high applied currents.

In the present work, the preparation of activated carbons from both winemaking wastes, bagasse (BAG), and cluster stalks (CS), is described. Hydrothermal carbonization as pre-treatment of chemical activation is used to obtain activated carbons with improved specific surface. Textural properties, and structural and morphological characterization have been investigated by several techniques, and their applicability to electrochemical energy storage systems has been addressed. The electrochemical performance of the obtained activated carbons from winemaking wastes is investigated using 1 M KOH aqueous electrolyte.

MATERIALS AND METHODS

Preparation of the Activated Carbons From the Biowastes

Activated carbons were generated from BAG and CS, winemaking wastes generated in the production of Albariño wine (Denomination of Origin “Rias Baixas,” Galicia, Spain). These biowastes were supplied by Mision Biológica de Galicia (CSIC). Both BAG and CS were separately ground to achieve a grain size of <2 mm. After that, aqueous suspensions of 75 g·L⁻¹ were prepared. The mixtures were introduced into a high-pressure reactor at 523 K for 3 h and 30 bar. Then, the aqueous suspensions were filtered through a pressure filter, obtaining the activated carbon precursors. Finally, these were chemically activated with KOH (1:2 ratio) in a tubular oven under a N₂ atmosphere (150 mL·min⁻¹) at 1,073 K for 2 h. After cooling down to room temperature, the obtained activated carbons were washed with MilliQ water until a neutral pH was achieved. These materials are henceforward denominated BAG and CS.

Physicochemical Characterization

The microporous structure of the obtained carbonaceous materials was evaluated by N₂ adsorption. Measurements were carried out using a Micromeritics ASAP 2010 Accelerated Surface Area and Porosimetry System at 77 K. The specific surfaces were determined by analyzing the N₂ adsorption isotherm from the Brunauer–Emmett–Teller (BET) equation (Brunauer et al., 1938) and Density Functional Theory (DFT) model (Nič et al., 2009) using a Micromeritics and Quantachrome software. The BET and DFT results were compared using Kaneko (Kaneko et al., 1992) and Dubinin (Nguyen and Do, 2001) equations. Micro-Raman measurements were carried out in a Horiba Jovin Yvon LabRAM HR800 system at room temperature. The samples were excited by a 633 nm He–Cd laser on an Olympus BX 41

confocal microscope with a $\times 40$ objective. A charge-coupled device detector was used to collect the scattered light dispersed by a $2,400 \text{ lines mm}^{-1}$ grating (micro-Raman) with a spectral resolution of 1.5 cm^{-1} . X-ray photoelectron spectroscopy (XPS) spectra were recorded using a Fisons MT500 spectrometer equipped with a hemispherical electron analyzer (CLAM2) and a non-monochromatic Mg K_{α} X-ray source operated at 300 W. Spectra were collected at a pass energy of 20 eV (typical for high-resolution conditions). The area under each peak was calculated after subtraction of the S-shaped background and fitting the experimental curve to a combination of Lorentzian and Gaussian lines of variable proportions. Binding energies were calibrated to the C 1s peak at 285.0 eV. The atomic ratios were computed from the peak intensity ratios and reported atomic sensitivity factors. Morphological characterization was performed by scanning electron microscopy (SEM) using a JEOL JSM-7600F. For these observations, the powder samples were placed on an adhesive conductive carbon disk.

Electrochemical Characterization

To evaluate the electrochemical properties of the activated carbons, a slurry was prepared using standard conditions reported elsewhere (Gören et al., 2015), that is, by mixing 80% of active material, 15% conductive carbon, and 5% PVDF dispersed in N-methyl-2-pyrrolidone. The slurry was impregnated on Toray Carbon Paper, which serves as conductive substrate, and then dried at 40°C for 12 h. Electrochemical performance was evaluated using 1 M KOH electrolyte in a three-electrode cell configuration. The coated carbon paper, a $2.5 \times 2.5 \text{ cm}^2$ platinum foil, and a saturated calomel electrode were employed as working, counter, and reference electrode, respectively. The electrochemical tests were performed in a Gamry Instruments IFC1000-07087 potentiostat. Cyclic voltammetry was performed at scan rates from 10 to $350 \text{ mV}\cdot\text{s}^{-1}$. Galvanostatic charge-discharge curves were obtained in the range -1.0 to 0.1 V at different specific currents (1 – $10 \text{ A}\cdot\text{g}^{-1}$). Electrochemical impedance spectroscopy (EIS) studies were performed after holding the electrode for 2,000 s open circuit potential to ensure signal stabilization, by applying a sinusoidal perturbation with 10 mV amplitude in the frequency range from 0.01 to 10^5 Hz . Material stability was tested by continuous galvanostatic charge-discharge experiments at $10 \text{ A}\cdot\text{g}^{-1}$ during 5,000 cycles.

RESULTS AND DISCUSSION

Characterization of the Activated Carbons Textural Features

The textural properties of the activated carbons were assessed by N_2 adsorption-desorption isotherms (Figure 1). For both activated carbons, the adsorbed N_2 volume ($\text{cm}^3\cdot\text{g}^{-1}$) significantly increases with the relative pressure (P/P_0) for relative pressures below 0.1, which indicates the presence of microporosity in both samples. At higher relative pressures, hysteresis loops were found, indicating the presence of mesopores (Beltrame et al., 2018). These results reveal the presence of both micropores and mesopores. According to the IUPAC (Thommes et al., 2015), the obtained shapes correspond

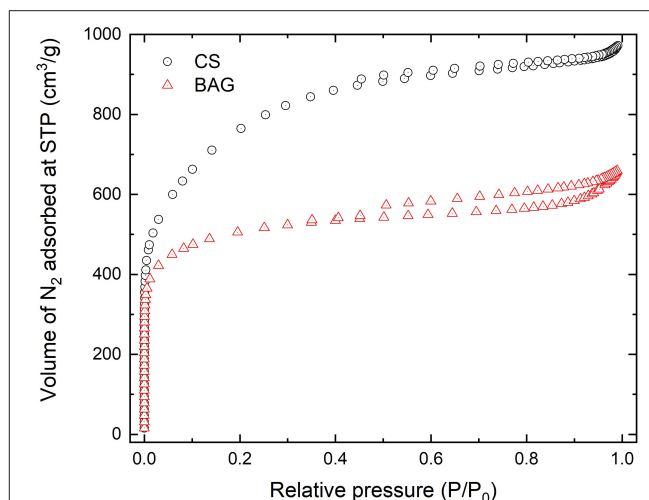


FIGURE 1 | N_2 adsorption-desorption isotherms for winemaking-derived activated carbons from bagasse (BAG) and cluster stalks (CS).

TABLE 1 | Textural properties for both activated carbons obtained from the winemaking wastes.

	BAG	CS
Total pore volume ($\text{cm}^3\cdot\text{g}^{-1}$)	0.8	1.4
Micropore volume ($\text{cm}^3\cdot\text{g}^{-1}$)	0.7	0.9
Average micropore size (nm)	1.2	1.7
Microporous surface ($\text{m}^2\cdot\text{g}^{-1}$)	1,244	1,111
Total surface area ($\text{m}^2\cdot\text{g}^{-1}$)	1,337	1,194
S_{BET} ($\text{m}^2\cdot\text{g}^{-1}$)	1,861	2,662

to type I and type IV isotherms, respectively. The volume of N_2 adsorbed was lower for the BAG sample than for the CS sample. However, the micropore volume (Table 1) was similar for both activated carbons. The total pore volume for the BAG sample was lower than for CS (0.8 and $1.4 \text{ cm}^3\cdot\text{g}^{-1}$, respectively). Also, the average pore sizes were 1.2 and 1.7 nm (lower than 2 nm in both cases), revealing that the obtained activated carbons mainly exhibit a microporous structure (Nič et al., 2009). The obtained results could indicate that the CS sample exhibits a greater number of mesopores. For this reason, the total volume of N_2 adsorbed was the highest. Finally, the specific surface areas were calculated using the Dubinin and the BET equations. Although the BET equation shall be carefully interpreted for microporous materials, it is widely used for determining the specific surface area of porous carbons (Guardia et al., 2018). Therefore, BET surface areas are included for comparison purposes. The obtained values were $1,337$ and $1,861 \text{ m}^2\cdot\text{g}^{-1}$ for the BAG sample and $1,194$ and $2,662 \text{ m}^2\cdot\text{g}^{-1}$ for the CS sample. The calculated BET surfaces were higher than the obtained total surface areas from the Dubinin equation, which could be associated to pore sizes being higher than 1 nm. In these cases, the BET equation tends to overestimate the results, as previously reported in literature (Centeno and Stoeckli, 2010).

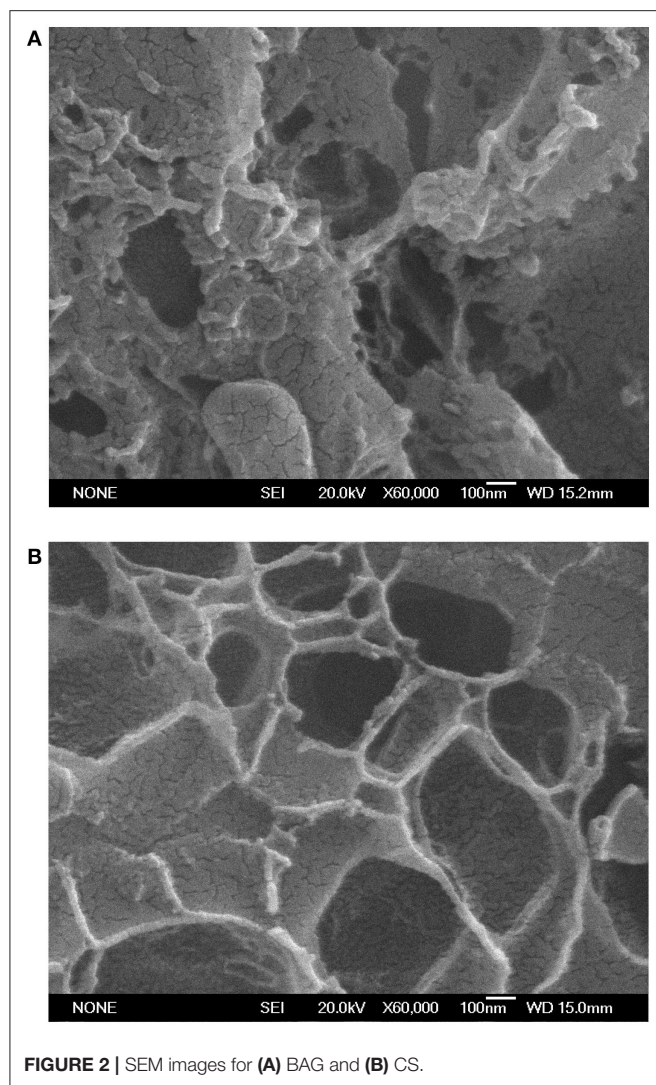


FIGURE 2 | SEM images for (A) BAG and (B) CS.

Scanning Electron Microscopy

SEM micrographs for the BAG and CS activated carbon samples (Figures 2A,B) exhibit a microporous microstructure. A large number of pores can be observed, caused by the chemical interaction between the precursor surface and the activation agent (KOH). The obtained pores were irregular and oval, like embedded deep holes typically observed after chemical activation (El-Naggar et al., 2015; Ravichandran et al., 2018). BAG images denote areas with material agglomerates, where porosity is found between these mass portions. Oppositely, images of carbon obtained from CS reveal low aggregated rates with larger porosity, which is in accordance with the results of nitrogen adsorption experiments.

Micro-Raman Spectroscopy

Two predominant bands can be observed in the Raman spectra for CS and BAG samples (Figure 3) with peaks at around 1,350 and 1,600 cm^{-1} . As previously reported for carbonaceous materials (Sfyris et al., 2017), these bands can be attributed to

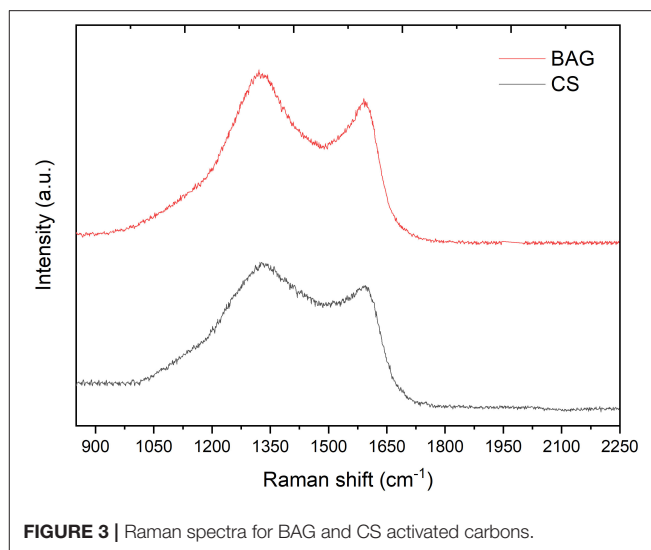
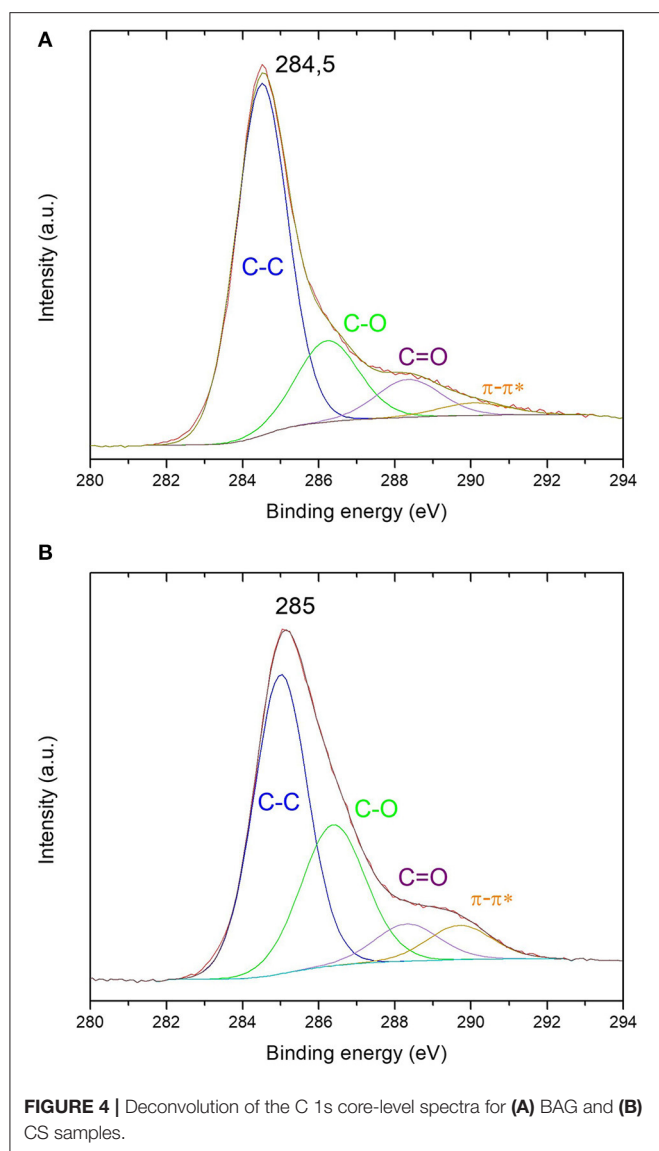


FIGURE 3 | Raman spectra for BAG and CS activated carbons.

A_{1g} and E_{2g} modes, also known as D and G bands, respectively. The D band indicates the disorder and degree of defective structure, whereas the G band is related to the graphitization of the samples. The intensity ratio (I_D/I_G) can provide information about the disorder and graphitization degree of the activated carbons (Zhang et al., 2018; Yagmur et al., 2020). Furthermore, it has been reported that overlapped bands in the range 1,400–1,500 cm^{-1} can be observed for amorphous carbons (Shimodaira and Masui, 2002). For the obtained carbon-based materials, in both cases, the D band was more intense than the G band. The calculated ratio of the D and G Raman signal was 1.08 and 1.1 for BAG and CS, respectively. In addition, a broadening of the D band for CS was found. Thus, the obtained results indicate that the CS sample exhibits a higher disorder degree than BAG.

X-Ray Photoelectron Spectroscopy

XPS measurements were performed to investigate the chemical composition of the samples. Asymmetric broad photoionizations were found in both cases (Figures 4A,B). The deconvolution of the C 1s core-level spectra shows four different peaks, which can be assigned to the sp^2 carbon bonding, C–O bonding, C=O bonding, and $\pi-\pi^*$ transitions (Estrade-Szwarczkopf, 2004; Jerng et al., 2011; Dwivedi et al., 2015). The binding energy values found for the main peak were 284.5 eV for BAG and 285.0 eV for CS. A slight shift toward lower binding energies was found. In addition, a difference in the width of the curve is appreciable when comparing both samples. These spectra are consistent with the presence of a main band with binding energy at 284 eV that corresponds to graphite, with a distortion of the peak, resulting from the appearance of disorder in the structure. The maximum of the CS photoionization appears at higher binding energies than the BAG sample and its width is considerably higher owing to this disorder. The obtained results reveal that the CS sample exhibits a lower graphitization degree, in good agreement with the obtained Raman results. $\pi-\pi^*$ transition peaks are the result of the stacking of the graphitic portion.



C–O/C=O signals exposed the presence of oxygen-containing surficial groups, which appears in carbonization processes in presence of oxygen and can only be eliminated at very high temperatures (Estrade-Szwarczkopf, 2004).

Electrochemical Characterization

Electrochemical Double-Layer Capacitance Analysis

BAG and CS wine biowaste-derived materials have been investigated as potential electrode materials in EDLCs. **Figures 5A,B** displays cyclic voltammetry results of the carbon-based materials in 1 M KOH in the -1.1 to 0.15 V range for CS and in the -1.0 to 0.1 V electrochemical window for BAG at different scan rates. Both present a quasi-ideal capacitive response at low scan rates. Nonetheless, when comparing the performance of both samples at scan rates over $200 \text{ mV}\cdot\text{s}^{-1}$, CS displays a tilted cyclic voltammogram, associated to increased

resistance whereas BAG's cyclic voltammetry maintains its shape even at the scan rate of $350 \text{ mV}\cdot\text{s}^{-1}$.

Discharge curves (**Figures 5C,D**) display a linear time-potential relationship in any case, as expected for a double-layer capacitance charge storage mechanism. On the one hand, BAG exhibits a capacitance of $134 \text{ F}\cdot\text{g}^{-1}$ at $1 \text{ A}\cdot\text{g}^{-1}$ and $129 \text{ F}\cdot\text{g}^{-1}$ at $10 \text{ A}\cdot\text{g}^{-1}$, which represents 96% capacitance retention when the applied current is ten-folded. On the other hand, CS has a capacitance of $95 \text{ F}\cdot\text{g}^{-1}$ at $1 \text{ A}\cdot\text{g}^{-1}$ and $86 \text{ F}\cdot\text{g}^{-1}$ at $10 \text{ A}\cdot\text{g}^{-1}$, corresponding to 90% capacitance retention at $10 \text{ A}\cdot\text{g}^{-1}$. Whereas, BAG has higher capacitance and better capacitance retention, CS is active in a slightly larger electrochemical window (**Figure 5E**). Both materials exhibit excellent capacitance retention at higher applied currents, indicating their potential for high-power applications.

Long-Term Stability

Capacitance retention was evaluated after 5,000 continuous charge-discharge cycles at $10 \text{ A}\cdot\text{g}^{-1}$ and presented in **Figure 5F**. CS retains $\sim 98\%$ of its initial capacitance, resulting in a capacitance of $84 \text{ F}\cdot\text{g}^{-1}$ after the electrochemical cycling stability evaluation. Alternatively, BAG has a slightly lower capacitance retention, with $120 \text{ F}\cdot\text{g}^{-1}$ at $10 \text{ A}\cdot\text{g}^{-1}$ after 5,000 cycles as compared with the initial $129 \text{ F}\cdot\text{g}^{-1}$, which represents 93% capacitance retention. Although CS shows slightly better performance, both materials display good capacitance retention after continuous charge-discharge, as expected for carbon-derived materials.

Table 2 presents a brief review of previously reported activated carbons obtained from winemaking wastes applied in electrochemical energy storage for comparison purposes. The results obtained in this work display comparable performance, even when high currents are applied. In addition, cycling stability is evaluated for the first time, to the best of author's knowledge, in wine biowaste-derived carbons.

Electrochemical Impedance Spectroscopy

Figure 6 illustrates the electrochemical impedance spectroscopy results for the CS and BAG-derived materials. Both display a quasi-ideal capacitive behavior, usually observed in carbon-based materials. This is in accordance with the results obtained by cyclic voltammetry and galvanostatic discharge. At high and mid-frequencies, from 10^5 to ~ 1 – 10 Hz, both materials display a purely resistive behavior, with a plateau in the modulus frequency (**Figure 6A**) and a close-to-zero phase angle (**Figure 6B**). The Nyquist plot (**Figure 5C**) shows an equivalent series resistance (ESR) of 2.65 Ohm for BAG and a charge-transfer resistance of 151 mOhm , whereas the CS-derived material displays an ESR of 3.8 Ohm and a charge-transfer resistance of 89 mOhm . Equivalent series resistance arises from the wiring and current collector resistance, the electrolyte resistance, and the contact and ionic resistances associated to the electrode-electrolyte interphase (Li et al., 2015). Both materials, prepared under the same conditions, present a depressed semi-circle, which accounts for the internal resistance of the electrode. In any case, both materials present a quasi-ideal behavior with a nearly parallel response to

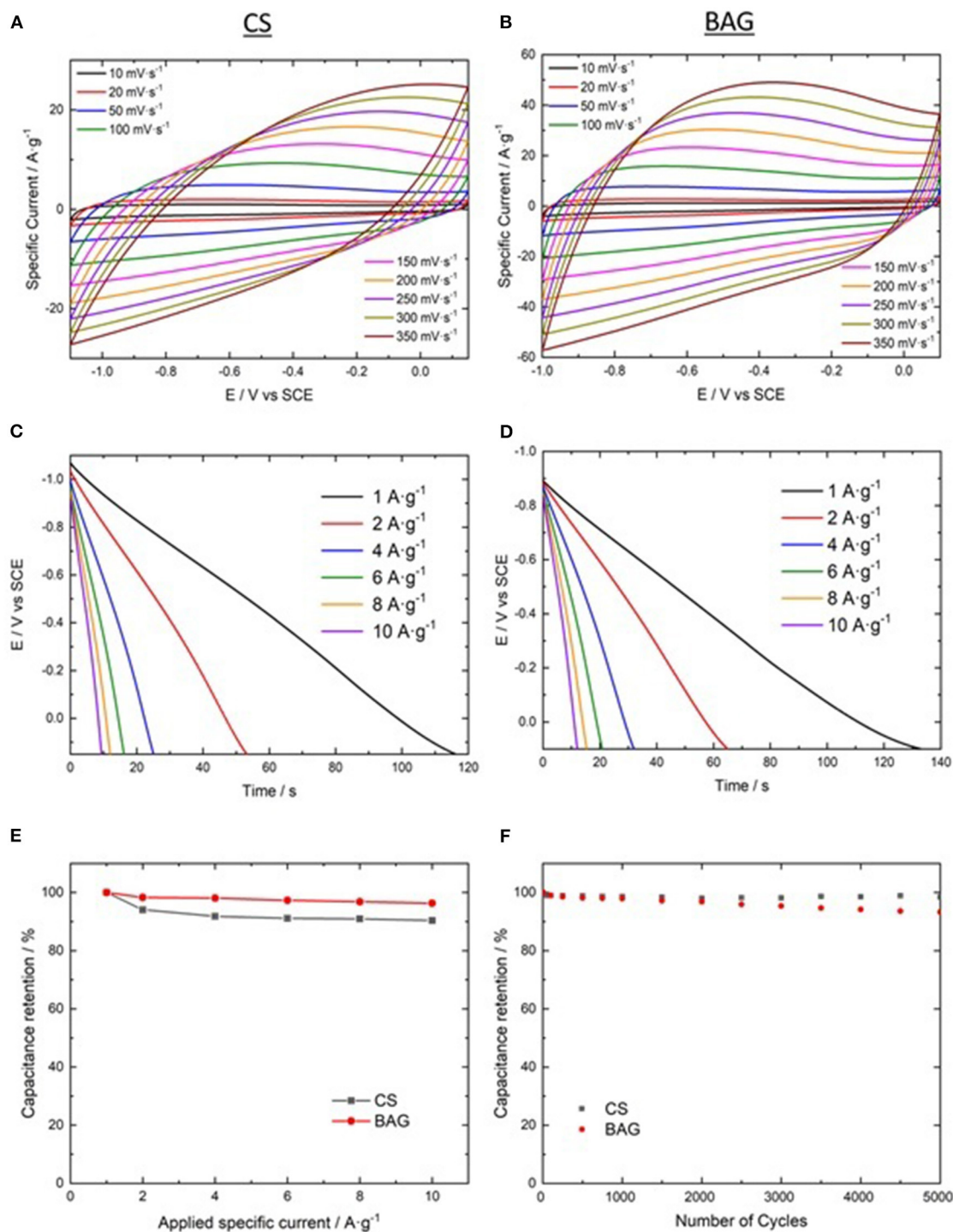


FIGURE 5 | Electrochemical characterization of CS (A,C) and BAG (B,D) by cyclic voltammetry (A,B) and galvanostatic charge–discharge (C,D) at different scan rates and applied currents, respectively. (E) Capacitance retention of each material at different applied specific currents. (F) Capacitance retention after 5,000 cycles of continuous charge–discharge at 10 A g⁻¹ in 1 M KOH.

the imaginary axis in the mid- and low-frequency range, as observed in the Nyquist plot, and a phase angle close to -80° . Nonetheless, a deviation from the ideal behavior is

explained by the contribution to the total impedance of certain diffusion-controlled phenomena that may be associated to the materials' porosity.

TABLE 2 | Comparison of obtained electrochemical results with previous work on activated carbons from winemaking waste.

Waste	Treatment	C (F·g ⁻¹)	I	Electrolyte	Cycling stability (%)	References
Grape seed	Air/O ₃ /HNO ₃	90–130	200 mA·g ⁻¹	H ₂ SO ₄ 1 M	–	Jiménez-Cordero et al., 2014
		50–70	200 mA·g ⁻¹	Na ₂ SO ₄ 1 M	–	
		80–110	200 mA·g ⁻¹	KOH 1 M	–	
Grape seed	KOH	75	200 mA·cm ⁻²	H ₂ SO ₄	–	Guardia et al., 2019
		45	200 mA·cm ⁻²	H ₂ SO ₄	–	
Bagasse	KOH	262–268	1 mA·cm ⁻²	H ₂ SO ₄ 2 M	–	Guardia et al., 2018
		142	1 mA·cm ⁻²	EMImBF ₄ /AN	–	
Stalks	KOH	289–296	1 mA·cm ⁻²	H ₂ SO ₄ 2 M	–	
		145–179	1 mA·cm ⁻²	EMImBF ₄ /AN	–	
Grape seed	KOH	262–269	1 mA·cm ⁻²	H ₂ SO ₄ 2 M	–	
		157–160	1 mA·cm ⁻²	EMImBF ₄ /AN	–	
Grape seed	KOH	210–300	1 mA·cm ⁻²	H ₂ SO ₄ 2 M	–	Suárez and Centeno, 2020
Bagasse	KOH	80–160	1 mA·cm ⁻²	H ₂ SO ₄ 2 M	–	
		260–270	1 mA·cm ⁻²	H ₂ SO ₄ 2 M	–	
		150–160	1 mA·cm ⁻²	H ₂ SO ₄ 2 M	–	
Stalks	KOH	260–270	1 mA·cm ⁻²	H ₂ SO ₄ 2 M	–	
Bagasse (BAG)	KOH	134	1 A·g ⁻¹	KOH 1 M	–	This work
		129	10 A·g ⁻¹	KOH 1 M	93 (5,000 cycles)	This work
Stalks (CS)	KOH	95	1 A·g ⁻¹	KOH 1 M	–	This work
		86	10 A·g ⁻¹	KOH 1 M	98 (5,000 cycles)	This work

Complex Capacitance Analysis

The real and imaginary capacitances as a function of the frequency are obtained using a complex capacitance analysis (Taberna et al., 2003), as described by the following equations and presented in **Figure 6D**.

$$C'(\omega) = -\frac{Z''(\omega)}{2\pi f |Z(\omega)|^2} \quad (1)$$

$$C'' = \frac{Z'(\omega)}{2\pi f |Z(\omega)|^2} \quad (2)$$

where Z' and Z'' are the real and imaginary parts of impedance in Ohm, respectively, f is the frequency in Hz, and $|Z(\omega)|$ is the modulus of impedance in Ohm. The real part of impedance attains a value of 145 mF·cm⁻² for BAG, whereas CS displays 88 mF·cm⁻², in accordance with the evolution observed by means of the galvanostatic discharge curves. As observed, the imaginary part goes through a maximum at a certain frequency (f_0) that defines a time constant, known as the characteristic relaxation time constant $\tau_0 = 1/f_0$. This is considered a supercapacitor's factor of merit and is defined as “the minimum time needed to discharge all the energy from the device with an efficiency >50%” (Pech et al., 2010). In this case, CS has a factor of merit of 3.9 s, whereas BAG displays only 1.6 s, in agreement with the ESR values and the good performance at high applied currents.

Finally, EIS is evaluated after the first and last discharge curve during the cycling stability test (**Figure 6**). Three main features can be observed after 5,000 cycles. First, there is a 10% increase in the ESR. Second, the charge-transfer resistance for CS is maintained whereas for BAG it is slightly reduced to 126 mOhm. Third, both materials present almost identical behavior at mid- and low frequencies before and after continuous cycling, with the exception of CS at frequencies below 0.5 Hz, that presents a slightly decreased phase angle to -82° and BAG at frequencies lower than 0.03 Hz, which decreases its phase angle in 2° . Considering these results altogether, the integrity of the energy storage process, correlated to the active surface and porosity of the activated carbon, is maintained through continuous charge-discharge, thus retaining most of the initial capacitance of the material, as observed in **Figure 5F**, but a slight increase in system resistance for BAG, probably as a result of pore clogging leading to a smaller capacitance retention than for CS. Nonetheless, both materials show excellent properties for electrochemical double layer applications.

The electrochemical performance of a material is the result of its morphological character, chemical composition, and their interaction with the electrolyte. As observed by means of N₂ adsorption experiments, both materials present great microporous surfaces, being slightly larger for BAG. This bagasse-derived carbon also possesses higher order and graphitic nature, as revealed by Raman and XPS. Therefore, this enhanced structure and chemical composition are reflected in the final

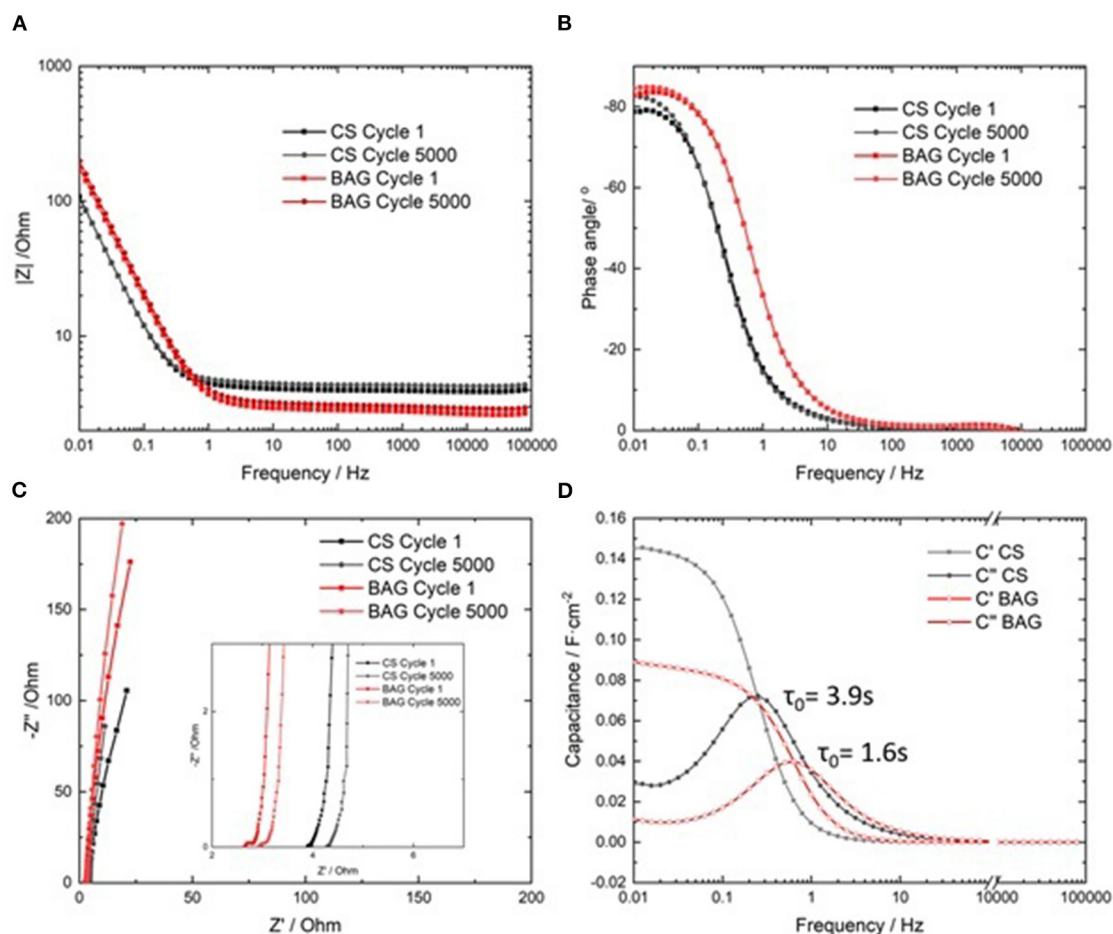


FIGURE 6 | (A–C) Electrochemical impedance spectroscopy results for CS and BAG after 1 and 5,000 charge–discharge cycles. **(D)** Complex analysis of impedance results.

electrochemical results, leading to lowered system resistance, as observed by cyclic voltammetry and electrochemical impedance spectroscopy, affecting final capacitance and performance at higher scan rates and applied currents. All these factors result in a better electrochemical performance of BAG when compared with CS. Nonetheless, both materials present excellent performance as negative electrodes for electrochemical energy storage. Therefore, BAG and CS can potentially be reinserted in a circular economy approach after their chemical activation.

CONCLUSIONS

Activated carbons were obtained from different winemaking wastes, bagasse (BAG) and cluster stalks (CS), by a hydrothermal process and subsequent chemical activation with KOH. This process leads to activated carbons with specific surfaces of 1,861 and 2,662 $m^2 \cdot g^{-1}$ for the BAG and CS samples, respectively. As adsorption–desorption N_2 isotherms reveal the presence of micropores and mesopores in both samples. Raman spectra for both activated carbons exhibit two predominant bands

assigned to the D and G bands, typical of carbonaceous materials. In addition, Raman measurements indicate that the CS-derived sample exhibits a higher disorder degree than BAG. The electrochemical properties of these activated carbons are studied for electrochemical double-layer capacitor applications. Capacitance values of 129 and 86 $F \cdot g^{-1}$ at 10 $A \cdot g^{-1}$ are obtained for BAG and CS, respectively, with stabilities over 90% in both cases after 5,000 cycles. These results endorse the future application of these materials as negative electrodes in electrochemical energy storage devices.

DATA AVAILABILITY STATEMENT

The raw data supporting the conclusions of this article will be made available by the authors, without undue reservation.

AUTHOR CONTRIBUTIONS

MM and FL conceived the study. LA, AA-M, and PA-C carried out the experiments, helped in the analyses

and discussion of the results, and wrote the article. All authors contributed to the review, edit, and approval of the paper.

FUNDING

Authors from Centro de Química Estrutural would like to thank the financial support of Fundação para a Ciência e a Tecnologia (FCT) under project numbers 1801P.00824.1.01, UID/QUI/00100/2019, and UIDB/00100/2020. We acknowledge support for the publication fee by the CSIC Open Access

Publication Support Initiative through its Unit of Information Resources for Research (URICI).

ACKNOWLEDGMENTS

Authors from the National Center for Metallurgical Researches, Spanish National Research Council (CENIM-CSIC) would like to thank the Viticulture Group at the Mision Biologica de Galicia (CSIC) for providing the winemaking wastes used in the present work, and to Dr. Irene Llorente for the XPS measurements carried out.

REFERENCES

- Alcaraz, L., Escudero, M. E., Alguacil, F. J., Llorente, I., Urbiet, A., Fernández, P., et al. (2019). Dysprosium removal from water using active carbons obtained from spent coffee ground. *Nanomaterials* 9:1372. doi: 10.3390/nano9101372
- Alcaraz, L., García-Díaz, I., Alguacil, F., and Lopez, F. (2020). Removal of copper ions from wastewater by adsorption onto a green adsorbent from winemaking wastes. *BioResources* 15, 1112–1133. doi: 10.15376/biores.15.1.1112-1133
- Alguacil, F., Alcaraz, L., García-Díaz, I., and López, F. (2018). Removal of Pb^{2+} in wastewater via adsorption onto an activated carbon produced from winemaking waste. *Metals* 8:697. doi: 10.3390/met8090697
- Beltrame, K. K., Cazetta, A. L., de Souza, P. S. C., Spessato, L., Silva, T. L., and Almeida, V. C. (2018). Adsorption of caffeine on mesoporous activated carbon fibers prepared from pineapple plant leaves. *Ecotoxicol. Environ. Saf.* 147, 64–71. doi: 10.1016/j.ecoenv.2017.08.034
- Brunauer, S., Emmett, P. H., and Teller, E. (1938). Adsorption of gases in multimolecular layers. *J. Am. Chem. Soc.* 60, 309–319. doi: 10.1021/ja01269a023
- Bubanal, S., and Shivashankar, M. R. (2017). History, method of production, structure and applications of activated carbon. *Int. J. Eng. Res.* V6, 495–498. doi: 10.17577/IJERTV6IS060277
- Centeno, T. A., and Stoeckli, F. (2010). The assessment of surface areas in porous carbons by two model-independent techniques, the DR equation and DFT. *Carbon* 48, 2478–2486. doi: 10.1016/j.carbon.2010.03.020
- Chan, O. S., Cheung, W. H., and McKay, G. (2011). Preparation and characterisation of demineralised tyre derived activated carbon. *Carbon* 49, 4674–4687. doi: 10.1016/j.carbon.2011.06.065
- Chang, S.-K., and Zainal, Z. (2019). “Activated carbon for supercapacitors,” in *Synthesis, Technology and Applications of Carbon Nanomaterials* (Elsevier), 309–334. doi: 10.1016/B978-0-12-815757-2.00012-7
- Chen, R., Li, L., Liu, Z., Lu, M., Wang, C., Li, H., et al. (2017). Preparation and characterization of activated carbons from tobacco stem by chemical activation. *J. Air Waste Manag. Assoc.* 67, 713–724. doi: 10.1080/10962247.2017.1280560
- Deiana, A. C., Sardella, M. F., Silva, H., Amaya, A., and Tancredi, N. (2009). Use of grape stalk, a waste of the viticulture industry, to obtain activated carbon. *J. Hazard. Mater.* 172, 13–19. doi: 10.1016/j.jhazmat.2009.06.095
- Dwivedi, N., Yeo, R. J., Satyanarayana, N., Kundu, S., Tripathy, S., and Bhatia, C. S. (2015). Understanding the role of nitrogen in plasma-assisted surface modification of magnetic recording media with and without ultrathin carbon overcoats. *Sci. Rep.* 5:7772. doi: 10.1038/srep07772
- El-Naggar, A. H., Alzhirani, A. K. R., Ahmad, M., Usman, A. R. A., Mohan, D., Ok, Y. S., et al. (2015). Preparation of activated and non-activated carbon from conocarpus pruning waste as low-cost adsorbent for removal of heavy metal ions from aqueous solution. *BioResources* 11, 1092–1107. doi: 10.15376/biores.11.1.1092-1107
- Estrade-Szwarckopf, H. (2004). XPS photoemission in carbonaceous materials: a “defect” peak beside the graphitic asymmetric peak. *Carbon* 42, 1713–1721. doi: 10.1016/j.carbon.2004.03.005
- Gonçalves, M., Castro, C. S., Boas, I. K. V., Soler, F. C., Pinto, E., de, C., et al. (2019). Glycerin waste as sustainable precursor for activated carbon production: adsorption properties and application in supercapacitors. *J. Environ. Chem. Eng.* 7:103059. doi: 10.1016/j.jece.2019.103059
- Gören, A., Costa, C. M., Silva, M. M., and Lanceros-Méndez, S. (2015). State of the art and open questions on cathode preparation based on carbon coated lithium iron phosphate. *Compos. B Eng.* 83, 333–345. doi: 10.1016/j.compositesb.2015.08.064
- Guardia, L., Suárez, L., Querejeta, N., Pevida, C., and Centeno, T. A. (2018). Winery wastes as precursors of sustainable porous carbons for environmental applications. *J. Clean. Prod.* 193, 614–624. doi: 10.1016/j.jclepro.2018.05.085
- Guardia, L., Suárez, L., Querejeta, N., Vretenár, V., Kotrusz, P., Skákalová, V., et al. (2019). Biomass waste-carbon/reduced graphene oxide composite electrodes for enhanced supercapacitors. *Electrochim. Acta* 298, 910–917. doi: 10.1016/j.electacta.2018.12.160
- Jain, A., Balasubramanian, R., and Srinivasan, M. P. (2016). Hydrothermal conversion of biomass waste to activated carbon with high porosity: a review. *Chem. Eng. J.* 283, 789–805. doi: 10.1016/j.cej.2015.08.014
- Jerng, S. K., Yu, D. S., Lee, J. H., Kim, C., Yoon, S., and Chun, S. H. (2011). Graphitic carbon growth on crystalline and amorphous oxide substrates using molecular beam epitaxy. *Nanoscale Res. Lett.* 6, 1–6. doi: 10.1186/1556-276X-6-565
- Jiménez-Cordero, D., Heras, F., Gilarranz, M. A., and Raymundo-Piñero, E. (2014). Grape seed carbons for studying the influence of texture on supercapacitor behaviour in aqueous electrolytes. *Carbon* 71, 127–138. doi: 10.1016/j.carbon.2014.01.021
- Kaneko, K., Ishii, C., Ruike, M., and Kuwabara, H. (1992). Origin of superhigh surface area and microcrystalline graphitic structures of activated carbons. *Carbon* 30, 1075–1088. doi: 10.1016/0008-6223(92)90139-N
- Lei, C., Amini, N., Markoulidis, F., Wilson, P., Tennison, S., and Lekakou, C. (2013). Activated carbon from phenolic resin with controlled mesoporosity for an electric double-layer capacitor (EDLC). *J. Mater. Chem. A* 1:6037. doi: 10.1039/c3ta01638b
- Li, K.-B., Shi, D.-W., Cai, Z.-Y., Zhang, G.-L., Huang, Q.-A., Liu, D., et al. (2015). Studies on the equivalent serial resistance of carbon supercapacitor. *Electrochim. Acta* 174, 596–600. doi: 10.1016/j.electacta.2015.06.008
- Maicas, S., and Mateo, J. J. (2020). Sustainability of wine production. *Sustainability* 12:559. doi: 10.3390/su12020559
- Mingo, E., Silván, J. M., and Martínez-Rodríguez, A. J. (2016). Selective antibacterial effect on campylobacter of a winemaking waste extract (WWE) as a source of active phenolic compounds. *LWT Food Sci. Technol.* 68, 418–424. doi: 10.1016/j.lwt.2015.12.052
- Nguyen, C., and Do, D. D. (2001). The dubinin-radushkevich equation and the underlying microscopic adsorption description. *Carbon* 39, 1327–1336. doi: 10.1016/S0008-6223(00)00265-7
- Nič, M., Jirát, J., Košata, B., Jenkins, A., and McNaught, A. (Eds.). (2009). *IUPAC Compendium of Chemical Terminology*. Durham, NC: IUPAC. doi: 10.1351/goldbook
- Pech, D., Brunet, M., Durou, H., Huang, P., Mochalin, V., Gogotsi, Y., et al. (2010). Ultrahigh-power micrometre-sized supercapacitors based on onion-like carbon. *Nat. Nanotechnol.* 5, 651–654. doi: 10.1038/nnano.2010.162
- Prabu, N., Saravanan, R. S. A., Kesavan, T., Maduraiveeran, G., and Sasidharan, M. (2019). An efficient palm waste derived hierarchical porous carbon for electrocatalytic hydrogen evolution reaction. *Carbon* 152, 188–197. doi: 10.1016/j.carbon.2019.06.016

- Rajamani, R., Vinoth Kumar, B., Sujith, A., and Karthick, E. (2018). Activated carbon production from waste biomass. *Int. J. Eng. Technol.* 7, 345–348. doi: 10.14419/ijet.v7i3.34.19222
- Ramón-Gonçalves, M., Alcaraz, L., Pérez-Ferreras, S., León-González, M. E., Rosales-Conrado, N., and López, F. A. (2019). Extraction of polyphenols and synthesis of new activated carbon from spent coffee grounds. *Sci. Rep.* 9, 1–11. doi: 10.1038/s41598-019-54205-y
- Ravichandran, P., Sugumaran, P., Seshadri, S., and Basta, A. H. (2018). Optimizing the route for production of activated carbon from *Casuarina equisetifolia* fruit waste. *R. Soc. Open Sci.* 5:171578. doi: 10.1098/rsos.171578
- Sardella, F., Gimenez, M., Navas, C., Morandi, C., Deiana, C., and Sapag, K. (2015). Conversion of viticultural industry wastes into activated carbons for removal of lead and cadmium. *J. Environ. Chem. Eng.* 3, 253–260. doi: 10.1016/j.jece.2014.06.026
- Senophiyah-Mary, J., Thomas, T., Loganath, R., and Meenambal, T. (2019). “Removal of copper from bioleachate of e-waste using orange activated carbon (OAC) and comparison with commercial activated carbon (CAC),” in *Waste Valorisation and Recycling*, ed G. Sadhan Kumar (Singapore: Springer Singapore), 373–383. doi: 10.1007/978-981-13-2784-1_35
- Sfyris, D., Sfyris, G. I., and Galiotis, C. (2017). Stress interpretation of graphene E-2 g and A-1 g vibrational modes: theoretical analysis. *arXiv:1706.04465* 1–30.
- Shimodaira, N., and Masui, A. (2002). Raman spectroscopic investigations of activated carbon materials. *J. Appl. Phys.* 92, 902–909. doi: 10.1063/1.1487434
- Suárez, L., and Centeno, T. A. (2020). Unravelling the volumetric performance of activated carbons from biomass wastes in supercapacitors. *J. Power Sources* 448:227413. doi: 10.1016/j.jpowsour.2019.227413
- Taberna, P. L., Simon, P., and Fauvarque, J. F. (2003). Electrochemical characteristics and impedance spectroscopy studies of carbon-carbon supercapacitors. *J. Electrochem. Soc.* 150, 292–300. doi: 10.1149/1.1543948
- Thommes, M., Kaneko, K., Neimark, A. V., Olivier, J. P., Rodriguez-Reinoso, F., Rouquerol, J., et al. (2015). Physisorption of gases, with special reference to the evaluation of surface area and pore size distribution (IUPAC Technical Report). *Pure Appl. Chem.* 87, 1051–1069. doi: 10.1515/pac-2014-1117
- Tsyntarski, B., Stoycheva, I., Tsoncheva, T., Genova, I., Dimitrov, M., Petrova, B., et al. (2015). Activated carbons from waste biomass and low rank coals as catalyst supports for hydrogen production by methanol decomposition. *Fuel Process. Technol.* 137, 139–147. doi: 10.1016/j.fuproc.2015.04.016
- Ukanwa, K. S., Patchigolla, K., Sakrabani, R., Anthony, E., and Mandavgane, S. (2019). A review of chemicals to produce activated carbon from agricultural waste biomass. *Sustainability* 11:6204. doi: 10.3390/su11226204
- Yaglikci, S., Gokce, Y., Yagmur, E., and Aktas, Z. (2020). The performance of sulphur doped activated carbon supercapacitors prepared from waste tea. *Environ. Technol.* 41, 36–48. doi: 10.1080/09593330.2019.1575480
- Yagmur, E., Gokce, Y., Tekin, S., Semerci, N. I., and Aktas, Z. (2020). Characteristics and comparison of activated carbons prepared from oleaster (*Elaeagnus angustifolia* L.) fruit using KOH and ZnCl₂. *Fuel* 267:117232. doi: 10.1016/j.fuel.2020.117232
- Zhang, G., Chen, Y., Chen, Y., and Guo, H. (2018). Activated biomass carbon made from bamboo as electrode material for supercapacitors. *Mater. Res. Bull.* 102, 391–398. doi: 10.1016/j.materresbull.2018.03.006

Conflict of Interest: The authors declare that the research was conducted in the absence of any commercial or financial relationships that could be construed as a potential conflict of interest.

Copyright © 2020 Alcaraz, Adán-Más, Arévalo-Cid, Montemor and López. This is an open-access article distributed under the terms of the Creative Commons Attribution License (CC BY). The use, distribution or reproduction in other forums is permitted, provided the original author(s) and the copyright owner(s) are credited and that the original publication in this journal is cited, in accordance with accepted academic practice. No use, distribution or reproduction is permitted which does not comply with these terms.



Advancements and Complexities in the Conversion of Lignocellulose Into Chemicals and Materials

Giulia Fiorani¹, Claudia Crestini^{1,2*}, Maurizio Selva^{1*} and Alvise Perosa¹

¹ Department of Molecular Sciences and Nanosystems, Ca' Foscari University of Venice, Venice, Italy, ² C4S Center for Sustainability, Ca' Foscari University Foundation, Calle Larga Ca' Foscari, Venice, Italy

OPEN ACCESS

Edited by:

Francesca Deganello,
Institute for the Study of
Nanostructured Materials, Italian
National Research Council, Italy

Reviewed by:

Gabriel Paes,
Fractionnement des Agro-Ressources
et de l'Environnement (FARE), France
Raffaele Cucciniello,
University of Salerno, Italy

*Correspondence:

Claudia Crestini
claudia.crestini@unive.it
Maurizio Selva
selva@unive.it

Specialty section:

This article was submitted to
Green and Sustainable Chemistry,
a section of the journal
Frontiers in Chemistry

Received: 04 June 2020

Accepted: 29 July 2020

Published: 21 August 2020

Citation:

Fiorani G, Crestini C, Selva M and
Perosa A (2020) Advancements and
Complexities in the Conversion of
Lignocellulose Into Chemicals and
Materials. *Front. Chem.* 8:797.
doi: 10.3389/fchem.2020.00797

This Perspective describes the challenges and objectives associated to the development of new chemical technologies for the conversion of lignocellulose (non-food or waste) into chemicals and materials; it also provides an outlook on the sources, potential products, and issues to be addressed.

Keywords: plant-based biomass, biobased platform chemicals, levulinic acid, dimethyl carbonate, lignin valorization, lignin characterization, lignin fractionation, lignin-based nanomaterials

INTRODUCTION

Plant-based biomass plays a pivotal role in the development of economically and environmentally sustainable biorefinery processes. Three different biopolymers are included in lignocellulosic biomass, namely cellulose, hemicellulose, and lignin, which are characterized by different chemical composition and reactivity. The chemical diversity of raw biomass represents a challenge toward the development of energy and resource efficient chemical processes and of the associated technological tools (Xu et al., 2019). For example, most of 50–70 MT/year of lignin produced by both the pulp and paper industry and modern saccharification processes are currently employed in low added-value applications (e.g., burned for energy co-generation) (Luo and Abu-Omar, 2017). Back in 2004, a rational selection of biobased *platform chemicals* was reported and became a strategic tool to develop focused valorization strategies (Werpy and Petersen, 2004); since then, the list of renewable-based platform chemicals and the associated chemical- and biochemical-based valorization strategies is constantly monitored and updated (Bozell et al., 2007; Bozell and Petersen, 2010; Esposito and Antonietti, 2015; Lee et al., 2019; Huo and Shanks, 2020). Currently, a plethora of commercial cellulose and hemicellulose valorization processes are available (Aresta et al., 2015), while examples of integrated biorefinery processes were reported only recently (BBI JU Annual Activity Report, 2019; Liao et al., 2020).

This Perspective showcases some recent examples of (i) preparation of selected building blocks derived from established biobased platform chemicals [e.g., levulinic acid (LVA) and OH-bearing biobased derivatives (BBDs)] and (ii) non-destructive technologies for the valorization of lignin. For both classes of biobased chemicals, valorization occurred employing mild, eco-friendly technologies.

LVA HYDROGENATION

LVA is an important renewable-based platform chemical, which can be obtained selectively upon acidic hydrolysis of polysaccharides (Bozell and Petersen, 2010; Kang et al., 2018). LVA is characterized by a significant synthetic potential in different fields of applications: for example, it is employed as intermediate for the preparation of drugs bearing heterocyclic scaffolds but can also be used as co-monomer for the preparation of renewable-based materials (Esposito and Antonietti, 2015; Adeleye et al., 2019). LVA can be selectively reduced to γ -valerolactone (GVL), which is a low-toxicity, biodegradable five-membered ring heterocyclic compound employed as a fully renewable-based aprotic solvent, fuel additive, and precursor for added-value chemicals (Alonso et al., 2013; Mellmer et al., 2014). LVA reduction to GVL is a sequential process composed of two steps by which LVA is initially hydrogenated to the intermediate γ -hydroxyvaleric acid that, in turn, undergoes a dehydration/cyclization reaction to give GVL (Figure 1, top). These transformations typically occur in solution in presence of homogeneous metal complexes based on Ru, Ir, Pd, and, more recently, Fe (Omoruyi et al., 2016). Nevertheless, GVL recovery by distillation is non-practical and anti-economical, due to its high boiling point ($T_{\text{eb}} = 207\text{--}208^\circ\text{C}$). Consequently, heterogenized Ru-based catalysts were developed, including complexes with sulfonated ligands for effective confinement in the aqueous phase, and/or Ru-based catalysts supported on mesoporous or amorphous materials (Wright and Palkovits, 2012). Performing LVA hydrogenation in multiphasic systems (MPs) represents a promising strategy to improve selective GVL formation as well as catalyst recovery. A MP consisting of three immiscible phases (e.g., water, an apolar solvent, *iso*-octane, and an ionic liquid, IL) was initially proposed. The catalyst (Ru/C) was effectively segregated in the IL phase and recycled up to eight times without losing its performance; in all catalytic runs, GVL was formed quantitatively (LVA Conv. = 81%; GVL Sel. > 99%) and exclusively in the aqueous solution (Selva et al., 2013). More recently, Ru/C catalyzed quantitative conversion of LVA to GVL was observed even in a simple biphasic $\text{H}_2\text{O}/\text{iso}$ -octane system. In the absence of any IL, the catalyst could be selectively confined (suspended) in the hydrocarbon medium, on condition that the aqueous solution was acidic in a pH range of 2.5–3. Ru-leaching in water was neglectable ($\text{Ru} < 0.01\%$ w/w) (Bellè et al., 2019).

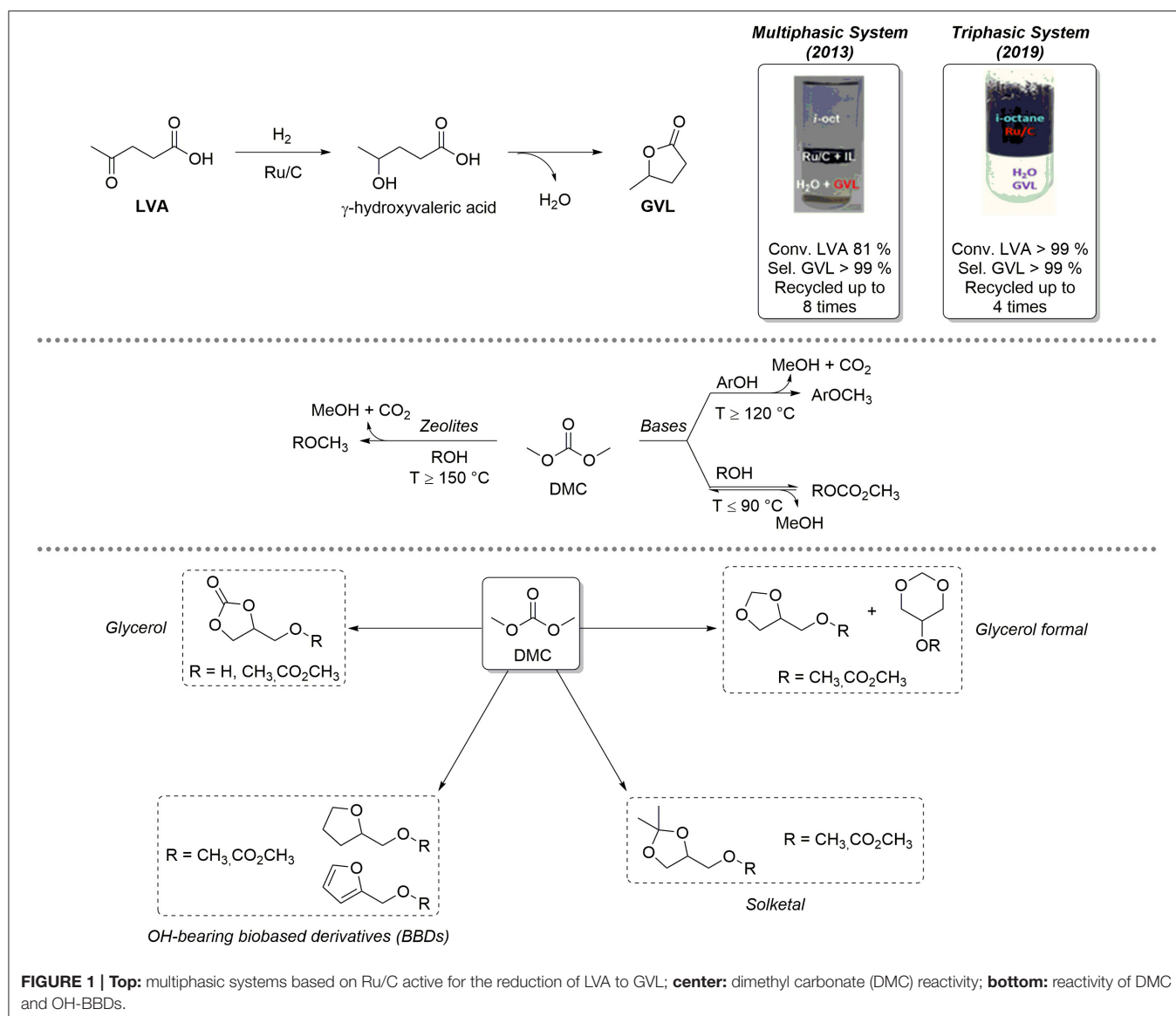
VALORIZATION OF OH-BEARING BBDs WITH DIMETHYL CARBONATE (DMC)

The lightest term of the dialkyl carbonates series, dimethyl carbonate (DMC), has an established role as a low environmental impact reagent and solvent (Fiorani et al., 2018; Selva et al., 2019). DMC embeds different non-equivalent electrophilic groups within its structure (one sp^2 carbonate C and two sp^3 hybridized methyl C) and can therefore react as an ambident reagent for selective carboxymethylation and/or methylation of a variety of O-, S-, C-, N-, and P-based nucleophiles (e.g., alcohols, phenols, methylene active compounds, amines, and

phosphines). Figure 1, center, exemplifies the case of alcohols and phenols. At low temperatures ($T \leq 90^\circ\text{C}$) and in the presence of base catalysts, only transcarbonation reactions take place via a $\text{B}_{\text{AC}}2$ mechanism: equilibrium product (ROCOOMe) formation is favored by continuous removal of MeOH via azeotropic distillation with DMC or by adding suitable adsorbing porous materials (molecular sieves, zeolites, etc.). At higher temperatures ($T > 120\text{--}150^\circ\text{C}$) and in the presence of weak bases or amphoteric catalysts like alkali metal exchanged faujasites, methylation occurs selectively following a $\text{B}_{\text{AI}}2$ mechanism. In the latter case, methylation products (ArOCH_3) are formed irreversibly with release of CO_2 . Within our long-lasting interest in eco-compatible processes using renewable-based starting materials, our group has developed a solid expertise on the use of DMC for the selective chemical upgrading of biosourced platform chemicals, as depicted in Figure 1, bottom. In-depth chemical valorization studies have been carried out by us on various OH-BBDs, including glycerol (Glyc), its cyclic acetals solketal and glycerol formal and other bioderived aliphatic alcohols. DMC-based protocols allowed for the selective preparation of OH-BBDs methyl ether derivatives, which find applications as fuel additives as well as solvents and chemical intermediates (Rorrer et al., 2019) or for the synthesis of symmetrical aliphatic dialkyl carbonates, which are rapidly gaining importance and expanding the range of applications as biobased polar aprotic solvents (Mao et al., 2019). For instance, the reactivity of Glyc and DMC under thermal (catalyst-free) conditions was thoroughly studied: (i) in batch mode, glycerol carbonate methyl ether was obtained selectively when working in large DMC excess ($\text{DMC}/\text{Glyc} = 60:1$ mol/mol, $T = 180^\circ\text{C}$, $t = 5$ h, yield = 82%). Interestingly, under a CO_2 atmosphere [$\text{DMC}/\text{Glyc} = 20:1$ mol/mol, $T = 180^\circ\text{C}$, $t = 5$ h, $p(\text{CO}_2) = 20$ bar], the reaction led to the formation of glycerol carbonate in up to 84% yield; (ii) in continuous-flow (CF) mode ($\text{DMC}/\text{MeOH}/\text{Glyc} = 10:6:1$ mol/mol, $p = 50$ bar, $F = 0.1$ ml·min $^{-1}$, $T = 230\text{--}250^\circ\text{C}$); instead, glycerol carbonate was achieved in up to 92% yield at $T = 230^\circ\text{C}$ (Guidi et al., 2016). The CF-reaction of DMC with OH-BBDs was further explored using weakly basic hydrotalcite catalysts (HTs). O-alkylation, with formation of the corresponding methyl ethers (> 99% yield) was the preferred pathway ($\text{DMC}/\text{ROH} = 20:1$ to $5:1$ mol/mol, $p = 1$ bar, $F = 0.1$ ml·min $^{-1}$, $T = 150\text{--}260^\circ\text{C}$) (Cattelan et al., 2017). Interestingly, HT catalysts displayed a high activity and selectivity also for the preparation of symmetrical dialkyl carbonates via a two-step carbonate interchange reaction (CIR). In this case, alkyl methyl carbonate intermediates were initially formed by batch reaction of various alcohol(s) with DMC at $T = 90^\circ\text{C}$. Thereafter, intermediates were converted into the desired symmetrical carbonates through disproportionation reactions carried out under CF conditions at high T ($T = 180\text{--}275^\circ\text{C}$) (Cattelan et al., 2018).

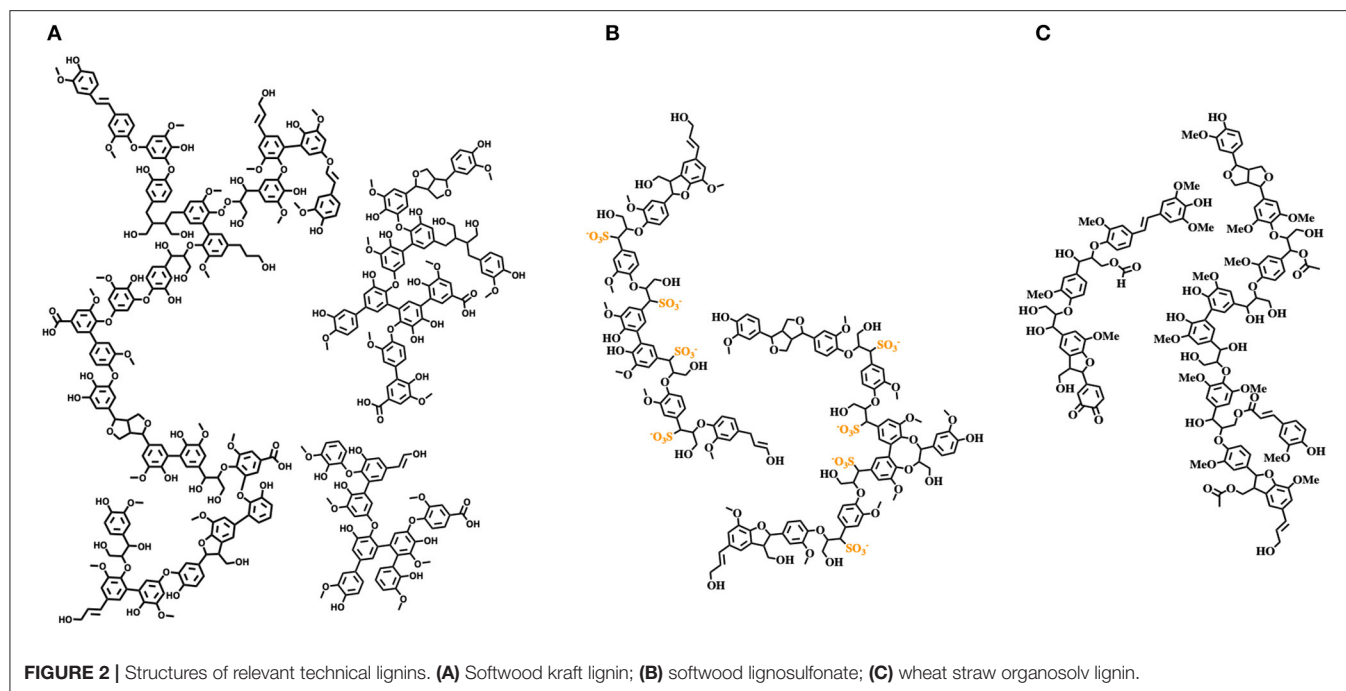
LIGNIN

The potential of lignin as a feedstock is enormous due to its abundance and rich chemical nature, consisting mainly



of aromatic and phenolic subunits. Different valorization pathways have been explored, such as direct lignin valorization, i.e., development of innovative renewable-based materials, or chemical transformation in aromatic commodities and chemicals such as for example, in the “lignin first” approach consisting in reductive treatments of biomass yield complex mixtures of partially reduced lignin derivatives useful for biofuel production (Sun et al., 2018). Nevertheless, industrially and commercially relevant lignin valorization processes are still needed (Argyropoulos and Crestini, 2016; Sun et al., 2018). Lignin stream valorization is hampered by two main factors: (i) lignin is an extremely complex biomaterial lacking a defined primary structure, with a specific composition severely affected by the botanical origin and location, altering monomers’ ratio and their linking modes; (ii) industrially available lignins are

highly variable heterogeneous, polyfunctional complex mixtures of unpredictable specifications, with distinct physicochemical properties compared to native lignin, largely due to the different processes required for their isolation (Figure 2). Therefore, to fully exploit lignin streams as feedstocks for further utilization, they should initially be refined to reproducible “cuts” with consistent specifications. At the same time, structural characterization studies and development of *ad hoc* analytical techniques are vibrant and challenging research topics useful to accelerate the development of circular lignin valorization value chains (Sette et al., 2011; Meng et al., 2019). For example, the structural features of milled wood lignin (MWL, which strongly resembles native lignin) were elucidated only in 2011 by an array of NMR techniques, unambiguously showing that MWL is a linear oligomer rather than a highly



branched polymer (Crestini et al., 2011). Structural elucidation studies performed on softwood kraft lignin highlight the presence of two different components: one derived from native lignin and the other composed of repolymerized oligomeric fragments generated during the Kraft pulping process (Crestini et al., 2017). Given the high variability and diversity of commercially available lignin streams, design and development of fractionation protocols for the isolation of distinct lignin fractions characterized by the same molecular weight distribution and chemical properties represent a key purification technology. Several studies on lignin fractionation have been reported, mainly relying on fractional precipitation and/or sequential dissolution in the presence of solvents with different polarity, aqueous solutions at different pHs, or membrane filtration (Cui et al., 2014; Sevastyanova et al., 2014; Duval et al., 2016; Lange et al., 2016). Lignin fractionation opens the door to a more widespread exploitation of commercial lignin stream derivatives in materials science. Moreover, specific fractions can be selectively modified (e.g., varying solubility, hydrophobicity, surface adhesion, antioxidant activity, UV screening, antimicrobial activity, anti-inflammatory activity, etc.). Development of accessible and reproducible tailoring processes will promote lignin inclusion in a large variety of consumer products, i.e., home and/or personal care products (Brooker et al., 2016a,b), composites, packaging materials coatings, and resins, retaining the desired macroscopic properties and, at the same time, mitigating the overall environmental footprint and improving their biodegradation.

The development of innovative materials derived from biomass is a timely fundamental research challenge. To this aim, in recent years, several different renewable-based

micro- and nanostructured materials were developed and successfully applied, among others, in microelectronics, cosmetics, nutraceutical, and pharmaceutical applications. Lignin nanoparticles were initially developed for agricultural applications as vectors for the controlled release of active principles, or in nanocomposites formulation (Tortora et al., 2014; Bartzoka et al., 2016; Sipponen et al., 2018). However, thanks to their high biocompatibility, lignin microcapsules can also be employed for the controlled and synergic release of pharmaceutical and/or cosmetic active principles and for the design and development of functional foods. The range of potential applications of lignin-based nanomaterials is expanding continuously and now also includes preparation of renewable-based lignin nanofibers suitable for carbon nanofiber production and use in structural composites and energy storage applications (Kumar et al., 2019).

CONCLUSIONS

Plant-based biomass plays a pivotal role in the development of economically and environmentally sustainable biorefinery processes. The chemical complexity of plant biomass, however, still represents a challenge toward the development of energy- and resource-efficient chemical processes and of the associated technological tools. Reliable convergent chemical strategies enabling transformations of biomass-derived matrices in discrete families of platform chemicals will be crucial to improve the biorefinery efficiency. This Perspective article, showcasing some recent examples of valorization of biopolymers and platform chemicals derived from lignocellulosic biomass, aims

at offering the Reader the scenario of issues associated to the implementation of new chemical technologies for the conversion of lignocellulose (non-food or waste) into chemicals and materials; at the same time, it also provides an outlook on the sources and potential products to be addressed using multiphase systems, eco-compatible reagents like DMC, and the design of protocols for lignin fractionation. Notably, this approach should be complemented with the advance of analytical techniques for the identification of the most promising added-value structures of a given valorization process.

REFERENCES

- Adeleye, A. T., Louis, H., Akakuru, O., Joseph, I., Enudi, O. C., and Michael, D. P. (2019). A review on the conversion of levulinic acid and its esters to various useful chemicals. *AIMS Energy* 7, 165–185. doi: 10.3934/energy.2019.2.165
- Alonso, D. M., Wettstein, S. G., and Dumesic, J. A. (2013). Gamma-valerolactone, a sustainable platform molecule derived from lignocellulosic biomass. *Green Chem.* 15:584. doi: 10.1039/c3gc37065h
- Aresta, M., Dibenedetto, A., and Dumeignil, F. (eds.). (2015). *Biorefineries: An Introduction*. Berlin; München; Boston, MA: DE GRUYTER.
- Argyropoulos, D. S., and Crestini, C. (2016). A perspective on lignin refining, functionalization, and utilization. *ACS Sustain. Chem. Eng.* 4, 5089–5089. doi: 10.1021/acssuschemeng.6b02173
- Bartzoka, E. D., Lange, H., Thiel, K., and Crestini, C. (2016). Coordination complexes and one-step assembly of lignin for versatile nanocapsule engineering. *ACS Sustain. Chem. Eng.* 4, 5194–5203. doi: 10.1021/acssuschemeng.6b00904
- BBI JU Annual Activity Report (2019). *Bio-Based Industries Joint Undertaking*. Available online at: <https://www.bbi-europe.eu/sites/default/files/documents/bbi-ju-aar-2019.pdf> (accessed July 7, 2020).
- Bellé, A., Tabanelli, T., Fiorani, G., Perosa, A., Cavani, F., and Selva, M. (2019). A multiphase protocol for selective hydrogenation and reductive amination of levulinic acid with integrated catalyst recovery. *ChemSusChem* 12, 3343–3354. doi: 10.1002/cssc.201900925
- Bozell, J. J., Holladay, J. E., Johnson, D., and White, J. F. (2007). *Top Value-Added Chemicals from Biomass Volume II — Results of Screening for Potential Candidates From Biorefinery Lignin*. Available online at: https://www.pnnl.gov/main/publications/external/technical_reports/PNNL-16983.pdf
- Bozell, J. J., and Petersen, G. R. (2010). Technology development for the production of biobased products from biorefinery carbohydrates—the US Department of Energy's "Top 10" revisited. *Green Chem.* 12:539. doi: 10.1039/b922014c
- Brooker, A. D. M., Vaccaro, M., Scialla, S., Benjelloun-Mlayah, B., Crestini, C., and Lange, H. (2016a). *Consumer Goods Products Comprising Lignin Oligomer*. Available online at: https://worldwide.espacenet.com/publicationDetails/biblio?CC=EP&NR=3108938A1&KC=A1&date=&FT=D&locale=en_EP
- Brooker, A. D. M., Vaccaro, M., Scialla, S., Crestini, C., and Lange, H. (2016b). *Consumer Goods Product Comprising Carboxylated Lignin Oligomer*. Available online at: <https://worldwide.espacenet.com/patent/search/family/053489876/publication/EP3108871A1?q=pn%3DEP3108871A1>
- Cattelan, L., Fiorani, G., Perosa, A., Maschmeyer, T., and Selva, M. (2018). Two-step synthesis of dialkyl carbonates through transcarboxylation and disproportionation reactions catalyzed by calcined hydrotalcites. *ACS Sustain. Chem. Eng.* 6, 9488–9497. doi: 10.1021/acssuschemeng.8b02106
- Cattelan, L., Perosa, A., Riello, P., Maschmeyer, T., and Selva, M. (2017). Continuous-flow O-alkylation of biobased derivatives with dialkyl carbonates in the presence of magnesium-aluminum hydrotalcites as catalyst precursors. *ChemSusChem* 10, 1571–1583. doi: 10.1002/cssc.201601765
- Crestini, C., Lange, H., Sette, M., and Argyropoulos, D. S. (2017). On the structure of softwood kraft lignin. *Green Chem.* 19, 4104–4121. doi: 10.1039/C7GC01812F
- Crestini, C., Melone, F., Sette, M., and Saladino, R. (2011). Milled wood lignin: a linear oligomer. *Biomacromolecules* 12, 3928–3935. doi: 10.1021/bm200948r
- Cui, C., Sun, R., and Argyropoulos, D. S. (2014). Fractional precipitation of softwood kraft lignin: isolation of narrow fractions common to a variety of lignins. *ACS Sustain. Chem. Eng.* 2, 959–968. doi: 10.1021/sc400545d
- Duval, A., Vilaplana, F., Crestini, C., and Lawoko, M. (2016). Solvent screening for the fractionation of industrial kraft lignin. *Holzforschung* 70, 11–20. doi: 10.1515/hf-2014-0346
- Espósito, D., and Antonietti, M. (2015). Redefining biorefinery: the search for unconventional building blocks for materials. *Chem. Soc. Rev.* 44, 5821–5835. doi: 10.1039/C4CS00368C
- Fiorani, G., Perosa, A., and Selva, M. (2018). Dimethyl carbonate: a versatile reagent for a sustainable valorization of renewables. *Green Chem.* 20, 288–322. doi: 10.1039/C7GC02118F
- Guidi, S., Calmanti, R., Noè, M., Perosa, A., and Selva, M. (2016). Thermal (Catalyst-Free) transesterification of diols and glycerol with dimethyl carbonate: a flexible reaction for batch and continuous-flow applications. *ACS Sustain. Chem. Eng.* 4, 6144–6151. doi: 10.1021/acssuschemeng.6b01633
- Huo, J., and Shanks, B. H. (2020). Bioprivileged molecules: integrating biological and chemical catalysis for biomass conversion. *Annu. Rev. Chem. Biomol. Eng.* 11, 63–85. doi: 10.1146/annurev-chembioeng-101519-121127
- Kang, S., Fu, J., and Zhang, G. (2018). From lignocellulosic biomass to levulinic acid: a review on acid-catalyzed hydrolysis. *Renew. Sustain. Energy Rev.* 94, 340–362. doi: 10.1016/j.rser.2018.06.016
- Kumar, M., Hietala, M., and Oksman, K. (2019). Lignin-based electrospun carbon nanofibers. *Front. Mater.* 6:62. doi: 10.3389/fmats.2019.00062
- Lange, H., Schiffels, P., Sette, M., Sevastyanova, O., and Crestini, C. (2016). Fractional precipitation of wheat straw organosolv lignin: macroscopic properties and structural insights. *ACS Sustain. Chem. Eng.* 4, 5136–5151. doi: 10.1021/acssuschemeng.6b01475
- Lee, S. Y., Kim, H. U., Chae, T. U., Cho, J. S., Kim, J. W., Shin, J. H., et al. (2019). A comprehensive metabolic map for production of bio-based chemicals. *Nat. Catal.* 2, 18–33. doi: 10.1038/s41929-018-0212-4
- Liao, Y., Koelewijn, S.-F., Van den Bossche, G., Van Aelst, J., Van den Bosch, S., Renders, T., et al. (2020). A sustainable wood biorefinery for low-carbon footprint chemicals production. *Science* 367, 1385–1390. doi: 10.1126/science.aau1567
- Luo, H., and Abu-Omar, M. M. (2017). "Chemicals from lignin," in *Encyclopedia of Sustainable Technologies*, ed M. A. Abraham (Amsterdam: Elsevier), 573–585. doi: 10.1016/B978-0-12-409548-9.10235-0
- Mao, S., Li, H., Shi, X., Soulé, J., and Doucet, H. (2019). Environmentally benign arylations of 5-membered ring heteroarenes by Pd-catalyzed C–H bonds activations. *ChemCatChem* 11, 269–286. doi: 10.1002/cctc.201801448
- Mellmer, M. A., Sener, C., Gallo, J. M. R., Luterbacher, J. S., Alonso, D. M., and Dumesic, J. A. (2014). Solvent effects in acid-catalyzed biomass conversion reactions. *Angew. Chem. Int. Ed.* 53, 11872–11875. doi: 10.1002/anie.201408359
- Meng, X., Crestini, C., Ben, H., Hao, N., Pu, Y., Ragauskas, A. J., et al. (2019). Determination of hydroxyl groups in biorefinery resources via quantitative ³¹P NMR spectroscopy. *Nat. Protoc.* 14, 2627–2647. doi: 10.1038/s41596-019-0191-1
- Omoruyi, U., Page, S., Hallett, J., and Miller, P. W. (2016). Homogeneous catalyzed reactions of levulinic acid: to γ -valerolactone and

AUTHOR CONTRIBUTIONS

All authors contributed to writing and revising the manuscript. All authors have read and agreed the final version of the Perspective.

FUNDING

CC kindly acknowledges Ca' Foscari Start up Funds (FPI) 2019 for funding.

- beyond. *ChemSusChem* 9, 2037–2047. doi: 10.1002/cssc.201600517
- Rorrer, J. E., Bell, A. T., and Toste, F. D. (2019). Synthesis of biomass-derived ethers for use as fuels and lubricants. *ChemSusChem* 12, 2835–2858. doi: 10.1002/cssc.201900535
- Selva, M., Gottardo, M., and Perosa, A. (2013). Upgrade of biomass-derived levulinic acid via Ru/C-catalyzed hydrogenation to γ -valerolactone in aqueous-organic-ionic liquids multiphase systems. *ACS Sustain. Chem. Eng.* 1, 180–189. doi: 10.1021/sc300088j
- Selva, M., Perosa, A., Rodríguez-Padrón, D., and Luque, R. (2019). Applications of dimethyl carbonate for the chemical upgrading of biosourced platform chemicals. *ACS Sustain. Chem. Eng.* 7, 6471–6479. doi: 10.1021/acssuschemeng.9b00464
- Sette, M., Wechselberger, R., and Crestini, C. (2011). Elucidation of lignin structure by quantitative 2D NMR. *Chem. Eur. J.* 17, 9529–9535. doi: 10.1002/chem.201003045
- Sevastyanova, O., Helander, M., Chowdhury, S., Lange, H., Wedin, H., Zhang, L., et al. (2014). Tailoring the molecular and thermo-mechanical properties of kraft lignin by ultrafiltration. *J. Appl. Polym. Sci.* 131:40799. doi: 10.1002/app.40799
- Sipponen, M. H., Lange, H., Ago, M., and Crestini, C. (2018). Understanding lignin aggregation processes. A case study: budesonide entrapment and stimuli controlled release from lignin nanoparticles. *ACS Sustain. Chem. Eng.* 6, 9342–9351. doi: 10.1021/acssuschemeng.8b01652
- Sun, Z., Fridrich, B., De Santi, A., Elangovan, S., and Barta, K. (2018). Bright side of lignin depolymerization: toward new platform chemicals. *Chem. Rev.* 118, 614–678. doi: 10.1021/acs.chemrev.7b00588
- Tortora, M., Cavalieri, F., Mosesso, P., Ciaffardini, F., Melone, F., and Crestini, C. (2014). Ultrasound driven assembly of lignin into microcapsules for storage and delivery of hydrophobic molecules. *Biomacromolecules* 15, 1634–1643. doi: 10.1021/bm500015j
- Werpy, T., and Petersen, G. (2004). *Top Value Added Chemicals From Biomass Volume I - Results of Screening for Potential Candidates From Sugars and Synthesis Gas*. Available online at: <https://www.nrel.gov/docs/fy04osti/35523.pdf>
- Wright, W. R. H., and Palkovits, R. (2012). Development of heterogeneous catalysts for the conversion of levulinic acid to γ -valerolactone. *ChemSusChem* 5, 1657–1667. doi: 10.1002/cssc.201200111
- Xu, C., Nasrollahzadeh, M., Selva, M., Issaabadi, Z., and Luque, R. (2019). Waste-to-wealth: biowaste valorization into valuable bio (nano) materials. *Chem. Soc. Rev.* 48, 4791–4822. doi: 10.1039/C8CS00543E

Conflict of Interest: The authors declare that the research was conducted in the absence of any commercial or financial relationships that could be construed as a potential conflict of interest.

Copyright © 2020 Fiorani, Crestini, Selva and Perosa. This is an open-access article distributed under the terms of the Creative Commons Attribution License (CC BY). The use, distribution or reproduction in other forums is permitted, provided the original author(s) and the copyright owner(s) are credited and that the original publication in this journal is cited, in accordance with accepted academic practice. No use, distribution or reproduction is permitted which does not comply with these terms.



A Way to Close the Loop: Physicochemical and Adsorbing Properties of Soybean Hulls Recovered After Soybean Peroxidase Extraction

OPEN ACCESS

Edited by:

Enrico Traversa,
University of Electronic Science and
Technology of China, China

Reviewed by:

John Zhanhu Guo,
University of Tennessee, Knoxville,
United States
Hassan Ait Ahsaine,
Mohammed V University, Morocco

*Correspondence:

Enzo Laurenti
enzo.laurenti@unito.it

† Present address:

Valentina Tolardo,
Smart Materials, Istituto Italiano di
Tecnologia and Department of
Informatics, Bioengineering, Robotics
and Systems Engineering, University
of Genova, Genoa, Italy
Razieh Sadraei,
Faculty of Science and Engineering,
University of Wolverhampton,
Wolverhampton, United Kingdom

Specialty section:

This article was submitted to
Green and Sustainable Chemistry,
a section of the journal
Frontiers in Chemistry

Received: 30 April 2020

Accepted: 22 July 2020

Published: 26 August 2020

Citation:

Tummino ML, Tolardo V,
Malandrino M, Sadraei R,
Magnacca G and Laurenti E (2020) A
Way to Close the Loop:
Physicochemical and Adsorbing
Properties of Soybean Hulls
Recovered After Soybean Peroxidase
Extraction. *Front. Chem.* 8:763.
doi: 10.3389/fchem.2020.00763

Maria Laura Tummino¹, Valentina Tolardo^{1†}, Mery Malandrino¹, Razieh Sadraei^{1†},
Giuliana Magnacca^{1,2} and Enzo Laurenti^{1*}

¹ Department of Chemistry, Università di Torino, Turin, Italy, ² Centre for Nanostructured Interfaces and Surfaces (NIS) and
INSTM Reference Centre, Turin, Italy

Soybean hulls are one of the by-products of soybean crushing and find application mainly in the animal feed sector. Nevertheless, soybean hulls have been already exploited as source of peroxidase (soybean peroxidase, SBP), an enzyme adopted in a wide range of applications such as bioremediation and wastewater treatment, biocatalysis, diagnostic tests, therapeutics and biosensors. In this work, the soybean hulls after the SBP extraction, destined to become a putrescible waste, were recovered and employed as adsorbents for water remediation due to their cellulose-based composition. They were studied from a physicochemical point of view using different characterization techniques and applied for the adsorption of five inorganic ions [Fe(III), Al(III), Cr(III), Ni(II), and Mn(II)] in different aqueous matrixes. The behavior of the exhausted soybean hulls was compared to pristine hulls, demonstrating better performances as pollutant adsorbents despite significant changes in their features, especially in terms of surface morphology, charge and composition. Overall, this work evidences that these kinds of double-recovered scraps are an effective and sustainable alternative for metal contaminants removal from water.

Keywords: soybean hulls, adsorption, wastewater treatments, scrap reuse, metals

INTRODUCTION

The origin and early history of soybeans are unknown, but some agronomic publications recorded origins of soybeans back to 2800 B.C. in China. Soybean (*Glycine max*) is an annual crop and today represents one of the major industrial and food crops grown in every continent (Bekabil, 2015), reaching a global production of over 360 million metric tons in 2018–2019 (USDA, 2019). Soybean hulls are one of the by-products of soybean crushing, a necessary step to produce soybean oil and meal (Poore et al., 2002; Scapini et al., 2018). Hulls represent around 8% (w/w) of the seed (Middelbos and Fahey, 2008; Robles Barros et al., 2020) and find application mainly in the animal feedstuff sector, due to their low nutrient value (Li et al., 2011; Balint et al., 2020; Robles Barros et al., 2020). When such use is not possible, hulls are burnt to recover heat or disposed in landfill as putrescible waste (Robles Barros et al., 2020). According to previous works, they are constituted by variable amounts of cellulose (38–51%), hemicellulose (20–25%), lignin (4–8%), pectin

(4–8%), proteins (11–15%), minor components (fatty acids, waxes, terpenes, essential oils, aromatic compounds, residual sucrose), and a little fraction of ashes (Wartelle and Marshall, 2000; Rojas et al., 2014).

One of the potential uses of soybean hulls in bio-chemistry field is their treatment to extract the soybean peroxidase (SBP). This enzyme is quite similar in structure and properties to the well-known horseradish peroxidase (HRP), adopted in a wide range of applications such as bioremediation and wastewater treatment, biocatalysis, diagnostic tests, therapeutics, and biosensors (Lopes et al., 2014; Krainer and Glieder, 2015). Respect to HRP, SBP shows a higher stability and a lower susceptibility both to thermal and chemical inactivation, making it suitable for biotechnological applications (Ryan et al., 2006; Steevensz et al., 2014; Al-Maqdi et al., 2018; Bilal et al., 2018; Donadelli et al., 2018; Sadraei et al., 2019; Yang et al., 2019). In a previous study regarding the prospects for a large-scale soybean peroxidase commercialization, Hailu et al. (2010) suggested that investments in an SBP extraction facility can be economically advantageous, estimating that, in a 0.5 ha plant, 6.2 metric tons of hulls can generate 0.56 billion units of crude SBP with a total annual revenue of 5.1 millions of CAD\$.

Another possible way to valorize the soybean hulls is their application as adsorbents of metal ions or organic molecules (among others, those indicated as Contaminants of Emerging Concerns) in polluted waters. The presence of these species in water bodies represents one of the most concerning environmental issues for their detrimental repercussions on aquatic organism, plants, human health, and climate changes (Inyinbor Adejumo et al., 2018). Within the scientific community, many efforts have been devoted to the development of different methods to solve this problem. Adsorption on biomasses results one of the most convenient solutions for two aspects: the adsorption does not favor secondary pollution if used with organic contaminants (i.e., transformation of the toxic substances into other kinds of polluting products) and it is a suitable method for capturing metal ions. In addition, the employment of residual biomasses is a key factor in a perspective of recycle and reuse. Carbon-based compounds, such as activated carbons, graphene, or graphene-oxides (De Gisi et al., 2016; Wang et al., 2018; Ali et al., 2019), and (hydro)oxide-based materials like SiO₂, Al₂O₃, zeolites, clays, etc. (Chen et al., 2017; Shi et al., 2020) have been widely described in the literature. More recently, supported humic-like substances, natural polysaccharides (as chitosan, alginate, starch, cellulose), but especially various types of agricultural/domestic scraps have been exploited for adsorption purposes (Dai et al., 2018; Singh et al., 2018; Tummino et al., 2019, 2020). In this context, soybean hulls, rich of hemicellulose and cellulose, containing oxygenated functional groups including carbonyl groups, hydroxyl groups, and ethers, can bind heavy metal ions and organic pollutants by different kinds of interaction (chelation, complexation, coordination, formation of hydrogen bonds). A short, but representative, list of substances removed by soybean hulls-based adsorbents, as reported in the literature, is shown in Table 1.

TABLE 1 | Inorganic ions and organic substances removed by adsorption with soybean hulls.

Substrates	References	Hulls pretreatments
Zn(II), Cu(II), Ni(II)	(Marshall and Johns, 1996; Marshall et al., 1999)	Different washings and/or citric acid-modification
Pb(II)	(Li et al., 2011)	Citric acid-modification
Cr(VI)	(Sheng-quan et al., 2012)	No treatments
Hg(II)	(Rizzuti et al., 2015)	No treatments
Safranin T, Remazol brilliant blue R, direct violet 51	(Rizzuti and Lancaster, 2013)	No treatments
BF-4B reactive red dye	(Módenes et al., 2019)	No treatments
BF-5G reactive blue dye	(Honorio et al., 2016)	No treatments
Methylene blue	(Fleira et al., 2019)	No treatments
Hormones	(Honorio et al., 2019)	No treatments
Herbicides (Diuron and Hexazinone)	(Takeshita et al., 2020)	No treatments

Moreover, in a previous paper, Marshall and Wartelle (2006) carried out modifications to make hulls act as dual-functional ion exchange resins and enhance their adsorbing properties, imparting a specific surface charge by reaction with citric acid (negatively charged) or choline chloride (positively charged).

Soybean hulls have been also considered as source of carbon (obtained by either thermal or chemical transformations) for the production of micro-mesoporous adsorbents (Girgis et al., 2011), biofillers (Balint et al., 2020), and can potentially be employed in those fields where carbons are required as active substrates for electrochemistry, electronics and biomedicine (Thiha et al., 2019; Sun et al., 2020; Wang C. et al., 2020). Finally, also cellulose and other polysaccharides, constituting the lignocellulosic hull biomass and obtained after proper extraction processes (Camiscia et al., 2018; Wang S. et al., 2020), can find outlet in different branches of biotechnology (food, medicine, bioremediation, paper industry, etc.) and of biorefinery, since they can be converted to biopolymers, bioethanol or even to fuels with high commercial value (Cassales et al., 2011; Camiscia et al., 2018; Dall Cortivo et al., 2020; Wang S. et al., 2020).

Given the benefits of promoting soybean hulls revalorization, this study is framed in the context of circular economy, aiming to (i) recover and reuse soybean hulls at the very end of their lifecycle after being subjected to the treatments for SBP extraction; (ii) study the physicochemical properties and adsorbing features of the treated hulls, also in comparison with the untreated ones. For these purposes, soybean hulls were characterized and tested toward solutions of the following

inorganic ions, Fe(III), Al(III), Cr(III), Ni(II) and Mn(II), in different aqueous matrixes, namely pure water, potable waters and landfill leachate.

MATERIALS AND METHODS

All the reagents were purchased from Merck Life Science S.r.l. (Italy) and used without further purification. All the experiments were performed in triplicate.

Preparation

For the extraction of soybean peroxidase (SBP) (Tolardo et al., 2019), the seeds were peeled, and the obtained hulls were stored at -12°C until use. SBP was extracted and purified by a process based on a previously published method (Calza et al., 2016): 100 g of soybean hulls were ground in a mortar, added to 600 mL of phosphate buffer (0.025 M, pH 7) and left under stirring for 2 h at room temperature. Then, the hulls were separated from the solution by filtration with a cotton gauze and subjected to the same treatment until the filtrate gave a negative response to enzymatic activity test for SBP. The hulls were successively dried at room temperature, cooled by N_2 at 77 K to favor their grinding and, then, homogenized in a mortar. Hulls not subjected to SBP extraction were homogenized in the same way and used as reference samples. In this paper, treated and untreated hulls were labeled SBH-A and SBH-B, respectively, where A and B stands for "After" and "Before" the extraction.

Characterization

ζ -potential measurements were performed on a Zetasizer (Malvern Instrument, Malvern, UK). The ζ -potential values were measured using principles of laser Doppler velocimetry and phase analysis light scattering (M3-PALS technique). All the suspensions were prepared by dispersing 10 mg of powder in 20 mL of double distilled water. The pH values were adjusted in a range of 2–10 by addition of 0.1 M HCl or 0.1 M NaOH aqueous solutions.

Attenuated total reflectance Fourier transform infrared (ATR-FTIR) spectra (16 scans/spectrum, 4 cm^{-1} resolution) were collected using a Universal ATR Sampling Accessory assembled in a Perkin-Elmer Spectrum 100 Fourier transform infrared spectroscope.

Scanning Electron Microscopy (SEM) analysis was carried out using a ZEISS EVO 50 XVP with LaB_6 source, equipped with detectors for secondary electrons collection and an Energy Dispersive X-ray Spectrometry (EDS) probe for elemental analyses. Samples were covered with a gold layer of $\sim 15\text{ nm}$ of thickness before the analysis to prevent charging (Bal-tec SCD050 sputter coater).

Surface area and pore volumes were obtained by N_2 adsorption at 77 K in an ASAP2020 gas-volumetric apparatus (Micromeritics, Norcross, GA, USA). The samples were previously outgassed overnight at 100°C until a standard residual pressure of 10^{-2} mbar was stably present in the outgassing system. The specific surface area of soybean hulls was calculated by the Brunauer-Emmett-Teller (BET) method (Brunauer et al., 1938).

The release of substances from SBH-A and SBH-B ($1,600\text{ mg L}^{-1}$) in MilliQ[®] water at pH 5 and 7 was monitored. After stirring for 24 h, hulls were separated by filtration in a Büchner funnel and the amount of each metal ion in solution was determined by Inductively Coupled Plasma Optical Emission Spectrometry (ICP-OES), model Optima 7000 DV (Perkin Elmer, Waltham, MA, USA), equipped with a crossflow nebulizer, a Scott spray chamber and a double monochromator (prism and Echelle grating). The instrumental conditions were: plasma power 1.3 kW, sample aspiration rate 1.5 mL min^{-1} , argon nebulizer flow 0.8 L min^{-1} , argon auxiliary flow 0.2 L min^{-1} and argon plasma flow 15 L min^{-1} . Moreover, in order to follow the simultaneous loss of organic substances, UV-visible spectra of the same solutions were recorded by an UV-visible spectrophotometer CARY 100 SCAN (Varian, Palo Alto, CA, USA) with a sample quartz cell of 1 cm path length.

Adsorption/Desorption Experiments

Following a previously reported procedure for the adsorption of metallic ions (Tummino et al., 2019), aqueous solutions (75 mL) of Iron, Aluminum, Nickel, Manganese and Chromium ions, prepared by concentrated commercial standards Tritisol[®] in MilliQ[®] water [respectively, FeCl_3 , $\text{Al}(\text{NO}_3)_3 \cdot 9\text{H}_2\text{O}$, NiCl_2 , MnCl_2 , CrCl_3], were put in contact at $25 \pm 1^{\circ}\text{C}$ with soybean hulls in a beaker and left under mechanical stirring throughout the measurement. During the experiments, pH and temperature were continuously monitored by means of a pH electrode and a thermometer introduced in the beaker. At different times, 10 mL of suspension were withdrawn and filtered with a cellulose filter ($0.45\text{ }\mu\text{m}$, Minisart, Sartorius, Göttingen, Germany) supported on syringes with plungers devoid of rubbery parts (BD DiscarditTM) to remove the adsorbent. After filtration, $10\text{ }\mu\text{L}$ of ultrapure HNO_3 (65%, Suprapur[®], Merck) were added to each sample and the solutions were stored at 4°C until further analysis. Inorganic ions concentration was determined by Inductively Coupled Plasma Optical Emission Spectrometry (ICP-OES), adopting the conditions previously described.

Initial tests were carried out by adding SBH-A or SBH-B at different concentrations (800 and $1,600\text{ mg L}^{-1}$) for 1 or 24 h to a solution containing all the metallic species: Fe(III), Al(III), Ni(II), Mn(II), and Cr(III) ($1 \times 10^{-5}\text{ M}$ for each ion). The pH was modulated by adding NaOH or HNO_3 solutions (0.2 M) in order to reach the stable pH value of 5, chosen after preliminary tests (not shown) to ensure the adsorption process without incurring precipitation problems. Then, for the most efficient system, namely SBH-A, the adsorption properties were studied more deeply in presence of: (i) solutions of a single inorganic ion ($1 \times 10^{-4}\text{ M}$) at pH 5; (ii) solutions of Cr(III) at different concentrations (from 1×10^{-3} to $2 \times 10^{-1}\text{ mM}$) to construct the adsorption isotherm at pH 5 and 25°C ; (iii) potable waters tested without any modification (pH 7.5); (iv) a landfill leachate tested without any modification (pH 5.6).

The experiments with potable waters and landfill leachate were performed for 6 h of contact time in order to optimize adsorption while maintaining the manipulation of the leachate within a typical working day (for safety reasons), in accordance with a previous procedure with similar samples (Tummino et al.,

2019). The potable waters, obtained from different municipal wells, and the landfill leachate were supplied by Acea Pinerolese Industriale S.p.A., a waste treatment facility connected with a water depuration plant located in Pinerolo, Italy.

The desorption tests were performed on SBH-A, recovered by filtration in a Büchner funnel after a 24 h-adsorption experiment in presence of the mixed ions solution (ions concentration: 1×10^{-5} M for each ion and hulls concentration: $1,600 \text{ mg L}^{-1}$). The desorption was conducted with two different solutions: (i) MilliQ[®] water at pH 5 and (ii) MilliQ[®] water at pH 5 containing NaCl salt in a 1:1 concentration ratio. The obtained suspensions were left under stirring for 24 h, then the hulls were separated from the solution by filtration. The ion concentrations in filtered solutions have been determined by ICP-OES.

RESULTS AND DISCUSSION

Hulls Characterization

The treatment employed for SBP extraction clearly modified the macroscopic aspects of hulls. The most visible effect was the adhesion of the SBH-A hulls to each other, not observable in SBH-B. This characteristic was assessed by measuring the hulls thickness by a digital thickness gauge on a casual and representative set of samples before grinding: the thickness values were $100 \pm 30 \mu\text{m}$ for SBH-B and $533 \pm 160 \mu\text{m}$ for SBH-A.

In order to better define the surface and structural modification induced by the SBP extraction process, SBH-A samples were characterized by means of ζ -potential measurements, ATR-FTIR analysis and electron microscopy, whose relative results were compared with SBH-B properties.

ζ -Potential

ζ -potential of SBH-A and SBH-B samples suspended in double distilled water were measured at different pH values. These measurements indicated that the surface of both the samples was always negatively charged also at acidic pH, approaching the point of zero charge at pH close to 2 (Figure 1). Moreover, the process for SBP extraction clearly influenced the surface of the hulls since the ζ -potential values of SBH-A are less negative than those recorded for SBH-B in the whole pH range, suggesting that the phosphate buffer is able in removing substances with a low pKa, which are negatively charged in a large range of pH values and therefore resulting more soluble than other not-charged substances (see release of organic matter in paragraph Release From SBH-A and SBH-B). The strong impact of this kind of pretreatment has been already ascertained by Giri et al. (2017) who observed the modification of physical structure and thermal stability of soybean hulls subjected to pyrolysis.

ATR-FTIR Measurements

ATR-FTIR spectrum of pure SBP enzyme (Figure 2) displayed absorbance bands between $3,000$ and $3,500 \text{ cm}^{-1}$ attributed to the N-H and O-H stretching modes, respectively, whereas the C-H asymmetric stretching was observed around $2,930 \text{ cm}^{-1}$. Bands at $1,645$ and $1,530 \text{ cm}^{-1}$ were ascribed to the amide I and amide II absorbance bands, respectively (Torres et al., 2017). The amide I band is mainly associated with the C=O stretching

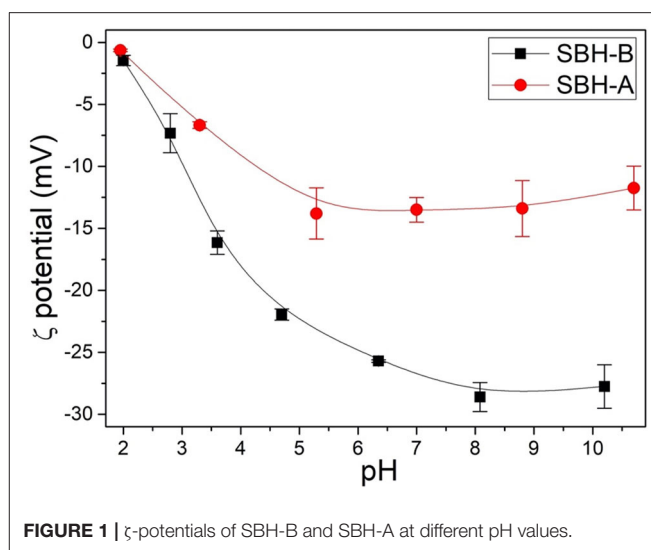


FIGURE 1 | ζ -potentials of SBH-B and SBH-A at different pH values.

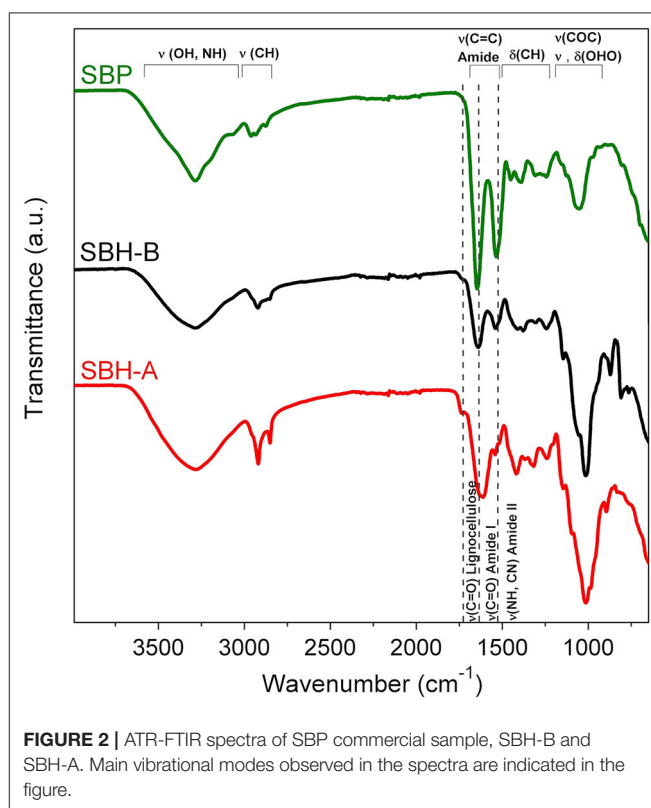


FIGURE 2 | ATR-FTIR spectra of SBP commercial sample, SBH-B and SBH-A. Main vibrational modes observed in the spectra are indicated in the figure.

vibrations of the peptide bonds and it is closely correlated to the protein secondary structure, whereas amide II results from the N-H bending vibration and the C-N stretching vibration (Barth, 2007). The region between $1,200$ and $1,400 \text{ cm}^{-1}$ involved mainly C-H bending modes (Torres et al., 2017), whereas the signal at ca. $1,050 \text{ cm}^{-1}$ was associated to O-H⁺-O stretching or bending of hydrated protons in proteins (Barth, 2007).

In general, ATR-FTIR spectra of hulls showed a broad band between $3,000$ and $3,500 \text{ cm}^{-1}$ of the N-H and O-H stretching

modes, the peaks at 2,920 and 2,850 cm^{-1} were attributed to $-\text{CH}_2$ asymmetric and symmetric stretching vibrations, respectively (Chandane and Singh, 2016). The peak at 1,740 cm^{-1} represents the carbonyl group ($-\text{C}=\text{O}$) stretching (Chandane and Singh, 2016), typical of ligno-cellulosic materials (Widiarto et al., 2019). The signal at 1,640 cm^{-1} (for SBH-B) and 1,620 cm^{-1} (for SBH-A) was associated to $\text{C}=\text{O}$ stretching vibrations of the peptide bonds, if present, (Torres et al., 2017), to olefinic $\text{C}=\text{C}$ stretching vibration (Qin et al., 2011) and to δ_{HOH} vibrations of molecularly adsorbed water (Widiarto et al., 2019). The peak at 1,540 cm^{-1} was due to N-H bending vibration and C-N stretching related to proteins (Torres et al., 2017) and/or to aromatic $-\text{C}=\text{C}-$ stretching, which are vibrations mainly related to the ligno-cellulosic backbone (Chandane and Singh, 2016). At 1,420 and 1,370 cm^{-1} there are the regions of CH_2 bending vibration and deformation of C-H in aromatic ring (Widiarto et al., 2019). The broad band centered at 1,010 cm^{-1} was assigned to ether ($-\text{C}-\text{O}-\text{C}-$) stretch (Chandane and Singh, 2016) and the peak at 870 cm^{-1} was attributed to glycoside bond of cellulose (Widiarto et al., 2019). The most remarkable differences between spectra of SBH-B and SBH-A concerned: (i) the peaks between 2,920 and 2,850 cm^{-1} , sharper in the case of SBH-A; (ii) the intensity of the peak at 1,740 cm^{-1} of the carbonyl group ($-\text{C}=\text{O}$), stronger for SBH-A; (iii) the shift of the peak at 1,640 to 1,620 cm^{-1} and the decrease of the signal at 1,540 cm^{-1} in the case of SBH-A. These evidences suggested that the peptidic portion on the surface hulls was almost completely lost after the SBP extraction treatment, whereas the ligno-cellulosic backbone signals became prevailing.

Morphological Characterization

Nitrogen adsorption at 77 K revealed a very low surface area, $<1 \text{ m}^2 \text{ g}^{-1}$, for both treated and untreated samples. On the other hand, SEM micrographs (Figure 3) confirmed the surface modifications highlighted before showing evident morphological differences between SBH-A and SBH-B. Indeed, SBH-B had a rough surface with some cavities (Chandane and Singh, 2016) and scales with a diameter comprised between 5 and 10 μm . After the SBP extraction, the hull surface structure seemed to collapse, the section appeared more compact and the order constituted by the scales was lost.

Release From SBH-A and SBH-B

The release of the metal ions involved in this study was detected at pH 5 and 7 after the hulls were soaked in pure water for 24 h (Table 2), in order to probe the metal content which could interfere in the adsorption/desorption tests. The reproducibility of the results is confirmed by low percent relative standard deviation (RSD %) which was always $<5\%$. SBH-B released a higher content of metals than SBH-A, confirming that SBP extraction procedure resulted in the removal of impurities present in the ligno-cellulosic structure of the hulls. Relevant amounts of iron, aluminum and, to a lesser extent, manganese were found in solution, in accordance to their ubiquitous presence as essential elements for living matter and their widespread diffusion in soils (Spehar, 1994; Noya et al., 2014). At increasing pH, the release process became less favorite.

Nevertheless, in all cases, the amount of metals detected in the solution was lower than the concentration used in the adsorption tests to evaluate hulls' sequestering capacity. The aqueous solutions were further analyzed by means of UV-vis technique, in order to follow the simultaneous loss of organic matter. The UV-visible spectra in Figure 4 show a non-negligible shoulder centered at 275 nm, indicating the release of water soluble organic substances (Khan et al., 2014), in particular in the case of SBH-B. A similar behavior have been already evidenced by Fieira et al. (2019), who evaluated such release in terms of Chemical Oxygen Demand (COD).

An overall view of the characterization outcomes for SBH assesses a sort of cleaning effect of the protein extraction with phosphate buffer from inorganic and organic substances present in the main lignocellulosic structure. It is reasonable to image that, together with the loss of a part of hulls' mass, the interactions keeping together the lignocellulosic matter components were subjected to changes: in particular, several functional groups, initially interacting each other in the non-modified structure, remained isolated, and available to form other interactions with other substrates (in this case, metal ions). Simultaneously, the changes induced in the surface morphology can be ascribable to the swelling of the lignocellulosic matter and subsequent drying that, probably, caused a partial structure collapse (Fidale et al., 2008).

Adsorption/Desorption Experiments

Adsorption of Metal Ions Mixture

SBH-A and SBH-B were tested for their adsorbing capability and the correspondent results are shown in Figure 5. Adsorption % was calculated by the following equation, where C_0 is the starting concentration of each ion ($1 \times 10^{-5} \text{ M}$) and C_{ion} is the concentration of each ion left in the solution at the end of the experiment. The error was calculated with respect to the total amount of the adsorbed ions. To highlight the differences in the adsorption of different metal ions, the contribute of each ion was indicated in a proper color in Figure 5.

$$\text{Adsorption \%} = \frac{[C_0 - C_{\text{Fe(III)}}] + [C_0 - C_{\text{Al(III)}}] + [C_0 - C_{\text{Cr(III)}}] + [C_0 - C_{\text{Ni(II)}}] + [C_0 - C_{\text{Mn(II)}}]}{5 \times 10^{-5}} \times 100$$

Figure 5, left panel, displays the different performances of SBH-A and SBH-B (800 mg L^{-1}) in contact with a solution containing the five metal ions ($1 \times 10^{-5} \text{ M}$ for each ion) for two different contact times: 1 and 24 h. Many differences are highlighted from the experimental data, both concerning the adsorption properties of the sample before and after the SBP extraction, and the behavior toward the metal ions. Observing the trends related to iron adsorption, the use of SBH-A was evidently advantageous with respect to SBH-B sample, particularly after a longer contact time. Similarly, 1 day-contact favored the removal of Cr(III), mostly for SBH-A. In the cases of Ni(II) and Mn(II), the adsorption levels resulted comparable for SBH-A and SBH-B both after 1 and 24 h, whereas a peculiar behavior was demonstrated toward Al(III), which was captured significantly only by SBH-A after 24 h.

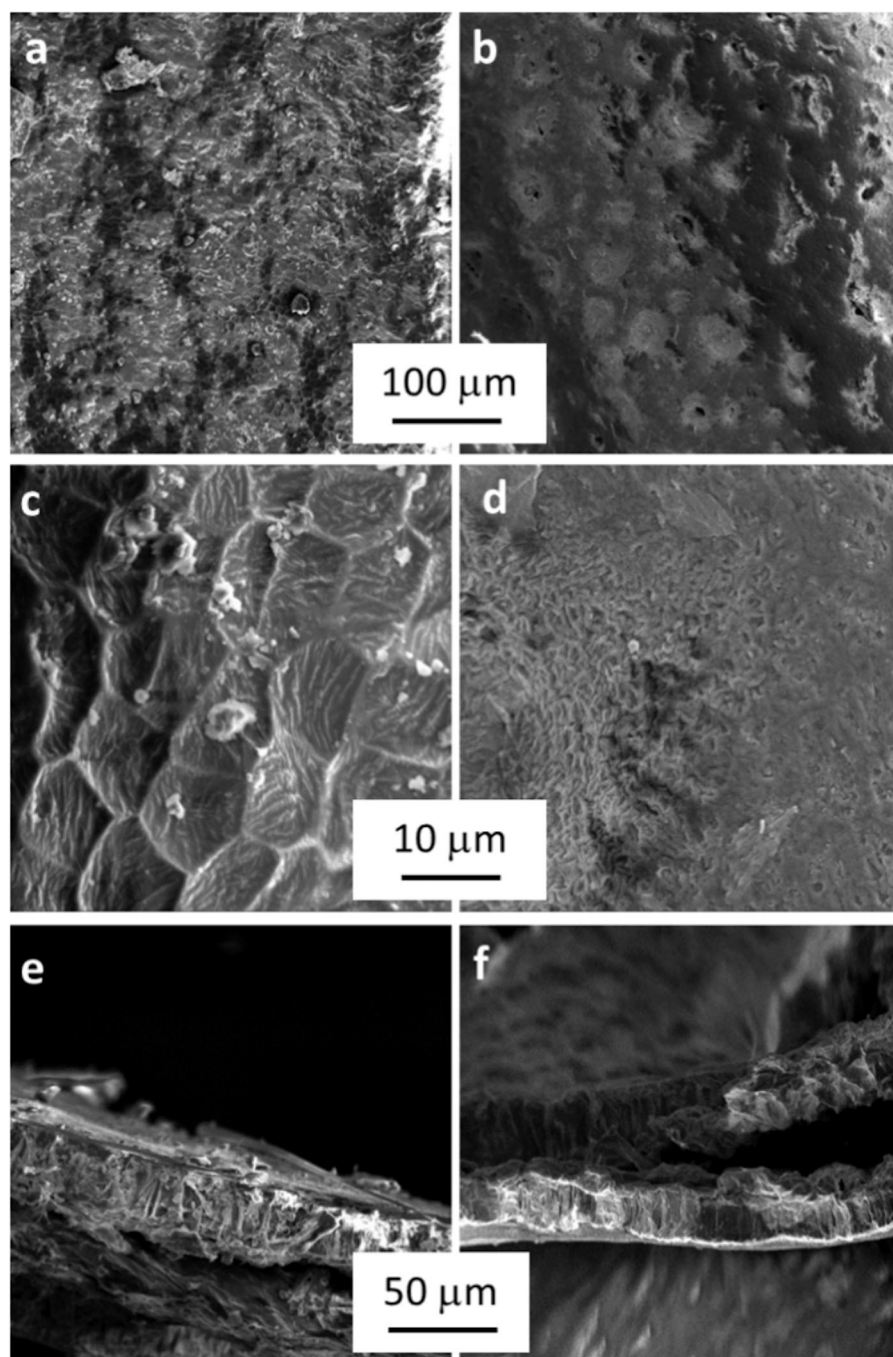


FIGURE 3 | Micrographs of SBH-B (a,c) and SBH-A (b,d) surfaces at different magnifications and, at the bottom, pictures of SBH-B (e) and SBH-A (f) sections.

In the right panel of **Figure 5**, the degrees of adsorption reached after 24 h with $1,600 \text{ mg L}^{-1}$ of hulls are represented. In general, the hull increment did not significantly affect the adsorption in the presence of the trivalent cations, whereas the adsorption observed for the two divalent cations, Mn(II) and Ni(II), almost doubled. A better adsorptive activity was

once more achieved by SBH-A than SBH-B toward iron and aluminum ions.

From the interpretation of the two graphs of **Figure 5**, it can be noticed that, although the adsorption is generally a fast process, involving the adsorbent surface and multiple interactions, the simultaneous presence of different ions slowed

down the process, establishing a certain selectivity, as well. The equilibria varied over time, favoring the species with a higher positive charge, Fe(III), Al(III) and Cr(III), possibly due to their electrostatic affinity with the negatively charged hulls surface. Nevertheless, the description of the adsorption phenomenon cannot be associated only to the electrostatic forces. Indeed, the hulls behavior toward aluminum resulted very peculiar: Al(III) has the lowest ionic radius (then, less steric hindrance) and a strong positive charge (3+), but it was not sequestered by SBH-B and 1 h was not a sufficient contact time to allow an efficient adsorption. This occurrence can be justified by taking into account the solvation degree: smaller ions with high density charge are more solvated and less rapidly attracted by the adsorbent surface (Zhu et al., 2016). In general, a complex frame of factors connected to the adsorbate nature influences the adsorption effectiveness, as valence, electronegativity, hydration radii, hydration enthalpies, solubility of the cations (Zhu et al., 2016) and hard—soft, acid—bases affinity [according to Pearson's principle (Alfarra et al., 2004)]. Moreover, it is worth to underline that the modifications induced by SBP extraction, including a lowering of the surface's negative charge, did not compromise the adsorptive properties of hulls, but rather improved them in some cases. The most probable reasons are the lower competition

with intrinsically present metal ions, which were mostly released during the SBP extraction treatment, and the exposure of a higher number of active sites on the surface of ligno-cellulosic matter after the same procedure. In particular, the SBH functionalities capable of positive ion attraction are mainly hydroxyl and carboxylic groups (Dai et al., 2018), which are present to a different extent in SBH-A and SBH-B, according to FTIR results.

Desorption Tests

Taking into account the adsorption capacity of SBH-A for most of the metals considered, the desorption tests were conducted on this material only. The hulls were recovered by filtration after 24-h adsorption experiment, the sample was divided in two aliquots and each successively added to a different solution, namely ultrapure water at pH 5 with or without NaCl. The intense interaction already found for hulls toward Al(III), Fe(III) and Cr(III) was responsible for the extremely reduced desorption observed for these ions, namely 1–3% maximum. Ni(II) and Mn(II) were slightly released, but always <20%. In general, the adsorption on SBH-A was not reversible in the adopted conditions, without any advantage provided by the presence of other metal ions (Na^+) in the washing solution.

Adsorption of Metal Ions Separately

Deepening the behavior of SBH-A, the hulls underwent adsorption of the same metal ions separately, using a concentration 10 times higher than the previous ones. As shown in Figure 6, high levels of metals removal were already reached in 1 h. Except for manganese, the entity of metals removal was ~90%, despite of different kinetic trends. In the absence of competition among different ions, the adsorption was favored for all the ions tested but the highly charged metal ions showed faster adsorption kinetic as confirmed by the first order k_{app} reported in Table 3. In particular, aluminum and iron ions show the highest k_{app} values and were almost totally adsorbed in few minutes, supporting the hypothesis that the present trials were mainly driven by charge interactions.

TABLE 2 | Species released from SBH-A and SBH-B ($1,600 \text{ mg L}^{-1}$) in MilliQ® water at pH 5 and 7.

		Species released (nM)				
		Fe	Al	Ni	Mn	Cr
pH 5	SBH-B	994	320	8.0	30	2.9
	SBH-A	103	19	1.1	6.3	3.2
pH 7	SBH-B	572	188	13	19	1.8
	SBH-A	64	16	1.7	5.7	1.6

Average errors (4–5%) are not shown in the table.

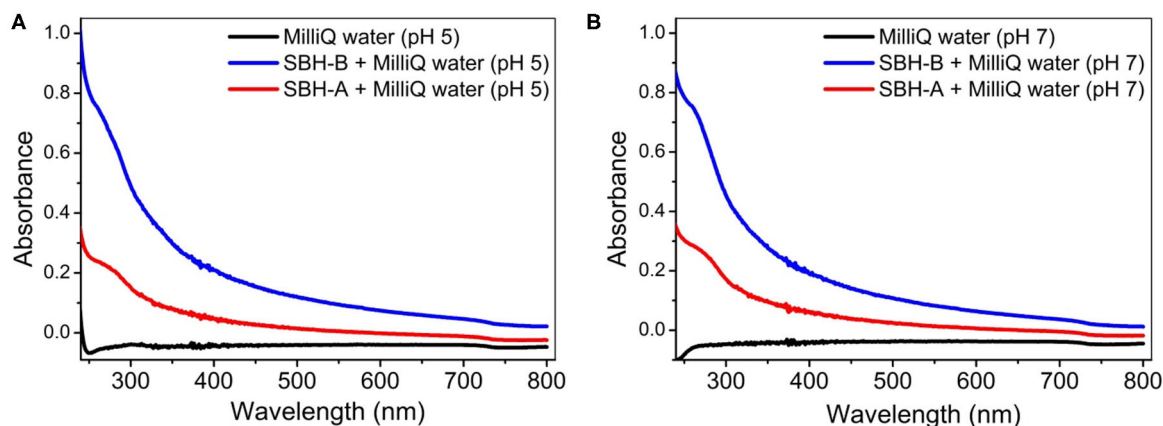


FIGURE 4 | UV-visible spectra of the solutions obtained after the release tests of SBH-A and SBH-B ($1,600 \text{ mg L}^{-1}$) in MilliQ® water at pH 5 (A) and 7 (B).

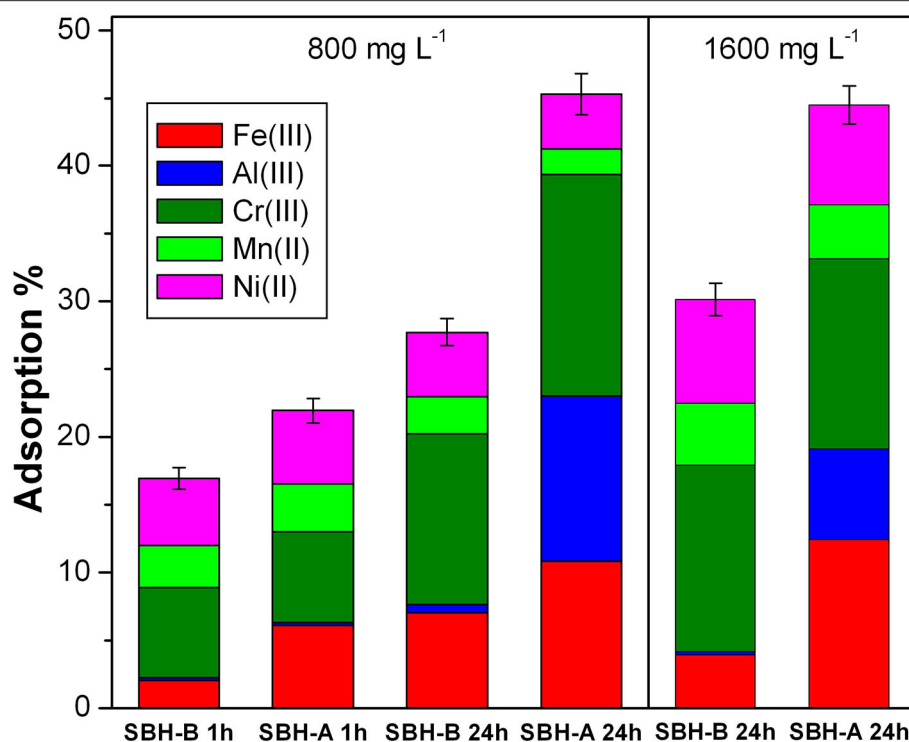


FIGURE 5 | Adsorption % of Fe(III), Al(III), Cr(III), Mn(II), and Ni(II) mixed together (1×10^{-5} M for each ion) at pH 5 in presence of SBH-B and SBH-A; Left panel conditions: hulls concentration 800 mg L^{-1} and contact times 1 or 24 h; Right panel conditions: hulls concentrations $1,600 \text{ mg L}^{-1}$, contact time 24 h. The adsorption % was calculated in relation to the total initial amount of metal ions in solution as described in the text.

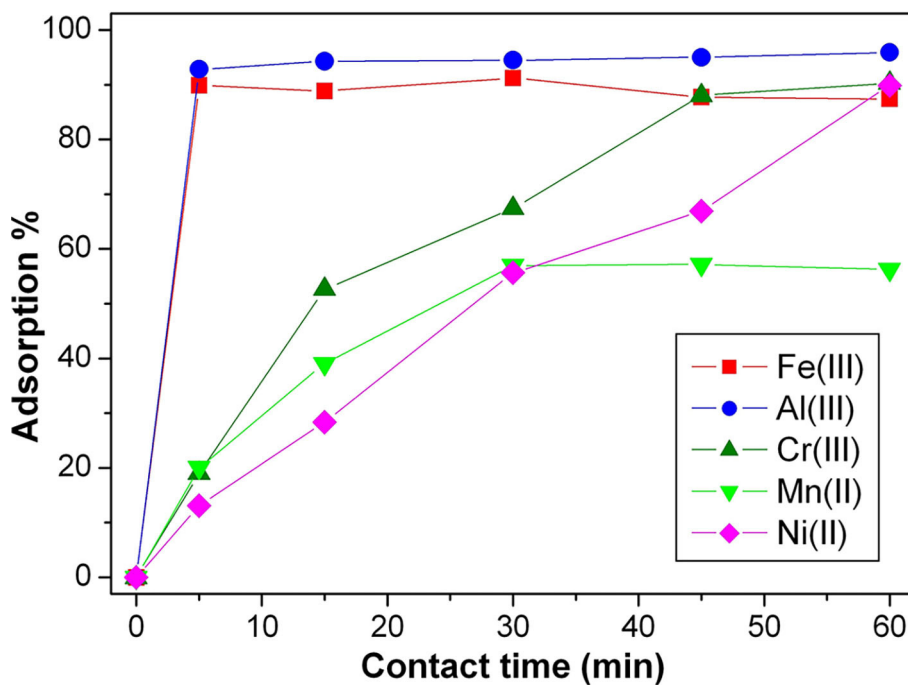


FIGURE 6 | Adsorption kinetics of Fe(III), Al(III), Cr(III), Mn(II), and Ni(II), single ion solutions 1×10^{-4} M at pH 5, in presence of SBH-A (800 mg L^{-1}).

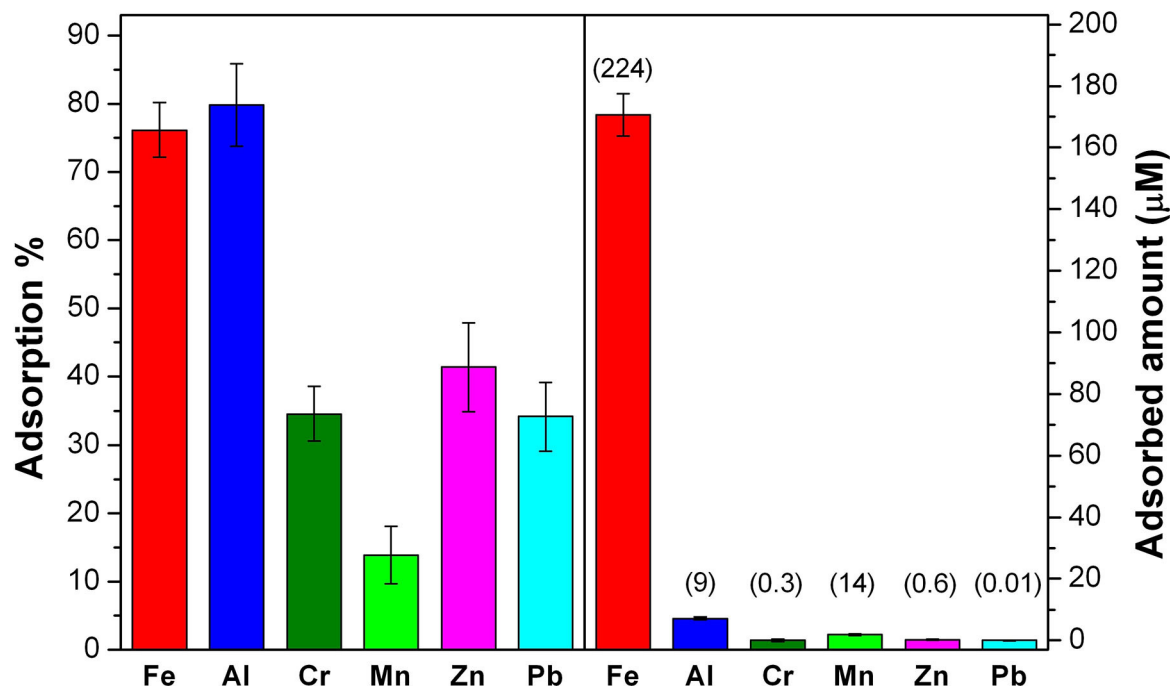


FIGURE 7 | Results of the 6 h-adsorption treatment of landfill leachate at its natural pH 5.6 with SBH-A. The left panel reports the adsorption % for each metal ion. On the right panel, the removed concentration (μM) of each ion is shown and the labels are referred to the starting concentration (μM) of each ion.

TABLE 3 | First order kinetic constants calculated on the basis of single ion adsorption reported in **Figure 6** (ion concentration 1×10^{-4} M at pH 5, in presence of SBH-A 800 mg L^{-1}).

Ion	$k_{app} \text{ (min}^{-1}\text{)}$	R^2
Fe(III)	0.823 ± 0.281	0.998
Al(III)	0.765 ± 0.081	0.999
Cr(III)	0.047 ± 0.009	0.992
Mn(II)	0.082 ± 0.012	0.992
Ni(II)	0.012 ± 0.006	0.993

To get some preliminary information on the adsorption mechanism of SBH-A, Cr(III) was chosen as a representative ion to obtain an adsorption isotherm. In this case, the amount of adsorbed Cr(III) by SBH-A was measured after 24 h of contact between SBH-A and variable concentrations of Cr(III). Preliminary measurements confirmed that the equilibrium was reached at all the Cr(III) concentrations considered in the experiment.

The experimental data were fitted both with the Langmuir and Freundlich equations reported below:

$$\text{Langmuir: } \frac{1}{q_e} = \frac{1}{q_m b C_e} + \frac{1}{q_m}$$

$$\text{Freundlich: } \log q_e = \log K_f + \frac{1}{n} \log C_e$$

TABLE 4 | Values of Langmuir and Freundlich constants, related to adsorption of Cr(III) ions on SBH-A (800 mg L^{-1}) at pH 5, time of contact 24 h.

Langmuir		Freundlich	
$q_m \text{ (mmol g}^{-1}\text{)}$	0.27	$K_f \text{ (L g}^{-1}\text{)}$	11.2
$b \text{ (L mmol}^{-1}\text{)}$	129	$1/n$	0.94
R^2	0.98	R^2	0.88

In both the equations, q_e is the concentration of adsorbate on the solid and C_e is the concentration of Cr(III) at equilibrium. In the Langmuir equation, q_m is the sorption capacity (namely the amount of adsorbate at complete monolayer coverage) and b the Langmuir isotherm constant that relates to the energy of adsorption. In Freundlich equation, the value of K_f is indicative of the adsorption capacity and $1/n$ represents the adsorption intensity (Islam et al., 2013).

The parameters determined by fitting the experimental data with the two equations are reported in **Table 4**. The highest value of R^2 obtained using the Langmuir model showed that it could be the most suitable model describing the system under study, indicating a homogenous distribution of adsorption sites and the presence of a single layer of Cr(III) ions on the surface of the hulls, rich of negatively charged functional groups (Saruchi and Kumar, 2019). On the other hand, from the Freundlich model, the value of $1/n$ value obtained in the range between 0 and 1, indicated that the interaction between Cr(III) and the hulls occurred easily (Saruchi and Kumar, 2019).

Tests on Potable Waters and Landfill Leachate

On the basis of previous results, final trials were carried out on real potable waters and a landfill leachate. Such experiments were performed as described above and in accordance to a previously reported procedure with similar samples (Tummino et al., 2019). Other metal ions (zinc and lead) were also followed, albeit not considered in the previous tests, but present in the real water samples.

Potable waters from two different urban well-sources were tested: in both cases the presence of iron, aluminum and chromium species were negligible, whereas low concentrations of nickel, zinc, and lead (respectively, 0.03, 0.61, and 0.006 μM) were observed. Adsorption test with SBH-A led to the removal of 63% of Ni, 85% of Zn and 41% of Pb.

In the case of the landfill leachate, it is important to note that the matrix was constituted also by organic molecules, creating a competition among the multiple components and then influencing SBH-A performances toward metallic ions. Nevertheless, the results showed in **Figure 7** are encouraging since SBH-A hulls maintained their sequestering ability, in particular toward Fe and Al, since more than 75% of these ions was removed from the solution. Moreover, it is also interesting to consider that, in the case of Fe, this percentage corresponds to a concentration of 1.7×10^{-4} M, confirming the good adsorption levels reached by SBH-A toward iron ions in ultrapure water, as previously discussed.

CONCLUSIONS

Soybean hulls were recovered after the extraction of soybean peroxidase, an enzyme employed as green biocatalyst. The results of hull physicochemical characterization evidenced a remarkable impact of the enzyme extraction procedure, which varied the hull surface morphology and decreased the content of intrinsically adsorbed metallic/organic substances. Such treated hulls were applied as adsorbents of metal ions [Fe(III), Al(III), Ni(II), Mn(II), Cr(III)] in different aqueous matrixes, revealing an improvement of their sequestering capability with respect to untreated samples. In conclusion, such residual hulls deriving from agro-industrial scraps, not only can be successfully

processed to obtain a high-value enzyme, but it is also possible to extend their exploitation in water remediation field, further decreasing their environmental impact as waste and giving them an additional technological and economical value.

DATA AVAILABILITY STATEMENT

The original contributions presented in the study are included in the article/supplementary material, further inquiries can be directed to the corresponding author.

AUTHOR CONTRIBUTIONS

MT, MM, GM, and EL contributed conception and design of the study. MT, VT, and RS performed the experiments. MT wrote the first draft of the manuscript. GM and EL wrote sections of the manuscript. All authors contributed to manuscript revision, read, and approved the submitted version.

FUNDING

This work was realized with the financial support for academic interchange by the Marie Skłodowska-Curie Research and Innovation Staff Exchange project funded by the European Commission H2020-MSCA-RISE-2014 within the framework of the research project Mat4treaT (Project number: 645551); and by Compagnia di San Paolo and University of Torino under the pluriannual convention (Project Torino_call2014_L2_126, project acronym: Microbusters, and Ex-post Projects, call 2018).

ACKNOWLEDGMENTS

MT work was supported by Bando Talenti della Società Civile—edizione 2016, promoted by Fondazione CRT (Italy), and managed by Fondazione Giovanni Gorla (Italy). Furthermore, we thank P. Bracco, Università di Torino, for her help in ATR-FTIR measurements; Roberta Gamberini and Raffaella Giordanino, Acea Pinerolese Industriale S.p.A., for the supply of samples of potable waters and landfill leachate and for their precious contribution in the discussion of results.

REFERENCES

- Alfarra, A., Frackowiak, E., and Béguin, F. (2004). The HSAB concept as a means to interpret the adsorption of metal ions onto activated carbons. *Appl. Surf. Sci.* 228, 84–92. doi: 10.1016/j.apsusc.2003.12.033
- Ali, I., Basheer, A. A., Mbianda, X. Y., Burakov, A., Galunin, E., Burakova, I., et al. (2019). Graphene based adsorbents for remediation of noxious pollutants from wastewater. *Environ. Int.* 127, 160–180. doi: 10.1016/j.envint.2019.03.029
- Al-Maqdi, K. A., Hisaindee, S., Rauf, M. A., and Ashraf, S. S. (2018). Detoxification and degradation of sulfamethoxazole by soybean peroxidase and UV + H₂O₂ remediation approaches. *Chem. Eng. J.* 352, 450–458. doi: 10.1016/j.cej.2018.07.036
- Balint, T., Chang, B. P., Mohanty, A. K., and Misra, M. (2020). Underutilized agricultural co-product as a sustainable biofiller for polyamide 6,6: effect of carbonization temperature. *Molecules* 25:1455. doi: 10.3390/molecules25061455
- Barth, A. (2007). Infrared spectroscopy of proteins. *Biochim. Biophys. Acta* 1767, 1073–1101. doi: 10.1016/j.bbaprot.2007.06.004
- Bekabil, U. T. (2015). Empirical review of production, productivity and marketability of soya bean in Ethiopia. *Int. J. U E Serv. Sci. Technol.* 8, 61–66. doi: 10.14257/ijunesst.2015.8.1.06
- Bilal, M., Rasheed, T., Iqbal, H. M. N., and Yan, Y. (2018). Peroxidases-assisted removal of environmentally-related hazardous pollutants with reference to the reaction mechanisms of industrial dyes. *Sci. Total Environ.* 644, 1–13. doi: 10.1016/j.scitotenv.2018.06.274
- Brunauer, S., Emmett, P. H., and Teller, E. (1938). Adsorption of gases in multimolecular layers. *J. Am. Chem. Soc.* 60, 309–319. doi: 10.1021/ja01269a023
- Calza, P., Zacchigna, D., and Laurenti, E. (2016). Degradation of orange dyes and carbamazepine by soybean peroxidase immobilized on silica monoliths and titanium dioxide. *Environ. Sci. Pollut. Res.* 23, 23742–23749. doi: 10.1007/s11356-016-7399-1

- Camiscia, P., Giordano, E. D. V., Brassesco, M. E., Fuciños, P., Pastrana, L., Cerqueira, M. F., et al. (2018). Comparison of soybean hull pre-treatments to obtain cellulose and chemical derivatives: physical chemistry characterization. *Carbohydr. Polym.* 198, 601–610. doi: 10.1016/j.carbpol.2018.06.125
- Cassales, A., de Souza-Cruz, P. B., Rech, R., and Záchia Ayub, M. A. (2011). Optimization of soybean hull acid hydrolysis and its characterization as a potential substrate for bioprocessing. *Biomass Bioenergy* 35, 4675–4683. doi: 10.1016/j.biombioe.2011.09.021
- Chandane, V., and Singh, V. K. (2016). Adsorption of safranin dye from aqueous solutions using a low-cost agro-waste material soybean hull. *Desalin. Water Treat.* 57, 4122–4134. doi: 10.1080/19443994.2014.991758
- Chen, G., Shah, K. J., Shi, L., and Chiang, P. C. (2017). Removal of Cd(II) and Pb(II) ions from aqueous solutions by synthetic mineral adsorbent: performance and mechanisms. *Appl. Surf. Sci.* 409, 296–305. doi: 10.1016/j.apsusc.2017.03.022
- Dai, Y., Sun, Q., Wang, W., Lu, L., Liu, M., Li, J., et al. (2018). Utilizations of agricultural waste as adsorbent for the removal of contaminants: a review. *Chemosphere* 211, 235–253. doi: 10.1016/j.chemosphere.2018.06.179
- Dall Cortivo, P. R., Hickert, L. R., Rosa, C. A., and Záchia Ayub, M. A. (2020). Conversion of fermentable sugars from hydrolysates of soybean and oat hulls into ethanol and xylitol by *Spathaspora hagerdaliae* UFMG-CM-Y303. *Ind. Crops Prod.* 146:112218. doi: 10.1016/j.indcrop.2020.112218
- De Gisi, S., Lofrano, G., Grassi, M., and Notarnicola, M. (2016). Characteristics and adsorption capacities of low-cost sorbents for wastewater treatment: a review. *Sustain. Mater. Technol.* 9, 10–40. doi: 10.1016/j.susmat.2016.06.002
- Donadelli, J. A., García Einschlag, F. S., Laurenti, E., Magnacca, G., and Carlos, L. (2018). Soybean peroxidase immobilized onto silica-coated superparamagnetic iron oxide nanoparticles: effect of silica layer on the enzymatic activity. *Colloids Surf. B Biointerfaces* 161, 654–661. doi: 10.1016/j.colsurfb.2017.11.043
- Fidale, L. C., Ruiz, N., Heinze, T., and El Seoud, O. A. (2008). Cellulose swelling by aprotic and protic solvents: what are the similarities and differences? *Macromol. Chem. Phys.* 209, 1240–1254. doi: 10.1002/macp.200800021
- Fieira, C., Batistella, E. P., Vincoski, J. V. A., Rosa, M. P. S., Pokrywiecki, J. C., Gomes, E. M. V., et al. (2019). Treatment of effluent containing thiamethoxam and efficiency evaluation of toxicity reduction. *Environ. Technol.* doi: 10.1080/09593330.2019.1703827. [Epub ahead of print].
- Girgis, B. S., Soliman, A. M., and Fathy, N. A. (2011). Development of micro-mesoporous carbons from several seed hulls under varying conditions of activation. *Microporous Mesoporous Mater.* 142, 518–525. doi: 10.1016/j.micromeso.2010.12.044
- Giri, G. F., Viarengo, G., Furlán, R. L. E., Suárez, A. G., Eleonora, G. V., and Spanevello, R. A. (2017). Soybean hulls, an alternative source of bioactive compounds: combining pyrolysis with bioguided fractionation. *Ind. Crops Prod.* 105, 113–123. doi: 10.1016/j.indcrop.2017.05.005
- Hailu, G., Weersink, A., and Cahlik, F. (2010). *Examining the Prospects for Commercialization of Soybean Peroxidase*. Available online at: <http://www.agbioforum.org/v13n3/v13n3a05-hailu.htm> (accessed July 2, 2020).
- Honorio, J. F., Veit, M. T., Da Cunha Gonçalves, G., De Campos, É. A., and Fagundes-Klen, M. R. (2016). Adsorption of reactive blue BF-5G dye by soybean hulls: kinetics, equilibrium and influencing factors. *Water Sci. Technol.* 73, 1166–1174. doi: 10.2166/wst.2015.589
- Honorio, J. F., Veit, M. T., and Tavares, C. R. G. (2019). Alternative adsorbents applied to the removal of natural hormones from pig farming effluents and characterization of the biofertilizer. *Environ. Sci. Pollut. Res.* 26, 28429–28435. doi: 10.1007/s11356-018-3558-x
- Inyinbor Adejumo, A., Adebisin Babatunde, O., Oluyori Abimbola, P., Adelani-Akande Tabitha, A., Dada Adewumi, O., and Oreofe Toyin, A. (2018). “Water pollution: effects, prevention, and climatic impact” in *Water Challenges of an Urbanizing World*, ed M. Glavan (InTech), 33–54. doi: 10.5772/intechopen.72018
- Islam, M., Mishra, P. C., and Patel, R. (2013). Microwave assisted synthesis of polycinnamamide Mg/Al mixed oxide nanocomposite and its application towards the removal of arsenate from aqueous medium. *Chem. Eng. J.* 230, 48–58. doi: 10.1016/j.cej.2013.06.037
- Khan, S., Yaoguo, W., Xiaoyan, Z., Youning, X., Jianghua, Z., and Sihai, H. (2014). Estimation of concentration of dissolved organic matter from sediment by using UV-visible spectrophotometer. *Int. J. Environ. Pollut. Rem.* 1, 24–29. doi: 10.11159/ijep.2014.003
- Krainer, F. W., and Glieder, A. (2015). An updated view on horseradish peroxidases: recombinant production and biotechnological applications. *Appl. Microbiol. Biotechnol.* 99, 1611–1625. doi: 10.1007/s00253-014-6346-7
- Li, J., Chen, E., Su, H., and Tan, T. (2011). Biosorption of Pb²⁺ with modified soybean hulls as adsorbent. *Chinese J. Chem. Eng.* 19, 334–339. doi: 10.1016/S1004-9541(11)60173-0
- Lopes, G. R., Pinto, D. C. G. A., and Silva, A. M. S. (2014). Horseradish peroxidase (HRP) as a tool in green chemistry. *RSC Adv.* 4, 37244–37265. doi: 10.1039/C4RA06094F
- Marshall, W. E., and Johns, M. M. (1996). Agricultural by-products as metal adsorbents: sorption properties and resistance to mechanical abrasion. *J. Chem. Technol. Biotechnol.* 66, 192–198. doi: 10.1002/(SICI)1097-4660(199606)66:2<192::AID-JCTB489andgt;3.0.CO;2-C
- Marshall, W. E., and Wartelle, L. H. (2006). Chromate (CrO₄²⁻) and copper (Cu²⁺) adsorption by dual-functional ion exchange resins made from agricultural by-products. *Water Res.* 40, 2541–2548. doi: 10.1016/j.watres.2006.04.030
- Marshall, W. E., Wartelle, L. H., Boler, D. E., Johns, M. M., and Toles, C. A. (1999). Enhanced metal adsorption by soybean hulls modified with citric acid. *Bioresour. Technol.* 69, 263–268. doi: 10.1016/S0960-8524(98)00185-0
- Middelbos, I. S., and Fahey, G. C. (2008). “Soybean carbohydrates,” in *Soybeans: Chemistry, Production, Processing, and Utilization*, eds L. A. Johnson, P. J. White, and R. Galloway (Urbana, IL: AOCS Press), 269–296. doi: 10.1016/B978-1-893997-64-6.50012-3
- Módenes, A. N., Hinterholz, C. L., Neves, C. V., Sanderson, K., Trigueros, D. E. G., Espinoza-Quifones, F. R., et al. (2019). A new alternative to use soybean hulls on the adsorptive removal of aqueous dyestuff. *Bioresour. Technol. Rep.* 6, 175–182. doi: 10.1016/j.biteb.2019.03.004
- Noya, A. I., Ghulamahdi, M., Sopandie, D., Sutandi, A., and Melati, M. (2014). Interactive effects of aluminum and iron on several soybean genotypes grown in nutrient solution. *Asian J. Plant Sci.* 13, 18–25. doi: 10.3923/ajps.2014.18.25
- Poore, M. H., Johns, J. T., and Burris, W. R. (2002). Soybean hulls, wheat middlings, and corn gluten feed as supplements for cattle on forage-based diets. *Vet. Clin. North Am. Food Anim. Pract.* 18, 213–231. doi: 10.1016/S0749-0720(02)00021-X
- Qin, L., Qiu, J., Liu, M., Ding, S., Shao, L., Lü, S., et al. (2011). Mechanical and thermal properties of poly(lactic acid) composites with rice straw fiber modified by poly(butyl acrylate). *Chem. Eng. J.* 166, 772–778. doi: 10.1016/j.cej.2010.11.039
- Rizzuti, A. M., Ellis, F. L., and Cosme, L. W. (2015). Biosorption of mercury from dilute aqueous solutions using soybean hulls and rice hulls. *Waste Biomass Valorization* 6, 561–568. doi: 10.1007/s12649-015-9391-2
- Rizzuti, A. M., and Lancaster, D. J. (2013). Utilizing soybean hulls and rice hulls to remove textile dyes from contaminated water. *Waste Biomass Valorization* 4, 647–653. doi: 10.1007/s12649-012-9167-x
- Robles Barros, P. J., Ramirez Ascheri, D. P., Siqueira Santos, M. L., Morais, C. C., Ramirez Ascheri, J. L., Signini, R., et al. (2020). Soybean hulls: optimization of the pulping and bleaching processes and carboxymethyl cellulose synthesis. *Int. J. Biol. Macromol.* 144, 208–218. doi: 10.1016/j.ijbiomac.2019.12.074
- Rojas, M. J., Siqueira, P. F., Miranda, L. C., Tardioli, P. W., and Giordano, R. L. C. (2014). Sequential proteolysis and cellulolytic hydrolysis of soybean hulls for oligopeptides and ethanol production. *Ind. Crops Prod.* 61, 202–210. doi: 10.1016/j.indcrop.2014.07.002
- Ryan, B. J., Carolan, N., and ÓFágáin, C. (2006). Horseradish and soybean peroxidases: comparable tools for alternative niches? *Trends Biotechnol.* 24, 355–363. doi: 10.1016/j.tibtech.2006.06.007
- Sadraei, R., Murphy, R. S., Laurenti, E., and Magnacca, G. (2019). Characterization methodology to evaluate the activity of supported soybean peroxidase. *Ind. Eng. Chem. Res.* 58, 19082–19089. doi: 10.1021/acs.iecr.9b03495
- Saruchi, and Kumar, V. (2019). Adsorption kinetics and isotherms for the removal of rhodamine B dye and Pb²⁺ ions from aqueous solutions by a hybrid ion-exchanger. *Arab. J. Chem.* 12, 316–329. doi: 10.1016/j.arabjc.2016.11.009
- Scapini, L. B., Rorig, A., Ferrarini, A., Fülber, L. M., Canavese, M., Silva, A. M., et al. (2018). Nutritional evaluation of soybean hulls with or without β -mannanase supplement on performance, intestinal morphometric and carcass yield of broilers chickens. *Braz. J. Poult. Sci.* 20, 633–642. doi: 10.1590/1806-9061-2017-0581

- Sheng-quan, Y., Si-yuan, G., Yi-gang, Y., Hui, W., and Han-Rui. (2012). Removal of the heavy metal ion Cr(VI) by soybean hulls in dyehouse wastewater treatment. *Desalin. Water Treat.* 42, 197–201. doi: 10.1080/19443994.2012.683144
- Shi, X., Wang, C., Zhang, J., Guo, L., Lin, J., Pan, D., et al. (2020). Zwitterionic glycine modified Fe/Mg-layered double hydroxides for highly selective and efficient removal of oxyanions from polluted water. *J. Mater. Sci. Technol.* 51, 8–15. doi: 10.1016/j.jmst.2019.12.034
- Singh, N. B., Nagpal, G., Agrawal, S., and Rachna. (2018). Water purification by using adsorbents: a review. *Environ. Technol. Innov.* 11, 187–240. doi: 10.1016/j.eti.2018.05.006
- Spehar, C. R. (1994). Seed quality of soya bean based on mineral composition of seeds of 45 varieties grown in a Brazilian savanna acid soil. *Euphytica* 76, 127–132. doi: 10.1007/BF00024030
- Steevensz, A., Cordova Villegas, L. G., Feng, W., Taylor, K. E., Bewtra, J. K., and Biswas, N. (2014). Soybean peroxidase for industrial wastewater treatment: a mini review. *J. Environ. Eng. Sci.* 9, 181–186. doi: 10.1680/jees.13.00013
- Sun, K., Wang, L., Wang, Z., Wu, X., Fan, G., Wang, Z., et al. (2020). Flexible silver nanowire/carbon fiber felt metacomposites with weakly negative permittivity behavior. *Phys. Chem. Chem. Phys.* 22, 5114–5122. doi: 10.1039/C9CP06196G
- Takeshita, V., Mendes, K. F., Pimpinato, R. F., and Tornisiello, V. L. (2020). Adsorption isotherms of diuron and hexazinone in drinking water using four agro-industrial residues. *Planta Daninha* 38:e020216260. doi: 10.1590/s0100-83582020380100013
- Thiha, A., Ibrahim, F., Muniandy, S., and Madou, M. J. (2019). Microplasma direct writing for site-selective surface functionalization of carbon microelectrodes. *Microsyst. Nanoeng.* 5, 1–12. doi: 10.1038/s41378-019-0103-0
- Tolardo, V., García-Ballesteros, S., Santos-Juanes, L., Vercher, R., Amat, A. M., Arques, A., et al. (2019). Pentachlorophenol removal from water by soybean peroxidase and iron(II) salts concerted action. *Water Air Soil Pollut.* 230:140. doi: 10.1007/s11270-019-4189-7
- Torres, J. A., Nogueira, F. G. E., Silva, M. C., Lopes, J. H., Tavares, T. S., Ramalho, T. C., et al. (2017). Novel eco-friendly biocatalyst: soybean peroxidase immobilized onto activated carbon obtained from agricultural waste. *RSC Adv.* 7, 16460–16466. doi: 10.1039/C7RA01309D
- Tummino, M. L., Magnacca, G., Cimino, D., Laurenti, E., and Nisticò, R. (2020). The innovation comes from the sea: chitosan and alginate hybrid gels and films as sustainable materials for wastewater remediation. *Int. J. Mol. Sci.* 21:550. doi: 10.3390/ijms21020550
- Tummino, M. L., Testa, M. L., Malandrino, M., Gamberini, R., Prevot, A. B., Magnacca, G., et al. (2019). Green waste-derived substances immobilized on SBA-15 silica: surface properties, adsorbing and photosensitizing activities towards organic and inorganic substrates. *Nanomaterials* 9:162. doi: 10.3390/nano9020162
- USDA (2019). *World Agricultural Production Report*. 33. Available online at: <https://apps.fas.usda.gov/psdonline/circulars/production.pdf> (accessed February 26, 2020).
- Wang, B., Wu, T., Angaiah, S., Murugadoss, V., Ryu, J.-E., Wujcik, E. K., et al. (2018). Development of nanocomposite adsorbents for heavy metal removal from wastewater. *ES Mater. Manuf.* 2, 35–44. doi: 10.30919/esmm5f175
- Wang, C., Makvandi, P., Zare, E. N., Tay, F. R., and Niu, L. (2020). Advances in antimicrobial organic and inorganic nanocompounds in biomedicine. *Adv. Therap.* 3:2000024. doi: 10.1002/adtp.202000024
- Wang, S., Shao, G., Yang, J., Liu, J., Wang, J., Zhao, H., et al. (2020). The production of gel beads of soybean hull polysaccharides loaded with soy isoflavone and their pH-dependent release. *Food Chem.* 313:126095. doi: 10.1016/j.foodchem.2019.126095
- Wartelle, L. H., and Marshall, W. E. (2000). Citric acid modified agricultural by-products as copper ion adsorbents. *Adv. Environ. Res.* 4, 1–7. doi: 10.1016/S1093-0191(00)00002-2
- Widiarto, S., Pramono, E., Suharto, Rochliadi, A., and Arcana, I. M. (2019). Cellulose nanofibers preparation from cassava peels via mechanical disruption. *Fibers* 7:44. doi: 10.3390/fib7050044
- Yang, H., Bever, C. S., Zhang, H., Mari, G. M., Li, H., Zhang, X., et al. (2019). Comparison of soybean peroxidase with horseradish peroxidase and alkaline phosphatase used in immunoassays. *Anal. Biochem.* 581:113336. doi: 10.1016/j.ab.2019.06.007
- Zhu, C., Dong, X., Chen, Z., and Naidu, R. (2016). Adsorption of aqueous Pb(II), Cu(II), Zn(II) ions by amorphous tin(VI) hydrogen phosphate: an excellent inorganic adsorbent. *Int. J. Environ. Sci. Technol.* 13, 1257–1268. doi: 10.1007/s13762-016-0964-9

Conflict of Interest: The authors declare that the research was conducted in the absence of any commercial or financial relationships that could be construed as a potential conflict of interest.

Copyright © 2020 Tummino, Tolardo, Malandrino, Sadraei, Magnacca and Laurenti. This is an open-access article distributed under the terms of the Creative Commons Attribution License (CC BY). The use, distribution or reproduction in other forums is permitted, provided the original author(s) and the copyright owner(s) are credited and that the original publication in this journal is cited, in accordance with accepted academic practice. No use, distribution or reproduction is permitted which does not comply with these terms.



Waste-Derived Nanoparticles: Synthesis Approaches, Environmental Applications, and Sustainability Considerations

Sabah M. Abdelbasir¹, Kelli M. McCourt², Cindy M. Lee^{2,3} and Diana C. Vanegas^{2,4*}

¹ Central Metallurgical Research and Development Institute, Cairo, Egypt, ² Department of Environmental Engineering and Earth Sciences, Clemson University, Clemson, SC, United States, ³ Department of Engineering and Science Education, Clemson University, Clemson, SC, United States, ⁴ Interdisciplinary Group for Biotechnological Innovation and Ecosocial Change-BioNovo, Universidad del Valle, Cali, Colombia

OPEN ACCESS

Edited by:

Francesca Deganello,
Italian National Research Council, Italy

Reviewed by:

Sergio Gonzalez-Cortes,
University of Oxford, United Kingdom
Il Je Yu,
Independent Researcher, Icheon,
South Korea

*Correspondence:

Diana C. Vanegas
dvanega@clemson.edu

Specialty section:

This article was submitted to
Green and Sustainable Chemistry,
a section of the journal
Frontiers in Chemistry

Received: 11 May 2020

Accepted: 27 July 2020

Published: 31 August 2020

Citation:

Abdelbasir SM, McCourt KM, Lee CM
and Vanegas DC (2020)
Waste-Derived Nanoparticles:
Synthesis Approaches, Environmental
Applications, and Sustainability
Considerations. *Front. Chem.* 8:782.
doi: 10.3389/fchem.2020.00782

For the past few decades, a plethora of nanoparticles have been produced through various methods and utilized to advance technologies for environmental applications, including water treatment, detection of persistent pollutants, and soil/water remediation, amongst many others. The field of materials science and engineering is increasingly interested in increasing the sustainability of the processes involved in the production of nanoparticles, which motivates the exploration of alternative inputs for nanoparticle production as well as the implementation of green synthesis techniques. Herein, we start by overviewing the general aspects of nanoparticle synthesis from industrial, electric/electronic, and plastic waste. We expand on critical aspects of waste identification as a viable input for the treatment and recovery of metal- and carbon-based nanoparticles. We follow-up by discussing different governing mechanisms involved in the production of nanoparticles, and point to potential inferences throughout the synthesis processes. Next, we provide some examples of waste-derived nanoparticles utilized in a proof-of-concept demonstration of technologies for applications in water quality and safety. We conclude by discussing current challenges from the toxicological and life-cycle perspectives that must be taken into consideration before scale-up manufacturing and implementation of waste-derived nanoparticles.

Keywords: carbon nanoparticles, metal nanoparticles, e-waste, plastic waste, industrial waste, nanoparticle-enabled technologies

INTRODUCTION

According to the Environment Program of the United Nations, nearly 11.2 billion tons of solid waste is generated every year, which is a significant source of environmental degradation and negative health impacts, particularly in low-income countries, where more than 90% of waste is openly dumped or burned (UNEP, 2020). In Southeast Asian countries with insufficient waste management capacity, such as Vietnam, Malaysia, the Philippines, and Thailand, waste-related issues are further exacerbated by the massive amounts of plastic, electric, and electronic waste imported from industrialized countries (Kaza et al., 2018; Dell, 2019; Sukanan, 2020). This situation has motivated the development, implementation, and strengthening of different policy strategies

including (i) international environmental agreements such as the Basel Convention on the control of transboundary movements of hazardous wastes and their disposal (Basel Action Network, 2019), (ii) source reduction, or complete bans on single-use plastics (UNEP, 2018), and (iii) shifts in political agendas toward the adoption of circular economy models for meeting environmental and resource-oriented goals in several countries (Bourguignon, 2014; Berg et al., 2018). However, there are significant technical, economic, environmental, and social challenges for realizing closed-loop management of engineered materials on a large scale. For example, many plastic and metal recycling processes involve the use of hazardous substances for extraction and purification, which results in new health risks for humans and the environment (Kral et al., 2019). Besides, the practical viability of strategies for recycling and repurposing materials is directly linked to the economic value of the end-products. Therefore, using “clean manufacturing” processes to yield “value-added” commodities from waste materials emerges as a desirable synergy for achieving both circularity and sustainability goals (Ferronato and Torretta, 2019).

Over the past few years, a plethora of engineered nanomaterials have demonstrated great promise for advanced applications ranging from energy transformation and storage (Hussein, 2015; Verma et al., 2016; Sonawane et al., 2017; Yang et al., 2019), pollution monitoring (Baruah and Dutta, 2009), intelligent packaging (Pereira de Abreu et al., 2012), precision agriculture and controlled delivery of food ingredients (Bindraban et al., 2015; Peters et al., 2016), membrane technology (Goh et al., 2015); water treatment (Westerhoff et al., 2013); drug delivery and diagnostics (Turcheniuk and Mochalin, 2017), bone and tissue engineering (Shadjou and Hasanzadeh, 2016), amongst others. In an effort to reduce negative environmental impacts and health risks associated with the production, use, and disposal of novel nanomaterials, the fields of materials engineering and nanotechnology are increasingly concerned with sustainability approaches, frameworks, and metrics (Dhingra et al., 2010; Mata et al., 2015; Falinski et al., 2018). For example, a Boolean search of the keywords “green synthesis” AND “nanomaterials” on the academic engine *Web of Science* (Clarivate™) returns a record count of 569 articles published on 2019 alone, which is 3-fold higher number than the year 2015, and 12-fold higher than the year 2009. This growing trend is expected to continue over the next few years, consistent with global trends on sustainable development.

Herein, we provide an overview of the current status, challenges, and future directions for the utilization of industrial wastes (e.g., large batteries, rubber tires, wastewater), e-waste (e.g., copper cables, printed circuit boards, electronic equipment), and plastic wastes (e.g., polyethylene, polypropylene, polyvinyl alcohol) as suitable inputs for production of nanoparticles (NPs) as added-value products. In addition, we review some proof-of-concept examples for the incorporation of waste-derived NPs in advanced technologies for pollution monitoring, treatment, and remediation of water (Figure 1). We conclude with some remarks from the sustainability viewpoint, that emphasize the critical aspects necessary for scale-up manufacturing and deployment of waste-derived nanomaterials.

WASTE AS STARTING MATERIALS FOR THE PRODUCTION OF NANOPARTICLES

Depending on the source of emission, highly problematic waste materials produced in massive amounts can be classified into wastes generated by industries, and wastes generated by consumers. Both industrial and consumer wastes can be utilized as inputs for processes that yield value-added products. From the industrial sector, large batteries, rubber tires, wastewater, and biosolids are prominent sources of carbon, lead, zinc, copper, and palladium. End-of-life consumer products result in overwhelming amounts of e-waste and plastic waste. E-waste can be a significant source of recoverable precious and semi-precious metals. Depending on the type of polymer and the degree of purity, plastic waste can be either recycled and reused as packaging material or, it can be used as raw material for other applications, including the production of construction materials, paper, fiber composites, new polymers, and carbon nanoparticles. In this section, we examine the recent research on the mechanisms and processes used for the recovery of valuable components from the different waste streams.

Industrial Waste

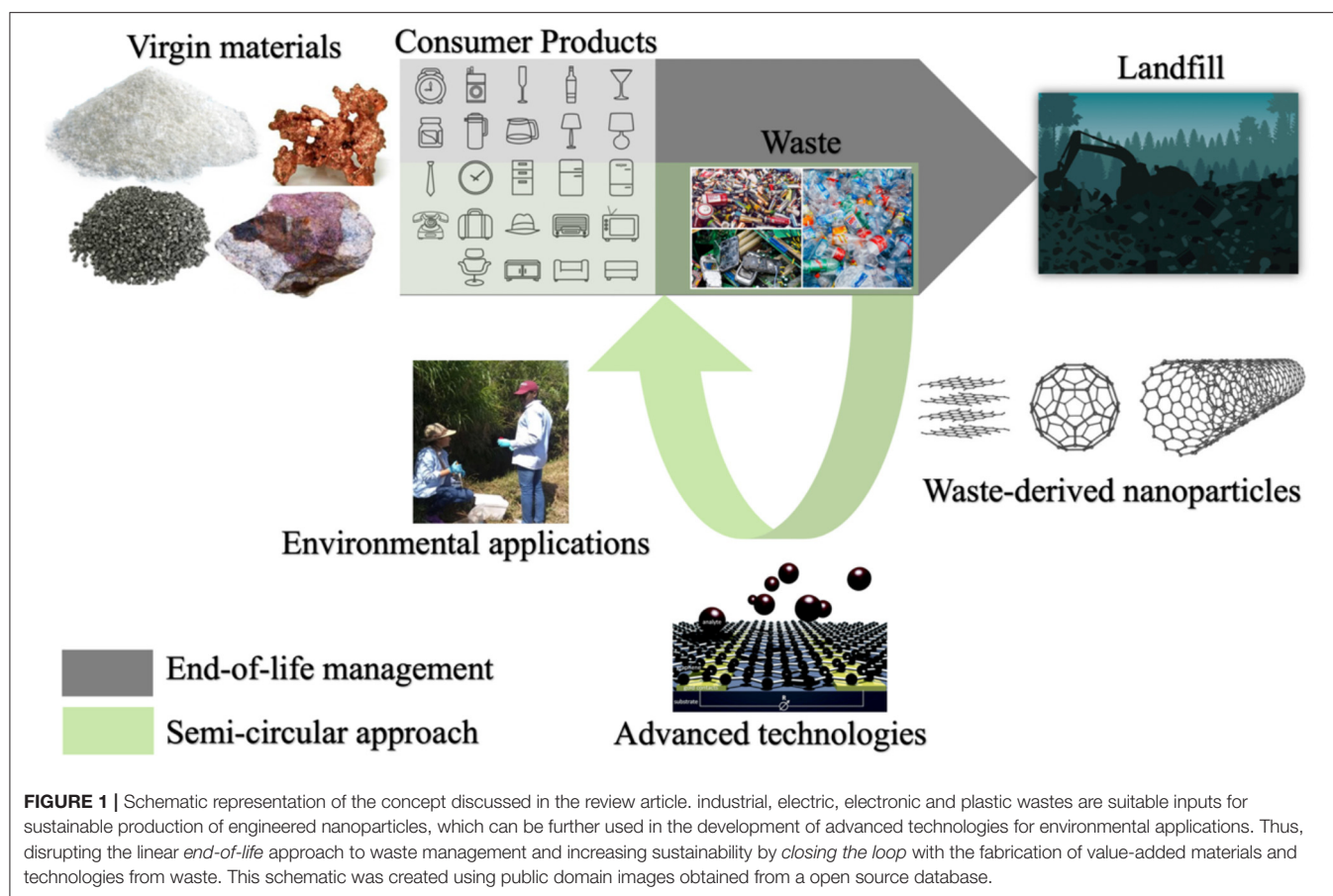
Up to this point in time, several industrial wastes such as batteries, tires, wastewater, and sludges have been studied as potential low-cost and ubiquitous starting materials for nanoparticles synthesis (Samaddar et al., 2018).

Lead Batteries

Over 50 million units of waste lead batteries are produced annually by China alone; considering the toxicological effects of lead exposure, along with its bioaccumulation capacity, recycling these batteries is a responsible approach while avoiding ecological and public health problems (Zhou et al., 2017). Lead pastes are made of metal oxide, dioxide, and sulfate forms that are difficult to recover and reuse because of their insolubility. However, pyrometallurgical processes can be employed to retrieve lead from spent lead-acid battery paste. For example, Zhou et al. (2017) designed a synthesis technique to make Pb nanopowder from simulated spent lead paste by the pyrolytic route. The authors produced submicron particles of lead oxide by a thermal process coadjuted by poly (N-vinyl-2-pyrrolidone), which helps decrease the particle size (Zhou et al., 2017). While the technique overcomes difficulties associated with the insolubility of lead paste in aqueous media, pyrometallurgical processes may have unfavorable consequences due to the high energy requirements as well as the undesirable emissions of air pollutants such as sulfur dioxide and lead dust.

Zinc-Manganese Batteries

Similarly, a large percent of transportable batteries in industrialized countries are made of zinc-manganese (Zn-Mn) composites. China alone produces more than 15 billion units every year (Xiang et al., 2015). Exposure to toxic concentrations of Zn can result in impaired calcium uptake and metabolic deficiencies in humans and other organisms (Valko et al., 2005). Thus, recovering Zn from recycled Zn-Mn batteries is a



convenient approach for enabling reuse of the metal in other applications while limiting its uncontrolled dissemination in the environment. Synthesis of Zn nanomaterials such as NPs, nanofibers, and flaky NPs using recycled Zn-Mn batteries as starting material, has been actively investigated in recent years. Xiang et al. (2015) demonstrated a facile and highly efficient method for separating zinc from spent batteries. Samples of recycled zinc-cathodes were put in a corundum crucible and subjected to a vacuum pressure of 1 Pa, heating temperature of 800°C, and condensing temperature 200°C. The simple technique can attain zinc separation efficiency up to 99.68%. By following the separation process with a nitrogen gas flow into the heating chamber, structured nanoparticles can be obtained with different morphologies including hexagonal prisms, fibers, and sheets (Xiang et al., 2015).

Rubber Tires

Worldwide, roughly 1,000 million scrap tires are generated every year (GoldsteinResearch, 2020). A significant portion is landfilled or openly burned, contributing to air pollution and environmental degradation (Moghaddasi et al., 2013). For that reason, the disposal of scrap rubber in landfills is banned in most developed countries (Turgut and Yesilata, 2008). Thus, there is interest in finding sustainable solutions for managing rubber tire waste. Generally, tires are composed of 45–47%

natural rubber, 21–22% carbon black, 12–25% metals, 5–10% textile, 6–7% additives and 1–2% zinc, ~1% sulfur (Evans and Evans, 2006; Samaddar et al., 2018). The synthesis of Zn NPs from used tires constitutes a suitable alternative with value-added potential. Moghaddasi et al. (2013) obtained NPs from recycled tires by applying ball milling for five consecutive hours. The method yielded rubber ash particles smaller than 500 nm; when aided with silicon waste, the particle size was further reduced to <50 nm. The effectiveness of rubber ash and ground tire rubber particles as a zinc source for plant nutrition was comparable to a commercial ZnSO₄ fertilizer (Moghaddasi et al., 2013).

As waste tires are composed, principally, of carbon (representing about 81.2 wt%) they are considered a promising source of carbon for various potential applications. Maroufi et al. (2017) synthesized high-value carbon nanoparticles (CNPs) from waste tire rubber (WTR), using a high-temperature approach. The transformation of WTRs was carried out at 1,550°C over various reaction times (5 s to 20 min). The total energy utilization for the process was acceptable as the decomposition of WTR and the formation of CNPs occurs quickly, and completely. Within 5 min, all the impurities, such as sulfur, zinc, and oxygen, have been removed (Maroufi et al., 2017). Another facile and low-cost method for the preparation of carbon black nanoparticles from waste tires was reported by Gómez-Hernández et al. (2019). Briefly, thermal transformation under the high temperature

(1,000°C) and self-pressurized conditions produced carbon nanoparticles (~22 nm) with high yield (about 81%) under the optimized conditions. The chain-like agglomerated nanoparticles showed good thermal stability and conductivity and the chemical analysis indicated that it was partly oxidized (C, 84.9%; O, 4.9%; S, 10.21%) (Gómez-Hernández et al., 2019). Many studies have been reported advising to choose an unconventional hydrocarbon waste as low-cost starting materials such as tires and plastics for the synthesis of CNTs (Sathiskumar and Karthikeyan, 2019). Multiwalled carbon nanotubes were synthesized from low boiling point hydrocarbon tire pyrolysis oil derived from waste tire material mixed with ferrocene as the catalyst on a quartz substrate with a flow rate of 20 ml/min at 950°C (Parasuram et al., 2018).

Wastewater and Bio-sludge

Wastewater effluents and industrial sludges have been identified as rich sources of valuable metals and metal oxides; therefore, these waste effluents have been extensively studied for the recovery of materials such as PbO, Mo, Ni, Co, Cu, Ag, SiO₂, rare earth elements, and Pt. While the concentration of trace elements is highly variable among waste effluents, there are associations with the specific activities performed in the emitting source, as well as the mineralogical diversity found within a single effluent source. For example, the U.S. Geological Survey has identified waste effluents from Zn ore mining as major sources of Ga and In. Through wastewater and biosolid mining, Ga and In could be recovered and used for the fabrication of integrated circuits, light-emitting diodes, photodetectors, semiconductors, and solar cells (Smith et al., 2015). An elemental analysis of waste stream samples (e.g., mining influenced waters) from different historical metal mining sites found concentrations of Ag (Mdn. ~10 ppm), Au (Mdn. ~0.3 ppm), Pd (Mdn. ~30 ppm), Pt (Mdn. ~1 ppm), Re (Mdn. ~0.01 ppm), Os (Mdn. ~0.02 ppm), Ir (Mdn. ~0.001 ppm), La (Mdn. ~20 ppm), Ce (Mdn. ~40 ppm), Nd (Mdn. ~20 ppm), Sm (Mdn. ~4 ppm), Gd (Mdn. ~4 ppm), Yb (Mdn. ~2 ppm), Th (Mdn. ~4 ppm), Zn (Mdn. ~1,000 ppm), Cu (Mdn. ~150 ppm), Ga (Mdn. ~15 ppm), In (Mdn. ~1 ppm), Sb (Mdn. ~10 ppm), and Te (Mdn. ~1.5 ppm). Although the recovery of some of these metals may not be economically attractive by itself, the removal and recovery of trace elements from waste streams may still offset treatment and disposal costs and reduce environmental and public health liability (Smith et al., 2015).

Urbina et al. (2019) demonstrated an innovative approach for metal recovery from aqueous waste such as those found in bioremediation or biomining processes. The method uses metal-binding peptides to functionalize fungal mycelia. *In silico* models have been developed for predicting binding affinity between metals and natural ligand-binding motifs. These models are useful because they enable the prediction of binding parameters based on open access protein databases (e.g., The Protein Data Bank <https://www.rcsb.org>) to describe the geometric features a cognate metal in a metalloprotein. As a proof-of-concept, the authors achieved binding affinity and specificity for Cu that show a high correlation between the natural motifs and those derived *in silico* (Urbina et al., 2019). Another study identified different morphologies of silica nano-fillers (100–500 nm) present in

polymer waste (Tran et al., 2017). Various metals have also been recovered from pickling wastes, spent catalysts, furnace slag, fly ash, e-waste, and metalized plastic waste (Khaloo et al., 2013; Bennett et al., 2016; Chaukura et al., 2016; Chen et al., 2016; El-Nasr et al., 2020; Elsayed et al., 2020). Aside from being a good source for the recovery of metals, various industrial effluents and bio-wastes have been used for the synthesis of carbon-based nanomaterials (Deng et al., 2016; Zhang et al., 2016). Deng et al. provided a comprehensive review highlighting the current status and prospects of green synthesis of carbon nanocomposites from bio-sludges and industrial wastes through microbiologically driven pathways (Deng et al., 2016).

Electric and Electronic Wastes

The overwhelming generation of end-of-life electric and electronic products and equipment (e-waste or WEEE) in the United States and Europe is causing severe environmental and public health issues in the e-waste receiving nations, which are primarily located in West Africa and Asia (Baldé et al., 2017; Tansel, 2017). For the past decades, there has been a steady increase in the development of efficient recycling techniques for e-waste led by the US and China, especially with regards to the recovery of metallic components (Bhat et al., 2012; Wibowo et al., 2014; Barletta et al., 2015; Park et al., 2017; Zeng et al., 2017). However, e-waste recycling is increasingly challenging because electronic devices are made of complex mixtures of various metals, plastics, glass, and even newly engineered nanomaterials (Abdelbasir et al., 2018b,c). Moreover, electronic components are continually being miniaturized, which diminishes the efficiency of conventional mechanical separation processes available in developing countries (Baldé et al., 2017). Despite the practical difficulties, the high economic value of precious metals, such as gold, silver, and palladium, continues to drive e-waste mining.

As shown in **Table 1**, Printed circuit boards and mobile phones contain the highest amounts of precious metals and a considerable portion of base metals. Printed circuit boards (PCBs) are an integral component of all electronics. On average, PCBs represent 3% of the total mass of waste electric and electronic equipment, but in the case of small appliances, it can account for almost 8% of the weight (Dalrymple et al., 2007; Luda, 2011; Abdelbasir et al., 2018c). In 2014 the value of metals in e-waste was roughly estimated at 52 billion U.S. dollars (Xu et al., 2016). The estimated overall composition of PCBs is 40% metals, 30% organics, and 30% persistent noxious materials (Abdelbasir et al., 2018b). Detailed elemental analysis of polymers present in PCB has revealed the following composition: 5.52 wt% C, 2.18 wt% H, 0.73 wt% N, and 7.86 wt% Br (Blazsó et al., 2002). Copper represents the highest amount of metals in PCBs, and it has the second-highest pecuniary value. The organics are generally made of a variety of polymers such as polyvinyl chloride (PVC), polycarbonate (PC), acrylonitrile butadiene styrene (ABS), polytetrafluoroethylene (PTFE), polyethylene (PE), and polypropylene (PP) (Stevens and Goosey, 2009). The toxicity of the materials found in PCBs is a recurrent concern in the characterization and treatment of waste PCBs. The lead-tin soldering material and the brominated flame retardants (BFRs) contained in PCBs are the most harmful

TABLE 1 | Composition of metals in various e-waste scraps.

Type of e-waste	Weight (%)					Weight* (ppm)		
	Cu	Fe	Al	Ni	Pb	Ag	Au	Pd
Printed circuit board	20	6	4	1	2.5	1,000	250	90
Mobile phone	13	5	1	0.1	0.3	1,380	350	210
TV board	10	28	10	0.3	1.0	280	20	10
Portable audio	21	23	1.0	0.03	0.14	150	10	4
DVD player	5	62	2	0.05	0.3	115	15	4
Calculator	3	4	5	0.5	0.1	260	50	5

This table was partially reproduced from Hsu et al. (2019) with republication license provided by the Royal Society of Chemistry (license ID: 1034053-1) (Hsu et al., 2019). *Minor components (<0.03 wt.%).

constituents. Additionally, copper catalyzes the formation of dioxins when the flame retardants are incinerated.

Conventional industrial waste management processes involve transport of e-waste over long distances, to only recover a small fraction of materials; primarily precious metals such as Au and Ag, and semi-precious metals, like Cu, Ni, Al, Zn, Pb, and Sn, leaving significant amounts of residual waste and toxic components (Mankhand et al., 2012). Generally, industrial recycling approaches start with energy-intensive mechanical operations such as bulk crushing, grinding, and separation based on density or magnetic properties (Long et al., 2010); chemical treatments are later applied for extraction and purification of copper and other precious metals (Quan et al., 2010; Mankhand et al., 2012).

Overall, the metal content in e-waste is much higher than in land-mined ores (Li et al., 2007; Duan et al., 2009; Zhao et al., 2012). For example, e-waste has a weight composition of 10–20% Cu, whereas the maximum concentration of Cu in virgin ore is 3%. Thus, recovering metallic elements from e-waste, rather than mining for ores in natural deposits, would significantly cut the environmental impacts associated with both the mining of metals and the accumulation of e-waste. Enormous energy savings have been estimated from the recovery of metals from e-waste in contrast with the conventional extraction from mined ores. Specific examples of comparative cost-benefits are 95% for Al, 85% for Cu, 75% for Zn, and 90% for Ni (Cui and Forssberg, 2003; Shokri et al., 2017). Conventional approaches for recovering metals from e-waste begin with the conversion of the metallic components found in e-waste to oxide or sulfite forms, followed by the iterative raising of the pure form of the elements. Recently, efficient processes such as pyro- and hydro- metallurgy of e-waste captured significant attention. In pyrometallurgy, crushed e-waste is placed into a molten bath where the plastic degrades while releasing energy, and the refractories are ejected as slag. This slag is subsequently processed for the extraction of base or precious metals (Cayumil et al., 2014). Alternatively, hydrometallurgy processing is more predictable and controllable, but also very costly since it requires recovery and treatment of spent liquids and preparation of fresh solutions. Furthermore, the presence of chlorides in hydrometallurgically-treated e-waste is likely detrimental to the environment (Mankhand et al., 2012).

While the high yields of precious and semiprecious metals from WEEE provide the economic incentive for recycling it, there is still a need for more efficient and sustainable approaches to WEEE management that use a more substantial fraction of the waste materials (not just the metal parts) and results in the generation of value-added products (Abdelbasir et al., 2018c).

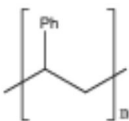
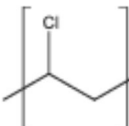
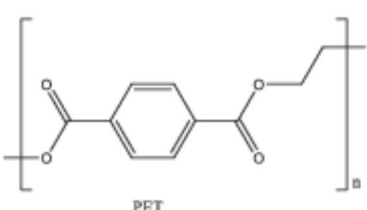
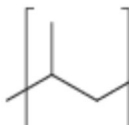
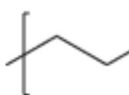
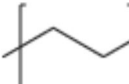
Plastic Wastes

The broad utilization of non-biodegradable plastics has arguably brought about the most significant and problematic class of waste materials in the world. Plastic polymers have been intensely used for about a century to fabricate an immense number of products. In fact, the production of synthetic plastics has increased vastly during the last decades (Gu and Ozbakkaloglu, 2016). Traditional plastics were designed to be durable and withstand variations in external environmental conditions, which is precisely the reason why they persist and accumulate in the environment (Pol and Thiyagarajan, 2010). On a global scale, plastics are now the major component in solid waste (Ritchie and Roser, 2020). The generation of plastic wastes (PW) accounts for over 150 million metric tons per year (Aboulkas et al., 2010).

Plastic debris and microplastics have been found in alarming concentrations in the ocean. These particles produce negative impacts not only on aquatic life and birds but also on humans via contamination of the trophic chain (Bouwmeester et al., 2015). Aside from the problems associated with their slow degradation, PWs are harmful because they contain pigments with several highly noxious trace elements that can migrate out of the polymeric matrix and into the environment (Gondal and Siddiqui, 2007). As a result, environmental pollution from synthetic PWs is now considered one of the most devastating and likely irreversible effects of contemporary anthropogenic activities (Zheng et al., 2005).

In many countries, separation at source (i.e., segregation of materials at the point of disposal) and recycling are main collective efforts initiated at the household level, which are aimed at reducing the need for producing new plastics from virgin materials and fossil fuels. Main synthetic polymers in household items include polystyrene (PS), polypropylene (PP), polyethylene terephthalate (PET), high-density polyethylene (HDPE), low-density polyethylene (LDPE), linear low-density polyethylene (LLDPE), polyvinyl chloride (PVC) and nylon. **Table 2** depicts

TABLE 2 | Properties and structure of polymers commonly found in plastic waste.

Plastic	Molecular weight (g/mol)	Density, (g cm ⁻³)	Chemical formula	Structure	Crystallinity
Polystyrene (PS)	104.1 (of repeat unit)	1.04–1.11	(C ₈ H ₈) _n		Highly amorphous (atactic), Highly crystalline (syndiotactic)
Polyvinylchloride (PVC)	62.50 (of repeat unit)	1.10–1.45	(C ₂ H ₃ Cl) _n		Highly amorphous
polyethylene terephthalate (PET)	192.17 (of repeat unit)	1.38–1.40	(C ₁₀ H ₈ O ₄) _n		Semi crystalline
Polypropylene (PP)	42.08 (of repeat unit)	0.855, amorphous 0.946, crystalline	(C ₃ H ₆) _n		Highly crystalline (isotactic), Highly amorphous (atactic)
High-density polyethylene (HDPE)	10 ³ –10 ⁷	0.93–0.97	(C ₂ H ₄) _n		High crystalline and low amorphous
Low-density polyethylene (LDPE)	8.9 × 10 ⁴ to 4.7 × 10 ⁵	0.910–0.940	(C ₂ H ₄) _n		Low crystalline and high amorphous

the properties of common plastic polymers. Considering the vast amount of solid waste generated worldwide, stakeholders are looking for avenues to use PWs as starting material for energy recovery or valued-added products manufacturing (Ackerman, 2000). From the thermodynamic perspective, energy recovery is less favorable as the energy content of plastic (42.6 MJ/l) is at least an order of magnitude lower than conventional fuels such as heating oil (443.5 MJ/kg) (Kumar et al., 2011; Banu et al., 2020). Additionally, using PW as an energy source can be seriously detrimental for public health since harmful dioxins are released during PW burning. Finally, the concept of using PWs as an alternative feedstock to generate syn-gas or oil for the later conversion into liquid fuels such as diesel and gasoline may incentivize the unnecessary perpetuation of dependence on carbon fuels, which ultimately leads to the release of greenhouse gases into the atmosphere, and all its encompassing effects on the planet.

On the other hand, turning PW into useful products is particularly challenging because of the chemical heterogeneity in the different waste streams. For instance, many packaging materials are made of compact composites of several thin layers of different polymers and often are lined with aluminum. These

composite plastics have to be landfilled because they are difficult to separate by conventional mechanical and/or chemical recovery processes (Al-Salem et al., 2009; Astrup et al., 2009; Singh et al., 2017). Recent approaches for valorizing mixed PWs include mixing them with materials such as wood, cement, and ash to turn them into construction materials (Sardot et al., 2012; Sofi et al., 2019), printable paper-like composites (Fan et al., 2020), fiber composites (Keskisaari and Kärki, 2017), new polymers (Rahimi and Garcíá, 2017), and polar waxes (Marek et al., 2015). Nanomaterials have also been prepared from single-polymer PW. For example, ultrafine nano-channeled carbon tubes and multi-walled carbon nanotubes (MWCNTs) have been synthesized from polyethylene terephthalate waste using an arc discharge method (Berkmans et al., 2014). **Table 3** summarizes the advantages and challenges of some of the potential value-added applications of PWs.

In summary, the depicted mechanisms show promising potential for reducing the amount of landfilled materials and noxious elements dispersed in the environment. It is worth noting that the majority of the reviewed processes are still in the early stages of research and development, thus the economics of scale have not yet been fully determined.

TABLE 3 | Potential value-added applications for recycled plastics.

Recycled plastics	Value-added applications	Expected advantages	Foreseen challenges	References
PET, PP, PS, LDPE, HDPE, PVC	Production of liquid fuels.	Reduced need for oil extraction from natural reserves.	High cost associated with complex thermochemical processes. Generation of hazardous byproducts.	Kumar et al., 2011; Banu et al., 2020
PP, LDPE, PS	Production of construction materials.	Possibility of utilizing mixed plastics.	Requires ultrafine grinding and thorough mixing to reduce variability in thermal and mechanical properties.	Sardot et al., 2012; Sofi et al., 2019
LLDPE	Production of printable paper.	High affinity with ink, hydrophobicity, and durability under harsh conditions.	Involves the use of hazardous organic solvents.	Fan et al., 2020
PVC, PET, PP	Production of fibers.	Reduced plastic waste volumes disposed to landfills.	Impurities and contamination potentially present in the recycled materials produce significant variations in the properties of the fibers.	Keskisaari and Kärki, 2017
LDPE, PET, HDPE, PVC, PS	Production of new polymers.	Reduced dependence on petrochemicals for plastic production. Catalytic methods for chemical recycling of polymers are less energy intensive than thermolysis methods.	Isolation and purification of monomers from chemically treated recycled polymers can be expensive. The mechanical properties of the newly synthesized polymers may not meet the conventional requirements.	Rahimi and García, 2017
PP	Production of polar waxes	Facile 2-step process. Requires low-toxic solvents that can be recirculated into the process. The rheological properties of the obtained waxes are similar to the commercial ones.	Overtime, wax deposition may affect the equipment required for the process.	Marek et al., 2015
PP, PET	Production of carbon nanoparticles	Attractive for applications in a plethora of advance technologies.	Toxicity concerns; particularly in occupational settings where the nanoparticles are manufactured and handled in large quantities.	Bazargan and McKay, 2012; Berkman et al., 2014; Zhuo and Levendis, 2014; Deng et al., 2016

Nonetheless, the proposed processes serve as a proof-of-concept demonstration of ways to divert from the business-as-usual approach to waste management. Perhaps, offsetting treatment and disposal costs, and reducing environmental and public health liabilities may be sufficient incentives to promote these alternative approaches.

SYNTHESIS OF NANOPARTICLES FROM RECYCLED MATERIALS

Metal and Metal Oxide Nanoparticles

Various procedures have been used for the synthesis of several types of nanomaterials from wastes after suitable pretreatment either physically or chemically or combinations of both. The most common physical pretreatment methods are grinding and milling. Chemical pretreatment is applied to separate any contaminants present in the waste sample by heating or treating with reagents such as strong acids (e.g., H₂SO₄, HNO₃, HCl) (Samaddar et al., 2018).

The most popular synthesis method for metallic NPs is reduction with sodium borohydride. Generally, the sodium borohydride solution is freshly prepared and rapidly added to the solution of waste materials. NPs produced via reaction are washed repetitively with ultrapure water and absolute alcohol for the removal of excess sodium borohydride. This method was

implemented by Fang et al. to prepare Fe NPs from steel pickling waste materials released from a steel plant (Fang et al., 2011).

Another important and widely used method is the solvent thermal method which involves chemical reactions in solvents contained in closed autoclave reactor and heated to a critical temperature (Dubin et al., 2010). When water is used as a solvent the process is known as “hydrothermal.” As an example, hematite NPs (α -Fe₂O₃) were synthesized via a solvent thermal method using ethanol as a solvent and heating the solution of the starting materials mixture (FeCl₃, and NaOH) at 150°C for 2 h to gain NPs (Tang et al., 2011). Another technique that uses voltage to promote chemical reactions in aqueous solutions for the synthesis of nanoparticles is electrodeposition. This method has been applied to produce nanowires, nanoporous materials, and nanocylinders. In addition to these mentioned techniques, green synthesis methods based on the use of environmentally friendly and biocompatible materials such as plants and microorganisms have recently arisen (Jeevanandam et al., 2016).

Metal nanoparticles (e.g., Pb, Hg, Cu, Fe, Au, Ag, Pd, Pt, and Rh) and polymers can be recovered from electronic wastes such as computer circuit boards, cellular phones, laptops, automobiles, and supercapacitors (Xiu and Zhang, 2012; Singh and Lee, 2016; Vermisoglou et al., 2016). To date, most efforts have focused on the recovery of metal nanoparticles from spent batteries. However, other forms of e-waste are also good

sources of a variety of valuable materials. For example, Cu nanoparticles were prepared from acidic CuCl_2 waste etchants generated in the manufacturing process for printed circuit boards by microemulsion processes (Mdlovu et al., 2018). Likewise, aqueous solutions of CuSO_4 from PCBs were chemically reduced to create organically stabilized Cu nanoparticles (Tatariants et al., 2018). Waste printed circuit boards (WPCBs) have also been recycled to obtain metals such as Cu, Pb, Fe, Au, and Hg (Calgaro et al., 2015; Chen et al., 2015a,b; Chu et al., 2015; Fogarasi et al., 2015; Hadi et al., 2015; Cui and Anderson, 2016). The metals recovered from WPCBs can be used to create nanoparticles. Cu from WPCBs has acted as a starting material in the synthesis of Cu nanoparticles (Yousef et al., 2018; El-Nasr et al., 2020). **Figure 2** portrays the morphological features of Cu nanoparticles obtained from WPCBs using the approach by El-Nasr et al. (2020).

WPCBs can also be used to create nanoparticles directly. $\text{Cu}_2\text{O}/\text{TiO}_2$ photocatalysts were recovered using electrokinetic processes (Xiu and Zhang, 2009). Cu_2O nanoparticles of different sizes were also created from WPCBs using supercritical water oxidation methods (SCWO) and electrokinetic processes (Xiu and Zhang, 2012). Copper–tin (Cu–Sn) nanoparticles were fabricated from the WPCBs of spent computers using selective thermal transformation while also separating toxic lead (Pb) and antimony (Sb) (Shokri et al., 2017). Lead (Pb) nanoparticles were synthesized from solders of WPCBs via evaporation under vacuum with forced flow inert gas condensation (Zhan et al., 2016). Various other forms of e-waste can be used to create nanoparticles such as purified carbon nanotubes, Cu_2O nanoparticles, and $\text{Cu}_2\text{O}/\text{TiO}_2$ catalysts. For example, Ag was completely recovered from incinerated organic solar cells (Søndergaard et al., 2016).

Wastes other than e-wastes can also be utilized. Ag, Cu, and bimetallic Ag/Cu nanoparticles were synthesized from a leachate solution (**Figure 3**). This solution was derived from a solution of leached metalized acrylonitrile butadiene styrene (ABS) from plastic wastes combined with nitric acid and ascorbic acid in the presence of chitosan at 60°C (Elsayed et al., 2020).

Researchers also utilize methods to reuse nanoparticles. For example, functionalized nanoparticles were successfully recycled to capture toxins from spiked blood plasma samples by applying a glycine buffer to free up the nanoparticles after their initial use (Hassanain et al., 2017). In another study, zinc oxide (ZnO) nanoparticles were synthesized from spent Zn–C battery via thermal technique at 900°C under an argon atmosphere using a horizontal quartz tube furnace. The produced nanoparticles were spherically shaped within a size range of 50 nm (**Figure 4**) (Farzana et al., 2018).

According to Dutta et al. recycling waste batteries and electronics to recover nanomaterials has ushered in a new era in nanotechnology and environmental research (Dutta et al., 2018).

Carbon Nanotubes

Carbon nanotubes (CNTs) synthesis from waste plastics is carried out in diverse systems, such as autoclaves, quartz tubes, crucibles, and muffle furnaces (Bazargan and McKay, 2012). Each method aims to disintegrate solid-state polymers into their

carbon precursors via pyrolysis (Zhuo and Levendis, 2014). Polyolefin ($\sim 85.7\text{wt } \%$ carbon content) is a polymeric material created from olefin monomer (C_nH_{2n}), and it is present in the large majority of plastic waste (Gong et al., 2012). Two waste polyolefins, polypropylene (PP) and polyethylene (PE) can be used for carbon materials synthesis. Other plastics integrated with additional elements such as polyvinyl alcohol (PVA) and polyethylene terephthalate (PET), can also be used for CNTs synthesis (Deng et al., 2016).

Gong et al. developed a new layer-by-layer assembling mechanism. In this method, waste PP was catalyzed via activated carbon and Ni_2O_3 in a quartz tube reactor. Activated carbon was effective in breaking PP into light hydrocarbons. Activated carbon also provided highly efficient catalytic conversion with Ni by encouraging dehydrogenation and aromatization with the formation of different aromatic groups. CNTs growth was accomplished based on benzene rings. The carboxylic moieties of activated carbon also enabled synergistic catalysis with Ni_2O_3 . The highest carbon yield ($\sim 50\text{ wt}\%$) was reached at 820°C with a proportion of raw materials of PP:10 Ni_2O_3 :8AC (wt%) (Gong et al., 2012). Considering the high energy demand of this method, the recovery of Ni_2O_3 could be an alternative for more sustainable scale-up manufacturing.

Zhou et al. reported another combustion method for PE decomposition. This method generates light hydrocarbon *in-situ* during an exothermic process. This method utilized a stainless-steel wire mesh as a catalyst and a substrate. A ceramic filter was placed before the stainless-steel wire mesh to eliminate the soot that could deactivate the mesh that served as a catalyst. The yield of CNTs was higher than 10 wt% (Zhuo et al., 2010).

In another synthesis process, Zhang et al. mixed PP ($\sim 2\text{ g}$), maleated PP ($\sim 0.5\text{ g}$), and Ni catalysis powders ($\sim 0.5\text{ g}$) in an autoclave. The resulting mixture was then heated for 12 h to a temperature of 700°C using an electric stove. It was then left to cool to ambient temperature. Carbon solid spheres were the only product obtained in absence of Ni from the reaction system which indicated that Ni powder catalyzed the decomposition of PP. MA-PP contributed to two actions in the growth process of CNTs, first improving the dispersion of Ni in PP, and then forming a homogenous system between carbon atoms and Ni catalysts. Ni particles were separated to form carbon-surrounded Ni particles and a high surface packing density of Ni particles enabled the nanotubes to grow along a consistent direction. This method of production of 160 nm CNTs had a yield of 80% (Zhang et al., 2008).

Bajad et al. attained approximately 45.8% yield in the production of MWNTs. These MWNTs were derived from PP waste catalyzed by Ni/Mo/MgO using a combustion technique (Bajad et al., 2015). The powdered catalysts and PP were placed in a covered silicon crucible and heated to 800°C in a muffle furnace. The Ni/Mo ratio was found to affect the yield and size of nanotubes. The HRTEM images exposed that the Ni/Mo ratio controlled both the yield and morphology of CNTs. Increasing the Mo content resulted in large diameter CNTs while lower Mo content gave higher yield with short-radius CNTs. The authors optimized the Ni/Mo mole ratio using response surface methodology (RSM) which proposed that 394% of carbon

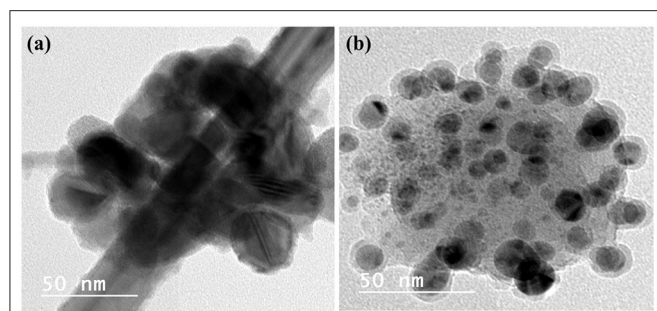


FIGURE 2 | High resolution TEM images of CuNPs obtained from WPCBs. These NPs were prepared from (a) ammoniacal ammonium chloride and (b) ammoniacal ammonium carbonate leachant by ascorbic acid in presence of cetyltrimethylammonium bromide (CTAB) as modifier. These images were reproduced from Seif El-Nasr et al. (2020) under the reproduction license number 4854300796766 provided by Elsevier and Copyright Clearance Center.

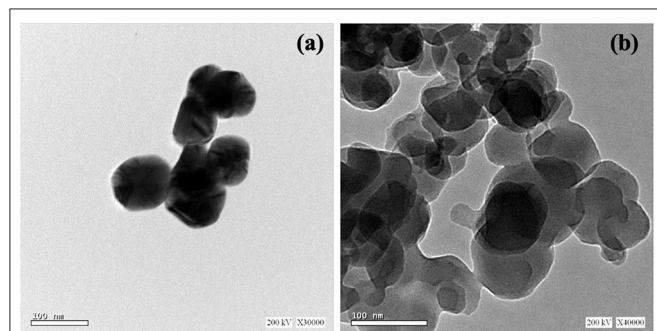


FIGURE 3 | TEM images of (a) Ag and (b) Cu NPs synthesized from metalized plastic waste. The NPs were prepared with leachant solution of metalized acrylonitrile butadiene styrene (ABS) using ascorbic acid as reductant and chitosan as stabilizer according to the methods described by Elsayed et al. (2020). These original images were provided by the authors of the manuscript and have not been previously published.

product could be yielded at a Ni/Mo mole ratio of 22.04. While 514% of CNTs would yield over $\text{Ni}_4\text{Mo}_{0.2}\text{MgO}_1$ catalyst at 800°C, 5 g polymer weight, 150 mg catalyst weight, and combustion time of 10 min.

Table 4 summarizes the different methods used in the production of CNTs from plastic polymers commonly found in solid waste.

Graphene

Graphene is a single-atom-thick sheet of sp^2 hybridized carbon atoms packed into a honeycomb lattice structure. Prominent properties of this material are high surface area, high electrical conductivity, good chemical stability, and strong mechanical strength (Nair et al., 2008; Rao et al., 2009; Luo et al., 2012; Novoselov et al., 2012). Graphene revolutionized the health, energy, and environment sectors (Liu et al., 2013a; Quesnel et al., 2015; Surwade et al., 2015; Yang et al., 2016a).

Its electrical, optical, and mechanical properties (Bonaccorso et al., 2010; Soldano et al., 2010; Marinho et al., 2012)

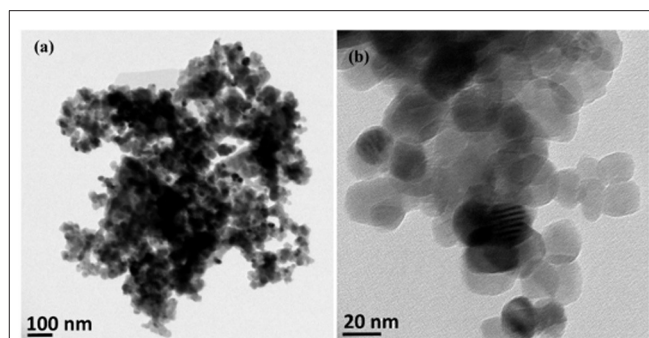


FIGURE 4 | Low resolution (a) and high resolution (b) TEM images of ZnO NPs recovered from spent Zn-C batteries via thermal route. This figure was reproduced from Farzana et al. (2018) under the terms and conditions of the Creative Commons Attribution (CC BY) license (<http://creativecommons.org/licenses/by/4.0/>).

make graphene eligible for any application. There are two essential sources for the preparation of graphene: graphite and organic molecules (Strudwick et al., 2015). Typical methods for graphene preparation include the bottom-up approach, the top-down approach, epitaxial growth on silicon carbide (Mishra et al., 2016), mechanical cleavage (Bonaccorso et al., 2012), and chemical reduction of graphene oxide (Abdolhosseinzadeh et al., 2015). The bottom-up approach utilizes chemical vapor deposition (CVD) on metallic films (Strudwick et al., 2015). The top-down approach utilizes liquid exfoliation of graphite crystal (Coleman, 2013). **Table 5** summarizes the recent approaches for graphene synthesis from waste materials.

Graphene can be synthesized from various waste plastics using a variety of methods. Gong et al. were able to create high yields of graphene flakes. Their method used waste polypropylene (PP) catalyzed by organically modified montmorillonite. A uniform mixture of PP (~89 wt %), talcum (~11 wt %), and modified montmorillonite, was placed in a crucible and heated to 700°C for 15 min to obtain the carbonized char. After cooling the carbonized char was immersed in HF and HNO_3 . HF dissolved the impurities and HNO_3 oxidized the amorphous carbon. After a repeated process of centrifuging and isolating from solution, graphene flakes were obtained (Gong et al., 2014b).

Manukyan et al. developed an energy-saving combustion method to prepare graphene sheets using waste polytetrafluoroethylene (PTFE) and silicon carbide (SiC). The process mechanism was similar to epitaxial growth on SiC, in which Si was removed by C_2F_4 through an exothermal reaction (Manukyan et al., 2013).

Ruan et al. developed a green synthesis method in which raw wastes including waste polystyrene, grass blades, waste food, and grass, were transformed into high-quality single-layered graphene. In this method, 10 mg of start materials were placed on a slightly bent piece of Cu foil held by a quartz boat in a CVD quartz tube. After low-pressure annealing at a temperature of approximately 1,050°C for 15 min in an inert atmosphere (Ar and H_2), graphene growth was observed on the back of the Cu foil (Ruan et al., 2011).

TABLE 4 | Synthesis methods of CNTs from waste plastics.

Waste plastics	Additives	Carbon yield (%)	References
PP	Stainless steel 316 tube that acted as reactor and catalyst	42	Tripathi et al., 2017
PP and PE	Ni/Al-SBA-15 catalysts	74.1	Yang et al., 2016b
PP	Ni/Ca-Al catalyst	>10	Wu et al., 2012
LDPE and PP	Ni-Mo/Al ₂ O ₃ catalyst	58	Aboul-Enein et al., 2018
PP	Ni/Mo/MgO catalyst	58	Song and Ji, 2011
HDPE and LDPE	Solvent free, cobalt acetate as catalyst	40	Pol and Thiagarajan, 2010
PE	CuBr and NiO	NR	Gong et al., 2014a
HDPE	Stainless steel wire mesh	NR	Zhuo et al., 2010
PP	Maleated polypropylene and Ni as catalysts	NR	Zhang et al., 2008
PP	Ni/Mo/MgO	45.8	Bajad et al., 2015
PP	Organic-modified clay and supported Ni catalyst	41.16	Tang et al., 2005
Polyvinyl alcohol	Fly ash	NR	Nath and Sahajwalla, 2011a,b, 2012
PP	Ni catalyst	85	Mishra et al., 2012
PET	Catalysts free	~39	Berkmans et al., 2014

NR, not reported in the manuscript.

TABLE 5 | Synthesis of graphene from waste materials.

Waste material	Fabrication technique	References
PP	Catalytic carbonization at 700°C	Gong et al., 2014b
PTFE	Epitaxial growth on SiC	Manukyan et al., 2013
PS, grass blades, waste food, and grass,	CVD using Cu foil as catalyst	Ruan et al., 2011
PE and PS	CVD synthesis	Sharma et al., 2014
PET	Thermal decomposition in a closed system.	El Essawy et al., 2017
Graphite electrode of waste dry cell zinc-carbon batteries	Acid treatment then, Hammer method	Roy et al., 2016
PET, PE, PVC, PP, PS, and polymethylmethacrylate (PMMA)	Solid-state CVD	Cui et al., 2017
PET	Pyrolysis at 900 °C then catalytic graphitization at 2,400 °C followed by exfoliation	Ko et al., 2020

Another CVD based graphene synthesis method used solid waste plastics roughly composed of 86% polyethylene and 14% polystyrene (Sharma et al., 2014). The method used two furnaces. In the first furnace, nearly 3 mg of plastic waste was put into a ceramic boat and kept at a temperature of approximately 500°C. In the second furnace, Cu foil was placed inside as substrate and kept at a temperature of approximately 1,020°C. Following pyrolysis, the degraded carbonaceous compounds were placed into the next furnace in a gas mixture (Ar/H₂: 98/2.5 sc cm). The products then interacted with a Cu substrate causing graphene growth. In this method, the injection rate of disintegrated products was crucial for graphene crystal formation. Large hexagonal single-layered graphene was produced at a low rate of pyrolysis and injection. On the other hand, under a high injection rate, a bilayer or multilayer graphene was formed (Sharma et al., 2014).

ENVIRONMENTAL APPLICATIONS OF WASTE-DERIVED NANOPARTICLES

The environmental applications of waste-derived nanoparticles will be discussed in this section and are presented in **Table 6**.

Wastewater Treatment and Water Remediation Adsorption

Industrial wastewater is contaminated with a mixture of pollutants unique to the industries that create them. For example, the textile industry produces waste streams contaminated with a variety of dyes. Water contaminated with these dyes must be treated to ensure public and environmental health (Arslan et al., 2016). Several research groups are attempting to find novel nanotechnology-enabled treatments for industrial wastewater using recycled nanoparticles, which helps meet circularity and sustainability goals. Arifin et al. (2017) developed iron oxide nanoparticles from mill scale and applied them to dye removal. In their process, iron oxide particles were removed from the unwanted components of mill scaling using magnetic separation techniques. The particles were then processed using conventional and high energy ball milling and treated with hexadecyltrimethylammonium bromide to prevent aggregation. In dye wastewater, the adsorption by the modified iron nanoparticles was above 99% with optimum adsorption of 99.93% with 53.76 nm particles (Arifin et al., 2017).

TABLE 6 | Environmental applications of waste nanoparticles.

	Nanoparticle	Source	Application	References
Wastewater treatment and water remediation	Iron oxide nanoparticles	Mill scale	Dye removal (adsorption)	Arifin et al., 2017
	Magnetite (Fe ₃ O ₄)	Iron ore tailings.	Dye removal (adsorption)	Giri et al., 2011
	Graphene	Polyethylene terephthalate (PET)	Dye removal (adsorption)	El Essawy et al., 2017
	CaCO ₃	Eggshell	Lead (Pb ²⁺) adsorption	Wang et al., 2018
	Porous aerogels	Paper, cotton textiles, and plastic bottles	Oil adsorption	Thai et al., 2019
	NiFe ₂ O ₄ / ZnCuCr-LDH composite	Saccharin wastewater	Dye removal (adsorption)	Zhang et al., 2020
	Silica nanoparticles (SiO ₂ NPs)	Sugar cane waste ash	Dye removal (adsorption)	Rovani et al., 2018
	Silica nanoparticles (MW-nSiO ₂ , nSiO ₂)	Corn husk waste	Dye removal (adsorption)	Peres et al., 2018
	Nnanocomposite of ZnO and CuO	Printed circuit boards	Dye removal (photocatalyst)	Nayak et al., 2019
	Metals-doped ZnO (M-ZnO)	Fabric filter dust	Dye removal (photocatalyst)	Wu et al., 2014
	Zero-valent iron nanoparticles	Pickling line of a steel plant	Nitrobenzene removal	Lee et al., 2015
	Carbon nanoparticles	Pomelo peels	Detection of mercury (Hg ²⁺)	Lu et al., 2012
Monitoring of pollutants in water	Nano-cuprous oxide	Electrical waste	Detecting dopamine and mercury	Abdelbasir et al., 2018a
Capture of air pollutants	Porous silica nanoparticles (PSNs)	Rice husks	CO ₂ capture	Zeng and Bai, 2016

Giri et al. (2011) developed a method for creating magnetite (Fe₃O₄) nanoparticles from iron ore tailings. The formation of these particles was confirmed through powder X-ray diffraction (XRD), ultraviolet-visible spectrophotometry (UV-Vis) and Fourier-transform infrared spectroscopy (FT-IR) spectra. These particles were fast and effective in the removal of methylene blue and Congo red dyes. In optimal conditions, the monolayer adsorption capacities were 70.4 mg g⁻¹ for methylene blue and 172.4 mg g⁻¹ for Congo red. These nanoparticles compared well with particles created from reagent grade materials and as such could be a value-added product with possible applications in large scale wastewater treatment (Giri et al., 2011).

El Essawy et al. (2017) explored another means of removing dye from water using recycled Polyethylene terephthalate (PET) as a starting material for NP production. Through thermal dissociation, PET creates graphene. The graphene was characterized using SEM, TEM, Raman, BET, TGA, and FT-IR. The produced graphene showed high micropore volume and surface area. Potential for adsorption was assessed with methylene blue and acid blue 25 dyes. This graphene showed good adsorption of methylene blue with optimal adsorption at a pH of 12. The methylene blue dye reached equilibrium within 30 min. The adsorption of the acid blue 25 dye was optimal in acidic solutions and the adsorbed dye reached an equilibrium in approximately 50 min. The PET-based graphene showed effectiveness in removing both dyes from solutions (El Essawy et al., 2017).

Wang et al. developed engineered biochar functionalized with waste eggshell particles. The biochar is composed of three types of biomass pretreated with eggshell waste and prepared through slow pyrolysis. The eggshell particles are prepared using a method shown to make colloidal and nanosized eggshell particles (Hassan et al., 2014). Using characterization tools such as scanning electron microscopy eggshell particles were found on the surface

and within the pore networks of the biochar. When studied the biochar treated with eggshells was more effective at lead (Pb²⁺) adsorption than pristine biochar due to the presence of CaCO₃ from the eggshells (Wang et al., 2018).

Thai et al. (2019) reviewed the synthesis of highly porous aerogels from recycled materials such as paper, cotton textiles, and plastic bottles. Paper-derived aerogels were made through a simple process that required sonication of a solution of recycled cellulose with polyamide-epichlorohydrin, followed by freeze-drying at -98°C. Similarly, textile-derived aerogels were prepared by blending scraps of cotton cloth with DI water, followed by sonication in a solution of polyamide-epichlorohydrin. The resulting dispersion was freeze-dried at -98°C and cured at 120°C. Aerogels from recycled PET bottles were obtained by immersing PET fibers in a solution of NaOH heated at 80°C; the fibers were subsequently rinsed with DI water and then mixed with a solution of polyvinyl alcohol, glutaraldehyde, and HCl. Next, the mixture was sonicated, heated at 80°C, and freeze-dried. To confer superhydrophobicity to these aerogels, a coating of methyltrimethoxysilane was added at the end of the fabrication process. The ultra-low density and high absorption capacity of these waste-derived aerogels make them especially attractive for remediation applications such as the clean-up of oil spills in water bodies. For example, aerogels from cotton can achieve an absorption capacity above 100 grams of motor oil per gram of aerogel, which significantly outperforms most commercial sorbents (Thai et al., 2019).

Zhang et al. (2020) proposed and tested another method for treating waste dyewater using iron derived from the manufacturing of saccharin. In this process, NiFe₂O₄ nanoparticles that are used as a catalyst, are first extracted from the saccharin wastewater, which is challenging to treat. A mesoporous magnet NiFe₂O₄/ ZnCuCr-LDH composite is then created using a hydrothermal method. The created NiFe₂O₄/

ZnCuCr-LDH composites had a removal efficiency for Congo red of over 97% in cases where the initial concentration of the dye was between 100 and 450 mg l⁻¹. The process treats the saccharin wastewater for iron contamination and reuses the waste iron to create a magnetic composite for the treatment of dye water (Zhang et al., 2020).

Rovani et al. and Peres et al. proposed methods of creating silicon nanoparticles from agricultural waste for the absorption of dyes. Rovani et al. created high purity silica nanoparticles (SiO₂NPs) from sugar cane waste ash. The nanoparticles were tested for their capacity as absorbent material for the removal of acid orange 8 (AO8) dye. The silicon nanoparticles had an absorption capacity of 230 mg/g and the nanoparticles were able to be reused for up to five cycles (Rovani et al., 2018). Peres et al. synthesized silica nanoparticles from corn husk waste through a standard synthesis and a microwave synthesis method. These silicon nanoparticles were applied for the absorption of methyl blue dye. The microwave silica nanoparticles show higher values for surface area, pore volume, pore diameter, porosity, and purity compared to the traditionally synthesized silica nanoparticles. The microwave silica nanoparticles had an absorption capacity of 679.9 mg/g and a removal percentage of 80%. The thermodynamic results for the absorbent revealed a favorable spontaneous exothermic reaction for both nano-silica particles (Peres et al., 2018).

Photocatalytic Degradation

Nayak et al. (2019) synthesized a nanocomposite of ZnO and CuO using electronic waste, specifically printed circuit boards. These composites were formed by applying nitric acid to the memory slots and processing the leached liquid using an alkaline hydrothermal treatment. The composites were characterized using high-resolution transmission electron microscopy (HR-TEM), diffuse reflectance ultraviolet-visible spectrophotometry (UV-DRS), and UV-Vis. The nanocomposites were composed of CuO cores with ZnO nanostructures precipitated onto the cores. The nanoparticles proved to be effective photocatalyst for methyl orange dye degradation in the presence of visible light and hydrogen peroxide. These nanoparticles show promise as photo-Fenton catalysts for organic pollutants (Nayak et al., 2019).

Wu et al. explored another strategy for the photocatalytic degradation of pollutants in wastewater. Wu et al. prepared a metals-doped ZnO (M-ZnO) nanomaterial using fabric filter dust. The dopants used (Fe, Mg, Ca, and Al) and the zinc were all obtained from fabric filter dust without the addition of chemicals as elemental sources. The doped M-ZnO nanoparticles were prepared through sulfolysis combining co-precipitation processes. The nanoparticle acts as a favorable photocatalyst for the breakdown of organic substances, specifically phenol, under visible light irradiation (Wu et al., 2014).

Decomposition

Lee et al. studied the removal of nitrobenzene using synthesized zero-valent iron nanoparticles. The iron oxide to synthesize the nanoparticles comes from the pickling line of a steel plant. These particles are approximately 500 nm. The particles showed a reaction activity much higher than commercial zero-valent

iron. Lee et al. proposed that in presence of the synthesized zero-valent iron nitrobenzene deoxidizes to nitrosobenzene. The nitrosobenzene is then reduced to aniline which is more biodegradable than nitrobenzene. When combined with biological processes these nanoparticles show promise in decomposing nitrobenzene in wastewater (Lee et al., 2015).

Monitoring of Pollutants in Water

Laboratory tests utilized to identify pollutants in water are cost-prohibitive in some communities because they require trained personnel and expensive equipment to run. To address this problem, researchers are developing low-cost sensors to monitor pollutants using nanoparticles. Some researchers take it a step further using recycled nanoparticles. Lu et al. (2012) developed an optical sensor that uses recycled carbon nanoparticles from waste pomelo peels. Pomelo (*Citrus maximus*) has a grapefruit-like flavor with a much thicker peel and is a popular fruit from Brazil to Southeast Asia. The particles, derived from the hydrothermal processing of the pomelo peels, need no further chemical modification. The carbon particles have a reported quantum yield of approximately 6.9%. These particles were tested for use in the detection of mercury (Hg²⁺) based on the mercury-induced fluorescence quenching of the carbon particles. The particles' selectivity and sensitivity were excellent, and the particles had a limit of detection as low as 0.23 nM. The carbon nanoparticles have also been successful in mercury detection in lake water samples (Lu et al., 2012).

Abdelbasir et al. (2018a) developed an electrochemical sensor for environmental protection applications. The sensor was fabricated by anchoring copper nanoparticles to laser-scribed graphene electrodes. The nano-cuprous oxide was synthesized from electrical waste. The unique structure of the nanoparticles made them stable, linker-free, and size-tunable. The anchoring of the particles to the graphene electrode reduced internal/charge transfer resistance enhancing electrochemical performance. The effectiveness of the sensors in detecting dopamine and mercury was evaluated. In the case of dopamine, the sensor shows a linear calibration curve between 300 nM and 5 μM, a limit of detection of 200 nM, a sensitivity of 30 nA μM⁻¹ cm⁻², and a response time of 2.4 ± 0.7 s. In the case of mercury, the sensor shows a linear calibration curve between 0.02 and 2.5 ppm, a limit of detection of 25 ppb, a sensitivity of 10 nA ppm⁻¹, and a response time of fewer than 3 min. The proposed approach presented to fabricate these sensors is scalable as wires are used in a variety of commonplace goods and industries (Abdelbasir et al., 2018a).

Capture of Air Pollutants

Zeng et al. tested a means of deriving porous silica nanoparticles (PSNs) from rice husks with a simple template-free method. This method is inexpensive, fast, simple, and energy saving. (NH₄)₂SiF₆ salt formed during the synthetic process serve as a porogen. Thus, providing control of the porosity of the PSNs without the need for extra pore-directing templates and post-heat-treatment by varying the molar ratios of HF/Si and NH₄OH/Si. The PSNs were evaluated as support for polyethyleneimine (PEI). The PEI/silica composite reached an adsorption capacity of 159 mg/g at 75°C under 15% CO₂.

According to Zeng et al. this is superior to waste silica precursors reported in the literature. The sorbent also showed high stability during 20 cycles of absorption and desorption. This implies that it has potential in post combustions CO₂ capture. The silica used could also be sourced from other waste streams such as bottom ash and fly ash (Zeng and Bai, 2016).

SUSTAINABILITY CONSIDERATIONS AND CONCLUDING REMARKS

Throughout this review, different possibilities for using waste materials as inputs for the production of NPs have been exemplified and discussed in the context of research. While the concept of turning waste into advanced technologies for environmental applications may, at first glance, look like an attractive full-circle approach, there are significant knowledge gaps about engineered nanomaterials that should be addressed before transitioning these ideas from the lab to the real world; particularly regarding energy use, generation of secondary wastes, fate and transport behavior, exposure routes in different environments, and toxicity levels in diverse organisms (Kumar et al., 2014). As viable processes emerge from the proof-of-concept stage, careful cost-benefit analyses must be conducted. Though there is no simple path for overcoming the negative implications of the current “end-of-life” waste management systems, many experts have highlighted the importance of conducting life cycle assessments and risk analysis early on during the development of new technologies and processes, and also, to account for aging transformations and potential release of nanomaterials and byproducts in the environment. Thus, minimizing the potential for the future unveiling of unintended consequences (Dhingra et al., 2010; Grillo et al., 2015; Mitrano et al., 2015). However, performing the pertinent life cycle assessment and risk analyses implies having access to a sufficiently large body of data on emissions and environmental concentrations on engineered NPs. Hence, most data available in the literature have been obtained through modeling and simulation of the release of NPs from containing products during consumer manipulation; thus, empirical information on release coefficients throughout all stages of the life cycle (including production, usage, and disposal) is a limiting factor (Aitken et al., 2006; Gottschalk and Nowack, 2011).

At the production stage, the twelve principles of green chemistry provide a suitable framework for manufacturing NPs and NP-enabled technologies. These principles are intended to guide the design of chemical routes that yield enhanced

sustainability outcomes (Gilbertson et al., 2015; Benelli, 2019). Nevertheless, the fact that NPs can be produced through sustainable approaches does not mean that the fabricated NPs are intrinsically safe and that their use and release in the environment will not cause harm. In the last decade, some studies have shown that engineered NPs that have already been used in different applications, including food manufacturing and packaging, could dramatically disrupt epigenetic mechanisms, and there are several questions regarding their ability to induce diseases (Smolkova et al., 2015). Perhaps, fullerenes are amongst the better-known class of engineered NPs. Several *in vitro* and *in vivo* studies have reported on the interactions and toxicity of carbon nanomaterials with various living systems (Liu et al., 2013b; Lalwani et al., 2016). Kagan et al. (2005) discussed how the very same properties that make CNTs so desirable for technological applications are also associated with inflammatory reactions and fibrogenic events that impair lung function in mice making their respiratory system more prone to infections (Kagan et al., 2005). The effects of inhalation of CNTs have been compared to those of asbestos fibers, which are known cytotoxic and carcinogenic particles (Sanchez et al., 2009).

In conclusion, to realize the potential benefits from the implementation of waste-derived NPs, a complex web of influencing factors must be understood, and decisions should err on the side of precaution and ethics. Scale and scope of the applications of these NPs, as well as strategies to enable closed-loop management of the engineered nanomaterials, should be defined on a regional basis and management policies should be informed by health and environmental science.

AUTHOR CONTRIBUTIONS

DV outlined and lead the drafting and editing of the manuscript. SA and KM performed an extensive literature search and contributed to the writing of sections and the construction of figures and tables. CL provided professional advice and participated in the revision of the final document. All authors read and approved the final manuscript.

FUNDING

The authors would like to acknowledge the support by the National Science Foundation (GRFPF award 2014124, for KM), the DUPC2-IHE program at Delft University (P: 1084731:111; Ref: 2019/061/108473/EWH), and the Open Access Publishing Initiative of Clemson University.

REFERENCES

- Abdelbasir, S. M., El-Sheikh, S. M., Morgan, V. L., Schmidt, H., Casso-Hartmann, L. M., Vanegas, D. C., et al. (2018a). Graphene-anchored cuprous oxide nanoparticles from waste electric cables for electrochemical sensing. *ACS Sustain. Chem. Eng.* 6, 12176–12186. doi: 10.1021/acssuschemeng.8b02510
- Abdelbasir, S. M., El-Sheltawy, C. T., and Abdo, D. M. (2018b). Green processes for electronic waste recycling: a review. *J. Sustain. Metall.* 4, 295–311. doi: 10.1007/s40831-018-0175-3
- Abdelbasir, S. M., Hassan, S. S. M., Kamel, A. H., and El-Nasr, R. S. (2018c). Status of electronic waste recycling techniques: a review. *Environ. Sci. Pollut. Res.* 25, 16533–16547. doi: 10.1007/s11356-018-2136-6
- Abdolhosseinzadeh, S., Asgharzadeh, H., and Kim, H. S. (2015). Fast and fully-scalable synthesis of reduced graphene oxide. *Sci. Rep.* 5, 1–7. doi: 10.1038/srep10160
- Aboul-Enein, A. A., Awadallah, A. E., Abdel-Rahman, A. A. H., and Haggag, A. M. (2018). Synthesis of multi-walled carbon nanotubes via pyrolysis of plastic waste using a two-stage process. *Fullerenes*

- Nanotub. Carbon Nanostructures 26, 443–450. doi: 10.1080/1536383X.2018.1447929
- Aboulkas, A., El harfi, K., and El Bouadili, A. (2010). Thermal degradation behaviors of polyethylene and polypropylene. Part I: pyrolysis kinetics and mechanisms. *Energy Convers. Manag.* 51, 1363–1369. doi: 10.1016/j.enconman.2009.12.017
- Ackerman, F. (2000). Waste management and climate change. *Local Environ.* 5, 223–229. doi: 10.1080/13549830050009373
- Aitken, R. J., Chaudhry, M. Q., Boxall, A. B. A., and Hull, M. (2006). Manufacture and use of nanomaterials: current status in the UK and global trends. *Occup. Med. (Chic. Ill.)* 56, 300–306. doi: 10.1093/occmed/kql051
- Al-Salem, S. M., Lettieri, P., and Baeyens, J. (2009). Recycling and recovery routes of plastic solid waste (PSW): a review. *Waste Manag.* 29, 2625–2643. doi: 10.1016/j.wasman.2009.06.004
- Arifin, S. A. R. A., Ismail, I., Halim Abdullah, A., Nabilah Shafiee, F., Nazlan, R., and Riati Ibrahim, I. (2017). Iron oxide nanoparticles derived from mill scale waste as potential scavenging agent in dye wastewater treatment for batik industry. *Solid State Phenom.* 268, 393–398. doi: 10.4028/www.scientific.net/SSP.268.393
- Arslan, S., Eyyaz, M., Gürbulak, E., and Yüksel, E. (2016). “A review of state-of-the-art technologies in dye-containing wastewater treatment – the textile industry case,” in *Textile Wastewater Treatment*. 1–29. doi: 10.5772/64140
- Astrup, T., Fruergaard, T., and Christensen, T. H. (2009). Recycling of plastic: accounting of greenhouse gases and global warming contributions. *Waste Manag. Res.* 27, 763–772. doi: 10.1177/0734242X09345868
- Bajad, G. S., Tiwari, S. K., and Vijayakumar, R. P. (2015). Synthesis and characterization of CNTs using polypropylene waste as precursor. *Mater. Sci. Eng. B Solid-State Mater. Adv. Technol.* 194, 68–77. doi: 10.1016/j.mseb.2015.01.004
- Baldé, C. P., Forti, V., Gray, V., Kuehr, R., and Stegmann, P. (2017). *Quantities, Flows, and Resources The Global E-waste*. Available online at: www.unu.edu (accessed May 10, 2020).
- Banu, J. R., Sharmila, V. G., Ushani, U., Amudha, V., and Kumar, G. (2020). Impervious and influence in the liquid fuel production from municipal plastic waste through thermo-chemical biomass conversion technologies - A review. *Sci. Total Environ.* 718:137287. doi: 10.1016/j.scitotenv.2020.137287
- Barletta, I., Johansson, B., Cullbrand, K., Björkman, M., and Reimers, J. (2015). “Fostering sustainable electronic waste management through intelligent sorting equipment,” in *IEEE International Conference on Automation Science and Engineering (CASE)* (Gothenburg), 459–461. doi: 10.1109/CoASE.2015.7294122
- Baruah, S., and Dutta, J. (2009). Nanotechnology applications in pollution sensing and degradation in agriculture. *Environ. Chem. Lett.* 7, 191–204. doi: 10.1007/s10311-009-0228-8
- Basel Action Network (2019). *Norwegian Proposal’ Puts Brakes on Global Plastic Waste ‘Tsunami’ 2020*. Available online at: https://www.ban.org/news/2019/5/10/basel-convention-agrees-to-control-plastic-waste-trade (accessed May 10 2020).
- Bazargan, A., and McKay, G. (2012). A review - Synthesis of carbon nanotubes from plastic wastes. *Chem. Eng. J.* 195–196, 377–391. doi: 10.1016/j.cej.2012.03.077
- Benelli, G. (2019). Green synthesis of nanomaterials. *Nanomaterials* 9:275. doi: 10.3390/nano9091275
- Bennett, J. A., Wilson, K., and Lee, A. F. (2016). Catalytic applications of waste derived materials. *J. Mater. Chem. A* 4, 3617–3637. doi: 10.1039/C5TA09613H
- Berg, A., Antikainen, R., Hartikainen, E., Kauppi, S., Kautto, P., Lazarevic, D., et al. (2018). *Circular Economy for Sustainable Development*. Helsinki: Finnish Environment Institute.
- Berkmans, J. A., Jagannatham, M., Priyanka, S., and Haridoss, P. (2014). Synthesis of branched, nano channeled, ultrafine and nano carbon tubes from PET wastes using the arc discharge method. *Waste Manag.* 34, 2139–2145. doi: 10.1016/j.wasman.2014.07.004
- Bhat, V., Rao, P., and Patil, Y. (2012). Development of an integrated model to recover precious metals from electronic scrap - a novel strategy for E-Waste management. *Procedia. Soc. Behav. Sci.* 37, 397–406. doi: 10.1016/j.sbspro.2012.03.305
- Bindrabn, P. S., Dimkpa, C., Nagarajan, L., Roy, A., and Rabbinge, R. (2015). Revisiting fertilisers and fertilisation strategies for improved nutrient uptake by plants. *Biol. Fertil. Soils* 51, 897–911. doi: 10.1007/s00374-015-1039-7
- Blazsó, M., Czégény, Z., and Csoma, C. (2002). Pyrolysis and debromination of flame retarded polymers of electronic scrap studied by analytical pyrolysis. *J. Anal. Appl. Pyrolysis* 64, 249–261. doi: 10.1016/S0165-2370(02)00035-9
- Bonaccorso, F., Lombardo, A., Hasan, T., Sun, Z., Colombo, L., and Ferrari, A. C. (2012). Production and processing of graphene and 2d crystals. *Mater. Today* 15, 564–589. doi: 10.1016/S1369-7021(13)70014-2
- Bonaccorso, F., Sun, Z., Hasan, T., and Ferrari, A. C. (2010). Graphene photonics and optoelectronics. *Nat. Publ. Gr.* 4, 611–622. doi: 10.1038/nphoton.2010.186
- Bourguignon, D. (2014). *Turning Waste Into a Resource - Moving Towards a “Circular Economy” - Think Tank. Brief. Eur. Parliam.* Available online at: https://www.europarl.europa.eu/thinktank/en/document.html?reference=EPRS_BRI(2014)545704 (accessed May 10, 2020).
- Bouwmeester, H., Hollman, P. C. H., and Peters, R. J. B. (2015). Potential health impact of environmentally released micro- and nanoplastics in the human food production chain: experiences from nanotoxicology. *Environ. Sci. Technol.* 49, 8932–8947. doi: 10.1021/acs.est.5b01090
- Calgaro, C. O., Schlemmer, D. F., Da Silva, M. D. C. R., Maziero, E. V., Tanabe, E. H., and Bertuol, D. A. (2015). Fast copper extraction from printed circuit boards using supercritical carbon dioxide. *Waste Manag.* 45, 289–297. doi: 10.1016/j.wasman.2015.05.017
- Cayumil, R., Khanna, R., Ikram-Ul-Haq, M., Rajarao, R., Hill, A., and Sahajwalla, V. (2014). Generation of copper rich metallic phases from waste printed circuit boards. *Waste Manag.* 34, 1783–1792. doi: 10.1016/j.wasman.2014.05.004
- Chaukura, N., Gwenzi, W., Bunhu, T., Ruziwa, D. T., and Pumure, I. (2016). Potential uses and value-added products derived from waste polystyrene in developing countries: a review. *Resour. Conserv. Recycl.* 107, 157–165. doi: 10.1016/j.resconrec.2015.10.031
- Chen, D., Li, Q., Shao, L., Zhang, F., and Qian, G. (2016). Recovery and application of heavy metals from pickling waste liquor (PWL) and electroplating wastewater (EPW) by the combination process of ferrite nanoparticles. *Desalin. Water Treat.* 57, 29264–29273. doi: 10.1080/19443994.2016.1172984
- Chen, M., Huang, J., Ogunseitan, O. A., Zhu, N., and Wang, Y., (2015a). Comparative study on copper leaching from waste printed circuit boards by typical ionic liquid acids. *Waste Manag.* 41, 142–147. doi: 10.1016/j.wasman.2015.03.037
- Chen, M., Zhang, S., Huang, J., and Chen, H. (2015b). Lead during the leaching process of copper from waste printed circuit boards by five typical ionic liquid acids. *J. Clean. Prod.* 95, 142–147. doi: 10.1016/j.jclepro.2015.02.045
- Chu, Y., Chen, M., Chen, S., Wang, B., Fu, K., and Chen, H. (2015). Micro-copper powders recovered from waste printed circuit boards by electrolysis. *Hydrometallurgy* 156, 152–157. doi: 10.1016/j.hydromet.2015.06.006
- Coleman, J. N. (2013). Liquid exfoliation of defect-free graphene. *Acc. Chem. Res.* 46, 14–22. doi: 10.1021/ar300009f
- Cui, H., and Anderson, C. G. (2016). Literature review of hydrometallurgical recycling of printed circuit boards (PCBs). *J. Adv. Chem. Eng.* 6, 1–11. doi: 10.4172/2090-4568.1000142
- Cui, J., and Forssberg, E. (2003). Mechanical recycling of waste electric and electronic equipment: a review. *J. Hazard. Mater.* 99, 243–263. doi: 10.1016/S0304-3894(03)00061-X
- Cui, L., Wang, X., Chen, N., Ji, B., and Qu, L. (2017). Trash to treasure: converting plastic waste into a useful graphene foil. *Nanoscale* 9, 9089–9094. doi: 10.1039/C7NR03580B
- Dalrymple, I., Wright, N., Kellner, R., Bains, N., Geraghty, K., Goosey, M., et al. (2007). An integrated approach to electronic waste (WEEE) recycling. *Circuit World* 33, 52–58. doi: 10.1108/03056120710750256
- Dell, J. (2019). *157,000 Shipping Containers of U.S. Plastic Waste Exported to Countries with Poor Waste Management in 2018 — Plastic Pollution Coalition*. Available online at: https://www.plasticpollutioncoalition.org/blog/2019/3/6/157000-shipping-containers-of-us-plastic-waste-exported-to-countries-with-poor-waste-management-in-2018 (accessed May 10, 2020).
- Deng, J., You, Y., Sahajwalla, V., and Joshi, R. K. (2016). Transforming waste into carbon-based nanomaterials. *Carbon N. Y.* 96, 105–115. doi: 10.1016/j.carbon.2015.09.033
- Dhingra, R., Naidu, S., Upreti, G., and Sawhney, R. (2010). Sustainable nanotechnology: through green methods and life-cycle thinking. *Sustainability* 2, 3323–3338. doi: 10.3390/su2103323

- Duan, C., Wen, X., Shi, C., Zhao, Y., Wen, B., and He, Y. (2009). Recovery of metals from waste printed circuit boards by a mechanical method using a water medium. *J. Hazard. Mater.* 166, 478–482. doi: 10.1016/j.jhazmat.2008.11.060
- Dubin, S., Gilje, S., Wang, K., Tung, V. C., Cha, K., Hall, A. S., et al. (2010). A one-step, solvothermal reduction method for producing reduced graphene oxide dispersions in organic solvents. *ACS Nano* 4, 3845–3852. doi: 10.1021/nn100511a
- Dutta, T., Kim, K. H., Deep, A., Szulejko, J. E., Vellingiri, K., Kumar, S., et al. (2018). Recovery of nanomaterials from battery and electronic wastes: a new paradigm of environmental waste management. *Renew. Sustain. Energy Rev.* 82, 3694–3704. doi: 10.1016/j.rser.2017.10.094
- El Essawy, N. A., Ali, S. M., Farag, H. A., Konsowa, A. H., Elnouby, M., and Hamad, H. A. (2017). Green synthesis of graphene from recycled PET bottle wastes for use in the adsorption of dyes in aqueous solution. *Ecotoxicol. Environ. Saf.* 145, 57–68. doi: 10.1016/j.ecoenv.2017.07.014
- El-Nasr, S. R., Abdelbasir, S. M., Kamel, A. H., and Hassan, S. S. M. (2020). Environmentally friendly synthesis of copper nanoparticles from waste printed circuit boards. *Sep. Purif. Technol.* 230, 115860. doi: 10.1016/j.seppur.2019.115860
- Elsayed, D. M., Abdelbasir, S. M., Abdel-Ghafar, H. M., Salah, B. A., and Sayed, S. A. (2020). Silver and copper nanostructured particles recovered from metalized plastic waste for antibacterial applications. *J. Environ. Chem. Eng.* 8:103826. doi: 10.1016/j.jece.2020.103826
- Evans, A., and Evans, R. (2006). *The Composition of a Tyre: Typical Components Creating markets for recycled resources. Waste Resour. Action Program.* 1–5. Available online at: <https://nanopdf.com/download/the-composition-of-a-tyre-typical-components.pdf> (accessed May 10, 2020).
- Falinski, M. M., Plata, D. L., Chopra, S. S., Theis, T. L., Gilbertson, L. M., and Zimmerman, J. B. (2018). A framework for sustainable nanomaterial selection and design based on performance, hazard, and economic considerations. *Nat. Nanotechnol.* 13, 708–714. doi: 10.1038/s41565-018-0120-4
- Fan, C., An, H., Du, J., and Luo, Y. (2020). High-performance printable paper-like composites derived from plastic flexible film wastes. *Polym. Int.* 69, 184–191. doi: 10.1002/pi.5935
- Fang, Z., Qiu, X., Chen, J., and Qiu, X. (2011). Degradation of the polybrominated diphenyl ethers by nanoscale zero-valent metallic particles prepared from steel pickling waste liquor. *Desalination* 267, 34–41. doi: 10.1016/j.desal.2010.09.003
- Farzana, R., Rajarao, R., Behera, P. R., Hassan, K., and Sahajwalla, V. (2018). Zinc oxide nanoparticles from waste Zn-C battery via thermal route: characterization and properties. *Nanomaterials* 8:717. doi: 10.3390/nano8090717
- Ferronato, N., and Torretta, V. (2019). Waste mismanagement in developing countries: a review of global issues. *Int. J. Environ. Res. Public Health* 16:1060. doi: 10.3390/ijerph16061060
- Fogarasi, S., Imre-Lucaci, F., Egedy, A., Imre-Lucaci, Á., and Ilea, P. (2015). Eco-friendly copper recovery process from waste printed circuit boards using Fe³⁺/Fe²⁺ redox system. *Waste Manag.* 40, 136–143. doi: 10.1016/j.wasman.2015.02.030
- Gilbertson, L. M., Zimmerman, J. B., Plata, D. L., Hutchison, J. E., and Anastas, P. T. (2015). Designing nanomaterials to maximize performance and minimize undesirable implications guided by the Principles of Green Chemistry. *Chem. Soc. Rev.* 44, 5758–5777. doi: 10.1039/C4CS00445K
- Giri, S. K., Das, N. N., and Pradhan, G. C. (2011). Synthesis and characterization of magnetite nanoparticles using waste iron ore tailings for adsorptive removal of dyes from aqueous solution. *Colloids Surfaces A Physicochem. Eng. Asp.* 389, 43–49. doi: 10.1016/j.colsurfa.2011.08.052
- Goh, P. S., Ng, B. C., Lau, W. J., and Ismail, A. F. (2015). Inorganic nanomaterials in polymeric ultrafiltration membranes for water treatment. *Sep. Purif. Rev.* 44, 216–249. doi: 10.1080/15422119.2014.926274
- GoldsteinResearch (2020). *Global Tire Recycling Market Report - Edition 2020*. Available online at: <https://www.goldsteinresearch.com/report/global-tire-recycling-industry-market-trends-analysis> (accessed May 10, 2020).
- Gómez-Hernández, R., Panecatí-Bernal, Y., and Méndez-Rojas, M. Á. (2019). High yield and simple one-step production of carbon black nanoparticles from waste tires. *Heliyon* 5:e02139. doi: 10.1016/j.heliyon.2019.e02139
- Gondal, M. A., and Siddiqui, M. N. (2007). Identification of different kinds of plastics using laser-induced breakdown spectroscopy for waste management. *J. Environ. Sci. Heal. Part A Toxic/Hazardous Subst. Environ. Eng.* 42, 1989–1997. doi: 10.1080/10934520701628973
- Gong, J., Liu, J., Jiang, Z., Feng, J., Chen, X., Wang, L., et al. (2014a). Striking influence of chain structure of polyethylene on the formation of cup-stacked carbon nanotubes/carbon nanofibers under the combined catalysis of CuBr and NiO. *Appl. Catal. B Environ.* 147, 592–601. doi: 10.1016/j.apcatb.2013.09.044
- Gong, J., Liu, J., Wan, D., Chen, X., Wen, X., Mijowska, E., et al. (2012). Catalytic carbonization of polypropylene by the combined catalysis of activated carbon with Ni₂O₃ into carbon nanotubes and its mechanism. *Appl. Catal. A Gen.* 449, 112–120. doi: 10.1016/j.apcata.2012.09.028
- Gong, J., Liu, J., Wen, X., Jiang, Z., Chen, X., Mijowska, E., et al. (2014b). Upcycling waste polypropylene into graphene flakes on organically modified montmorillonite. *Ind. Eng. Chem. Res.* 53, 4173–4181. doi: 10.1021/ie4043246
- Gottschalk, F., and Nowack, B. (2011). The release of engineered nanomaterials to the environment. *J. Environ. Monit.* 13, 1145–1155. doi: 10.1039/c0em00547a
- Grillo, R., Rosa, A. H., and Fraceto, L. F. (2015). Engineered nanoparticles and organic matter: a review of the state-of-the-art. *Chemosphere* 119, 608–619. doi: 10.1016/j.chemosphere.2014.07.049
- Gu, L., and Ozbakkaloglu, T. (2016). Use of recycled plastics in concrete: a critical review. *Waste Manag.* 51, 19–42. doi: 10.1016/j.wasman.2016.03.005
- Hadi, P., Xu, M., Lin, C. S. K., Hui, C. W., and McKay, G. (2015). Waste printed circuit board recycling techniques and product utilization. *J. Hazard. Mater.* 283, 234–243. doi: 10.1016/j.jhazmat.2014.09.032
- Hassan, T. A., Rangari, V. K., and Jeelani, S. (2014). Value-added biopolymer nanocomposites from waste eggshell-based CaCO₃ nanoparticles as fillers. *ACS Sustain. Chem. Eng.* 2, 706–717. doi: 10.1021/sc400405v
- Hassanain, W. A., Izake, E. L., Schmidt, M. S., and Ayoko, G. A. (2017). Gold nanomaterials for the selective capturing and SERS diagnosis of toxins in aqueous and biological fluids. *Biosens. Bioelectron.* 91, 664–672. doi: 10.1016/j.bios.2017.01.032
- Hsu, E., Barmak, K., West, A. C., and Park, A. H. A. (2019). Advancements in the treatment and processing of electronic waste with sustainability: a review of metal extraction and recovery technologies. *Green Chem.* 21, 919–936. doi: 10.1039/C8GC03688H
- Hussein, A. K. (2015). Applications of nanotechnology in renewable energies - A comprehensive overview and understanding. *Renew. Sustain. Energy Rev.* 42, 460–476. doi: 10.1016/j.rser.2014.10.027
- Jeevanandam, J., Chan, Y. S., and Danquah, M. K. (2016). Biosynthesis of metal and metal oxide nanoparticles. *Chem. Bio. Eng. Rev.* 3, 55–67. doi: 10.1002/cben.201500018
- Kagan, V. E., Bayir, H., and Shvedova, A. A. (2005). Nanomedicine and nanotoxicology: two sides of the same coin. *Nanomed. Nanotechnol. Biol. Med.* 1, 313–316. doi: 10.1016/j.nano.2005.10.003
- Kaza, S., Yao, L., Bhada-Tata, P., Van Woerden, F., and Ionkova, K. (2018). *What a Waste 2.0: a Global Snapshot of Solid Waste Management to 2050*. Washington, DC: World Bank. doi: 10.1596/978-1-4648-1329-0
- Keskisaari, A., and Kärki, T. (2017). Raw material potential of recyclable materials for fiber composites: a review study. *J. Mater. Cycles Waste Manag.* 19, 1136–1143. doi: 10.1007/s10163-016-0511-2
- Khaloo, S. S., Torabbeigi, M., Jazani, R. K., Douraghi, M., and Ghalavand, Z. (2013). Laboratory waste minimization by recovery of silver as nano-silver colloidal dispersion from waste silver chloride. *J. Mater. Cycles Waste Manag.* 15, 342–347. doi: 10.1007/s10163-013-0123-z
- Ko, S., Kwon, Y. J., Lee, J. U., and Jeon, Y. P. (2020). Preparation of synthetic graphite from waste PET plastic. *J. Ind. Eng. Chem.* 83, 449–458. doi: 10.1016/j.jiec.2019.12.018
- Kral, U., Morf, L. S., Vyzinkarova, D., and Brunner, P. H. (2019). Cycles and sinks: two key elements of a circular economy. *J. Mater. Cycles Waste Manag.* 21, 1–9. doi: 10.1007/s10163-018-0786-6
- Kumar, A., Kumar, P., Anandan, A., Fernandes, T. F., Ayoko, G. A., and Biskos, G. (2014). Engineered nanomaterials: knowledge gaps in fate, exposure, toxicity, and future directions. *J. Nanomater.* 130198. doi: 10.1155/2014/130198
- Kumar, S., Panda, A. K., and Singh, R. K. (2011). A review on tertiary recycling of high-density polyethylene to fuel. *Resour. Conserv. Recycl.* 55, 893–910. doi: 10.1016/j.resconrec.2011.05.005

- Lalwani, G., D'Agati, M., Khan, A. M., and Sitharaman, B. (2016). Toxicology of graphene-based nanomaterials. *Adv. Drug Deliv. Rev.* 105, 109–144. doi: 10.1016/j.addr.2016.04.028
- Lee, H., Kim, B.-H., Park, Y.-K., Kim, S.-J., and Jung, S.-C. (2015). Application of recycled zero-valent iron nanoparticle. *J. Nanomater.* 2015:392537. doi: 10.1155/2015/392537
- Li, J., Lu, H., Guo, J., Xu, Z., and Zhou, Y. (2007). Recycle technology for recovering resources and products from waste printed circuit boards. *Environ. Sci. Technol.* 41, 1995–2000. doi: 10.1021/es0618245
- Liu, J., Cui, L., and Losic, D. (2013a). Graphene and graphene oxide as new nanocarriers for drug delivery applications. *Acta Biomater.* 9, 9243–9257. doi: 10.1016/j.actbio.2013.08.016
- Liu, Y., Zhao, Y., Sun, B., and Chen, C. (2013b). Understanding the toxicity of carbon nanotubes. *Acc. Chem. Res.* 46, 702–713. doi: 10.1021/ar300028m
- Long, L., Sun, S., Zhong, S., Dai, W., Liu, J., and Song, W. (2010). A novel approach to recycling of glass fibers from nonmetal materials of waste printed circuit boards. *J. Hazard. Mater.* 177, 626–638. doi: 10.1016/j.jhazmat.2009.12.078
- Lu, W., Qin, X., Liu, S., Chang, G., Zhang, Y., Luo, Y., et al. (2012). Economical, green synthesis of fluorescent carbon nanoparticles and their use as probes for sensitive and selective detection of mercury(II) ions. *Anal. Chem.* 84, 5351–5357. doi: 10.1021/ac3007939
- Luda, P. M. (2011). Recycling of printed circuit boards. *Integr. Waste Managem. Vol. II (InTech)* 285–298.
- Luo, B., Liu, S., and Zhi, L. (2012). Chemical approaches toward graphene-based nanomaterials and their applications in energy-related areas. *Small* 8, 630–646. doi: 10.1002/smll.201101396
- Mankhand, T. R., Singh, K. K., Gupta, K., and Das, S. (2012). Pyrolysis of printed circuit boards. *Int. J. Metallurgical Eng.* 1, 102–107. doi: 10.5923/j.ijmee.20120106.01
- Manukyan, K. V., Rouvimov, S., Wolf, E. E., and Mukasyan, A. S. (2013). Combustion synthesis of graphene materials. *Carbon N. Y.* 62, 302–311. doi: 10.1016/j.carbon.2013.06.014
- Marek, A. A., Zawadiak, J., Piotrowski, T., and Hefczyc, B. (2015). A new efficient method for the processing of post-consumer polypropylene and other polyolefin wastes into polar waxes. *Waste Manag.* 46, 62–67. doi: 10.1016/j.wasman.2015.08.042
- Marinho, B., Ghislandi, M., Tkalya, E., Koning, C. E., and de With, G. (2012). Electrical conductivity of compacts of graphene, multi-wall carbon nanotubes, carbon black, and graphite powder. *Powder Technol.* 221, 351–358. doi: 10.1016/j.powtec.2012.01.024
- Maroufi, S., Mohammad, M., and Veena, S. (2017). Nano-carbons from waste tyre rubber: an insight into structure and morphology. *Waste Managem.* 69, 110–116. doi: 10.1016/j.wasman.2017.08.020
- Mata, M. T., Martins, A. A., Costa, A. V. C., and Sikdar, K. S. (2015). *Nanotechnology and Sustainability - Current Status and Future Challenges. Life Cycle Anal. Nanoparticles. Risk Assessment Sustain. DEStech Publ.* 271–306. Available online at: https://www.researchgate.net/profile/Antonio_Martins2/publication/280836162_Nanotechnology_and_Sustainability_-_Current_Status_and_Future_Challenges/links/55c8a54b08aea2d9bdc9158c.pdf
- Mdllovu, N. V., Chiang, C. L., Lin, K. S., and Jeng, R. C. (2018). Recycling copper nanoparticles from printed circuit board waste etchants via a microemulsion process. *J. Clean. Prod.* 185, 781–796. doi: 10.1016/j.jclepro.2018.03.087
- Mishra, N., Boeckl, J., Motta, N., and Iacopi, F. (2016). Graphene growth on silicon carbide: a review. *Phys. Status Solidi* 213, 2277–2289. doi: 10.1002/pssa.201600091
- Mishra, N., Das, G., Ansaldo, A., Genovese, A., Malerba, M., Povia, M., et al. (2012). Pyrolysis of waste polypropylene for the synthesis of carbon nanotubes. *J. Anal. Appl. Pyrolysis* 94, 91–98. doi: 10.1016/j.jaap.2011.11.012
- Mitrano, D. M., Motellier, S., Clavaguera, S., and Nowack, B. (2015). Review of nanomaterial aging and transformations through the life cycle of nano-enhanced products. *Environ. Int.* 77, 132–147. doi: 10.1016/j.envint.2015.01.013
- Moghaddasi, S., Khoshgoftarmansh, A. H., Karimzadeh, F., and Chaney, R. L. (2013). Preparation of nano-particles from waste tire rubber and evaluation of their effectiveness as zinc source for cucumber in nutrient solution culture. *Sci. Hortic. (Amsterdam)*. 160, 398–403. doi: 10.1016/j.scienta.2013.06.028
- Nair, R. R., Blake, P., Grigorenko, A. N., Novoselov, K. S., Booth, T. J., Stauber, T., et al. (2008). Fine structure constant defines visual transparency of graphene. *Science* 80, 320–1308. doi: 10.1126/science.1156965
- Nath, D. C. D., and Sahajwalla, V. (2011a). Growth mechanism of carbon nanotubes produced by pyrolysis of a composite film of poly (vinyl alcohol) and fly ash. *Appl. Phys. A Mater. Sci. Process.* 104, 539–544. doi: 10.1007/s00339-011-6405-1
- Nath, D. C. D., and Sahajwalla, V. (2011b). Application of fly ash as a catalyst for synthesis of carbon nanotube ribbons. *J. Hazard. Mater.* 192, 691–697. doi: 10.1016/j.jhazmat.2011.05.072
- Nath, D. C. D., and Sahajwalla, V. (2012). Analysis of carbon nanotubes produced by pyrolysis of composite film of poly (Vinyl Alcohol) and modified fly ash. *Mater. Sci. Appl.* 3, 103–109. doi: 10.4236/msa.2012.32016
- Nayak, P., Kumar, S., Sinha, I., and Singh, K. K. (2019). ZnO/CuO nanocomposites from recycled printed circuit board: preparation and photocatalytic properties. *Environ. Sci. Pollut. Res.* 26, 16279–16288. doi: 10.1007/s11356-019-04986-6
- Novoselov, K. S., Fal'Ko, V. I., Colombo, L., Gellert, P. R., Schwab, M. G., and Kim, K. (2012). A roadmap for graphene. *Nature* 490, 192–200. doi: 10.1038/nature11458
- Parasuram, B., Sundaram, S., Sathiskumar, C., and Karthikeyan, S. (2018). Synthesis of multi-walled carbon nanotubes using tire pyrolysis oil as a carbon precursor by spray pyrolysis method. *Inorg. Nano-Metal Chem.* 48, 103–106. doi: 10.1080/24701556.2017.1357578
- Park, E. K., Jung, B. B., Choi, W. Z., and Oh, S. K. (2017). A basic study on sorting of black plastics of waste electrical and electronic equipment (WEEE). *J. Korean Inst. Resour. Recycl.* 26, 69–77. doi: 10.7844/kirr.2017.26.1.69
- Pereira de Abreu, D. A., Cruz, J. M., and Losada, P. P. (2012). Active and intelligent packaging for the food industry. *Food Rev. Int.* 28, 146–187. doi: 10.1080/87559129.2011.595022
- Peres, E. C., Slaviero, J. C., Cunha, A. M., Hosseini-Bandegharai, A., and Dotto, G. L. (2018). Microwave synthesis of silica nanoparticles and its application for methylene blue adsorption. *J. Environ. Chem. Eng.* 6, 649–659. doi: 10.1016/j.jece.2017.12.062
- Peters, R. J. B., Bouwmeester, H., Gottardo, S., Amenta, V., Arena, M., Brandhoff, P., et al. (2016). Nanomaterials for products and application in agriculture, feed and food. *Trends Food Sci. Technol.* 54, 155–164. doi: 10.1016/j.tifs.2016.06.008
- Pol, V. G., and Thiagarajan, P. (2010). Remediating plastic waste into carbon nanotubes. *J. Environ. Monit.* 12, 455–459. doi: 10.1039/B914648B
- Quan, C., Li, A., and Gao, N. (2010). Synthesis of carbon nanotubes and porous carbons from printed circuit board waste pyrolysis oil. *J. Hazard. Mater.* 179, 911–917. doi: 10.1016/j.jhazmat.2010.03.092
- Quesnel, E., Roux, F., Emieux, F., Faucherand, P., Kymakis, E., Volonakis, G., et al. (2015). Graphene-based technologies for energy applications, challenges and perspectives. *2D Mater.* 2:030204. doi: 10.1088/2053-1583/2/3/030204
- Rahimi, A. R., and García, J. M. (2017). Chemical recycling of waste plastics for new materials production. *Nat. Rev. Chem.* 1, 1–11. doi: 10.1038/s41570-017-0046
- Rao, C. N. R., Sood, A. K., Subrahmanyam, K. S., and Govindaraj, A. (2009). Graphene: the new two-dimensional nanomaterial. *Angew. Chemie Int. Ed.* 48, 7752–7777. doi: 10.1002/anie.200901678
- Ritchie, H., and Roser, M. (2020). *Plastic Pollution*. Available online at: <https://ourworldindata.org/plastic-pollution>
- Rovani, S., Santos, J. J., Corio, P., and Fungaro, D. A. (2018). Highly pure silica nanoparticles with high adsorption capacity obtained from sugarcane waste ash. *ACS Omega* 3, 2618–2627. doi: 10.1021/acsomega.8b00092
- Roy, I., Sarkar, G., Mondal, S., Rana, D., Bhattacharyya, A., Saha, N. R., et al. (2016). Synthesis and characterization of graphene from waste dry cell battery for electronic applications. *RSC Adv.* 6, 10557–10564. doi: 10.1039/C5RA21112C
- Ruan, G., Sun, Z., Peng, Z., and Tour, J. M. (2011). Growth of graphene from food, insects, and waste. *ACS Nano* 5, 7601–7607. doi: 10.1021/nn202625c
- Samaddar, P., Ok, Y. S., Kim, K. H., Kwon, E. E., and Tsang, D. C. W. (2018). Synthesis of nanomaterials from various wastes and their new age applications. *J. Clean. Prod.* 197, 1190–1209. doi: 10.1016/j.jclepro.2018.06.262
- Sanchez, V. C., Pietruska, J. R., Miselis, N. R., Hurt, R. H., and Kane, A. B. (2009). Biopersistence and potential adverse health impacts of fibrous nanomaterials: what have we learned from asbestos? *Wiley Interdiscip. Rev. Nanomed. Nanobiotechnol.* 1, 511–529. doi: 10.1002/wnan.41

- Sardot, T., Smith, G., and McDonald, A. (2012). Valorizing mixed plastic wastes from cardboard recycling by amendment with wood, cement and ash. *J. Reinf. Plast. Compos.* 31, 1488–1497. doi: 10.1177/0731684412459984
- Sathiskumar, C., and Karthikeyan, S. (2019). Recycling of waste tires and its energy storage application of by-products – a review. *Sustain. Mater. Technol.* 22. doi: 10.1016/j.susmat.2019.e00125
- Shadjou, N., and Hasanzadeh, M. (2016). Graphene and its nanostructure derivatives for use in bone tissue engineering: recent advances. *J. Biomed. Mater. Res. Part A* 104, 1250–1275. doi: 10.1002/jbm.a.35645
- Sharma, S., Kalita, G., Hirano, R., Shinde, S. M., Papon, R., Ohtani, H., et al. (2014). Synthesis of graphene crystals from solid waste plastic by chemical vapor deposition. *Carbon N. Y.* 72, 66–73. doi: 10.1016/j.carbon.2014.01.051
- Shokri, A., Pahlevani, F., Levick, K., Cole, I., and Sahajwalla, V. (2017). Synthesis of copper-tin nanoparticles from old computer printed circuit boards. *J. Clean. Prod.* 142, 2586–2592. doi: 10.1016/j.jclepro.2016.11.017
- Singh, J., and Lee, B. K. (2016). Recovery of precious metals from low-grade automobile shredder residue: a novel approach for the recovery of nanozero-valent copper particles. *Waste Manag.* 48, 353–365. doi: 10.1016/j.wasman.2015.10.019
- Singh, N., Hui, D., Singh, R., Ahuja, I. P. S., Feo, L., and Fraternali, F. (2017). Recycling of plastic solid waste: a state of art review and future applications. *Compos. Part B Eng.* 115, 409–422. doi: 10.1016/j.compositesb.2016.09.013
- Smith, K. S., Hageman, P. L., Plumlee, G. S., Budahn, J. R., and Bleiwas, D. I. (2015). “Potential metal recovery from waste streams,” in *International Applied Geochemistry Symposium (IAGS)* (Tucson, AZ).
- Smolkova, B., El Yamani, N., Collins, A. R., Gutleb, A. C., and Dusinska, M. (2015). Nanoparticles in food: epigenetic changes induced by nanomaterials and possible impact on health. *Food Chem. Toxicol.* 77, 64–73. doi: 10.1016/j.fct.2014.12.015
- Sofi, M., Sabri, Y., Zhou, Z., and Mendis, P. (2019). Transforming municipal solid waste into construction materials. *Sustain* 11:2611. doi: 10.3390/su11092661
- Soldano, C., Mahmood, A., and Dujardin, E. (2010). Production, properties and potential of graphene. *Carbon N. Y.* 48, 2127–2150. doi: 10.1016/j.carbon.2010.01.058
- Sonawane, J. M., Yadav, A., Ghosh, P. C., and Adeloju, S. B. (2017). Recent advances in the development and utilization of modern anode materials for high performance microbial fuel cells. *Biosens. Bioelectron.* 90, 558–576. doi: 10.1016/j.bios.2016.10.014
- Søndergaard, R. R., Zimmermann, Y. S., Espinosa, N., Lenz, M., and Krebs, F. (2016). Incineration of organic solar cells: efficient end of life management by quantitative silver recovery. *Energy Environ. Sci.* 9, 857–861. doi: 10.1039/C6EE00021E
- Song, R., and Ji, Q. (2011). Synthesis of carbon nanotubes from polypropylene in the presence of Ni/Mo/MgO catalysts via combustion. *Chem. Lett.* 40, 1110–1112. doi: 10.1246/cl.2011.1110
- Stevens, G. C., and Goosey, M. (2009). “Materials used in manufacturing electrical and electronic products,” in *Electronic Waste Management* (Cambridge, UK: RSC Publishing), 40–74. doi: 10.1039/9781847559197-00040
- Strudwick, A. J., Weber, N. E., Schwab, M. G., Kettner, M., Weitz, R. T., Wunsch, J. R., et al. (2015). Chemical vapor deposition of high quality graphene films from carbon dioxide atmospheres. *ACS Nano* 9, 31–42. doi: 10.1021/nn504822m
- Sukanan, D. (2020). *Waste Imports Are Flooding Asian Countries Like Thailand*. Available at: <https://www.sustainability-times.com/environmental-protection/asian-countries-like-thailand-are-flooded-by-waste-imports/> (accessed May 10, 2020).
- Surwade, S. P., Smirnov, S. N., Vlassioulis, I. V., Unocic, R. R., Veith, G. M., Dai, S., et al. (2015). Water desalination using nanoporous single-layer graphene. *Nat. Nanotechnol.* 10, 459–464. doi: 10.1038/nnano.2015.37
- Tang, T., Chen, X., Meng, X., Chen, H., and Ding, Y. (2005). Synthesis of multiwalled carbon nanotubes by catalytic combustion of polypropylene. *Angew. Chemie Int. Ed.* 44, 1517–1520. doi: 10.1002/anie.200461506
- Tang, W., Li, Q., Gao, S., and Shang, J. K. (2011). Arsenic (III,V) removal from aqueous solution by ultrafine α -Fe₂O₃ nanoparticles synthesized from solvent thermal method. *J. Hazard. Mater.* 192, 131–138. doi: 10.1016/j.jhazmat.2011.04.111
- Tansel, B. (2017). From electronic consumer products to e-wastes: global outlook, waste quantities, recycling challenges. *Environ. Int.* 98, 35–45. doi: 10.1016/j.envint.2016.10.002
- Tatarants, M., Yousef, S., Sakalauskaite, S., Daugelavičius, R., Denafas, G., and Bendikiene, R. (2018). Antimicrobial copper nanoparticles synthesized from waste printed circuit boards using advanced chemical technology. *Waste Manag.* 78, 521–531. doi: 10.1016/j.wasman.2018.06.016
- Thai, Q. B., Le, D. K., Luu, T. P., Hoang, N., Nguyen, D., and Duong, H. M. (2019). Aerogels from wastes and their applications. *JOJ Mater. Sci.* 5:555663. doi: 10.19080/JOJMS.2019.05.555663
- Tran, D. T., Joubert, A., Venditti, D., Durecu, S., Meunier, T., Le Bihan, O., et al. (2017). Characterization of polymer waste containing nano-fillers prior its end-of-life treatment. *Waste Biomass Valorization* 8, 2463–2471. doi: 10.1007/s12649-016-9757-0
- Tripathi, P. K., Durbach, S., and Coville, N. J. (2017). Synthesis of multi-walled carbon nanotubes from plastic waste using a stainless-steel CVD reactor as catalyst. *Nanomater* 7:284. doi: 10.3390/nano7100284
- Turcheniuk, K., and Mochalin, V. N. (2017). Biomedical applications of nanodiamond (Review). *Nanotechnology* 28, 252001. doi: 10.1088/1361-6528/aa6ae4
- Turgut, P., and Yesilata, B. (2008). Physico-mechanical and thermal performances of newly developed rubber-added bricks. *Energy Build.* 40, 679–688. doi: 10.1016/j.enbuild.2007.05.002
- UNEP (2018). *SINGLE-USE PLASTICS A Roadmap for Sustainability*.
- UNEP (2020). *Solid Waste Management | UNEP - UN Environment Programme*. Available online at: <https://www.unenvironment.org/explore-topics/resource-efficiency/what-we-do/cities/solid-waste-management> (accessed May 10, 2020).
- Urbina, J., Patil, A., Fujishima, K., Paulino-Lima, G., Saltikov, C., and Rothschild, L. J. (2019). A new approach to biomining: bioengineering surfaces for metal recovery from aqueous solutions. *Sci. Reports (Nature Publ. Group)* 9, 16422. doi: 10.1038/s41598-019-52778-2
- Valko, M., Morris, H., and Cronin, M. T. D. (2005). *Metals, Toxicity and Oxidative Stress*. doi: 10.2174/0929867053764635
- Verma, M. L., Puri, M., and Barrow, C. J. (2016). Recent trends in nanomaterials immobilised enzymes for biofuel production. *Crit. Rev. Biotechnol.* 36, 108–119. doi: 10.3109/07388551.2014.928811
- Vermisoglou, E. C., Giannouri, M., Todorova, N., Giannakopoulou, T., Lekakou, C., and Trapalis, C. (2016). Recycling of typical supercapacitor materials. *Waste Manag. Res.* 34, 337–344. doi: 10.1177/0734242X15625373
- Wang, H., Gao, B., Fang, J., Ok, Y. S., Xue, Y., Yang, K., et al. (2018). Engineered biochar derived from eggshell-treated biomass for removal of aqueous lead. *Ecol. Eng.* 121, 124–129. doi: 10.1016/j.ecoleng.2017.06.029
- Westerhoff, P. K., Kiser, A., and Hristovski, K. (2013). Nanomaterial removal and transformation during biological wastewater treatment. *Environ. Eng. Sci.* 30, 109–117. doi: 10.1089/ees.2012.0340
- Wibowo, S., Deng, H., and Zhang, X. (2014). “Evaluating the performance of e-waste recycling programs using fuzzy multiattribute group decision making model,” in *Proceedings of the 2014 9th IEEE Conference on Industrial Electronics and Applications, ICIEA 2014* (Institute of Electrical and Electronics Engineers Inc.), 1989–1994. doi: 10.1109/ICIEA.2014.6931495
- Wu, C., Wang, Z., Wang, L., Williams, P. T., and Huang, J. (2012). Sustainable processing of waste plastics to produce high yield hydrogen-rich synthesis gas and high quality carbon nanotubes. *RSC Adv.* 2, 4045–4047. doi: 10.1039/c2ra20261a
- Wu, Z. J., Huang, W., Cui, K. K., Gao, Z. F., and Wang, P. (2014). Sustainable synthesis of metals-doped ZnO nanoparticles from zinc-bearing dust for photodegradation of phenol. *J. Hazard. Mater.* 278, 91–99. doi: 10.1016/j.jhazmat.2014.06.001
- Xiang, X., Xia, F., Zhan, L., and Xie, B. (2015). Preparation of zinc nano structured particles from spent zinc manganese batteries by vacuum separation and inert gas condensation. *Sep. Purif. Technol.* 142, 227–233. doi: 10.1016/j.seppur.2015.01.014
- Xiu, F. R., and Zhang, F. S. (2009). Preparation of nano-Cu₂O/TiO₂ photocatalyst from waste printed circuit boards by electrokinetic process. *J. Hazard. Mater.* 172, 1458–1463. doi: 10.1016/j.jhazmat.2009.08.012
- Xiu, F. R., and Zhang, F. S. (2012). Size-controlled preparation of Cu₂O nanoparticles from waste printed circuit boards by supercritical water combined with electrokinetic process. *J. Hazard. Mater.* 233–234, 200–206. doi: 10.1016/j.jhazmat.2012.07.019

- Xu, Y., Li, J., and Liu, L. (2016). Current status and future perspective of recycling copper by hydrometallurgy from waste printed circuit boards. *Procedia Environ. Sci.* 31, 162–170. doi: 10.1016/j.proenv.2016.02.022
- Yang, K., Feng, L., and Liu, Z. (2016a). Stimuli responsive drug delivery systems based on nano-graphene for cancer therapy. *Adv. Drug Deliv. Rev.* 105, 228–241. doi: 10.1016/j.addr.2016.05.015
- Yang, R. X., Chuang, K. H., and Wey, M. Y. (2016b). Carbon nanotube and hydrogen production from waste plastic gasification over Ni/Al-SBA-15 catalysts: effect of aluminum content. *RSC Adv.* 6, 40731–40740. doi: 10.1039/C6RA04546D
- Yang, Z., Tian, J., Yin, Z., Cui, C., Qian, W., and Wei, F. (2019). Carbon nanotube- and graphene-based nanomaterials and applications in high-voltage supercapacitor: a review. *Carbon N. Y.* 141, 467–480. doi: 10.1016/j.carbon.2018.10.010
- Yousef, S., Tatarians, M., Makarevičius, V., Lukošius, S. I., Bendikiene, R., and Denafas, G. (2018). A strategy for synthesis of copper nanoparticles from recovered metal of waste printed circuit boards. *J. Clean. Prod.* 185, 653–664. doi: 10.1016/j.jclepro.2018.03.036
- Zeng, W., and Bai, H. (2016). High-performance CO₂ capture on amine-functionalized hierarchically porous silica nanoparticles prepared by a simple template-free method. *Adsorption* 22, 117–127. doi: 10.1007/s10450-015-9698-0
- Zeng, X., Yang, C., Chiang, J. F., and Li, J. (2017). Innovating e-waste management: from macroscopic to microscopic scales. *Sci. Total Environ.* 575, 1–5. doi: 10.1016/j.scitotenv.2016.09.078
- Zhan, L., Xiang, X., Xie, B., and Sun, J. (2016). A novel method of preparing highly dispersed spherical lead nanoparticles from solders of waste printed circuit boards. *Chem. Eng. J.* 303, 261–267. doi: 10.1016/j.cej.2016.06.002
- Zhang, H., Bussini, D., Hortal, M., Elegir, G., Mendes, J., and Jordá Beneyto, M. (2016). PLA coated paper containing active inorganic nanoparticles: material characterization and fate of nanoparticles in the paper recycling process. *Waste Manag.* 52, 339–345. doi: 10.1016/j.wasman.2016.03.045
- Zhang, H., Xia, B., Wang, P., Wang, Y., Li, Z., Wang, Y., et al. (2020). From waste to waste treatment: mesoporous magnetic NiFe₂O₄/ZnCuCr-layered double hydroxide composite for wastewater treatment. *J. Alloys Compd.* 819, 153053. doi: 10.1016/j.jallcom.2019.153053
- Zhang, J., Li, J., Cao, J., and Qian, Y. (2008). Synthesis and characterization of larger diameter carbon nanotubes from catalytic pyrolysis of polypropylene. *Mater. Lett.* 62, 1839–1842. doi: 10.1016/j.matlet.2007.10.015
- Zhao, Y. M., Duan, C. L., Wu, L. L., Zhang, H. J., He, J. F., and He, Y. Q. (2012). The separation mechanism and application of a tapered diameter separation bed. *Int. J. Environ. Sci. Technol.* 9, 719–728. doi: 10.1007/s13762-012-0105-z
- Zheng, Y., Yanful, E. K., and Bassi, A. S. (2005). A review of plastic waste biodegradation. *Crit. Rev. Biotechnol.* 25, 243–250. doi: 10.1080/07388550500346359
- Zhou, H., Su, M., Lee, P. H., and Shih, K. (2017). Synthesis of submicron lead oxide particles from the simulated spent lead paste for battery anodes. *J. Alloys Compd.* 690, 101–107. doi: 10.1016/j.jallcom.2016.08.094
- Zhuo, C., Brendan, H., Henning, R., and Yiannis, L. (2010). Synthesis of carbon nanotubes by sequential pyrolysis and combustion of polyethylene. *Carbon* 48, 4024–4034. doi: 10.1016/j.carbon.2010.07.007
- Zhuo, C., and Levendis, Y. A. (2014). Upcycling waste plastics into carbon nanomaterials: a review. *J. Appl. Polym. Sci.* 131:931. doi: 10.1002/app.39931

Conflict of Interest: The authors declare that the research was conducted in the absence of any commercial or financial relationships that could be construed as a potential conflict of interest.

Copyright © 2020 Abdelbasir, McCourt, Lee and Vanegas. This is an open-access article distributed under the terms of the Creative Commons Attribution License (CC BY). The use, distribution or reproduction in other forums is permitted, provided the original author(s) and the copyright owner(s) are credited and that the original publication in this journal is cited, in accordance with accepted academic practice. No use, distribution or reproduction is permitted which does not comply with these terms.



Adsorption of Orange II Onto Zn₂Al-Layered Double Hydroxide Prepared From Zinc Ash

Andra Tămaș¹, Ioana Cozma², Laura Cochei^{1*}, Lavinia Lupa^{1*} and Gerlinde Rusu¹

¹ Faculty of Industrial Chemistry and Environmental Engineering, University Politehnica Timisoara, Timisoara, Romania,

² "Coriolan Dragulescu" Institute of Chemistry, Timisoara, Romania

OPEN ACCESS

Edited by:

Enrico Traversa,
University of Electronic Science and
Technology of China, China

Reviewed by:

Priyanka Sharma,
Stony Brook University, United States
Inderjeet Tyagi,
Zoological Survey of India, India

*Correspondence:

Laura Cochei
laura.cochei@upt.ro
Lavinia Lupa
lavinia.lupa@upt.ro

Specialty section:

This article was submitted to
Green and Sustainable Chemistry,
a section of the journal
Frontiers in Chemistry

Received: 17 June 2020

Accepted: 07 October 2020

Published: 30 November 2020

Citation:

Tămaș A, Cozma I, Cochei L, Lupa L
and Rusu G (2020) Adsorption of
Orange II Onto Zn₂Al-Layered Double
Hydroxide Prepared From Zinc Ash.
Front. Chem. 8:573535.
doi: 10.3389/fchem.2020.573535

The dye industry is one of the largest water consuming industries, and at the same time generates large quantities of wastewaters. The resulting wastewaters require proper treatment before discharge, because the dye contents have a negative effect on the water body and organisms present in it. The most efficient treatment method for water containing dyes is represented by adsorption processes. The challenge with these adsorption processes is to develop new, efficient, viable, and economic adsorbent materials. Therefore, in the present paper, the performance of Zn₂Al-layered double hydroxide, prepared from an industrial waste (zinc ash) as a zinc source, was investigated in the Orange II dye adsorption process. The Zn₂Al-layered double hydroxide prepared from secondary sources presents similar morphological and structural characteristics as those prepared from analytical grade reagents. The influence of initial dye concentration, adsorption time, solid:liquid ratio, pH, and temperature was evaluated in order to confirm the benefit of this waste valorization. A comparison with the reference Zn₂Al-layered double hydroxide prepared from analytical grade reagents was performed and the results show that due to the small presence of impurities, the material prepared from zinc ash shows better adsorption capacities ($q_{\text{max,exp}} = 42.5 \text{ mg/g}$ at 293 K) than the material prepared from reagents ($q_{\text{max,exp}} = 36.9 \text{ mg/g}$ at 293 K), justifying the utilization of secondary sources for layered double hydroxides preparation. The proposed treatment process presents advantages from both economic and environmental protection point of view.

Keywords: layered double hydroxides, zinc ash waste, Orange II adsorption, equilibrium, kinetics, thermodynamics

INTRODUCTION

Synthetic dyes are used in many industries, such as the textile, plastics, leather, pharmaceutical, paint, and electroplating industries. Their intensive use leads to an increase of discharged effluents with dye content in water streams, representing an increased danger for environmental protection and human health (Jin et al., 2008; Hsiu-Mei et al., 2009; Kousha et al., 2012). In particular, the International Agency for Research on Cancer (IARC) classified Orange II dye as a category 3 carcinogen in humans (Pan et al., 2011). Their property of fast dispersion in water and their complex aromatic structure slow down the efficiency of the water treatment process, such as biological treatment and the oxidation processes (Abramian and El-Rassy, 2009; Hsiu-Mei et al., 2009; Jin et al., 2014; Asfaram et al., 2015; Ghaedi et al., 2015).

From all the conventional processes used for treatment of water containing dye pollutants, adsorption proved to be the most efficient. If the formation of toxic sludge is avoided, it could be used for a wide range of water compositions—implying low operational costs (Bouhent et al., 2011; Mahmoodi et al., 2011; Kousha et al., 2012; Kaur et al., 2015). The most important factor which has the greatest influence on the efficiency of an adsorption process is represented by the adsorbent material type. An efficient adsorbent material must fulfill the following criteria: high adsorption kinetics, great selectivity, high adsorption capacity, thermal and chemical stability, and easy preparation. These properties are accomplished by layered double hydroxides (LDHs), also called hydrotalcite-like compounds, due to their distinctive characteristics; positively charged metal hydroxide layers and interlayer balancing anions which lead to large interlayer spaces, tunable chemical composition, and the reasonable number of exchangeable anions (Aguilar et al., 2013; Lafi et al., 2016; Mandal and Sandhya, 2019). In the last few years, in order to decrease the synthesis costs and also to reduce the quantity of waste discharged in the environment, attention has been focused on the LDH synthesis starting from secondary sources (Li et al., 2012; Murayama et al., 2012; Santini and Fey, 2012; Barik et al., 2014). Therefore, the novelty of this paper consists of the use of a Zn₂Al-layered double hydroxide, prepared from an industrial waste zinc source (zinc ash), as the adsorbent material in the removal process of Orange II dye from aqueous solutions. The influence of initial dye concentration, time of adsorption, solid:liquid ratio, pH, and temperature was evaluated in order to confirm the benefit of this waste valorization. A comparison of the adsorption performance of the studied materials with a reference Zn₂Al-layered double hydroxide, prepared from analytical grade reagents, was performed. The proposed method of using, as adsorbent materials, LDH obtained from an industrial waste, presents multiple advantages, such as: decreasing the waste discharged in the environment, minimizing the use of primary materials, and reducing costs of the adsorption process.

MATERIALS AND METHODS

All reagents utilized in this study were purchased from Merck (Germany) and were used as received. The layered double hydroxides (Zn₂Al-CO₃ - type) utilized in this study were prepared and characterized in a previous study (Cocheci et al., 2018). The sample Zn₂Al - R was prepared by starting of analytical grade reagents and utilizing the co-precipitation at low oversaturation method, as described by Cavani et al. (1991). The sample Zn₂Al - W was prepared starting from fine grained zinc ash ($d < 0.315$ mm), a waste produced by the hot-dip galvanizing process. The schematic procedure of the Zn₂Al - W sample preparation is presented in **Figure 1**. After mixing the zinc ash with 20% HCl in order for zinc dissolution to occur, the zinc chloride solution was separated by filtration from unreacted compounds and utilized as a zinc precursor for the Zn₂Al - type layered double hydroxide preparation, by utilizing the same co-precipitation method. The zinc chloride

solution was mixed with a defined quantity of aluminum nitrate in order to obtain a molar ratio $\text{Zn}^{2+} : \text{Al}^{3+} = 2 : 1$ and a total molar concentration of the 1 M in 200 cm³ metal precursors solution. This solution was added drop by drop to a Na₂CO₃ 1M solution under vigorous magnetic stirring. The pH was kept constant to pH = 10.5 by adding a 2M NaOH solution and was monitored with an InoLab pH-meter. After total addition of metal precursors solution, the precipitate was aged at 70°C overnight, washed with distilled water until all impurities and unreacted compounds were removed, filtered, and dried at 70°C. The LDH samples were crushed and sieved in order to obtain particles with dimensions <90 µm.

The structural characterization of prepared LDH reveals that the sample prepared from zinc ash has similar characteristics to the sample prepared from analytical grade reagents **Supplementary Table 1** presents the unit cell parameters for the two materials and the morphological characteristics (BET surface area and the pore volumes) for the synthesized samples (Cocheci et al., 2018). The SEM images are presented in **Figure 2**, together with the EDX spectra. From the SEM images of the materials, it is evident that the formation of highly agglomerated hexagonal plates with different sizes and good crystallinity, stacked with one another—this behavior being well-known for this type of materials synthesized by a co-precipitation method. In case of LDH-W (**Figure 2A**), due to the presence of a small quantity of impurities (Fe, Pb, Ca) from the zinc ash, an inhomogeneity of the surface and a smaller crystallinity is evidenced.

Orange II dye adsorption experiments were developed in batch mode in order to obtain information about the adsorptive behavior of the two materials. In order to study the benefit of waste valorization onto LDH, kinetic, thermodynamics and equilibrium studies were performed. The kinetic studies were performed studying the influence of different parameters such as: pH, solid:liquid ratio, initial dye concentration, and temperature at various stirring times upon the adsorption performance developed by the two studied LDHs. The adsorption characteristics were obtained by contacting a defined amount of adsorbent (Zn₂Al - R or Zn₂Al - W) with 50 cm³ solutions of different concentrations of dye (10 – 200 mg/L).

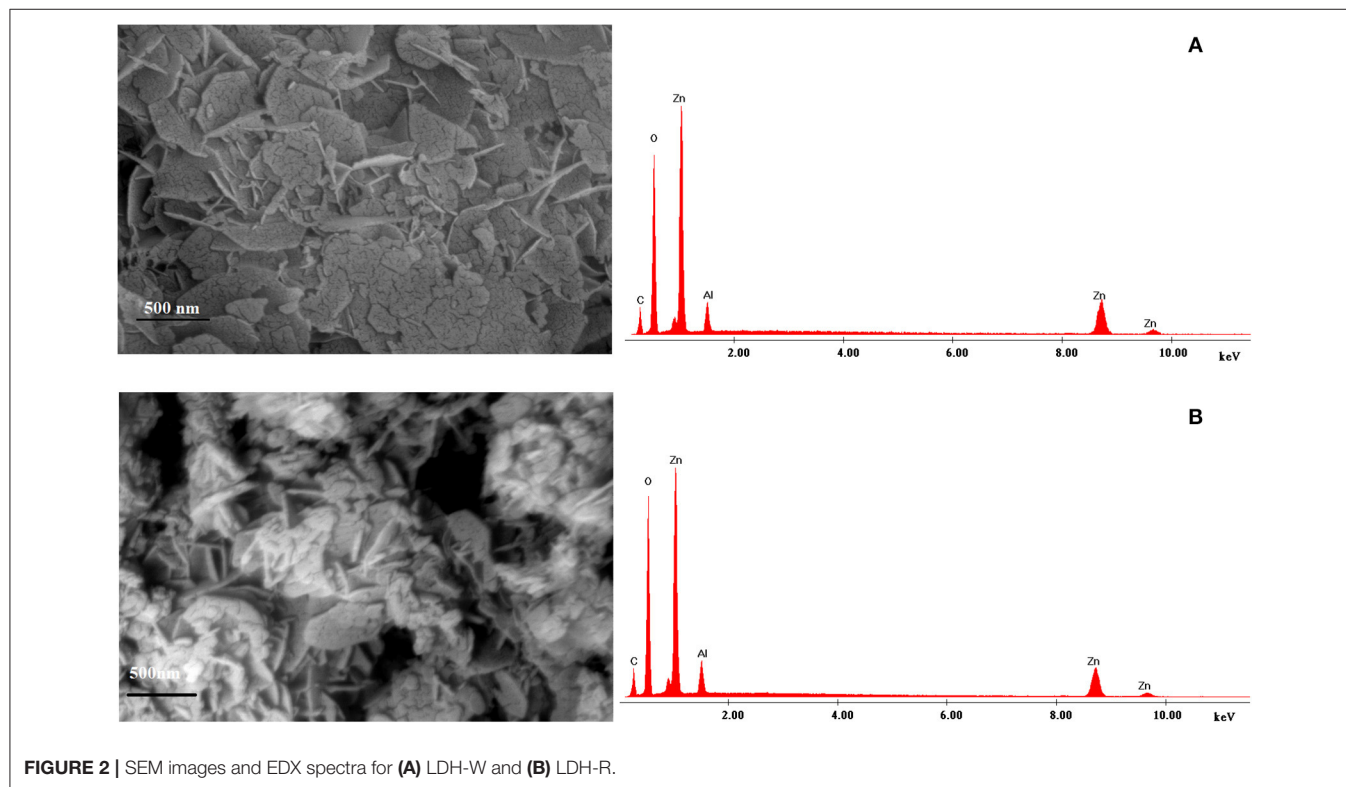
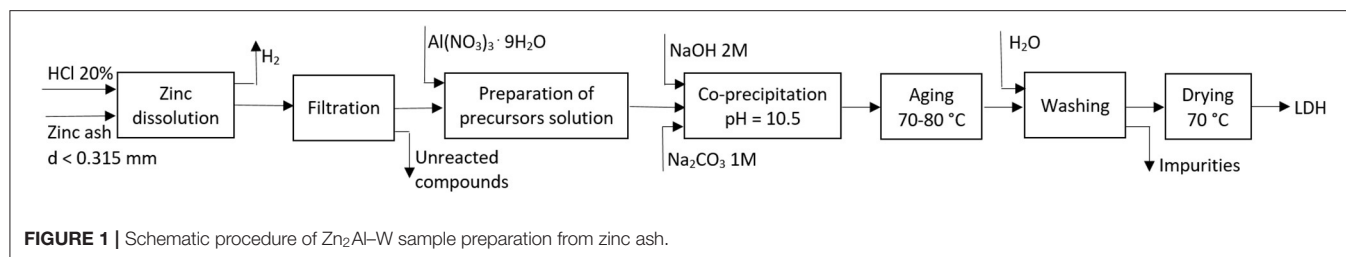
The adsorption capacity at equilibrium (q_e) and at time t (q_t) were calculated taking into account the mass balance of Orange II dye adsorbed onto the LDH surface:

$$q_e = \frac{(C_0 - C_e) \cdot V}{m} \quad (1)$$

where q_e is the adsorption capacity of adsorbent at equilibrium (mg/g), V the volume of the solution (L), C_0 (mg/L) and C_e (mg/L) the initial and equilibrium concentrations of Orange II, and m the mass of adsorbent (g).

$$q_t = \frac{(C_0 - C_t) \cdot V}{m} \quad (2)$$

where q_t is the adsorption capacity of adsorbent at time t (mg/g), V the volume of the solution (L), C_0 (mg/L) the initial



concentration of Orange II, and C_t (mg/L) the concentration of Orange II at time t , and m the mass of adsorbent (g).

The structural characterization of exhausted materials after adsorption was performed by utilization of XRD and FTIR techniques. The X-ray diffractograms were recorded using a Rigaku Ultima IV X-ray diffractometer (40 kV, 40 mA) with $\text{CuK}\alpha$ radiation. The Fourier-transform infrared spectra (FTIR) were recorded in the domain $400\text{--}4,000\text{ cm}^{-1}$ using Bruker Vertex 70 FTIR equipment. The concentrations of Orange II dye solutions were spectrometrically determined at 480 nm using a Varian 100 UV-VIZ spectrometer.

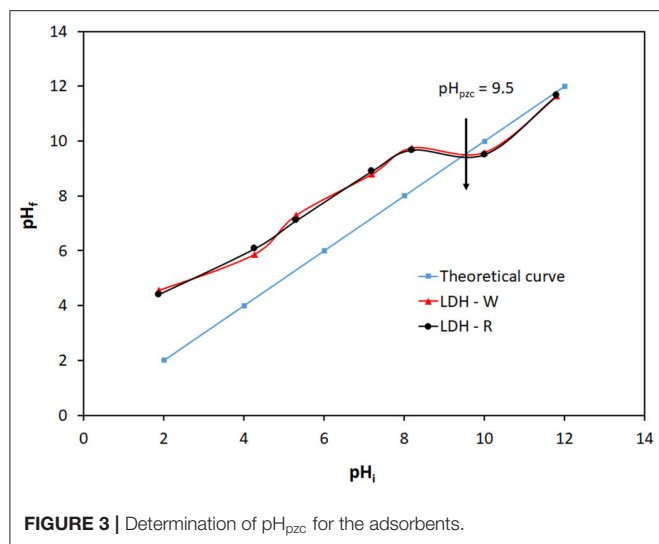
RESULTS AND DISCUSSION

Determination of pH_{pzc} for the Adsorbents

Due to the fact that layered double hydroxides consist in positive layers of mixed metal hydroxides, the pH of working solutions plays an important role in the adsorption behavior of these materials. Depending on the value of the initial pH of the working

solution, the surface of the materials can be either negatively charged, neutral at a particular pH, or positively charged. The value of pH at which the surface of the materials is neutral (the so-called pH of point of zero charged pH_{pzc}) was determined by contacting 0.0050 g of solid materials with 50 cm^3 of solutions of HNO_3 or NaOH with defined pH_i values. After 24 h of mixing, the values of final pH (pH_f) of the solutions were determined. By plotting $\text{pH}_f = f(\text{pH}_i)$, the pH_{pzc} can be determined as the intersection point of the obtained curve with the theoretical curve $\text{pH}_i = \text{pH}_f$. The pH of point of zero charged for the studied materials is presented in Figure 3.

From Figure 3 it can be observed that the behavior of the materials (LDH – R, prepared from analytical grade reagents and LDH – W, prepared from waste) is similar and the $\text{pH} = 9.5$ represents the point of zero charge of the surfaces for both materials. At pH values lower than $\text{pH}_{\text{pzc}} = 9.5$ the surface of LDH became positive due to the protonation effect, while at pH values greater than $\text{pH}_{\text{pzc}} = 9.5$ the surface of LDH became negative due to the deprotonation effect (Xu et al., 2008). From



a practical point of view, if the initial pH of the working solution has values lower than $\text{pH} = 4$, or greater than $\text{pH} = 12$, the mixed hydroxides can be dissolved.

On the other hand, the Orange II dye exists in aqueous solutions in various forms (Bourikas et al., 2005), but in the pH range of 2 – 9 only the partial ionized species (HL^-) is present; the fully ionized species being predominant at $\text{pH} > 12$ (Zaheer et al., 2019).

Kinetic Studies

At Different pH Values

The studies about pH influence on the adsorption process were performed by starting with 40 mg/L dye solutions, 1 g/L solid:liquid ratio, and an experimental temperature of 20°C. The influence of pH on the adsorption process is presented in **Figure 4A**.

It is evident that acidic conditions are favorable for the adsorption capacity of materials. As the pH of the dye solution increases, the adsorption capacity decreases. Comparing the sample prepared from analytical grade reagent (LDH – R) and that prepared from waste (LDH – W), at $\text{pH} = 4$ and after 90 min of adsorption, the adsorption capacities are similar. At initial $\text{pH} = 6.3$, the LDH prepared from waste (sample LDH – W) adsorbed better than the sample LDH – R (prepared from analytical grade reagents). We decided to run the following experiments at natural pH of initial Orange II solutions ($5 < \text{pH} < 7$) for practical convenience. It can also be observed that at each pH and for both studied adsorbents, the quantity of the adsorbed dye takes place very fast in the first 5 min of stirring. After that, the increase of the adsorption capacity is not so significant.

At Different Solid:Liquid Ratios

To study the influence of the quantity of adsorbent material on the removal of Orange II dye, different amounts of LDH were added, ranging between 25–100 mg, into the flask containing 50 mL of dye solution. The experiments were performed at $\text{pH} \sim 6.3$, temperature 293K and the initial dye concentration of 40

mg/L. The resulting suspensions were stirred in a Julabo SW 22 multishaker at 200 rot/min. The samples were removed from stirring at predetermined time intervals and solids were removed by filtration and the filtrate was analyzed to establish the residual dye concentration. The results are shown in **Figure 4B**.

It is evident that the increase in the adsorbent dose lead to the decrease of the quantity of adsorbed dye. In case of the highest S:L ratio there is not a great difference between the adsorption capacity developed by the studied adsorbent. At a lower S:L ratio the adsorption capacity developed by LDH-W is higher than the adsorption capacity developed by LDH-R. Because the main purpose is to decrease the treatment costs, it is more efficient to use a lower S:L ratio. Therefore, further studies were performed using 1 g of LDH for the treatment of 1 L of aqueous solutions containing Orange II. By studying the second parameters, solid:liquid ratio, at different stirring times, the same conclusion can be drawn—that the main quantity of dye is adsorbed in the first 5 min of stirring. At higher stirring time, the adsorption capacity presents a slow increase, regardless of working conditions.

At Different Initial Concentrations of Dye

The effect of stirring time upon the adsorption performance was also studied using three different initial concentrations of dye (20, 40 and 80 mg/L). The experiments were performed at $\text{pH} \sim 6.3$, temperature 293K, and the dosage of adsorbent 1 g/L. The results are shown in **Figure 4C**.

The difference between the adsorption capacities developed by the two studied adsorbents is more relevant when it is used at higher initial concentrations of Orange II in solution. The presence, in the LDH structure (in case of the LDH-W, obtained from waste), of impurities (such as: Fe, Ca, Pb) lead to the decrease of its crystallinity, conferring inhomogeneity to the adsorbent surface and increasing the number of available sites for dye adsorption (Cocheci et al., 2018). At the same time, the LDH obtained from waste presents larger pores. All of this leads to the fact that LDH-W develops much higher adsorption capacity than LDH-R in the removal process of Orange II from aqueous solutions.

The performance of the studied materials developed in the adsorption process of Orange II from aqueous solutions was compared with the adsorption performance of other materials reported in specialty literature (**Table 1**). It can be observed that the Zn₂Al-LDH prepared from secondary sources present better adsorption capacity than other similar materials studied for the removal of Orange II from aqueous solutions.

At Different Temperatures

The kinetic studies were also performed at three different temperatures (293, 308, and 323 K) in order to determine the effect of temperature on the Orange II adsorption process, using LDH-R and LDH-W as adsorbent materials. The experiments were performed at $\text{pH} \sim 6.3$, the initial dye concentration of 40 mg/L and the dosage of adsorbent 1 g/L. The results are shown in **Figure 4D**.

The temperature increase lead to a slow increase of the quantity of dye adsorbed onto the studied materials. At the

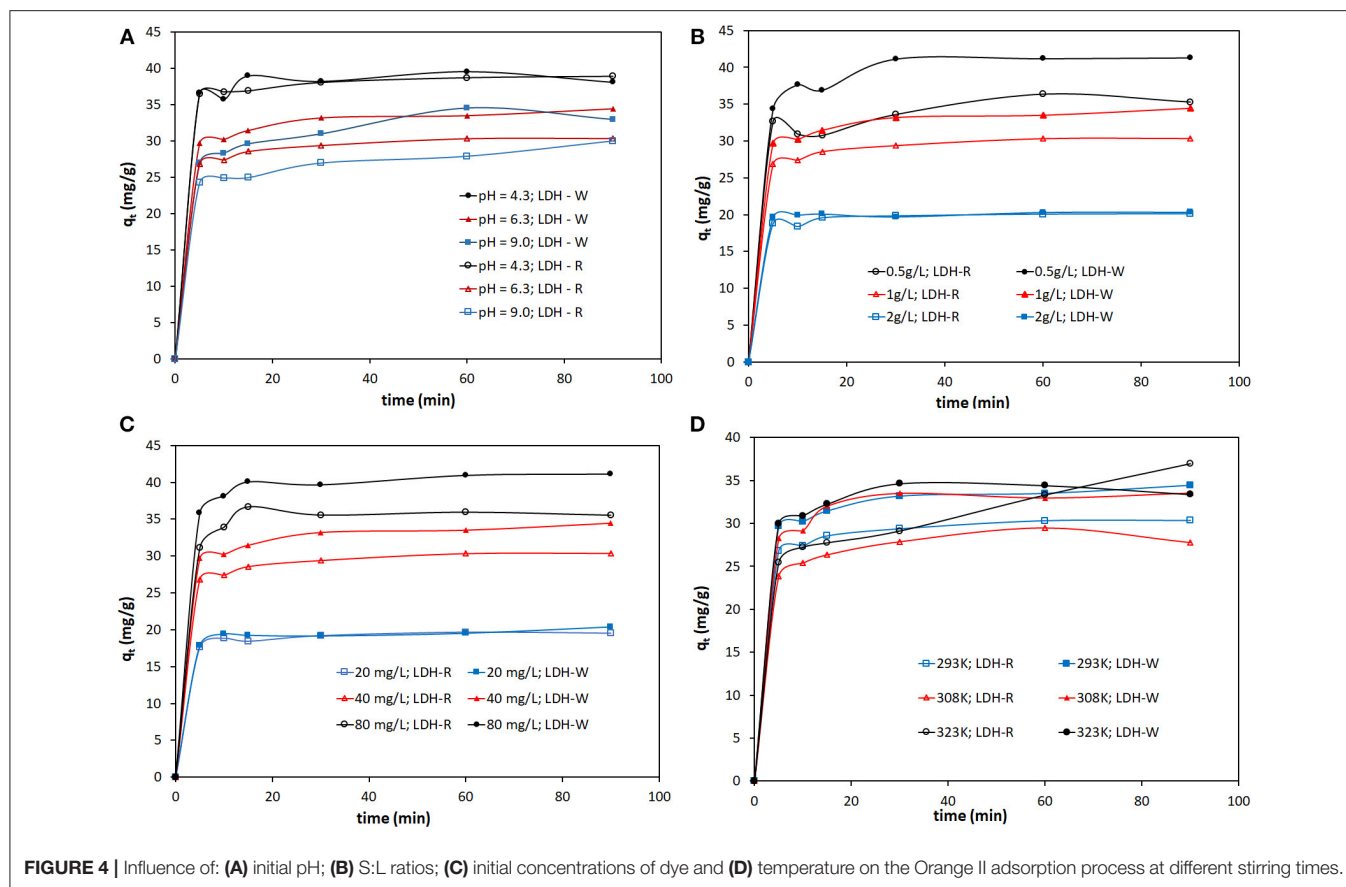


FIGURE 4 | Influence of: (A) initial pH; (B) S:L ratios; (C) initial concentrations of dye and (D) temperature on the Orange II adsorption process at different stirring times.

TABLE 1 | The comparison between the adsorption capacities of similar adsorbents developed in the treatment processes of aqueous solutions containing Orange II.

Adsorbent	q_m , mg/g	References
HDTMA coated zeolite	33.9	Jin et al., 2014
DMDOA-palygorskite (100% CEC equivalent modification)	38.61	Sarkar et al., 2011
2% Hexadecylammonium bromide (HDTMA)-modified zeolite	3.38	Jin et al., 2008
Spent brewery grains	28.54	Silva et al., 2004
Bottom ash	13.24	Gupta et al., 2006
LDH-R	35.75	Present paper
LDH-W	42.5	

same temperature, the LDH obtained from waste developed a higher adsorption performance than the LDH obtained from the reagent.

It can be concluded that the equilibrium between the studied LDHs and the adsorbate is achieved quite quickly, regardless of working parameters. The largest quantity of Orange II is retained by the studied LDHs in the first 5 min of stirring, then the adsorption capacities of the material present a slow increase in time due to the decrease of the active site available for adsorption.

After 15 min of contact between the two phases, the adsorption capacities of the studied materials are not influenced by the stirring time. It can be concluded that the studied layered double hydroxides are more efficient adsorbent materials for Orange II removal, than other adsorbents reported in literature due to the fact that in this case the equilibrium is achieved more quickly. In case of Orange II adsorption onto metal-Organic Framework (MOF) iron-benzenetricarboxylate (Fe(BTC)), the equilibrium is achieved between 80 and 140 min (García et al., 2014) and through adsorption onto phosphoric-acid modified clam shell powder after 90 min of stirring (Ma et al., 2013).

In order to investigate the mechanism of adsorption of Orange II onto LDH-R and LDH-W, kinetic models are used to test the experimental data. The experimental curves were fitted with the linear forms of the pseudo-first order (PFO) (Equation 3) (Georgin et al., 2016) and pseudo-second order (PSO) (Equation 4) (Hu et al., 2010; Plazinski et al., 2013; Georgin et al., 2016; Zaheer et al., 2019) models:

$$\ln(q_e - q_t) = \ln q_e - k_1 t \quad (3)$$

$$\frac{t}{q_t} = \frac{1}{k_2 \cdot q_e^2} + \frac{1}{q_e} \cdot t \quad (4)$$

where k_1 (min^{-1}) and k_2 ($\text{g mg}^{-1} \text{min}^{-1}$) are the rate constants of the PFO and PSO models, respectively; q_e and q_t (mg g^{-1}) are

the equilibrium adsorption capacity and the adsorption capacity at time t (min), respectively.

The kinetic parameters k_1 and q_e were determined from the slope and intercept of the linear plot $\ln(q_e - q_t)$ vs. t (figures omitted for the sake of brevity). For the PSO the graphical representations of $t/q_t = f(t)$ were used in order to determine the kinetic parameters k_2 and q_e (Figure 5). The kinetic parameter

together with the obtained correlation coefficients are presented in **Supplementary Table 2**.

The plots of t/q_t vs. t show good linearity, regardless of the working conditions, implying that the adsorption system follows the pseudo-second-order kinetic model. In all cases the correlations coefficients obtained for the fitting of the experimental data with the PSO model is close to unity compared

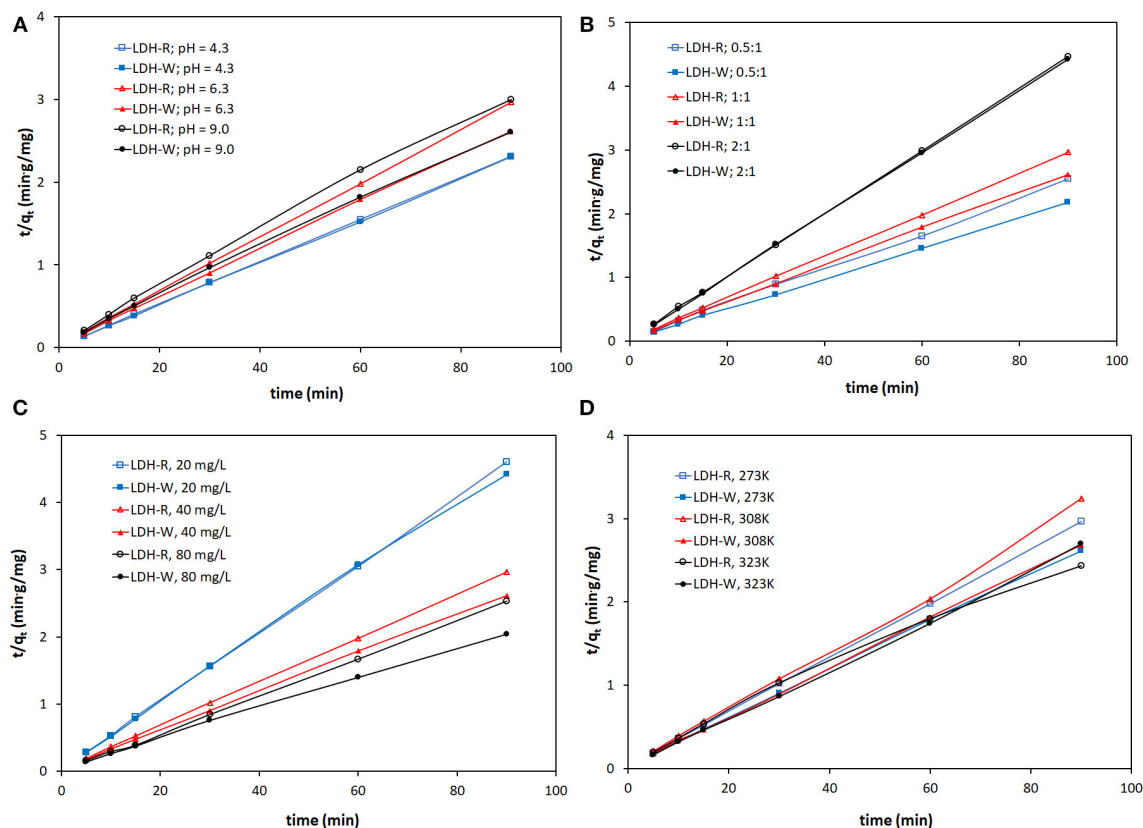


FIGURE 5 | Pseudo-second-order kinetic models for adsorption of Orange II at: (A) different pH; (B) different S:L ratio; (C) different dye concentrations; (D) different temperatures.

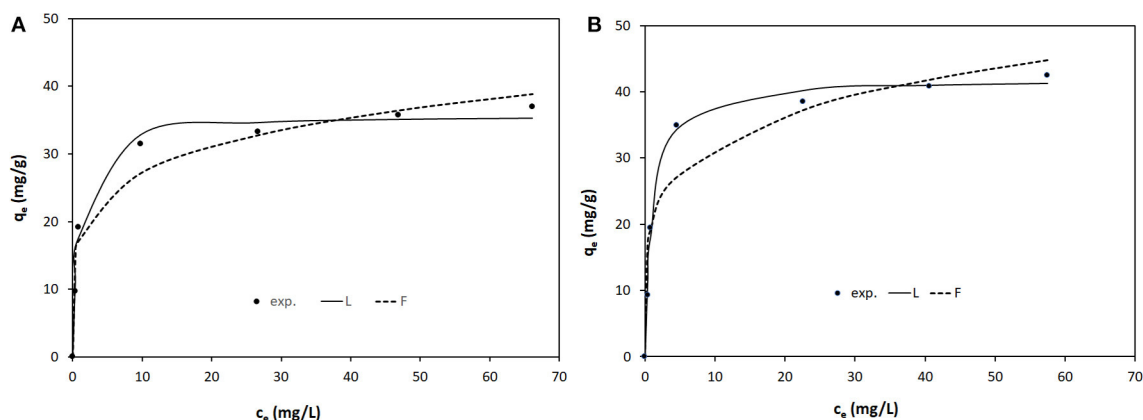
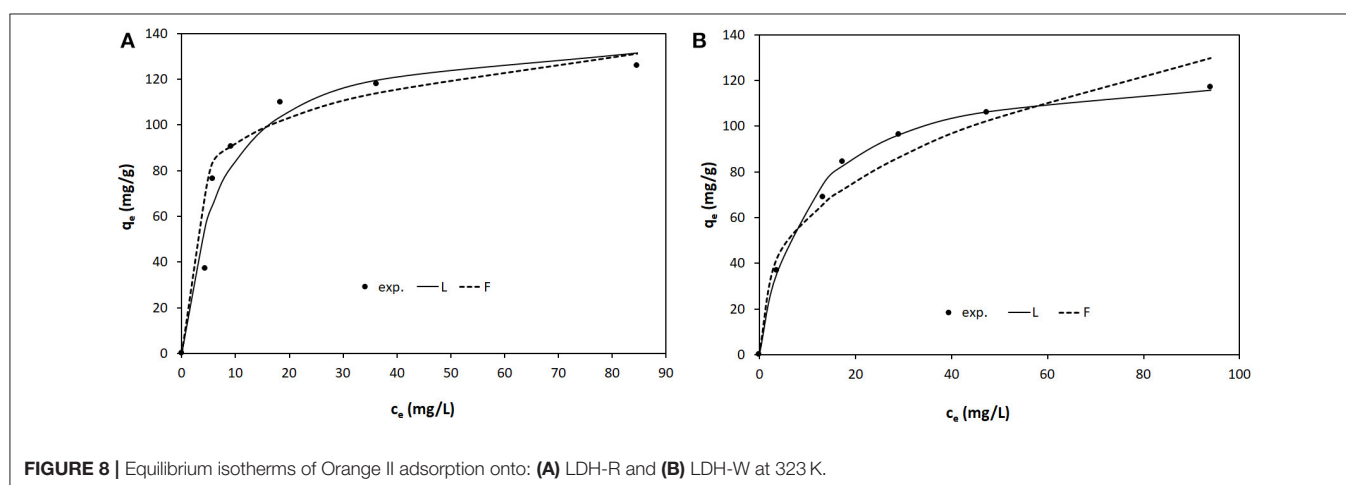
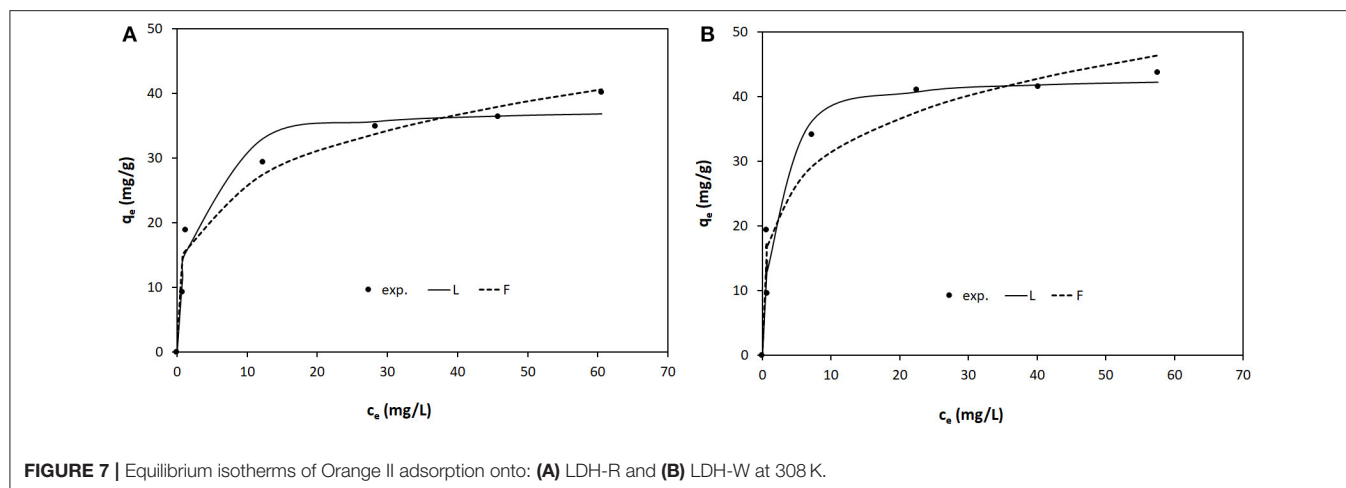


FIGURE 6 | Equilibrium isotherms of Orange II adsorption onto: (A) LDH-R and (B) LDH-W at 293 K.



with the correlation's coefficients obtained in case of the fitting of the experimental data with the PFO model. Furthermore, the q_e calculated from the linear plot of the PSO kinetic model are close to those experimentally determined. All of this suggests that the pseudo second order kinetic model describes the adsorption of Orange II onto the studied LDH, implying a chemisorption process.

Equilibrium Studies

In order to determine the maximum adsorption capacities of the studied materials, equilibrium studies were performed with solutions containing initial concentration of Orange II between 10 and 100 mg/L, a S:L ratio of 1 g/L, at three different temperatures (293, 308, and 323 K). Due to the fact that, at 323 K, the equilibrium was not reached with the same starting dye solutions as in previous experiments, we performed the equilibrium studies with an initial concentration of Orange II between 40 and 200 mg/L.

The experimental data were fitted with the non-linear form of the Langmuir and Freundlich isotherms in order to describe the equilibrium between the adsorbent materials and Orange II. The non-linear mathematical expression of Langmuir model is

represented in Equation (5) (Tran et al., 2016):

$$q_e = \frac{q_{\max} \cdot K_L \cdot c_e}{1 + K_L \cdot c_e} \quad (5)$$

where q_{\max} (mg/g) is the maximum saturated monolayer adsorption capacity under the given conditions and K_L (L/mg) is the Langmuir constant related to the affinity between an adsorbent and adsorbate.

The non-linear form of Freundlich isotherm is described by Equation (6):

$$q_e = K_F \cdot c_e^{\frac{1}{n}} \quad (6)$$

where K_F (mg/g)(L/mg) $^{1/n}$ is the Freundlich constant and $1/n$ ($0 < n < 10$) is a Freundlich intensity parameter.

The equilibrium isotherms of Orange II adsorption onto LDH-R and LDH-W at the studied temperatures are shown in **Figures 6–8**. The equilibrium isotherms parameters, together with the obtained correlation coefficients, are presented in **Table 2**.

The adsorption performance of the studied materials increases with the increase of the working temperatures. At 323 K the

TABLE 2 | Equilibrium parameters for Orange II adsorption onto LDH-R and LDH-W.

Model	T(K)	LDH-R				LDH-W			
		q_{\max} , mg/g		K_L , L/mg	R^2	q_{\max} , mg/g		K_L , L/mg	R^2
		Exp	Calc			Exp	Calc		
Langmuir	293	36.9	35.75	1.161	0.9814	42.5	42.00	0.991	0.9871
	308	40.17	37.93	0.551	0.9412	43.72	43.22	0.715	0.9201
	323	117	127.34	0.106	0.9949	126	142.02	0.147	0.9542
	T(K)	LDH-R				LDH-W			
		K_F , (mg/g)(L/mg) $^{1/n}$		1/n	R^2	K_F , (mg/g)(L/mg) $^{1/n}$		1/n	R^2
Freundlich	293		17.69	0.187	0.9111		20.11	0.198	0.8643
	308		14.88	0.245	0.9431		18.79	0.223	0.8831
	323		26.68	0.348	0.9388		34.34	0.324	0.8128
	T(K)	LDH-R				LDH-W			
		q'_{\max} , mg/g	$B_D \times 10^7$, mol 2 /J 2	E, kJ/mol	R^2	q'_{\max} , mg/g	$B_D \times 10^7$, mol 2 /J 2	E, kJ/mol	R^2
Dubinin-Radushkevich	293	33.87	1.305	1.957	0.9819	39.96	1.464	1.848	0.9863
	308	35.33	2.964	1.299	0.9681	38.83	1.696	1.717	0.8164
	323	77.01	3.11	1.268	0.8050	87.46	5.11	0.99	0.8335

maximum adsorption capacities developed by LDH-R and LDH-W is 117 and 126 mg/g, respectively. These values are almost 3 times higher than the maximum adsorption capacities resulted at 293 K. Due to the fact that the isotherms present an S shape at 323 K the initial concentration of Orange II was increased until the equilibrium was reached. According to Giles and et al., this shape is obtained when the compounds containing a sulfonate group and an aromatic ring are absorbed vertically to the adsorbent surface, implying strong intermolecular forces (Giles et al., 1960). At a higher temperature, the diffusion and mobility of the Orange II particles are increased leading to a higher mass transfer rate from solutions to the surface of the studied LDHs. Furthermore, this behavior suggests that the adsorption of Orange II onto LDHs materials is a chemisorption. By increasing the temperature, the rate of the chemical reaction increases, the favorable intermolecular forces between the LDHs surface and dye are much stronger than those between adsorbate and solvent (Kaur et al., 2013; Gupta et al., 2017). The increase in adsorption capacities of adsorbents with an increase in temperature may also be attributed to the pore size enlargement (Demirbas et al., 2008; Banerjee and Chattopadhyaya, 2017).

It is observed that for both adsorbents the curves obtained from the two models reproduce, with sufficient accuracy, the experimental data. Also, for various temperatures and both models, the values of the correlation coefficient R^2 are higher for LDH-R and, for the same type of adsorbent, these values are higher for the Langmuir model (Table 2). Furthermore, the maximum adsorption capacities developed by the studied adsorbent and experimentally determined are close to those calculated from the Langmuir isotherm, regardless of the working temperatures. These data indicate that the Langmuir model described the adsorption of Orange II onto the studied

LDHs on the entire concentration range, suggesting that the adsorption takes place from a monolayer onto the adsorbent surface (Tran et al., 2016). The LDH obtained from waste developed a higher maximum adsorption capacity than the LDH synthesized from reagents (Table 2).

The strength of adsorption is indicated by the magnitude of the Freundlich constant (K_F), which is the highest at the highest temperature (for both adsorbents) and for LDH-W (at the same temperature). For all the cases the Freundlich parameters $1/n$ present sub unitary values which indicates the affinity of Orange II for the studied adsorbents (Gupta et al., 2017).

In order to determine if the Orange II adsorption takes place due to a physisorption or a chemisorption process, the adsorption energy E was estimated by applying the Dubinin-Radushkevich (D-R) isotherm. The linearized form of this isotherm is given in Equation (7) (Hadi et al., 2010):

$$\ln q_e = \ln q_m - B_D \cdot \varepsilon^2 \quad (7)$$

where B_D is the D-R model constant (mol 2 /kJ 2) and ε is the Polanyi potential (Equation 8):

$$\varepsilon = R \cdot T \cdot \ln \left(1 + \frac{1}{c_e} \right) \quad (8)$$

The adsorption energy E whose magnitude can provide information on adsorption mechanisms is determined from Equation (9), B_D being determined from the linear representation of $\ln q_e = f(\varepsilon^2)$:

$$E = \frac{1}{\sqrt{2 \cdot B_D}} \quad (9)$$

The D-R isotherm parameters are presented in **Table 2**. The low values of the adsorption energy confirm that the dye adsorption on both adsorbents is physically achieved. The maximum adsorption capacities calculated from the D-R isotherms present values lower than those experimentally obtained.

Due to the fact that the Langmuir isotherm best described the adsorption of Orange II onto the studied LDHs, the equilibrium experimental data were also fitted with its four linear forms which are presented in Equations (10)–(13) (Tran et al., 2016):

Langmuir linearization (type 1):

$$\frac{c_e}{q_e} = \frac{1}{q_{\max}} \cdot c_e + \frac{1}{q_{\max} \cdot K_L} \quad (10)$$

Langmuir linearization (type 2):

$$\frac{1}{q_e} = \frac{1}{q_{\max} \cdot K_L} \cdot \frac{1}{c_e} + \frac{1}{q_{\max}} \quad (11)$$

Langmuir linearization (type 3):

$$q_e = q_{\max} - \frac{1}{K_L} \cdot \frac{q_e}{c_e} \quad (12)$$

Langmuir linearization (type 4):

$$\frac{q_e}{c_e} = K_L \cdot q_{\max} - K_L \cdot q_e \quad (13)$$

The symbols have the same meaning as described before. The applicability of these isotherms was compared based on the error function values: correlation coefficient R^2 , chi-square test χ^2 (Equation 14) (Hadi et al., 2010), average relative error ARE (Equation 15) (Li et al., 2017), and normalized standard deviation Δq (Equation 16) (Lv et al., 2007):

$$\chi^2 = \sum_{i=1}^n \frac{(q_{e,\text{exp}} - q_{e,\text{calc}})^2}{q_{e,\text{calc}}} \quad (14)$$

$$\text{ARE} = \frac{100}{n} \cdot \sum_{i=1}^n \left| \frac{q_{e,\text{calc}} - q_{e,\text{exp}}}{q_{e,\text{calc}}} \right|_i \quad (15)$$

$$\Delta q = 100 \cdot \sqrt{\frac{1}{n-1} \cdot \sum_{i=1}^n \left(\frac{q_{e,\text{exp}} - q_{e,\text{calc}}}{q_{e,\text{exp}}} \right)_i^2} \quad (16)$$

The Langmuir parameters determined from its linear representations (figures omitted for the sake of brevity) are presented in **Supplementary Tables 3, 4**.

Each of the four linear forms of the Langmuir isotherm will result in different parameter estimates as shown in **Supplementary Tables 3, 4**. The adsorption of Orange II onto LDH-R and LDH-W adsorbents is well-represented by the Langmuir type I model with highest coefficient of determinations; R^2 values as shown in **Supplementary Tables 3, 4**, indicate that there is strong evidence that the sorption of the chosen dye onto the prepared samples follows the Langmuir isotherm.

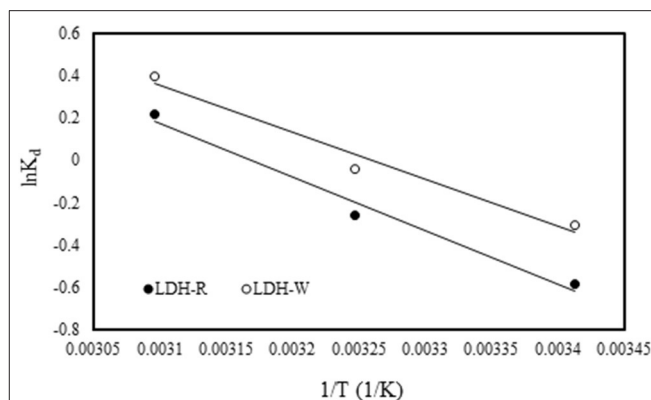


FIGURE 9 | Effect of temperature on the adsorption of Orange II onto the studied materials.

TABLE 3 | Thermodynamic parameters of Orange II adsorption onto the studied materials.

Adsorbent	T (K)	R^2	ΔG° (kJ/mol)	ΔH° (kJ/mol)	ΔS° (J/mol K)
LDH-R	293	0.9798	-0.126	19.3	66.3
	308		-1.12		
	323		-2.11		
LDH-W	293	0.9708	-0.163	17.3	59.6
	308		-1.06		
	323		-1.95		

Thermodynamic Studies

The thermodynamic parameters were calculated according to the following equations (Kaur et al., 2013; Banerjee and Chattopadhyaya, 2017; Gupta et al., 2017):

$$\Delta G^\circ = -RT \ln K_d \quad (17)$$

$$\Delta G^\circ = \Delta H^\circ - T \Delta S^\circ \quad (18)$$

$$\ln K_d = \frac{\Delta S^\circ}{R} - \frac{\Delta H^\circ}{RT} \quad (19)$$

$$K_d = \frac{q_e}{C_e} \quad (20)$$

where: ΔG° is Gibbs free energy (KJ/mol), ΔS° is the entropy and heat of adsorption (J/mol K), ΔH° is enthalpy (kJ/mol), T is the absolute temperature (K), R is universal gas constant (8.314 J/(mol·K)), and K_d is the distribution coefficient.

ΔH° and ΔS° were obtained from the slope and intercept of van't Hoff plots of $\ln K_d$ vs. $1/T$ (**Figure 9**) and the resulted values, together with the Gibbs free energy calculated with Equation (17) and the correlation coefficients, are presented in **Table 3**.

The positive value of ΔH° thermodynamically substantiates the assumption that the adsorption of Orange II on the studied LDH is endothermic in nature. The feasibility and spontaneity of the adsorption process was confirmed by the obtained negative values of ΔG° . The positive value of ΔS° suggested an increase in randomness at the solid/liquid interface during adsorption of

Orange II dye onto the studied materials. Adsorption is then likely to occur spontaneously at a high temperature because $\Delta H^\circ > 0$ and $\Delta S^\circ > 0$ (see Table 3) (Kaur et al., 2013; Banerjee and Chattopadhyaya, 2017; Gupta et al., 2017).

The Structural Characterization of Exhausted Materials After Adsorption

The XRD patterns of exhausted adsorbents are presented in Figure 10. The diffraction peaks of materials after Orange II dye adsorption are characteristic for layered double hydroxides with carbonate as an interlayer anion, since no modification in the position of the main peaks and basal spacing occurred. The basal spacing d_{003} and the d_{110} distances (cation-cation distance in the hydroxides layer) of the as-synthesized materials were $d_{003} = 7.605 \text{ \AA}$ ($d_{110} = 3.082 \text{ \AA}$) for Zn₂Al-LDH prepared

from zinc ash and $d_{003} = 7.598 \text{ \AA}$ ($d_{110} = 3.080 \text{ \AA}$) for Zn₂Al-LDH prepared from analytical grade reagents (Cocheci et al., 2018). For the materials separated after Orange II adsorption, the basal spacing and d_{110} distances are: $d_{003} = 7.593 \text{ \AA}$ ($d_{110} = 3.079 \text{ \AA}$) for LDH-W (prepared from waste) and $d_{003} = 7.587 \text{ \AA}$ ($d_{110} = 3.077 \text{ \AA}$) for LDH-R (prepared from analytical grade reagents). Studies regarding Orange II intercalation in the interlayer space of layered double hydroxides find that the basal spacing became larger due to this intercalation (Geraud et al., 2007; Liu et al., 2007). The unchanged basal spacing in our case suggests that, due to the presence of a carbonate anion in the interlayer space of LDH (due to the strong electrostatic attraction and the hydrogen bonds that the carbonate creates with the hydroxides layer), the organic dye was adsorbed on the surface of the layered double hydroxides.

The FTIR spectrum of Orange II (Figure 11) presents several absorption bands between 1,700 and 1,000 cm^{-1} ; the bands with maxima at 1,662 and 1,622 cm^{-1} correspond to a combination of phenyl ring vibrations with stretching of the C = N groups (Stylidi et al., 2004; Zhang et al., 2007). The band with a maximum at 1,614 cm^{-1} correspond to carbonyl (C = O) stretching vibrations and the maximum at 1,473 cm^{-1} are attributable to N = N stretching vibrations. The bands with maxima at 1,396 cm^{-1} and 1,320 cm^{-1} could be attributed to O – H bending vibrations (Stylidi et al., 2003). The absorption band with a maximum at 1,090 cm^{-1} could be attributed to the $\nu(\text{N} - \text{N})$ stretching vibrations, and the maxima located at 1,153 cm^{-1} and 1,045 cm^{-1} correspond to the coupling between the phenyl ring and the $\nu_s(\text{SO}_3)$ mode of the sulfonate group (Zhang et al., 2007).

The FTIR spectra of exhausted adsorbents present the main absorption bands that are characteristic of layered double hydroxides but also show some small shoulders that correspond

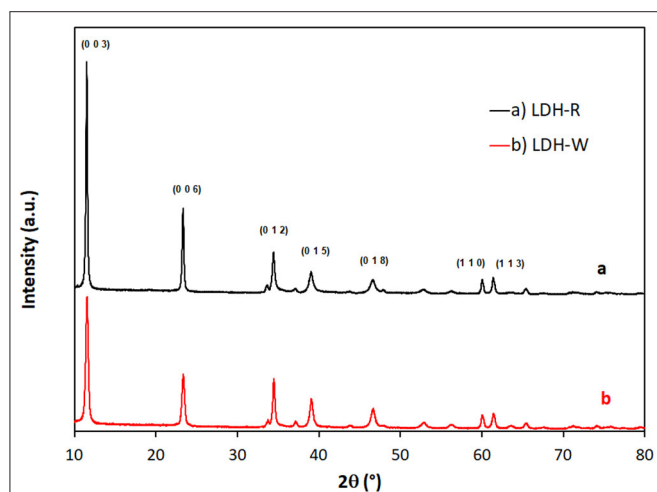


FIGURE 10 | The XRD patterns of (A) LDH-R and (B) LDH-W after Orange II adsorption.

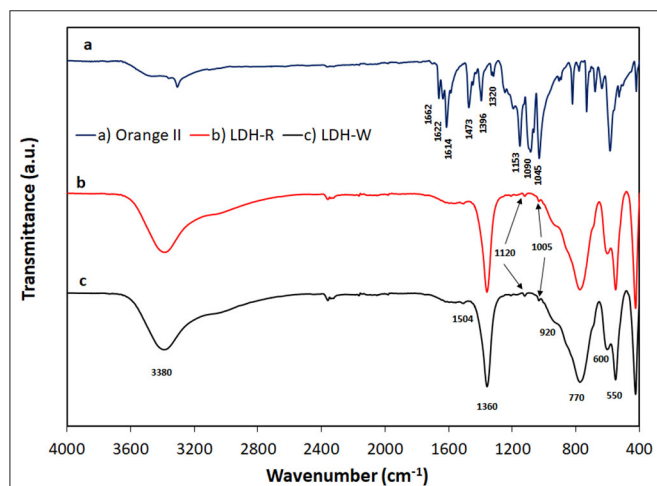


FIGURE 11 | FTIR spectra of (A) Orange II dye; (B) LDH-R after adsorption; (C) LDH-W after adsorption.

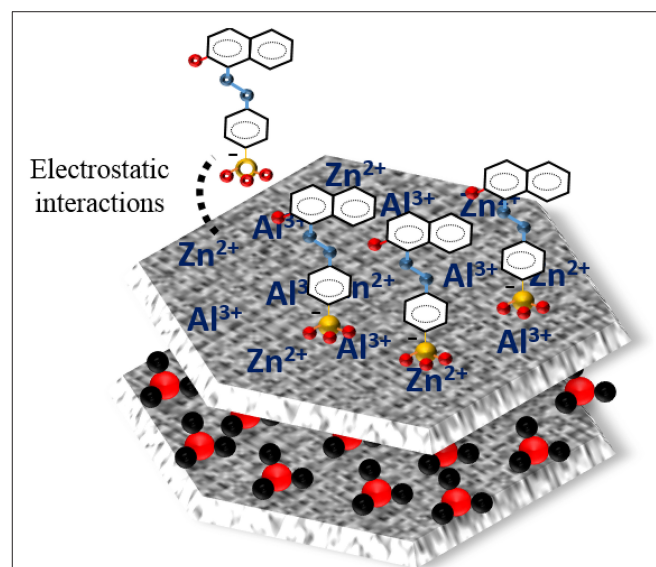


FIGURE 12 | Schematic representation on Orange II adsorption onto surface of adsorbents.

to the vibrations of sulfonate groups of Orange II dye (**Figure 11**). The main FTIR absorption bands of LDH – R (**Figure 11B**) and LDH – W (**Figure 11C**) could be attributed as follows: the strong band at $3,380\text{ cm}^{-1}$ is attributable to O – H stretching vibrations of Zn and Al hydroxides from the layer, the band with a maximum at $1,360\text{ cm}^{-1}$ could be assigned to the stretching ν_3 mode of carbonate. The small shoulders at $1,504\text{ cm}^{-1}$ can be attributed to a lowered carbonate symmetry that activated the ν_1 vibration mode of carbonate (Carja et al., 2001). The lowering of the carbonate symmetry activated the appearances of some weak shoulders corresponding to the ν_2 and ν_4 vibration mode of carbonate, visible at around 920 cm^{-1} and 600 cm^{-1} , respectively (Klopprogge et al., 2002). The band located around 770 cm^{-1} and the band at around 550 cm^{-1} may be due to the Al – O or Zn – Al – O bond vibrations in the brucite-like layer (Cocheci et al., 2018). The small shoulders that are located at $1,120\text{ cm}^{-1}$ and $1,005\text{ cm}^{-1}$ could be assigned to the bands of sulfonate group of Orange II dye that are shifted to lower frequencies due to the interactions with the hydroxides layer (Geraud et al., 2007).

The adsorption mechanism of Orange II onto the LDH-R or LDH-R adsorbents might involve two paths: external surface adsorption of dye *via* electrostatic interactions or replacement of carbonate anions from the interlayer region by the sulfonate group *via* anionic exchange (Lei et al., 2017; Srilakshmi and Thirunavukkarasu, 2019). From the structural characterization of exhausted materials after adsorption, it could be concluded that, in this case, the mechanism of Orange II adsorption onto the studied materials involves electrostatic interactions. This conclusion is in agreement with reports of other researchers who studied the adsorption of different anionic dyes on similar adsorbent materials (Geraud et al., 2007; Khosla et al., 2013; García et al., 2014; Jin et al., 2014). The schematic representation on Orange II adsorption onto the surface of adsorbents is presented in **Figure 12**.

CONCLUSIONS

In the present paper, the performance of Zn₂Al-layered double hydroxide, prepared from an industrial waste (zinc ash) as a source of zinc, and of Zn₂Al-layered double hydroxide prepared from analytical grade reagents, as a reference, in the Orange II dye adsorption process, was investigated. The influence of initial dye concentration, time of adsorption, solid:liquid ratio, pH,

and temperature was evaluated in order to confirm the benefit of this waste valorization. It was observed that the Orange II adsorption is strongly influenced by the studied parameters, the most efficient results being obtained at an initial pH value around 6, using a solid:liquid ratio of 1 g/L. The Orange II adsorption onto the studied LDH takes place very quickly, most of the dye content being adsorbed in the first 5 min, then the equilibrium is achieved in 15 min, regardless of the working conditions. The kinetic studies showed that the adsorption is described by the pseudo-second order and the equilibrium data presented a good fit with the Langmuir isotherm. The adsorption capacities increase with the increase of working temperature, and the thermodynamic parameters suggest the process of removal was spontaneous and endothermic. These results correlated with the results obtained from the structural characterization of exhausted materials after adsorption, through RX and FTIR, suggesting that the Orange II adsorption onto the studied materials occurs due to a chemisorption, implying strong intermolecular forces between the sulfonate group of the dye and the active sites of the adsorbent surface. For all the working conditions the LDH obtained from zinc ash shows better adsorption capacities than the material prepared from reagents, justifying the utilization of secondary sources for layered double hydroxides preparation. The proposed treatment process presents advantages from both an economic and environmental protection point of view.

DATA AVAILABILITY STATEMENT

The raw data supporting the conclusions of this article will be made available by the authors, without undue reservation.

AUTHOR CONTRIBUTIONS

LC and LL designed the study. AT and IC performed the experiments. LL and GR performed the instrumental analysis. AT, LC, and LL analyzed the data and wrote the paper with input from all authors.

SUPPLEMENTARY MATERIAL

The Supplementary Material for this article can be found online at: <https://www.frontiersin.org/articles/10.3389/fchem.2020.573535/full#supplementary-material>

REFERENCES

- Abramian, L., and El-Rassy, H. (2009). Adsorption kinetics and thermodynamics of azo-dye orange II onto highly porous titania aerogel. *Chem. Eng. J.* 150, 403–410. doi: 10.1016/j.cej.2009.01.019
- Aguiar, J. E., Bezerra, B. T. C., de Melo Braga, B., da Silva Lima, P. D., Nogueira, R. E. F. Q., de Lucena, S. M. P., et al. (2013). Adsorption of anionic and cationic dyes from aqueous solution on non-calcined Mg-Al layered double hydroxide: experimental and theoretical study. *Sep. Sci. Technol.* 48, 2307–2316. doi: 10.1080/01496395.2013.804837
- Asfaram, A., Ghaedi, M., Agarwal, S., Tyagi, I., and Kumar Gupta, V. (2015). Removal of basic dye Auramine-O by ZnS:Cu nanoparticles loaded on activated carbon: optimization of parameters using response surface methodology with central composite design. *RSC Adv.* 5, 18438–18450. doi: 10.1039/C4RA15637D
- Banerjee, S., and Chattopadhyaya, M. S. (2017). Adsorption characteristics for the removal of a toxic dye, tartrazine from aqueous solutions by a low cost agricultural by-product. *Arab. J. Chem.* 10, S1629–S1638. doi: 10.1016/j.arabjc.2013.06.005
- Barik, G., Padhan, E., Dash, B., Sarangi, K., and Subbaiah, T. (2014). Preparation of layered nickel aluminium double hydroxide from waste solution of nickel. *Miner. Eng.* 69, 107–112. doi: 10.1016/j.mineng.2014.07.015

- Bouhent, M. M., Derriche, Z., Denoyel, R., Prevot, V., and Forano, C. (2011). Thermodynamical and structural insights of orange II adsorption by Mg₂AlNO₃ layered double hydroxides. *J. Solid State Chem.* 184, 1016–1024. doi: 10.1016/j.jssc.2011.03.018
- Bourikas, K., Styliad, M., Kondarides, D. I., and Verykios, X. E. (2005). Adsorption of acid orange 7 on the surface of titanium dioxide. *Langmuir* 21, 9222–9230. doi: 10.1021/la051434g
- Carja, C., Nakamura, R., Aida, T., and Niiyama, H. (2001). Textural properties of layered double hydroxides: effect of magnesium substitution by copper or iron. *Microporous Mesoporous Mater.* 47, 275–284. doi: 10.1016/S1387-1811(01)00387-0
- Cavani, F., Trifiro, F., and Vaccari, A. (1991). Hydrotalcite-type anionic clays: preparation, properties, and applications. *Catal. Today* 11, 173–301. doi: 10.1016/0920-5861(91)80068-K
- Cocheci, L., Lupa, L., Gheju, M., Golban, A., Lazău, R., and Pode, R. (2018). Zn-Al-CO₃ layered double hydroxides prepared from a waste of hot-dip galvanizing process. *Clean Technol. Environ. Policy* 20, 1105–1112. doi: 10.1007/s10098-018-1533-3
- Demirbas, E., Kobya, M., and Sulak, M. T. (2008). Adsorption kinetics of a basic dye from aqueous solutions onto apricot stones activated carbon. *Bioresour. Technol.* 99, 5368–5373. doi: 10.1016/j.biortech.2007.11.019
- García, E., Medina, R., Lozano, M., Hernández Pérez, I., Valero, M., and Franco, A. (2014). Adsorption of azo-dye orange II from aqueous solutions using a metal-organic framework material: iron-benzenetricarboxylate. *Materials* 7, 8037–8057. doi: 10.3390/ma7128037
- Georgin, J., Dotto, G. L., Mazutti, M. A., and Foletto, E. L. (2016). Preparation of activated carbon from peanut shell by conventional pyrolysis and microwave irradiation-pyrolysis to remove organic dyes from aqueous solutions. *J. Environ. Chem. Eng.* 4, 266–275. doi: 10.1016/j.jece.2015.11.018
- Geraud, E., Bouhent, M., Derriche, Z., Leroux, F., Prevot, V., and Forano, C. (2007). Texture effect of layered double hydroxides on chemisorption of orange II. *J. Phys. Chem. Solids* 68, 818–823. doi: 10.1016/j.jpcs.2007.02.053
- Ghaedi, M., Hajjati, S., Mahmudi, S., Tyagi, I., Agarwal, S., Maity, A., et al. (2015). Modeling of competitive ultrasonic assisted removal of the dyes-Methylene blue and Safranin-O using Fe₃O₄ nanoparticles. *Chem. Eng. J.* 268, 28–37. doi: 10.1016/j.cej.2014.12.090
- Giles, C. H., Macewan, T. H., Nakhwa, S. N., and Smith, D. (1960). Studies in Adsorption. Part XI. A System of classification of solution adsorption isotherms, and its use in diagnosis of adsorption mechanisms and in measurement of specific surface areas of solids. *J. Chem. Soc.* 3973–3993. doi: 10.1039/jr9600003973
- Gupta, V. K., Agarwal, S., Sadegh, H., Ali, G. A. M., Bharti, K. A., and Makhoulouf, A. S. H. (2017). Facile route synthesis of novel graphene oxide-β-cyclodextrin nanocomposite and its application as adsorbent for removal of toxic bisphenol A from the aqueous phase. *J. Mol. Liq.* 237, 466–472. doi: 10.1016/j.molliq.2017.04.113
- Gupta, V. K., Mittal, A., Gajbe, V., and Mittal, J. (2006). Removal and recovery of the hazardous azo dye acid orange 7 through adsorption over waste materials: bottom ash and de-oiled soya. *Ind. Eng. Chem. Res.* 45, 1446–1453. doi: 10.1021/ie051111f
- Hadi, M., Samarghandi, M. R., and McKay, G. (2010). Equilibrium two-parameter isotherms of acid dyes sorption by activated carbons: study of residual errors. *Chem. Eng. J.* 160, 408–416. doi: 10.1016/j.cej.2010.03.016
- Hsiu-Mei, C., Ting-Chien, C., San-De, P., and Chiang, H.-L. (2009). Adsorption characteristics of orange II and chrysophenine on sludge adsorbent and activated carbon fibers. *J. Hazard. Mater.* 161, 1384–1390. doi: 10.1016/j.jhazmat.2008.04.102
- Hu, Z., Chen, H., Ji, F., and Yuan, S. (2010). Removal of congo red from aqueous solution by cattail root. *J. Hazard. Mater.* 173, 292–297. doi: 10.1016/j.jhazmat.2009.08.082
- Jin, X., Jiang, M., Shan, X., Pei, Z., and Chen, Z. (2008). Adsorption of methylene blue and orange II onto unmodified and surfactant-modified zeolite. *J. Colloid Interf. Sci.* 328, 243–247. doi: 10.1016/j.jcis.2008.08.066
- Jin, X., Yu, B., Chen, Z., Arocena, J. M., and Thring, R. W. (2014). Adsorption of orange II dye in aqueous solution onto surfactant-coated zeolite: characterization, kinetic, and thermodynamic studies. *J. Colloid Interf. Sci.* 435, 15–20. doi: 10.1016/j.jcis.2014.08.011
- Kaur, S., Rani, S., Kumar, V., Mahajan, R. K., Asif, M., Tyagi, I., et al. (2015). Synthesis, characterization and adsorptive application of ferrocene based mesoporous material for hazardous dye congo red. *J. Ind. Eng. Chem.* 26, 234–242. doi: 10.1016/j.jiec.2014.11.035
- Kaur, S., Rani, S., and Mahajan, R. K. (2013). Adsorption kinetics for the removal of hazardous dye congo red by biowaste materials as adsorbents. *J. Chem. NY.* 2013:628582. doi: 10.1155/2013/628582
- Khosla, E., Kaur, S., and Dave, P. N. (2013). Mechanistic study of adsorption of acid orange-7 over aluminum oxide nanoparticles. *J. Eng.* 2013:593534. doi: 10.1155/2013/593534
- Klopprogge, J. T., Wharton, D., Hickey, L., and Frost, R. L. (2002). Infrared and Raman study of interlayer anions CO₃²⁻, NO₃⁻, SO₄²⁻ and ClO₄⁻ in Mg/Al-hydrotalcite. *Am. Miner.* 87, 623–629. doi: 10.2138/am-2002-5-604
- Kousha, M., Daneshvar, E., Sohrabi, M. S., Jokar, M., and Bhatnagar, A. (2012). Adsorption of acid orange II dye by raw and chemically modified brown macroalga *Stoechospermum marginatum*. *Chem. Eng. J.* 192, 67–76. doi: 10.1016/j.cej.2012.03.057
- Lafi, R., Charradi, K., Djebbi, M. A., Ben Haj Amara, A., and Hafiane, A. (2016). Adsorption study of congo red dye from aqueous solution to Mg-Al-layered double hydroxide. *Adv. Powder Technol.* 27, 232–237. doi: 10.1016/j.apt.2015.12.004
- Lei, C., Pi, M., Kuang, P., Guo, Y., and Zhang, F. (2017). Organic dye removal from aqueous solutions by hierarchical calcined Ni-Fe layered double hydroxide: isotherm, kinetic, and mechanism studies. *J. Colloid Interface Sci.* 496, 158–166. doi: 10.1016/j.jcis.2017.02.025
- Li, S., Wang, F., Jing, X., Wang, J., Saba, J., Liu, Q., et al. (2012). Synthesis of layered double hydroxides from eggshells. *Mater. Chem. Phys.* 132, 39–43. doi: 10.1016/j.matchemphys.2011.10.049
- Li, W., Lin, Q., Gao, M., and Ma, H. (2017). Adsorption studies of orange II onto polyaniline/bentonite nanocomposite. *Water Sci. Technol.* 76, 337–354. doi: 10.2166/wst.2017.211
- Liu, L. Y., Pu, M., Yang, L., Li, D. Q., Evans, D. G., and He, J. (2007). Experimental and theoretical study on the structure of acid orange 7-pillared layered double hydroxide. *Mater. Chem. Phys.* 106, 422–427. doi: 10.1016/j.matchemphys.2007.06.022
- Lv, L., He, J., Wei, M., Evans, D. G., and Zhou, Z. (2007). Treatment of high fluoride concentration water by MgAl-CO₃ layered double hydroxides: kinetic and equilibrium studies. *Water Res.* 41, 1534–1542. doi: 10.1016/j.watres.2006.12.033
- Ma, J., Zou, J., Cui, B., Yao, C., and Li, D. (2013). Adsorption of orange II dye from aqueous solutions using phosphoric-acid modified clam shell powder. *Desalin. Water Treat.* 51, 6536–6544. doi: 10.1080/19443994.2013.770114
- Mahmoodi, N. M., Salehi, R., Arami, M., and Bahrami, H. (2011). Dye removal from colored textile wastewater using chitosan in binary systems. *Desalination* 267, 64–72. doi: 10.1016/j.desal.2010.09.007
- Mandal, S., and Sandhya, K. (2019). Layered double hydroxide-poly(diallyldimethylammonium chloride) nanocomposites: synthesis, characterization, and adsorption studies. *Mater. Today Proc.* 18, 1044–1053. doi: 10.1016/j.matpr.2019.06.549
- Murayama, N., Maekawa, I., Ushiro, H., Miyoshi, T., Shibata, J., and Valix, M. (2012). Synthesis of various layered double hydroxides using aluminum dross generated in aluminum recycling process. *Int. J. Miner. Process.* 110–111, 46–52. doi: 10.1016/j.minpro.2012.03.011
- Pan, H., Feng, J., Cerniglia, C. E., and Chen, H. (2011). Effects of orange II and sudan III azo dyes and their metabolites on staphylococcus aureus. *J. Ind. Microbiol. Biotechnol.* 38, 1729–1738. doi: 10.1007/s10295-011-0962-3
- Plazinski, W., Dziuba, J., and Rudzinski, W. (2013). Modeling of sorption kinetics: the pseudo-second order equation and the sorbate intraparticle diffusivity. *Adsorption* 19, 1055–1064. doi: 10.1007/s10450-013-9529-0
- Santini, T. C., and Fey, M. V. (2012). Synthesis of hydrotalcite by neutralization of bauxite residue mud leachate with acidic saline drainage water. *Appl. Clay Sci.* 55, 94–99. doi: 10.1016/j.clay.2011.10.011
- Sarkar, B., Xi, Y., Megharaj, M., and Naidu, R. (2011). Orange II adsorption on palygorskites modified with alkyl trimethylammonium and dialkyl dimethylammonium bromide—an isothermal and kinetic study. *Appl. Clay Sci.* 51, 370–374. doi: 10.1016/j.clay.2010.11.032

- Silva, J. P., Sousa, S., Rodrigues, J., Antunes, H., Porter, J. J., Gonçalves, I., et al. (2004). Adsorption of acid orange 7 dye in aqueous solutions by spent brewery grains. *Sep. Purif. Technol.* 40, 309–315. doi: 10.1016/j.seppur.2004.03.010
- Srilakshmi, C., and Thirunavukkarasu, T. (2019). Enhanced adsorption of congo red on microwave synthesized layered Zn-Al double hydroxides and its adsorption behaviour using mixture of dyes from aqueous solution. *Inorg. Chem. Commun.* 100, 107–117. doi: 10.1016/j.inoche.2018.12.027
- Stylidi, M., Kondarides, D. I., and Verykios, X. E. (2003). Pathways of solar light-induced photocatalytic degradation of azo dyes in aqueous TiO₂ suspensions. *Appl. Catal. B* 40, 271–286. doi: 10.1016/S0926-3373(02)00163-7
- Stylidi, M., Kondarides, D. I., and Verykios, X. E. (2004). Visible light-induced photocatalytic degradation of acid orange 7 in aqueous TiO₂ suspensions. *Appl. Catal. B* 47, 189–201. doi: 10.1016/j.apcatb.2003.09.014
- Tran, H. N., You, S.-J., and Chao, H.-P. (2016). Thermodynamic parameters of cadmium adsorption onto orange peel calculated from various methods: a comparison study. *J. Environ. Chem. Eng.* 4, 2671–2682. doi: 10.1016/j.jece.2016.05.009
- Xu, Z. P., Jin, Y., Liu, S., Hao, Z. P., and Lu, G. Q. (2008). Surface charging of layered double hydroxides during dynamic interactions of anions at the interfaces. *J. Colloid Interface Sci.* 326, 522–529. doi: 10.1016/j.jcis.2008.06.062
- Zaheer, Z., Bawazir, W. A., Al-Bukhari, S. M., and Basaleh, A. S. (2019). Adsorption, equilibrium isotherm, and thermodynamic studies to the removal of acid orange 7. *Mater. Chem. Phys.* 232, 109–120. doi: 10.1016/j.matchemphys.2019.04.064
- Zhang, G., Qu, J., Liu, H., Cooper, A. T., and Wu, R. (2007). CuFe₂O₄/activated carbon composite: a novel magnetic adsorbent for the removal of acid orange II and catalytic regeneration. *Chemosphere* 68, 1058–1066. doi: 10.1016/j.chemosphere.2007.01.081

Conflict of Interest: The authors declare that the research was conducted in the absence of any commercial or financial relationships that could be construed as a potential conflict of interest.

Copyright © 2020 Tămaş, Cozma, Cochei, Lupa and Rusu. This is an open-access article distributed under the terms of the Creative Commons Attribution License (CC BY). The use, distribution or reproduction in other forums is permitted, provided the original author(s) and the copyright owner(s) are credited and that the original publication in this journal is cited, in accordance with accepted academic practice. No use, distribution or reproduction is permitted which does not comply with these terms.

Advantages of publishing in Frontiers



OPEN ACCESS

Articles are free to read
for greatest visibility
and readership



FAST PUBLICATION

Around 90 days
from submission
to decision



HIGH QUALITY PEER-REVIEW

Rigorous, collaborative,
and constructive
peer-review



TRANSPARENT PEER-REVIEW

Editors and reviewers
acknowledged by name
on published articles

Frontiers

Avenue du Tribunal-Fédéral 34
1005 Lausanne | Switzerland

Visit us: www.frontiersin.org

Contact us: frontiersin.org/about/contact



REPRODUCIBILITY OF RESEARCH

Support open data
and methods to enhance
research reproducibility



DIGITAL PUBLISHING

Articles designed
for optimal readership
across devices



FOLLOW US

@frontiersin



IMPACT METRICS

Advanced article metrics
track visibility across
digital media



EXTENSIVE PROMOTION

Marketing
and promotion
of impactful research



LOOP RESEARCH NETWORK

Our network
increases your
article's readership